



Density functional perturbation theory for modeling of weak interactions and spectroscopy in the condensed phase

Arne Scherrer

► To cite this version:

Arne Scherrer. Density functional perturbation theory for modeling of weak interactions and spectroscopy in the condensed phase. Theoretical and/or physical chemistry. Université Pierre et Marie Curie - Paris VI; Martin-Luther-Universität Halle-Wittenberg, 2016. English. NNT : 2016PA066716 . tel-01617081

HAL Id: tel-01617081

<https://theses.hal.science/tel-01617081>

Submitted on 16 Oct 2017

HAL is a multi-disciplinary open access archive for the deposit and dissemination of scientific research documents, whether they are published or not. The documents may come from teaching and research institutions in France or abroad, or from public or private research centers.

L'archive ouverte pluridisciplinaire **HAL**, est destinée au dépôt et à la diffusion de documents scientifiques de niveau recherche, publiés ou non, émanant des établissements d'enseignement et de recherche français ou étrangers, des laboratoires publics ou privés.

DENSITY FUNCTIONAL PERTURBATION THEORY
FOR MODELING OF
WEAK INTERACTIONS AND SPECTROSCOPY
IN THE CONDENSED PHASE

DISSERTATION

TO ACQUIRE THE DOCTORAL DEGREE OF THE

Naturwissenschaftliche Fakultät II
Chemie, Physik und Mathematik
Martin-Luther-Universität Halle-Wittenberg

AND THE

ED 388 Chimie physique et chimie analytique de Paris Centre
Institut PASTEUR ENS-CNRS-UPMC
Sorbonne Universités, UPMC Université Paris 06

PRESENTED BY

Arne Scherrer

BORN THE 15TH JULY 1987 IN BERLIN

SUPERVISED IN CO-TUTELLE BY

Prof. Dr. Daniel Sebastiani
Prof. Dr. Rodolphe Vuilleumier

CONTENTS

ABSTRACT	vii
INTRODUCTION	I
1 ELECTRONIC STRUCTURE METHODS	5
1.1 Ab-initio molecular dynamics	5
1.2 The CPMD program package	12
1.3 Position operator and periodic boundary conditions	16
1.4 Vibrational circular dichroism	19
1.5 Exact factorization of the electron-nuclear wave function	29
1.6 Electronic susceptibility	32
2 ARTICLES PUBLISHED WITHIN THIS THESIS	36
2.1 Overview	36
2.2 Derivation of the nuclear velocity perturbation theory	38
2.3 Implementation of the nuclear velocity perturbation theory	51
2.4 Moment expansion of the electronic susceptibility	61
2.5 Molecular geometry dependence of the electronic susceptibility	72
2.6 Discussion	80
3 FURTHER RESULTS NOT YET PUBLISHED	81
3.1 Overview	81
3.2 Gauge in the liquid phase and first applications	82
3.3 Modern theory of magnetization and the nuclear velocity perturbation theory	97
3.4 Non-local pseudopotentials and Galilean invariance	100
3.5 On the mass of atoms in molecules: Beyond the Born-Oppenheimer approximation	104
3.6 Direct moment expansion algorithm	119
3.7 Discussion	121
CONCLUSION	123
BIBLIOGRAPHY	130
LIST OF FIGURES	154
LIST OF TABLES	155
APPENDICES	156
APPENDIX A ELECTRONIC STRUCTURE METHODS	156
A.1 Derivation of the exact factorization	156
A.2 Relating microscopic and macroscopic perspectives	158

A.3	Harmonic approximations	161
APPENDIX B GAUGE IN THE LIQUID PHASE AND FIRST APPLICATIONS		163
B.1	Projected nuclear velocity perturbation theory with density functional perturbation theory .	163
B.2	Radially resolved vibrational spectra	164
B.3	Computational details	167
APPENDIX C ON THE MASS OF ATOMS IN MOLECULES		169
C.1	The adiabatic limit of the exact factorization	169
C.2	Separation of the center of mass	169
C.3	Numerical details of the position dependent mass	171

ACKNOWLEDGMENTS

This work has been accomplished in co-tutelle between Daniel Sebastiani at the Martin-Luther-Universität Halle-Wittenberg and Rodolphe Vuilleumier at the École normale supérieure and Université Pierre et Marie Curie in Paris. I would like to thank both of them for their continued support, mentoring and advice in scientific and personal matters. Without their enthusiasm and commitment, this work and the venture of a thesis in co-tutelle would not have been possible. Furthermore, I am obliged to my co-workers and external collaborators, who contributed a great deal to this work, foremost Federica Agostini from the Max-Planck Institut für Mikrostrukturphysik in Halle for the common work on the nuclear velocity perturbation theory and Christian Dreßler, Sascha Jähnigen and Paul Ahlert for the joint efforts in the electronic susceptibility and vibrational circular dichroism projects. I also want to thank all my colleagues and co-workers in Halle and Paris for this inspiring and fantastic time. It has been and is a great pleasure to be part of your lives, which made the moves from Berlin to Halle and from Halle to Paris a very enriching experience. Finally, my gratitude belongs to my parents, who supported me throughout the duration of my education and whose continued support enabled me to undertake this inspiring venture.



Financially, this research project was supported by the Ländergraduierstenstipendium des Landes Sachsen-Anhalt, the PROCOPE program of the German Academic Exchange Service and by the co-tutelle scholarship of the Deutsch-Französische Hochschule. My special thanks go to Daniel Sebastiani for making this project and the co-tutelle possible.

ABSTRACT

This thesis deals with the development and application of computational methods for the efficient and accurate calculation of spectroscopic parameters and non-covalent inter-molecular interactions in condensed-phase systems from quantum chemical methods. Specifically, electronic current densities and electronic polarizability effects are computed in the framework of density functional perturbation theory. These phenomena are relevant in the context of vibrational spectroscopy and fragment-based methods for the simulation of very large systems, respectively. The nuclear velocity perturbation theory of vibrational circular dichroism is rigorously derived from the framework of the exact factorization of the electron-nuclear wave function. In the time-dependent picture, this theory is shown to be the lowest order correction to the Born-Oppenheimer approximation. The first successful implementation within a large-scale electronic structure program package is reported, efficiently yielding electronic currents densities along molecular dynamics trajectories of condensed phase systems, at unprecedented time- and length scales. In the first application, the first fully ab-initio calculation of dynamical vibrational circular dichroism in the condensed phase is demonstrated. The evaluation of magnetic observables in the condensed phase is achieved by means of an orbital-dependent Wannier gauge. The choice of the gauge for the liquid phase is rigorously analyzed and discussed. A generalization towards dynamical vibrational optical activity spectra is sketched. Furthermore, the rigorous derivation of the nuclear velocity perturbation theory yields a theoretical framework to treat weak, non-adiabatic nuclear-electronic couplings via a kinetic coupling of slow and fast degrees of freedom. One conceptually outreaching implication is the emergence of a position-dependent mass of nuclei in molecules, answering the fundamental questions as to how masses move in a molecule. As a second line of research, first steps towards a density-based modeling of inter-molecular interactions are devised. An explicit spatial representation of the interacting electronic susceptibility linear response function is employed. The response function is partitioned into a small, low-dimensional part, relevant for inter-molecular interaction potentials, and a large remainder accounting for more complex perturbation potentials. This partitioning is achieved by means of a change of representation, termed the moment expansion, which is further analyzed from the mathematical and algorithmic perspective. As a first step towards an application in the fragmented molecular dynamics framework, the explicit molecular geometry dependence of the response function is calculated.

INTRODUCTION

The context of this work is the development and application of theoretical methods for the modeling of complex molecular systems and their spectroscopic responses, focusing on the condensed phase at ambient conditions.

Examples of these systems are e.g. molecules in solution. They are characterized by their lack of long-range order and dynamically changing conformations. Furthermore, they can exhibit significant electronic polarization effects due to solvent-solute interactions and weak inter-molecular interactions like hydrogen-bonding. The accurate description of their molecular dynamics and the consideration of their chemical environment are central for a sound understanding of their physical and chemical properties and ultimately their biological function.

Optical spectroscopy is a powerful experimental tool to study these kind of physical properties. It gives access to molecular arrangements, absolute configuration, dynamics and weak inter-molecular interactions. Its underlying principle is very general: the system is exposed to a perturbative force and the responses of its observables are measured. In dielectrics and paramagnets, an external electric or magnetic field induces an electric polarization or a magnetization. In most cases, these responses are significantly determined by the change of the electronic structure, even if the frequency of the perturbation matches the one of the nuclear vibrations. Examples are infrared absorption, Raman scattering or nuclear magnetic resonance spectroscopies. In all of these, the accurate description of the electronic response is central. If the perturbations and the responses are sufficiently small, these effects can be described by linear response perturbation theory.

From a theoretical point of view, weak inter-molecular interactions can be considered as perturbations to the isolated molecular properties. In this way, the polarizing effect of the chemical environment or even hydrogen-bonding can be described in a perturbative way, based on a fragmentation of the system into its molecular constituents. Such a fragmentation can considerably reduce the computational complexity of the quantum mechanical problem.

Our method of choice to study these kind of effects is *ab-initio* molecular dynamics^{1,2} (AIMD). In this method, the molecular systems are described in a semi-classical approach, combining classical nuclei interacting with quantum electrons. This combination gives access to pico- to nano-second simulation times which are relevant for solvation, hydrogen-bonding and electronic polarization effects. The AIMD allows a dynamical description of complex polarizable molecular systems, applicable to phenomena such as bond breaking and formation and changing chemical environments. Its main advantages for spectroscopic applications is its capability to provide meaningful sampling of phase space and to naturally include weak-interactions and anharmonic effects.

In the field of AIMD, the established methodology for the solution of the electronic structure problem is Kohn-Sham density functional theory (DFT).^{3,4} In case of DFT, the perturbative calculation of ground state response properties is possible using linear density functional perturbation theory⁵⁻⁹ (DFPT). The main application of DFPT is the calculation of spectroscopic parameters along AIMD in the condensed phase, but also inter-molecular interaction energies can be obtained in this framework.¹⁰⁻¹² Important properties accessible at this level of theory are e.g. electric polarizabilities for Raman scattering intensities^{9,13} or nuclear magnetic resonance (NMR) chemical shifts.^{9,14}

This work extends the application range of DFPT in two closely related yet distinct directions, the effi-

cient calculation of electronic probability currents, used e.g. for spectroscopy in the condensed phase, and of electronic polarizability effects for the modeling of weak interactions in the condensed phase. Both aspects strive for efficient approximations of the complex fundamental equations employing linear response perturbation theory.

In the remainder of this introduction, both lines of research are introduced separately. Chapter 1 then provides a review of the employed electronic structure methods and introduces the notation for the subsequent developments and discussions. The results already published are presented in chapter 2. Further not yet published work is included in chapter 3. Finally, a summary and perspective of further developments are provided in the conclusion.

ELECTRONIC PROBABILITY CURRENTS FOR VIBRATIONAL CIRCULAR DICHROISM

Our principal application of electronic probability currents is the calculation of response properties of complex chiral systems in the condensed phase. In particular, we focus on the understanding and interpretation of vibrational optical activity (VOA) spectra in the condensed phase, aiming at applications to molecular crystals, molecules in solutions and macro molecules. Vibrational spectroscopy is an experimental tool for the investigation of the structure of chemical compounds, ranging from molecular crystals and solutions up to biochemical macromolecules such as proteins. It is a complementary approach to techniques such as X-ray and neutron scattering, electron crystallography and NMR spectroscopy.

In many biological systems, the lack of long-range order, which is required in most of these techniques, limits their applicability. Complementary to this, VOA is able to probe absolute configuration and secondary structure of chiral systems without the need of long-range order. VOA has become of major interest to scientists in academia and industry because virtually all biomolecules contain chiral centers and due to the general availability of modern accurate measurement instrumentation. Its intrinsic connection to the underlying molecular structure makes it one of the most structurally sensitive spectroscopic techniques available. In particular its applicability to controlling and characterizing molecular chirality has proven to be important in the pharmaceutical industry.

Despite the increasing popularity of experimental VOA spectroscopy, its theoretical groundings still lag behind, especially in comparison to the better-understood IRA or NMR counterparts. In particular, this applies to the treatment of condensed phase systems, for which at present no satisfying first-principles theory has been reported. In this work, we aim for an improved interpretation and theoretical evaluation of experimental vibrational circular dichroism¹⁵⁻¹⁸ (VCD) spectra. VCD denotes the difference in absorption of left and right circularly polarized light in the infrared region of the electromagnetic spectrum. It is closely related to infrared absorbance intensities (IRA) and provides a very sensitive probe of the environment of chiral centers.

Experimentally, VCD is typically measured in the liquid phase and provides detailed structural and absolute configuration information.¹⁹⁻²¹ Recently, it has found increasing popularity for probing chirality transfer²²⁻²⁷ and enantioselective synthesis.^{28, 29} The theoretical description of VCD has a long-standing history³⁰⁻³⁸ and its generalization to the liquid phase still is evolving.^{39, 40} An accurate description of vibrational spectroscopy in the condensed phase is given in the time correlation function (TCF) formalism.^{41, 42} This dynamical approach has been successfully applied to IRA of bulk solutions and solvated molecules, based

on AIMD⁴³⁻⁴⁷ or even more sophisticated methods.⁴⁸ However, even about 20 years after the milestone work of Silvestrelli,⁴³ a fully AIMD-based TCF VCD spectrum has not been reported. First attempts using partial charges or density-based reconstructed currents show the interest in this direction.⁴⁹⁻⁵²

This discrepancy between the IRA and VCD has a deeper physical reason. The advance of AIMD IRA spectra results from the fact that only adiabatic information of the electronic wave function is needed. Hence working within the Born-Oppenheimer (BO) approximation⁵³ is sufficient. In contrast, VCD requires the calculation of the magnetic dipole moment and thus requires a non-adiabatic electronic wave function, carrying an electronic current density.^{32, 33, 54}

This aspect of VCD has been addressed in the fundamental works by Stephens and Nafie. Their magnetic field perturbation theory³⁴ (MFPT) and nuclear velocity perturbation theory³³ (NVPT) provide elegant and efficient ways to obtain the required magnetic dipole moments. They are, however, usually applied in the double harmonic approximation to isolated systems.

A natural extension of the theoretical description of VCD is the combination of these approaches with AIMD-based TCF spectra in the condensed phase. This combination provides a general and rigorous extension of the established methods and is also naturally capable of describing weak inter-molecular interactions, chirality transfer²²⁻²⁷ and conformational changes^{55, 56} in solution at ambient conditions. In other words, it is in principle able to describe what experiments actually measure.

The missing link to realize this extension is an efficient scheme to compute the magnetic moments along a molecular dynamics. The MFPT is not particularly suited for a condensed phase implementation due to the ill-definition of the position operator under periodic boundary conditions.⁵⁷ In this work, we develop the necessary theoretical and computational means for this task by developing, implementing and benchmarking the NVPT in condensed phase systems.

THE ELECTRONIC SUSCEPTIBILITY FOR INTER-MOLECULAR INTERACTIONS

As mentioned above, perturbation theory can also be used to model weak inter-molecular interactions, e.g. for the accurate evaluation of inter-molecular electrostatic interactions, which is of great importance in large scale molecular dynamics simulations. In many cases, a fragmentation approach can be used to increase the efficiency of such calculations. Common methods employed are based on multipole expansions,⁵⁸⁻⁶³ density fitting⁶⁴⁻⁶⁶ or perturbation theories.^{10, 67-69} Provided that polarization effects are taken into account, this involves the calculation of *response* properties of the fragments, e.g. in the simplest case the dipole-dipole-polarizability α .

Wave function and density functional theory based perturbation theories are very successful in providing chemically accurate inter-molecular interaction energies, yielding instructive energy decomposition schemes.^{10, 67-69} However, their power comes at the price of a high computational complexity. In view of their application to molecular dynamics simulations, the dependence of the involved quantities on the atomic configuration has to be considered explicitly.

During a molecular dynamics simulation, an orbital-based evaluation of the electronic response corresponds to solving the unperturbed ground state electronic structure of each fragment and configuration and subsequently a series of self-consistent solutions of the perturbation equations for each pairwise interaction of the fragments. This is evidently a very costly undertaking, limiting its applicability to comparatively small

system sizes.

Density-based methods provide a considerable reduction of dimensionality.^{70,71} The long-range regime of the electrostatic interaction is elegantly described by the (distributed) point multipole approximation, which drastically simplifies its description.^{58-61,72,73} In larger molecules, distributed point multipoles have proven to work even if the single point multipole approximation diverges.^{72,74} A further generalization, allowing for polarization effects, is the distributed polarizability method that attributes multipole polarizabilities to different sites of the molecules.⁷⁵⁻⁷⁸ By construction, point multipoles give a poor description of the short range regime of the interaction.⁷⁹ Strategies to overcome this problem employ a spatial representation of the electronic density via Gaussian charge distributions^{80,81} or Gaussian multipoles.^{63,82-89}

Our work aims to push this approach to the next level, combining the advantages of a reduced computational complexity of the evaluation of the response density while keeping the response density in its full non-local spatial dependence and not only its multipole moments. In analogy to Gaussian multipole moments^{63,88} (as a generalization of point multipoles), we use the full non-local representation of the electronic susceptibility, providing a generalization of the multipole-multipole-polarizabilities.^{75-78,90,91}

In this work, we aim for a higher usability of the approach without the need of solving the DFPT equations self-consistently for each (i) novel external perturbation potential and (ii) new molecular conformation. We develop a very condensed representation of the full response function for inter-molecular interactions and show that the explicit representation of the full non-local response function on the molecular geometry can be achieved by means of a Taylor expansion in the nuclear coordinates.

CHAPTER I

ELECTRONIC STRUCTURE METHODS

In this chapter, we present the employed methods and introduce the notation for the subsequent developments and discussions. It is not meant as a didactic review of these methods but sets the focus on the aspects relevant for the later developments. We include corresponding references to more comprehensive presentations. In section 1.1, we introduce the basic concepts and notations of the used theories for the modeling of chemical systems from first principles. The prerequisites for the description of the implementation are given in section 1.2. An outline of the position operator problem under periodic boundary conditions is provided in section 1.3. The macroscopic and microscopic foundations of vibrational circular dichroism and its theoretical descriptions are presented in section 1.4. As a starting point of approximations, we introduce the framework of the exact factorization of the electron-nuclear wave function in section 1.5. Finally, we deal with electronic polarization effects and the electronic susceptibility in section 1.6.

1.1 AB-INITIO MOLECULAR DYNAMICS

For the microscopic description of matter, we resort to a first principles description of its constituent molecules. We start with the non-relativistic Hamiltonian, describing a system of interacting electrons and nuclei⁹²

$$\hat{\mathcal{H}} = \hat{T}_n + \hat{T}_e + V_{ee}(\mathbf{r}) + V_{en}(\mathbf{r}, \mathbf{R}) + V_{nn}(\mathbf{R}) + V_{n,ext}(\mathbf{R}, t) + V_{e,ext}(\mathbf{r}, t), \quad (1.1.1)$$

with the nuclear and electronic kinetic energies \hat{T}_n and \hat{T}_e , the interaction potentials of electron-electron $V_{ee}(\mathbf{r})$, nuclear-nuclear $V_{nn}(\mathbf{R})$ and electron-nuclear $V_{en}(\mathbf{r}, \mathbf{R})$ interactions and external potentials of nuclei $V_{n,ext}(\mathbf{R}, t)$ and electrons $V_{e,ext}(\mathbf{r}, t)$. The symbols \mathbf{r} and \mathbf{R} are used to collectively indicate the coordinates of N_e electrons and N_n nuclei, respectively. The full Hamiltonian enters the time-dependent Schrödinger equation (TDSE) that governs the time evolution of the full electron-nuclear wave function $\Psi(\mathbf{r}, \mathbf{R}, t)$

$$i\hbar\partial_t\Psi(\mathbf{r}, \mathbf{R}, t) = \hat{\mathcal{H}}\Psi(\mathbf{r}, \mathbf{R}, t). \quad (1.1.2)$$

The exact solution of eq. (1.1.2) is a formidable task that is only feasible at few degrees of freedom.⁹³ One common way to solve it is provided by the Born-Huang expansion,^{53,92} which is outlined in section 1.1.1 along the lines of ref.² We introduce the central concepts of Born-Oppenheimer molecular dynamics in section 1.1.2. The approximate solution of the electronic structure problem, employing density functional theory and its perturbation variant density functional perturbation theory, are reviewed in sections 1.1.3 and 1.1.4. Throughout this work, we assume that the electronic ground state is a non-degenerate singlet, such that the electron spin is not considered explicitly.

1.1.1 BORN-OPPENHEIMER APPROXIMATION AND BORN-HUANG EXPANSION

In ab-initio molecular dynamics² (AIMD), one typically employs a mixed quantum-classical approach, combining a quantum mechanical treatment of the electronic degrees of freedom with a classical treatment of the

nuclei. Underlying this approach is the Born-Oppenheimer⁵³ (BO) approximation to the electron-nuclear problem. It can be recovered via appropriate limits from the exact factorization of the electron-nuclear wave function (c.p. section 1.5), as shown in sections 2.2 and 3.5. Here, we only wish to introduce the working equations of the AIMD implementation and follow the conventional route via the Born-Huang expansion⁹² to do so.

We start from the full TDSE in eq. (1.1.2), with the total Hamiltonian of eq. (1.1.1), which is partitioned in the nuclear kinetic energy operator and external potentials on the one side, and the standard BO electronic Hamiltonian $\hat{\mathcal{H}}_{BO}$ on the other side

$$\hat{\mathcal{H}} = \hat{T}_n + \hat{\mathcal{H}}_{BO} + V_{n,ext}(\mathbf{R}, t) + V_{e,ext}(\mathbf{r}, t) \quad (1.1.3)$$

$$\hat{\mathcal{H}}_{BO} = \hat{T}_e + V_{ee}(\mathbf{r}) + V_{en}(\mathbf{r}, \mathbf{R}) + V_{nn}(\mathbf{R}). \quad (1.1.4)$$

In the Born-Huang expansion, we use the stationary eigenfunctions $\varphi_{\mathbf{R},l}(\mathbf{r})$ of the electronic BO Hamiltonian in eq. (1.1.4) as a basis to expand the total wave function

$$\Psi(\mathbf{r}, \mathbf{R}, t) = \sum_l^{\infty} \varphi_{\mathbf{R},l}(\mathbf{r}) \chi_l(\mathbf{R}, t), \quad (1.1.5)$$

with time dependent expansion coefficients $\chi_l(\mathbf{R}, t)$. By projection on $\varphi_{\mathbf{R},k}(\mathbf{r})$, this yields a set of coupled partial differential equations

$$\left[\hat{T}_n + \epsilon_{BO,k}(\hat{\mathbf{R}}) \right] \chi_k + \sum_l \hat{C}_{kl} \chi_l = i\hbar \partial_t \chi_k, \quad (1.1.6)$$

with the BO eigenvalues $\epsilon_{BO,k}(\mathbf{R})$ and the non-adiabatic coupling operator

$$\hat{C}_{kl} = \langle \varphi_{\mathbf{R},k} | \hat{T}_n | \varphi_{\mathbf{R},l} \rangle_{\mathbf{r}} + \sum_{\nu} \frac{1}{M_{\nu}} \langle \varphi_{\mathbf{R},k} | -i\hbar \nabla_{\nu} | \varphi_{\mathbf{R},l} \rangle_{\mathbf{r}} \cdot (-i\hbar \nabla_{\nu}). \quad (1.1.7)$$

If all couplings are taken into account in the solution, the problem is solved exactly, i.e. fully non-adiabatic. This is, however, only possible in very small molecular or model systems. The adiabatic solution corresponds to considering the diagonal terms C_{kk} only, i.e. the energies of the eigenstates are modified, but there are no transitions possible. In the clamped nuclei approximation, also the diagonal coupling terms are neglected and the electron-nuclear problem is reduced to

$$\left[\hat{\mathcal{H}}_{BO} - \epsilon_{BO,k}(\mathbf{R}) \right] |\varphi_{\mathbf{R},k}\rangle = 0 \quad \text{and} \quad \left[\hat{T}_n + \epsilon_{BO,k}(\hat{\mathbf{R}}) \right] \chi_k = i\hbar \partial_t \chi_k. \quad (1.1.8)$$

The electronic-nuclear coupling then is mediated only via the potential energy surface without any vibronic effects.

1.1.2 GROUND STATE BORN-OPPENHEIMER MOLECULAR DYNAMICS

The classical limit of the nuclei is obtained by rewriting the nuclear wave function in a polar representation,² with amplitude $A_k(\mathbf{R}, t)$ and phase $S_k(\mathbf{R}, t)$

$$\chi_k(\mathbf{R}, t) = A_k(\mathbf{R}, t) e^{iS_k(\mathbf{R}, t)/\hbar}. \quad (1.1.9)$$

Separating the real and imaginary part of the nuclear TDSE (1.1.8) gives rise to two coupled partial differential equations for the amplitude and phase. The amplitude equation can be written as a continuity equation in terms of the nuclear probability density $\rho_k = |\chi_k|^2 = A_k^2$ and the associated nuclear current density $\mathbf{J}_{k,\nu} = \rho_k \nabla_I S_k / M_\nu$ as

$$\frac{\partial \rho_k}{\partial t} + \sum_\nu \nabla_\nu \cdot \mathbf{J}_{k,\nu} = 0. \quad (1.1.10)$$

For the phase, one obtains in the classical limit ($\hbar \rightarrow 0$)

$$\frac{\partial S_k}{\partial t} + \sum_\nu \frac{1}{2M_\nu} (\nabla_\nu S_k)^2 + \epsilon_{BO,k} = \lim_{\hbar \rightarrow 0} \hbar^2 \sum_\nu \frac{1}{2M_\nu} \frac{\nabla_\nu^2 A_k}{A_k} = 0. \quad (1.1.11)$$

This equation is isomorphic to the equation of motion in the Hamilton-Jacobi formulation of classical mechanics, with a classical Hamiltonian^{2,94}

$$\mathcal{H}_k(\mathbf{R}, \mathbf{P}) = T(\mathbf{P}) + \epsilon_{BO,k}(\mathbf{R}), \quad (1.1.12)$$

expressed in terms of generalized coordinates $\mathbf{R} = \mathbf{R}(t)$ and their conjugate canonical momenta $\mathbf{P}_\nu = \mathbf{P}_\nu(t) = \nabla_\nu S_k$. The nuclear equation of motion

$$M_\nu \ddot{\mathbf{R}}_\nu = -\nabla_\nu \epsilon_{BO,k}(\mathbf{R}) \quad (1.1.13)$$

then is governed solely by the potential generated by the electronic degrees of freedom at the corresponding nuclear configuration. The ground state BO molecular dynamics, which is employed in this work, simultaneously solves the electronic and nuclear equations

$$M_\nu \ddot{\mathbf{R}}_\nu = -\nabla_\nu \min_{\varphi_{\mathbf{R},0}} \{ \langle \varphi_{\mathbf{R},0} | \hat{\mathcal{H}}_{BO} | \varphi_{\mathbf{R},0} \rangle \} \quad \text{and} \quad \hat{\mathcal{H}}_{BO} | \varphi_{\mathbf{R},0} \rangle = \epsilon_{BO,0}(\mathbf{R}) | \varphi_{\mathbf{R},0} \rangle. \quad (1.1.14)$$

This requires the solution of the time-independent electronic Schrödinger equation at the given nuclear configuration. The evaluation of the nuclear gradient of the electronic potential energy surface is, via the Hellman-Feynman theorem,^{95,96} the expectation value of the analytical derivative of the Hamiltonian.

1.1.3 DENSITY FUNCTIONAL THEORY

The exact solution of eq. (1.1.14) is still very expensive in systems with more than a few degrees of freedom. Already calculations of small molecules require an approximate treatment of the electronic structure problem. The established methodology in the field of AIMD is the use of Kohn-Sham (KS) density functional theory (DFT).^{3,4,97-99} We will not provide a detailed discussion of this vast field of research but focus on the relevant aspects for the introduction of density functional perturbation theory. A more comprehensive presentation can be found in the references already given and in ref.¹⁰⁰ which we follow in this presentation. For simplicity, we drop the explicit notation of the parametric dependence on the nuclear positions.

HOHENBERG-KOHN THEOREMS

The powerful idea of DFT is to reduce the electronic degrees of freedom of a system by using the electronic density instead of the electronic wave function. Although this approach dates back already to Fermi and

Wigner,⁹⁷ modern DFT is based on the two theorems of Hohenberg-Kohn³ (HK). They point out that the whole information of the electronic ground state is contained in its electronic density.

The first HK theorem states that, for a system of interacting particles in an external potential $V_{ext}(\mathbf{r})$, this potential is determined uniquely (up to a constant) by the ground state particle density $n_0(\mathbf{r})$. Therefore, there exists a one-to-one correspondence of the density with the underlying external potential, as schematically illustrated in fig. 1.1.

$$\begin{array}{ccc}
 V_{ext}(\mathbf{r}) & \xleftrightarrow{HK} & n_0(\mathbf{r}) \\
 \Downarrow & & \Uparrow \\
 \Psi_i(\mathbf{r}) & \Longrightarrow & \Psi_0(\mathbf{r})
 \end{array}$$

Figure 1.1: Schematic illustration of the first Hohenberg-Kohn theorem in analogy to ref.¹⁰⁰ The solution of the Schrödinger equation for the Hamiltonian with an external potential $V_{ext}(\mathbf{r})$ yields the electronic wave functions $\Psi_i(\mathbf{r})$, among others the ground state one $\Psi_0(\mathbf{r})$, from which its electronic density $n_0(\mathbf{r})$ can be determined. The first Hohenberg-Kohn (HK) theorem closes the circle, proving a one-to-one correspondence of the ground state density to the underlying external potential.

Since the external potential determines $\hat{\mathcal{H}}_{BO}$ and in turn all other physical properties, this means that it is possible to express the full many particle ground state as a unique functional of n_0 .

The second HK theorem states the existence of such a unique functional of the electronic ground state density for the electronic ground state energy $\mathcal{E}[n_0]$. It further applies the Rayleigh-Ritz¹⁰¹ variational principle to show that this functional takes its global minimum for the exact ground state density n_0 . That is, for any valid trial density \tilde{n} , we have

$$\epsilon_{BO,0} = \mathcal{E}[n_0] \leq \mathcal{E}[\tilde{n}] = T[\tilde{n}] + \mathcal{E}_{en}[\tilde{n}] + \mathcal{E}_{ee}[\tilde{n}], \quad (1.1.15)$$

where the functional is split in the kinetic energy functional T and the functionals for the energies due to electron-nuclear \mathcal{E}_{en} and electron-electron \mathcal{E}_{ee} interaction. Even though the electronic density contains all required information, we do not have an explicit formulation of it. In particular, there exists no good approximation for the kinetic energy functional of the electronic ground state density. This shortcoming has been circumvented by Kohn and Sham, as discussed in the following.

KOHN-SHAM DENSITY FUNCTIONAL THEORY

In the Kohn and Sham (KS) ansatz,⁴ one introduces a non-interacting single determinant reference system of KS orbitals ϕ_o that yields the same ground state density n_0 as the fully interacting wave function

$$n_0(\mathbf{r}) \stackrel{!}{=} n(\mathbf{r}) = \sum_o |\phi_o(\mathbf{r})|^2. \quad (1.1.16)$$

By applying the HK theorems to this system of non-interacting electrons, the exact ground state energy functional becomes the KS functional

$$\mathcal{E}^{KS}[\{\phi_o\}] = \underbrace{\sum_o \langle \phi_o | -\frac{1}{2} \nabla^2 | \phi_o \rangle}_{T_s[\{\phi_o\}]} + \underbrace{\int V_{en}(\mathbf{r}, \mathbf{R}) n(\mathbf{r}) d^3r}_{\mathcal{E}_{en}[n]} + \underbrace{\frac{1}{2} \iint \frac{n(\mathbf{r}) n(\mathbf{r}') d^3r' d^3r}{|\mathbf{r} - \mathbf{r}'|}}_{\mathcal{E}_H[n] = \frac{1}{2} \int V_H(\mathbf{r}) n(\mathbf{r}) d^3r} + \mathcal{E}_{xc}[n], \quad (1.1.17)$$

with the KS kinetic energy T_s and the classical Hartree potential V_H and energy functional \mathcal{E}_H . The last term \mathcal{E}_{xc} is the exchange-correlation energy, defined as

$$\mathcal{E}_{xc}[\{\phi_o\}] \equiv T[n] - T_s[\{\phi_o\}] + \mathcal{E}_{ee}[n] - \mathcal{E}_H[n]. \quad (1.1.18)$$

It accounts for exchange effects due to the quantum nature of the electrons and for the error made by omitting correlation in the reference system. With an exact expression of $\mathcal{E}_{xc}[n]$, the KS formalism would give the exact ground state energy. However, only approximate functionals are available at present. Hence we resort to the generalized gradient approximation to the exchange-correlation functional,^{102–105} which employs functional dependences on the density and its gradient.¹⁰⁰

Even though this ansatz introduces a wave function again, it greatly reduces the computational complexity of the mathematical problem. This is due to the fact that the interaction is only due to the density and not due to the wave function.

By variational minimization of the KS functional with respect to the density $n(\mathbf{r})$, one obtains a KS Hamiltonian eigenvalue problem

$$(\hat{\mathcal{H}}_{KS} - \epsilon_o)|\phi_o\rangle = 0 \quad \text{with} \quad \hat{\mathcal{H}}_{KS} = -\frac{1}{2}\nabla^2 + V_{en}(\hat{\mathbf{r}}, \mathbf{R}) + V_{Hxc}[n], \quad (1.1.19)$$

introducing the Hartree-exchange-correlation potential $V_{Hxc}[n]$ as the functional derivative of the Hartree-exchange-correlation functional $\mathcal{E}_{Hxc} = \mathcal{E}_H + \mathcal{E}_{xc}$ with respect to the electronic density.

1.1.4 DENSITY FUNCTIONAL PERTURBATION THEORY

If an electronic system is exposed to an external perturbation, e.g. due to electro-magnetic fields, the eigenfunctions of the unperturbed Hamiltonian are no longer eigenfunctions of the perturbed Hamiltonian, but the new eigenfunctions can be calculated using perturbation theory.¹⁰⁶ We do not present the conventional Hamiltonian formulation of perturbation theory of DFT^{6–8} but use a more general variational approach.⁹ This theoretical concept of density functional perturbation theory (DFPT) is based on the variational principle applied to a perturbed system. In case of an unperturbed system in its electronic ground state, the variational principle states that the ground state KS orbitals are those that minimize the KS energy. In presence of a perturbation, the electronic structure adjusts such that the perturbed energy is again minimized. This property is used to calculate the perturbed states by a variational approach, which allows to treat perturbations that are not representable in a Hamiltonian form.⁹ This review of DFPT is adapted from ref.¹⁰⁷

In presence of a small perturbation, the response of a property X of the system can be obtained to arbitrary order by a perturbative expansion around its unperturbed value $X^{(0)}$ according to

$$X = \sum_{k=0}^{\infty} \lambda^k X^{(k)} \quad \text{with} \quad X^{(k)} = \frac{1}{k!} \frac{d^k X}{d\lambda^k}. \quad (1.1.20)$$

Common choices of X are the energy E , the KS orbitals $|\phi_o\rangle$ or the density n . The perturbation parameter λ is an infinitesimally small auxiliary variable that helps to separate different orders of the response with respect to the perturbation and does not occur in the final expressions. The presence of the perturbation is represented by an additional linearized energy term in the total energy functional

$$\mathcal{E}^{tot}[\{\phi_o\}] = \mathcal{E}^{KS}[\{\phi_o\}] + \lambda \mathcal{E}^{pert}[\{\phi_o\}], \quad (1.1.21)$$

depending on the ensemble of occupied KS orbitals $\{\phi_o\}$. In the variational approach, the total energy in presence of the perturbation is minimized by varying with respect to the electronic states.⁹ Its explicit expansion is given as

$$\mathcal{E}^{tot} = \mathcal{E}^{tot}[\{\phi_o^{(0)} + \lambda\phi_o^{(1)} + \dots\}] = \mathcal{E}^{(0)} + \lambda\mathcal{E}^{(1)} + \lambda^2\mathcal{E}^{(2)} + \mathcal{O}(\lambda^3). \quad (1.1.22)$$

Due to the variational property of the ground state energy, the ground state orbitals minimize the perturbed functional. At the extremal point, the linear order energy vanishes due to stationarity. The first non-vanishing term is thus the second order energy $\mathcal{E}^{(2)}$. The variation of the electronic states is supplemented by additional constraints, in order to maintain orthonormality. A particularly convenient choice is the orthogonalization of the response orbitals $\{\phi^{(1)}\}$ with respect to the occupied unperturbed orbitals $\{\phi^{(0)}\}$ in the parallel-transport gauge^{6,9}

$$\langle\phi_o^{(1)}|\phi_{o'}^{(0)}\rangle = 0 \quad \forall o, o'. \quad (1.1.23)$$

Instead of using canonical orbitals $\phi^{(0)}$, we can formulate the second order variation of the energy also in terms of unitary transformations of these φ_o ¹⁴

$$\begin{aligned} \mathcal{E}^{(2)} = & \sum_{oo'} \left[\langle\varphi_o^{(1)}|\hat{\mathcal{H}}_{KS}^{(0)}\delta_{oo'} - \langle\varphi_{o'}^{(0)}|\hat{\mathcal{H}}_{KS}^{(0)}|\varphi_o^{(0)}\rangle|\varphi_{o'}^{(1)}\rangle \right] + \frac{1}{2} \iint d^3r d^3r' K(\mathbf{r}, \mathbf{r}') n^{(1)}(\mathbf{r}) n^{(1)}(\mathbf{r}') \\ & + \sum_o \left[\langle\varphi_o^{(1)}|\frac{\delta\mathcal{E}^{pert}}{\delta\langle\varphi_o^{(0)}|} + \frac{\delta\mathcal{E}^{pert}}{\delta|\varphi_o^{(0)}\rangle}|\varphi_o^{(1)}\rangle \right], \end{aligned} \quad (1.1.24)$$

with the Hartree-exchange-correlation kernel $K(\mathbf{r}, \mathbf{r}') = \frac{\delta(\mathcal{E}_H + \mathcal{E}_{xc})}{\delta n(\mathbf{r})\delta n(\mathbf{r})}$ and the unperturbed KS Hamiltonian according to eq. (1.1.19). The functional derivative of the exchange-correlation potentials are usually realized via a finite-difference scheme,⁹ but in principle can be computed analytically. A variational minimization under the orthogonality constraints of eq. (1.1.23) yields inhomogeneous Sternheimer equations^{9,14,108}

$$-\hat{P}_e \sum_{o'} \left(\hat{\mathcal{H}}_{KS}^{(0)}\delta_{oo'} - \langle\varphi_{o'}^{(0)}|\hat{\mathcal{H}}_{KS}^{(0)}|\varphi_o^{(0)}\rangle \right) \hat{P}_e |\varphi_{o'}^{(1)}\rangle = \hat{P}_e \left[\int d^3r' n^{(1)}(\mathbf{r}') \langle\mathbf{r}'|\hat{K}|\varphi_o^{(0)}\rangle + \frac{\delta\mathcal{E}_{KS}^{pert}}{\delta\langle\varphi_o^{(0)}|} \right], \quad (1.1.25)$$

where $\hat{P}_e = \sum_o 1 - |\varphi_o\rangle\langle\varphi_o|$ is a projection operator on the empty orbitals. This equation can be solved self-consistently by linear algebra algorithms as e.g. conjugated-gradient minimization.² It has the advantage to contain ground state information only, i.e. its solution does not require the knowledge of unoccupied electronic states. With this result, it is possible to efficiently calculate the response properties of various perturbations such as nuclear displacements or electric and magnetic fields in the condensed phase.

NUCLEAR DISPLACEMENT AND MAGNETIC FIELD PERTURBATIONS

In this work, we use the nuclear displacement perturbation (NDP) implementation of ref.⁹ Furthermore, magnetic field perturbations¹⁴ (MFP) in the condensed phase are discussed in section 1.4.4. The NDP can be done with canonical orbitals. Its perturbation functional

$$\mathcal{E}_{KS}^{NDP} = \sum_o \left\langle \phi_o^{(0)} \left| \frac{\partial \hat{\mathcal{H}}_{KS}}{\partial \mathbf{R}} \right| \phi_o^{(0)} \right\rangle \quad (1.1.26)$$

yields Sternheimer equations that on both sides depend on the response orbitals and hence have to be solved self-consistently

$$-\hat{P}_e(\hat{\mathcal{H}}_{KS}^{(0)} - \epsilon_o^{(0)})\hat{P}_e|\phi_o^{(\mathbf{R})}\rangle = \hat{P}_e \left[\int d^3r' n^{(1)}(\mathbf{r}') \langle \mathbf{r}' | \hat{K} | \phi_o^{(0)} \rangle + \frac{\partial \hat{\mathcal{H}}_{KS}}{\partial \mathbf{R}} |\phi_o^{(0)}\rangle \right]. \quad (1.1.27)$$

The response orbitals are written in a compact notation as $|\phi_o^{(\mathbf{R})}\rangle$, where the superscript in parentheses indicates the derivative.

MFPs in the condensed phase pose additional complications due to the ill-definition of the position operator under periodic boundary conditions (c.p. section 1.3). Implementations of MFPs have been realized in different ways.^{14,109,110} We review the implementation by Sebastiani et al.,¹⁴ which employs the combination of a plane wave basis and maximally localized Wannier orbitals^{m1,m2} (MLWOs) w_o . This approach uses the continuous set of gauge transformations^{m3} as the physical gauge of the magnetic field. That is, for the evaluation of the electronic current density $\mathbf{j}(\mathbf{r}')$ at position \mathbf{r}' , the gauge origin \mathbf{r}_0 of the electro-magnetic vector potential $\mathbf{A}(\mathbf{r}) = -\frac{1}{2}(\mathbf{r} - \mathbf{r}_0) \times \mathbf{B}$ is set to \mathbf{r}' . In this gauge, the current density reduces to its paramagnetic part

$$\mathbf{j}(\mathbf{r}') = \frac{e}{mc} \sum_o \langle w_o^{(0)} | (\hat{\mathbf{p}}|\mathbf{r}'\rangle\langle\mathbf{r}'| + |\mathbf{r}'\rangle\langle\mathbf{r}'|\hat{\mathbf{p}}) [|w_o^{(\mathbf{r} \times \mathbf{p})}\rangle - \mathbf{r}' \times |w_o^{(\mathbf{p})}\rangle] \cdot \mathbf{B}. \quad (1.1.28)$$

In this formula, the position operator enters as an absolute position such that it is not well defined under periodic boundary conditions. Since the MFP linear response orbitals are purely imaginary, the linear density response vanishes and no self-consistency is required to solve the corresponding Sternheimer equations. We can therefore introduce a compact Green's function notation of the response calculation as

$$|w_o^{(\mathcal{O})}\rangle = \sum_{o'} \hat{G}_{oo'} \hat{\mathcal{O}} |w_{o'}^{(0)}\rangle \quad \text{with} \quad \hat{G}_{oo'} = - \left(\hat{\mathcal{H}}_{KS}^{(0)} \delta_{oo'} - \langle w_{o'}^{(0)} | \hat{\mathcal{H}}_{KS}^{(0)} | w_o^{(0)} \rangle \right)^{-1}, \quad (1.1.29)$$

which is only used for compact representation of the formula. Introducing the orbital-dependent position operator reference frames (c.p. section 1.3) \mathbf{r}_o , eq. (1.1.28) can be rewritten in a computationally practicable way

$$\mathbf{j}(\mathbf{r}') = \frac{e}{mc} \sum_{oo'} \langle w_o^{(0)} | (\hat{\mathbf{p}}|\mathbf{r}'\rangle\langle\mathbf{r}'| + |\mathbf{r}'\rangle\langle\mathbf{r}'|\hat{\mathbf{p}}) \left[\hat{G}_{oo'} \left((\hat{\mathbf{r}} - \mathbf{r}_{o'}) \times \hat{\mathbf{p}} \right) |w_{o'}^{(0)}\rangle - (\mathbf{r}' - \mathbf{r}_o) \times \hat{G}_{oo'} \hat{\mathbf{p}} |w_{o'}^{(0)}\rangle \right] \cdot \mathbf{B} + \Delta\mathbf{j}(\mathbf{r}'), \quad (1.1.30)$$

with a correction

$$\Delta\mathbf{j}(\mathbf{r}') = -\frac{e}{mc} \sum_{oo'} \langle w_o^{(0)} | (\hat{\mathbf{p}}|\mathbf{r}'\rangle\langle\mathbf{r}'| + |\mathbf{r}'\rangle\langle\mathbf{r}'|\hat{\mathbf{p}}) \hat{G}_{oo'} \left((\mathbf{r}_o - \mathbf{r}_{o'}) \times \hat{\mathbf{p}} \right) |w_{o'}^{(0)}\rangle \cdot \mathbf{B}. \quad (1.1.31)$$

Since only relative positions occur, these expressions are well defined also under periodic boundary conditions. The evaluation of eq. (1.1.30) requires 6 non self-consistent perturbation calculations, whereas eq. (1.1.31) requires one calculation for each state o or each group of states of sufficient proximity.

1.2 THE CPMD PROGRAM PACKAGE

The theoretical developments of this work are implemented in the CPMD^{m4} program package, in which a plane wave basis is employed. This choice is particularly well suited for linear response calculations. We introduce only the concepts and notation necessary for the description of the implementation in section 2.3. In particular, we do not discuss details like the explicit implementation of the exchange correlation energy, the different choices of norm conserving non-local pseudopotentials or algorithmic subtleties of high-performance parallel computing. A complete presentation of the implementation and the employed concepts is given in ref.²

1.2.1 PLANE WAVE BASIS AND SUPER CELL

The unit cell under periodic boundary conditions is described by its Bravais lattice vectors $\mathbf{h} = [\mathbf{a}_1, \mathbf{a}_2, \mathbf{a}_3]$ yielding the cell volume $\Omega = \det\{\mathbf{h}\}$. The reciprocal space vectors $\mathbf{G} = 2\pi(\mathbf{h}^T)^{-1}\mathbf{g}$ are given by a set of integers $\mathbf{g} = [i, j, k]$. All periodic functions $f(\mathbf{r})$ are expanded in plane waves

$$f(\mathbf{r}) = f(\mathbf{r} + \mathbf{L}) = \frac{1}{\sqrt{\Omega}} \sum_{\mathbf{G}} f(\mathbf{G}) e^{i\mathbf{G}\cdot\mathbf{r}}, \quad (1.2.1)$$

which allows to express equivalent points in different cells via the direct lattice vectors \mathbf{L} . Since the potentials exhibit the same periodicity as the lattice, the KS orbitals can be written in general Bloch form

$$\phi_o(\mathbf{r}, \mathbf{k}) = e^{i\mathbf{k}\cdot\mathbf{r}} u_o(\mathbf{r}, \mathbf{k}), \quad (1.2.2)$$

with the crystal moment \mathbf{k} .¹⁰⁰ The periodic functions $u_o(\mathbf{r}, \mathbf{k})$ are expanded in plane waves with expansion coefficients $c_o(\mathbf{G}, \mathbf{k})$

$$\phi_o(\mathbf{r}, \mathbf{k}) = \frac{1}{\sqrt{\Omega}} \sum_{\mathbf{G}} c_o(\mathbf{G}, \mathbf{k}) e^{i(\mathbf{G}+\mathbf{k})\cdot\mathbf{r}}. \quad (1.2.3)$$

The reciprocal-space sums are restricted to \mathbf{G} vectors with a kinetic energy $\frac{1}{2}|\mathbf{k} + \mathbf{G}|^2 \leq E_{cut}$. Real-space and reciprocal-space are converted via fast Fourier transforms, which allows to efficiently evaluate potential and kinetic energies as well as position and momentum operator derived expectation values. We work only in the Γ -point approximation, employing large enough unit cells in disordered systems. Therefore we drop the \mathbf{k} dependence in the following.

1.2.2 TOTAL ENERGIES

The total energy of the system is partitioned into kinetic, electro static, local pseudopotential, non-local pseudopotential and exchange-correlation energy contributions

$$E_{tot} = E_{kin} + E_{es} + E_{loc} + E_{nl} + E_{xc}. \quad (1.2.4)$$

The evaluation of the kinetic energy is conveniently done in reciprocal space

$$E_{kin} = \sum_o \sum_{\mathbf{G}} \frac{1}{2} f_o |\mathbf{G}|^2 |c_o(\mathbf{G})|^2, \quad (1.2.5)$$

with the occupation numbers f_o of the occupied KS orbitals. We use Ewald's method^{2,100} for the evaluation of the electro static energy of extended systems, introducing smeared nuclear core charges $n_c^\nu(\mathbf{r})$

$$n_{tot}(\mathbf{r}) = n(\mathbf{r}) + \sum_\nu n_c^\nu(\mathbf{r}) \quad \text{with} \quad n_c^\nu(\mathbf{r}) = -\frac{Z_\nu}{(R_c^\nu)^3} \pi^{-3/2} e^{-\left[(\mathbf{r}-\mathbf{R}^\nu)/R_c^\nu\right]^2}. \quad (1.2.6)$$

This gives the total electro static energy

$$E_{es} = 2\pi\Omega \sum_{\mathbf{G} \neq 0} \frac{|n_{tot}(\mathbf{G})|^2}{G^2} - \sum_\nu \frac{1}{\sqrt{2\pi}} \frac{Z_\nu^2}{R_c^\nu} + E_{ovrl} \quad (1.2.7)$$

$$E_{ovrl} = \sum'_{\nu, \nu'} \sum_{\mathbf{L}} \frac{Z_\nu Z_{\nu'}}{|\mathbf{R}^\nu - \mathbf{R}^{\nu'} - \mathbf{L}|} \operatorname{erfc} \left\{ \frac{|\mathbf{R}^\nu - \mathbf{R}^{\nu'} - \mathbf{L}|}{\sqrt{R_c^{\nu 2} + R_c^{\nu' 2}}} \right\}. \quad (1.2.8)$$

The advantages of the use of a plane wave basis come with the price that the representation of core electrons is very expensive. In order to further reduce the degrees of freedom and required basis set size, we treat the chemically more inert core electrons in the frozen core approximation and account for their presence by employing pseudopotentials.¹⁰⁰ We use norm-conserving non-local pseudopotentials in a separable form¹¹⁵⁻¹¹⁷

$$V_{psp}^\nu(\mathbf{r}, \mathbf{r}') = (V_{core}^\nu(\mathbf{r}) + \Delta V_{loc}^\nu(\mathbf{r})) \delta(\mathbf{r} - \mathbf{r}') + V_{nl}^\nu(\mathbf{r}, \mathbf{r}'), \quad (1.2.9)$$

with $\hat{V}_{nl}^\nu = \sum_l \sum_{m, m'} |p_{lm}^\nu\rangle w_{lmm'}^\nu \langle p_{lm'}^\nu|$ and the Hartree potential $V_{core}^\nu(\mathbf{r})$ of the Gaussian core charges $n_c^\nu(\mathbf{r})$. The local potential $\Delta V_{loc}^\nu(\mathbf{r})$ and the projectors $p_{lm}^\nu(\mathbf{r})$ are stored in reciprocal space for each atom species and are translated to the atomic positions with the structure factor $S_\nu(\mathbf{G}) = e^{-i\mathbf{G} \cdot \mathbf{R}^\nu}$ via

$$p_{lm}^\nu(\mathbf{r}) = \sum_{\mathbf{G}} p_{lm}(G) e^{i\mathbf{G} \cdot \mathbf{r}} S_\nu(\mathbf{G}) Y_{lm}(\tilde{\theta}, \tilde{\phi}), \quad (1.2.10)$$

with polar coordinates $\mathbf{G} = (G, \tilde{\theta}, \tilde{\phi})$. The projection on the wave function yields

$$F_{lm,o}^\nu = \frac{1}{\sqrt{\Omega}} \sum_{\mathbf{G}} p_{lm}^\nu(\mathbf{G}) S_\nu(\mathbf{G}) c_o^*(\mathbf{G}) \quad (1.2.11)$$

and provides simple expressions of the energy contributions of the pseudopotentials

$$E_{loc} = \sum_\nu \sum_{\mathbf{G}} \Delta V_{loc}^\nu(\mathbf{G}) S_\nu(\mathbf{G}) n^*(\mathbf{G}) \quad (1.2.12)$$

$$E_{nl} = \sum_o f_o \sum_\nu \sum_{lm \in \nu} F_{lm,o}^{\nu*} w_{lmm'}^\nu F_{lm',o}^\nu. \quad (1.2.13)$$

We employ generalized gradient corrected exchange correlation functionals. Their energy contribution can be expressed as

$$E_{xc} = \Omega \sum_{\mathbf{G}} \varepsilon_{xc}(\mathbf{G}) n^*(\mathbf{G}). \quad (1.2.14)$$

1.2.3 NUCLEAR GRADIENTS

We need the gradient of the total energy with respect to the nuclear positions for the calculation of forces during molecular dynamics simulations, structure optimizations or NDP calculations. The corresponding expressions are

$$\frac{\partial E_{loc}}{\partial R_\alpha^\nu} = -\Omega \sum_{\mathbf{G}} iG_\alpha \Delta V_{loc}^\nu S_\nu(\mathbf{G}) n^*(\mathbf{G}) \quad (1.2.15)$$

$$\frac{\partial E_{nl}}{\partial R_\alpha^\nu} = \sum_o f_o \sum_\nu \sum_{lm \in \nu} \left\{ F_{lm,o}^{\nu*} w_{lmm'}^\nu \frac{\partial F_{lm',o}^\nu}{\partial R_\alpha^\nu} + \frac{\partial F_{lm,o}^{\nu*}}{\partial R_\alpha^\nu} w_{lmm'}^\nu F_{lm',o}^\nu \right\} \quad (1.2.16)$$

$$\frac{\partial E_{es}}{\partial R_\alpha^\nu} = -\Omega \sum_{\mathbf{G} \neq 0} iG_\alpha \frac{n_{tot}^*(\mathbf{G})}{G^2} n_c^\nu(\mathbf{G}) S_\nu(\mathbf{G}) + \frac{\partial E_{ovrl}}{\partial R_\alpha^\nu}, \quad (1.2.17)$$

where the most complicated term is the derivative of the non-local pseudopotential projectors. The perturbation functional of a NDP of nucleus ν in direction α is

$$E_{\text{pert}}[\{\phi_o\}] = \frac{\partial E_{loc}}{\partial R_\alpha^\nu} + \frac{\partial E_{nl}}{\partial R_\alpha^\nu} + \frac{\partial E_{es}}{\partial R_\alpha^\nu}. \quad (1.2.18)$$

One advantage of the use of a plane wave basis is the independence of the basis on the nuclear positions. There are no Pulay forces¹¹⁸ in the expressions of the nuclear gradient, which greatly simplifies the perturbation calculations.

1.2.4 NON-LOCAL PSEUDOPOTENTIALS AND GAUGE INVARIANCE

The coupling of non-local pseudopotentials to external electro-magnetic fields requires special attention in order to achieve gauge invariant expressions of the Hamiltonian and eigenvalue spectrum of the system. If working with magnetic fields, the gauge including projector augmented waves (GIPAW) correction assures this gauge invariance.^{119,120} An alternative approach is the ICL method,^{121,122} which is used in this work.

The GIPAW method bases on the projector augmented wave method,¹²³ which introduces a linear transformation between the Hilbert spaces of the all-electron wave functions and of the pseudo wave functions. In order to obtain a gauge invariant Hamiltonian and eigenvalue spectrum, the non-local pseudopotentials have to be corrected

$$\langle \mathbf{r} | \hat{V}_{nl}^{\nu, \mathbf{A}} | \mathbf{r}' \rangle = \hat{V}_{nl}^\nu(\mathbf{r}, \mathbf{r}') \exp \left\{ -i \frac{e}{\hbar c} \int_{\mathbf{r}' \rightarrow \mathbf{R}^\nu \rightarrow \mathbf{r}} \mathbf{A}(\mathbf{r}'', t) \cdot d\mathbf{r}'' \right\}, \quad (1.2.19)$$

where the integration path goes over the atomic position \mathbf{R}^ν of the pseudopotential.

The ICL method does not rely on the long wavelength limit, which is assumed in the GIPAW method. At variance with the GIPAW, the integration is along the direct connection of the two points

$$\langle \mathbf{r} | \hat{V}_{nl}^{\nu, \mathbf{A}} | \mathbf{r}' \rangle = \hat{V}_{nl}^\nu(\mathbf{r}, \mathbf{r}') \exp \left\{ -i \frac{e}{\hbar c} \int_{\mathbf{r}'}^{\mathbf{r}} \mathbf{A}(\mathbf{r}'', t) \cdot d\mathbf{r}'' \right\}. \quad (1.2.20)$$

This choice also guarantees gauge-invariance of the eigenenergies but does not match all-electron and pseudo eigenenergies.¹²⁰ In our case, the correction is not due to external electro-magnetic vector potentials but due to nuclear velocities, as discussed in section 3.4.

1.2.5 FINITE TEMPERATURE MOLECULAR DYNAMICS

The parameters controlled in experimental measurements usually are the chemical potential, the temperature and the pressure (μPT). However, Hamiltonian mechanics conserves the energy and particle number, i.e. its statistics follow the microcanonical ensemble (NVE). It is possible to do molecular dynamics simulations in different ensembles by using extended Lagrangian techniques.⁹⁴ In these approaches, the Lagrangian of the system is extended by additional fictitious degrees of freedom that couple to variables of the original Hamiltonian. In case of the canonical ensemble (NVT), the additional degrees of freedom are coupled to the momenta of the particles. The extended systems no longer follow Hamiltonian dynamics, but their dynamics yield the proper ensemble averages.

We rely on the fact that the canonical ensemble (NVT) is a good approximation to the experimental conditions if the experimentally studied systems are large. This is the case in the liquid or condensed phase, which we are interested in. To generate AIMD in the canonical ensemble, we employ Nosé-Hover thermostat chains^{2,124,125}

$$M_\nu \ddot{\mathbf{R}}_\nu = -\nabla_\nu \epsilon_0(\mathbf{R}) - M_\nu \dot{\xi}_1 \dot{\mathbf{R}}_\nu \quad (1.2.21)$$

$$Q_1^n \ddot{\xi}_1 = \left[\sum_\nu M_\nu \dot{\mathbf{R}}_\nu^2 - g k_B T \right] - Q_1^n \dot{\xi}_1 \dot{\xi}_2 \quad (1.2.22)$$

$$Q_k^n \ddot{\xi}_k = \left[Q_{k-1}^n \dot{\xi}_{k-1}^2 - k_B T \right] - Q_k^n \dot{\xi}_k \dot{\xi}_{k+1} (1 - \delta_{k,K}) \quad \text{where } k = 2, \dots, K, \quad (1.2.23)$$

which couple additional fictitious degrees of freedom to the momenta of the particles. However, the additional couplings change the dynamics of the system. This violates the assumptions of linear response theory (c.p. section A.2), which assumes the system to be in thermal equilibrium and to follow Hamiltonian dynamics at the same time.

In order to combine both aspects, we use the representation of the canonical ensemble as a set of microcanonical ensembles that yields the correct canonical ensemble averages.^{126,127} Computationally, this is realized by sampling statistically independent initial conditions from a thermostated molecular dynamics, which in turn are propagated independently in the microcanonical ensemble.

1.3 POSITION OPERATOR AND PERIODIC BOUNDARY CONDITIONS

One of the central problems dealt with in this work is the ill-definition of the position operator when periodic boundary conditions are used. In the Schrödinger representation, the position operator acts on the bound eigenstates of a finite system simply by multiplication with the real space coordinate.⁵⁷ However, under periodic boundary conditions, the position operator is ill-defined since its operation on a wave function $\mathbf{r}\varphi(\mathbf{r})$ is no longer periodic and hence not part of the same Hilbert space as $\varphi(\mathbf{r})$. The simple application of the periodic sawtooth position operator yields unphysical results due to the jump of the operator at the cell boundary.

Directly connected to this problem is the choice of a gauge of the magnetization or magnetic dipole moment under periodic boundary conditions. Both aspects have been addressed in different ways via the modern theories of polarization and magnetization, presented in the following. Using the Berry phase^{128–130} position operator, it is possible to define maximally localized Wannier orbitals,^{111,112} which are used in this work.

1.3.1 MODERN THEORY OF POLARIZATION

The modern theory of (microscopic) polarization^{57,129–133} (MTP) provides a way to express the microscopic polarization in terms of periodic bulk properties. It starts from the observation that experiments actually do not measure the polarization itself but the changes in polarization. This means that the total polarization of a periodic system depends on the choice of the unit cell, whereas the change of polarization does not (as illustrated in fig. 1.2).

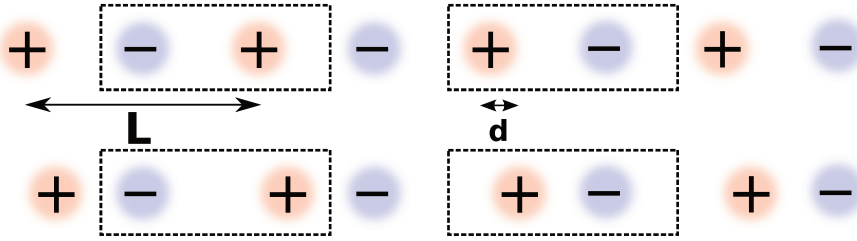


Figure 1.2: Illustrations of polarization and polarization changes. In the upper panel, the polarization of the unit cell of this one dimensional chain depends on the choice of the unit cell. A displacement of the charges changes the polarization (lower panel) and the change of the polarization is the same in both cells.

The MTP employs a geometric phase¹²⁸ to calculate the expectation value of a periodic operator that coincides with the position operator in the limit of large unit cells. This genuine many-body operator has the form

$$\langle \hat{r}_j \rangle = \frac{L_j}{2\pi} \text{Im} \ln \langle \varphi_0 | \exp \left\{ i \frac{2\pi}{L_j} \hat{r}_j \right\} | \varphi_0 \rangle \quad (1.3.1)$$

and, if evaluated in the Γ -point approximation in terms of bulk Bloch orbitals, reads

$$\langle \hat{r}_j \rangle = \lim_{L_j \rightarrow \infty} \frac{L_j}{2\pi} \text{Im} \ln \det \mathbf{S}^j \quad \text{with} \quad S_{o,o'}^j = \int_0^{L_j} \phi_o^*(r_j) \exp \left\{ i \frac{2\pi}{L_j} \hat{r}_j \right\} \phi_{o'}(r_j) dr_j. \quad (1.3.2)$$

This position operator is only defined modulo jumps of $2\pi/L_j$. In polarization differences, these “polarization quanta” have to be taken into account.

1.3.2 MAXIMALLY LOCALIZED WANNIER ORBITALS

The definition of the position operator under periodic boundary conditions can be used to adapt the concept of localized molecular orbitals to the condensed phase.^{134,135} The maximally localized Wannier orbitals^{III,112} (MLWOs) w_o are unitary transformations of Bloch orbitals $\phi_{o'}$ that minimize the spread functional S

$$|w_o\rangle = \sum_{o'} U_{o'o}^{loc} |\phi_{o'}\rangle \quad \text{with} \quad S = \sum_o \left(\langle \hat{r}^2 \rangle_o - \langle \hat{r} \rangle_o^2 \right). \quad (1.3.3)$$

We omit unnecessary technical details here and work directly in the Γ -point approximation.^{2,136} The minimization of the spread functional is equivalent to maximizing the functional

$$\Omega_s = \sum_j \sum_o |r_{j,oo}|^2 \quad \text{with} \quad r_{j,oo'} = \langle \phi_o | e^{-i\frac{2\pi}{L_j} \hat{r}_j} | \phi_{o'} \rangle. \quad (1.3.4)$$

The unitary transformation $\mathbf{U} = \exp[-\mathbf{A}]$ is parametrized as the exponential of an anti-symmetric matrix \mathbf{A} that is obtained via steepest decent optimization in the direction of the gradient

$$\frac{\partial \Omega_s}{\partial A_{oo'}} = 0. \quad (1.3.5)$$

In insulating systems, the MLWOs decay exponentially.¹³⁷ If working in a large enough super cell, which

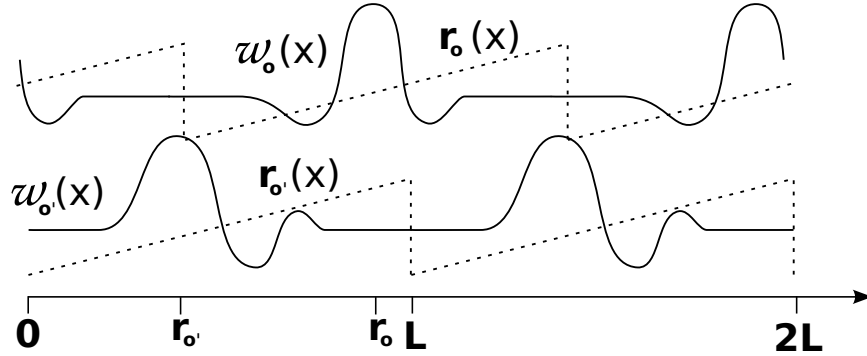


Figure 1.3: The position operator is evaluated in a different reference system for each state, i.e. with the corresponding Wannier center \mathbf{r}_o as origin. The jump of the sawtooth position operator occurs in a region where the orbitals are practically zero.

is anyway required in the Γ -point approximation, the MLWOs are practically zero in some region of the unit cell. This property can be used to center the sawtooth position operator under periodic boundary conditions at the center of charge of the MLWO, the Wannier center $\mathbf{r}_o \equiv \sum_j \hat{e}_j r_{joo}$, such that the jump of the sawtooth position operator occurs in a region where the orbitals are practically zero (c.p. figure 1.3). This technique has been applied to the calculation of chemical shifts of the nuclear magnetic resonance shielding in the condensed phase^{14,138} and is used in this work for the calculation of magnetic dipole moments in the condensed phase.¹³⁹

1.3.3 MODERN THEORY OF MAGNETIZATION

The ill-definition of the position operator under periodic boundary condition also leads to an ill-definition of angular momentum and hence the magnetic moment operator. This poses two related, yet distinct prob-

lems. First, the operator evaluation itself and secondly the calculation of the total magnetization of the sample. The first problem of the operator evaluation can be resolved employing a distributed origin gauge, as described in the preceding section. However, the overall magnetization cannot be straightforwardly defined with respect to a common origin.

This second issue is addressed by the modern theory of magnetization^{132,140,141} (MTM), which expresses the total magnetization of an extended sample in terms of properties of the bulk MLWOs. It turns out that the total magnetization is given by the sum of two contributions

$$\mathbf{M} = -\frac{e}{2V_C} \left[\sum_{\mathbf{L}} \sum_i \langle w_i(\mathbf{L}) | (\hat{\mathbf{r}} - \mathbf{L}) \times \hat{\mathbf{v}} | w_i(\mathbf{L}) \rangle + \mathbf{L} \times \langle w_i(\mathbf{L}) | \hat{\mathbf{v}} | w_i(\mathbf{L}) \rangle \right]. \quad (1.3.6)$$

The first term is due to local currents (LC) and defined with respect to a common origin in the unit cell $\mathbf{0}$

$$\mathbf{M}_{LC} = -\frac{e}{2V_C} \sum_i \langle w_i(\mathbf{0}) | (\hat{\mathbf{r}} - \mathbf{0}) \times \hat{\mathbf{v}} | w_i(\mathbf{0}) \rangle. \quad (1.3.7)$$

The second term stems from an itinerary current (IC) that cancels within the bulk but yields a significant surface current

$$\mathbf{M}_{IC} = -\frac{e}{2V_C} \sum_{\mathbf{L}} \sum_i \mathbf{L} \times \langle w_i(\mathbf{L}) | \hat{\mathbf{v}} | w_i(\mathbf{L}) \rangle. \quad (1.3.8)$$

The first term can be evaluated in a distributed origin gauge with subsequent translation to the common origin, whereas the second term has to be recast in terms of inter cell currents. This is achieved by evaluating the current operator between different MLWOs

$$\langle \hat{\mathbf{v}} \rangle_{i0,j\mathbf{L}} = 2\text{Im} \langle w_i(0) | \hat{\mathbf{r}} | w_j(\mathbf{L}) \rangle \langle w_j(\mathbf{L}) | \hat{\mathcal{H}} | w_i(0) \rangle. \quad (1.3.9)$$

The total sample is partitioned into a bulk part B and a surface part S and the currents between MLWOs inside $i \in B$ and outside $j \in S$ are calculated. Since in the thermodynamic limit, the surface can also be taken in the bulk, this formalism requires bulk properties only. The final expression of the itinerary current contribution is

$$\mathbf{M}_{IC} = -\frac{e}{4V_C} \sum_{\mathbf{L}} \sum_{ij} \mathbf{L} \times \langle \hat{\mathbf{v}} \rangle_{i0,j\mathbf{L}}. \quad (1.3.10)$$

1.4 VIBRATIONAL CIRCULAR DICHROISM

Having introduced the necessary theoretical concepts, we turn to the first intended application. Vibrational circular dichroism (VCD) is a form of optical activity. In the following discussion, we review how VCD can be described mathematically from a macroscopic perspective, i.e. in terms of macroscopically accessible quantities like electro-magnetic fields (1.4.1). We then turn to its microscopic origins on the molecular level (1.4.2), followed by the theory of dynamical VCD spectra (1.4.3) and a review of the current state of the art of ab-initio calculations of VCD (1.4.4).

1.4.1 MACROSCOPIC PERSPECTIVE

Macroscopically, optical activity refers to the different interaction of chiral substances with electro-magnetic radiation via circular birefringence (CB) and circular dichroism (CD).¹⁴² CB denotes the rotation of the polarization of linearly polarized light and CD is the difference in differential absorbance of circularly polarized light. Both effects are described by different refractive indices for the different handedness of the radiation and are related to their real part (CB) and imaginary part (CD) respectively. This work focuses on vibrational CD (VCD), i.e. CD in the infrared region of the electro-magnetic spectrum, where the energy matches the transition energies of vibrational excitations of molecules. Throughout this work we assume that the strength of the external fields is weak compared to the intra molecular interactions such that the interaction can be described by the linear response of the system to the applied external fields.

ISOTROPIC CHIRAL MEDIA

In this work, we focus on the infrared radiation-matter interaction of chiral molecules in the gas or liquid phase, both at ambient conditions. These kind of systems are homogeneous (no spatial dispersion) and isotropic (no preferential directions). Due to the presence of chiral molecules, the medium is chiral, and we are interested in the temporal dispersion of the interaction, i.e. how the interaction changes with the frequency of the electro-magnetic wave. We limit ourselves to dielectric materials but keep track of the magnetic terms in the derivation. In other words, we want to describe homogeneous isotropic chiral dielectric-magnetic media with temporal dispersion.¹⁴³

MAXWELL'S EQUATIONS AND CONSTITUTIVE RELATIONS

We start with Maxwell's equations in absence of free charges and currents (in cgs units)⁷³

$$\nabla \cdot \mathbf{D} = 0 \quad \nabla \times \mathbf{E} = -\frac{1}{c} \frac{\partial \mathbf{B}}{\partial t} \quad \nabla \cdot \mathbf{B} = 0 \quad \nabla \times \mathbf{H} = \frac{1}{c} \frac{\partial \mathbf{D}}{\partial t}, \quad (1.4.1)$$

with the electric field strength $\mathbf{E}(\mathbf{r}, t)$, the dielectric displacement $\mathbf{D}(\mathbf{r}, t)$, the magnetic flux density $\mathbf{B}(\mathbf{r}, t)$, the magnetic field strength $\mathbf{H}(\mathbf{r}, t)$ and the speed of light c . For brevity, we omit the spatial dependence of the fields if not explicitly necessary. We have to choose a set of constitutive relations to describe linear homogeneous isotropic chiral dielectric-magnetic media with temporal dispersion.¹⁴³ The isotropy reduces the coupling matrices to scalar coefficients. Following the arguments of Silverman,¹⁴⁴ we choose the sym-

metrized constitutive relations of Condon¹⁴⁵

$$\tilde{\mathbf{P}}(\omega) = \tilde{\chi}_e(\omega)\tilde{\mathbf{E}}(\omega) + \tilde{\chi}_{em}(\omega)\tilde{\mathbf{H}}(\omega) \quad \text{and} \quad \tilde{\mathbf{M}}(\omega) = \tilde{\chi}_m(\omega)\tilde{\mathbf{H}}(\omega) + \tilde{\chi}_{me}(\omega)\tilde{\mathbf{E}}(\omega). \quad (1.4.2)$$

Here, $\tilde{\chi}_e$ is the electric susceptibility, $\tilde{\chi}_m$ the magnetic susceptibility and $\tilde{\chi}_{em}$ and $\tilde{\chi}_{me}$ the magnetoelectric cross-susceptibilities. We work in the frequency domain (ω) to express the convolutions in time domain as simple products. In the following, complex numbers are denoted by a tilde and the explicit notation of the frequency dependence is dropped. In contrast to the Drude-Born-Fedorov¹⁴³ relations, the choice in eq. (1.4.2) decouples permittivity and permeability from the magnetoelectric cross-susceptibilities. Alternative choices are discussed in the literature.^{143,146} We can relate the cross-susceptibilities by imposing Lorentz-reciprocity¹⁴⁷ $\tilde{\chi}_{em} = -\tilde{\chi}_{me}$, which yields

$$\tilde{\mathbf{D}} = \tilde{\mathbf{E}} + 4\pi\tilde{\mathbf{P}} = \tilde{\epsilon}\tilde{\mathbf{E}} + i\tilde{\gamma}\tilde{\mathbf{H}} \quad \text{and} \quad \tilde{\mathbf{B}} = \tilde{\mathbf{H}} + 4\pi\tilde{\mathbf{M}} = \tilde{\mu}\tilde{\mathbf{H}} - i\tilde{\gamma}\tilde{\mathbf{E}}, \quad (1.4.3)$$

with the permittivity $\tilde{\epsilon}$, permeability $\tilde{\mu}$ and chiral index $\tilde{\gamma}$ defined as follows:

$$\tilde{\epsilon} = (1 + 4\pi\tilde{\chi}_e), \quad \tilde{\mu} = (1 + 4\pi\tilde{\chi}_m), \quad \tilde{\gamma} = 4\pi i\tilde{\chi}_{me}. \quad (1.4.4)$$

CHIRALITY AND SYMMETRIES

In order to see how the introduced $\tilde{\chi}_{me}$ are related to the chirality of the system, we recall that Maxwell's equations (1.4.1) are form-invariant under⁷³

- a) proper rotations b) spatial inversion (SI) $\mathbf{r} \rightarrow -\mathbf{r}$ c) time reversal (TR) $t \rightarrow -t$.

The involved physical quantities can be characterized by their transformation properties. A polar/axial vector transforms odd/even under SI. The projection of an axial vector on a polar vector is an example of a pseudo scalar that also changes sign under SI. Furthermore we have to differentiate between even and odd functions under TR. An overview of the transformation properties is given in table 6.1 of ref.⁷³

The constitutive relations in eq. (1.4.2) have to transform consistently as well

$$\tilde{\mathbf{P}} = \tilde{\chi}_e\tilde{\mathbf{E}} + \tilde{\chi}_{em}\tilde{\mathbf{H}} \quad \tilde{\mathbf{M}} = \tilde{\chi}_m\tilde{\mathbf{H}} + \tilde{\chi}_{me}\tilde{\mathbf{E}}. \quad (1.4.5)$$

Since $\tilde{\mathbf{P}}$ and $\tilde{\mathbf{E}}$ transform odd under SI and even under TR, it follows that $\tilde{\chi}_e$ has to transform even under SI and TR. From similar arguments we see that $\tilde{\chi}_m$ has to transform even under SI and TR. Since $\tilde{\mathbf{H}}$ transforms even under SI and odd under TR, we find $\tilde{\chi}_{em}$ to behave odd under SI and TR. Similarly we find $\tilde{\chi}_{me}$ to transform odd under SI and TR. $\tilde{\chi}_{em}$ and $\tilde{\chi}_{me}$ are hence pseudo scalar quantities. They involve transition dipole moments of a polar and an axial vector, the electric current dipole and magnetic dipole moment. For electronic states of a definite parity, it is not possible to simultaneously have non-vanishing transition moments of a polar and an axial vector. However, if the parity is broken by the chirality, a non-vanishing contribution arises.⁷³

EIGENMODES OF THE ELECTRO-MAGNETIC FIELDS

With the chosen constitutive relations, we can determine the eigenmodes of the electro-magnetic fields. By eliminating $\tilde{\mathbf{B}}$ and $\tilde{\mathbf{D}}$ from eqs. (1.4.1) and (1.4.3), we obtain

$$\nabla \times \begin{pmatrix} \tilde{\mathbf{E}} \\ \tilde{\mathbf{H}} \end{pmatrix} = \underline{\underline{\mathbf{K}}} \begin{pmatrix} \tilde{\mathbf{E}} \\ \tilde{\mathbf{H}} \end{pmatrix} \quad \text{and} \quad \nabla \cdot \begin{pmatrix} \tilde{\mathbf{E}} \\ \tilde{\mathbf{H}} \end{pmatrix} = \begin{pmatrix} 0 \\ 0 \end{pmatrix} \quad \text{with} \quad \underline{\underline{\mathbf{K}}} = -\frac{i\omega}{c} \begin{pmatrix} i\tilde{\gamma}\underline{\underline{I}} & -\tilde{\mu}\underline{\underline{I}} \\ \tilde{\epsilon}\underline{\underline{I}} & i\tilde{\gamma}\underline{\underline{I}} \end{pmatrix} \quad (1.4.6)$$

Diagonalization of $\tilde{\mathbf{K}}$ yields eigenvalues $\tilde{\mathbf{k}}_{\pm} = \frac{\omega}{c}(\tilde{n} \pm \tilde{\gamma})$, with the complex refractive index $\tilde{n}^2 = \tilde{\epsilon}\tilde{\mu}$. The fields corresponding to the eigenmodes of the medium satisfy $\tilde{\mathbf{H}}_{\pm} = \mp i \frac{\tilde{n}}{\mu} \tilde{\mathbf{E}}_{\pm}$. Since they fulfill Helmholtz's equation $(\nabla^2 + \tilde{\mathbf{k}}_{\pm}^2)\tilde{\mathbf{E}}_{\pm} = 0$, we can identify them as circularly polarized plane waves with wave vector $\tilde{\mathbf{k}}_{\pm}$. We choose the propagation direction as ϵ_3 , with $\tilde{\mathbf{k}}_{\pm} = \tilde{k}_{\pm}\epsilon_3$, and obtain the electric field solution that is given in eq. (1.4.9).

CIRCULAR AND ELLIPTICAL POLARIZATION

A monochromatic electro-magnetic wave propagating in ϵ_3 -direction, with $\epsilon_1 \times \epsilon_2 = \epsilon_3$, can be described by⁷³

$$\mathbf{E}(\mathbf{r}, t) = E_1(\mathbf{r}, t)\epsilon_1 + E_2(\mathbf{r}, t)\epsilon_2. \quad (1.4.7)$$

Right (−) and left (+) elliptical polarization is given at a phase-difference of $\frac{\pi}{2}$. The convention of right circular polarization is that, when the radiation is viewed propagating toward an observer, the polarization vector rotates clockwise.^{17,148} Circular polarization is obtained at the special case of equal amplitudes. To introduce optical activity, we use a complex index of refraction that differs for left and right circularly polarized light, rewriting $\tilde{n}_{\pm} = \tilde{n} \pm \tilde{\gamma}$ as

$$\tilde{n}_{\pm} = n'_{\pm} + i n''_{\pm} = n' \pm \frac{1}{2}\Delta n' + i n'' \pm \frac{i}{2}\Delta n'', \quad (1.4.8)$$

where the real part n'_{\pm} is related to the dispersion and the complex part n''_{\pm} to the absorbance of the wave. A circularly polarized wave is described by

$$\mathbf{E}_{\pm}(\mathbf{r}, t) = E_0 \text{Re} \left[e^{i(\tilde{k}_{\pm} z - \omega t)} \tilde{\epsilon}_{\pm} \right] = \frac{E_{\pm}(z)}{\sqrt{2}} \left[\epsilon_1 \cos(k'_{\pm} z - \omega t) \mp \epsilon_2 \sin(k'_{\pm} z - \omega t) \right], \quad (1.4.9)$$

with wave vector $\tilde{\mathbf{k}}_{\pm} = \frac{\omega \tilde{n}_{\pm}}{c} \epsilon_3$, polarization vectors $\tilde{\epsilon}_{\pm} = \frac{1}{\sqrt{2}}(\epsilon_1 \pm i \epsilon_2)$ and amplitude $E_{\pm}(z) = \frac{A_0 \omega}{c} e^{-\frac{1}{2}\alpha_{\pm} z}$. The attenuation of the amplitude $E_{\pm}(z)$ is governed by the absorption coefficient α_{\pm} , according to the Lambert-Beer law $\alpha_{\pm} = \frac{2\omega}{c} n''_{\pm}$.⁷³ To illustrate the relation of CB and CD, we decompose a linearly polarized wave (polarization in ϵ_1 -direction) into two circularly polarized waves and obtain

$$\mathbf{E}(\mathbf{r}, t) = \frac{E_0}{\sqrt{2}} e^{-\frac{1}{2}\alpha z} \mathcal{R}(\theta) \text{Re} \left[(\cosh(\eta) \epsilon_1 - i \sinh(\eta) \epsilon_2) e^{i \frac{\omega n' z}{c}} e^{-i \omega t} \right], \quad (1.4.10)$$

in terms of the mean absorptivity α , the azimuth θ and the ellipticity η

$$\alpha = \frac{2\omega}{c} n'', \quad \theta = \frac{\omega}{2c} \Delta n' z, \quad \eta = \frac{\omega}{2c} \Delta n'' z. \quad (1.4.11)$$

Eq. (1.4.10) is an elliptically polarized wave (c.p. fig. 1.4) with its major axis rotated by θ in the ϵ_1, ϵ_2 -plane (clockwise at $\theta > 0$). $\mathcal{R}(\theta)$ is the rotation matrix of rotations in the ϵ_1, ϵ_2 -plane. At $\eta > 0$ follows a right elliptical polarization.¹⁴⁸ We can see from eq. (1.4.11) how the different parts of the refractive index effect the wave propagation and how VCD is measured experimentally

$$\tanh(\eta) = -\frac{|\mathbf{E}_+|^2 - |\mathbf{E}_-|^2}{|\mathbf{E}_+|^2 + |\mathbf{E}_-|^2} \approx \frac{\Delta \epsilon z}{4}. \quad (1.4.12)$$

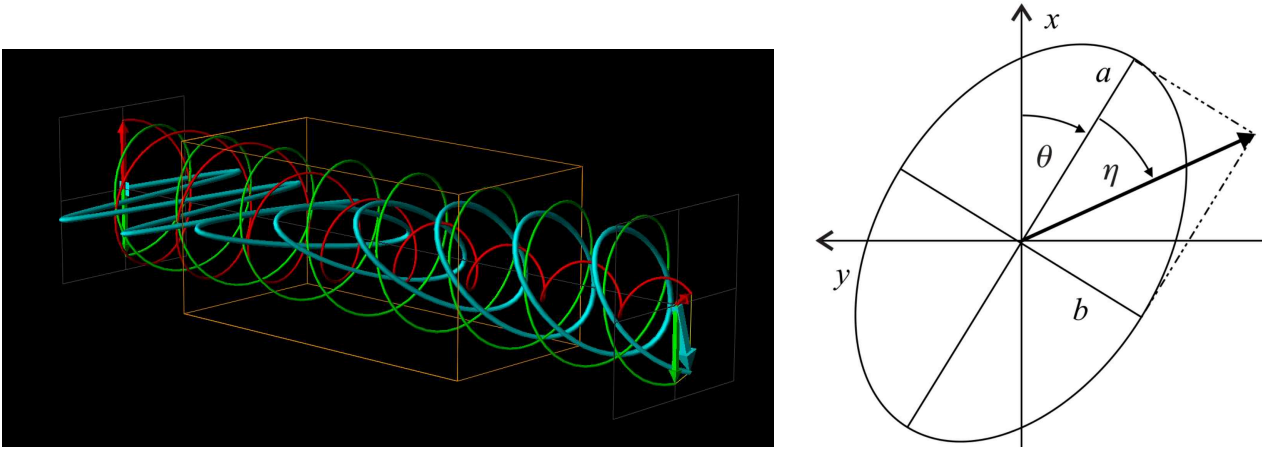


Figure 1.4: Left: Illustration of CB and CD in a medium (yellow box). The originally linearly polarized wave obtains an ellipticity due to the stronger attenuation of the red wave. The difference in propagation velocity leads to a rotation of the axes of the ellipse. Right: Elliptical polarization. The ellipticity of the polarization is defined as the ratio of the minor (b) to the major amplitude (a), with the convention that the ellipticity is positive for a right elliptical polarization.

1.4.2 MICROSCOPIC PERSPECTIVE

Microscopically, optical activity of chiral substances emerges due to the properties of their constituent molecules. To describe this, we consider a system in thermal equilibrium described by the density matrix of the canonical ensemble.^{126,127} At ambient conditions, most of the constituent molecules are in their electronic and vibrational ground states. For the radiation-matter interaction, we use a classical description of the external fields, interacting with the molecule described as a quantum system.¹⁴⁸ Since we are interested in the infrared spectral region, we can apply the long wavelength limit and expand the interaction Hamiltonian to first order in the wave vector.^{149–151} The interaction Hamiltonian can be equivalently chosen in the “position” or the “velocity” form.¹⁴⁸ In an isotropic system, the relevant part of perturbation Hamiltonian in the position form reads

$$\hat{\mathcal{H}}^{(1)}(t) = -\hat{\boldsymbol{\mu}} \cdot \mathbf{E}(t) - \hat{\mathbf{m}} \cdot \mathbf{H}(t). \quad (1.4.13)$$

The electric quadrupolar moment does not contribute to the vibrational optical activity in the isotropic average.¹⁴⁹ The electric $\hat{\boldsymbol{\mu}}$ and magnetic $\hat{\mathbf{m}}$ dipole moment operators are defined as

$$\hat{\boldsymbol{\mu}} = \hat{\boldsymbol{\mu}}^e + \hat{\boldsymbol{\mu}}^n = -\sum_{i=1}^{N_e} e\hat{\mathbf{r}}_i + \sum_{\nu=1}^{N_n} Z_{\nu}e\hat{\mathbf{R}}_{\nu} \quad (1.4.14)$$

$$\hat{\mathbf{m}} = \hat{\mathbf{m}}^e + \hat{\mathbf{m}}^n = -\sum_{i=1}^{N_e} \frac{e}{2mc} \hat{\mathbf{r}}_i \times \hat{\mathbf{p}}_i + \sum_{\nu=1}^{N_n} \frac{Z_{\nu}e}{2M_{\nu}c} \hat{\mathbf{R}}_{\nu} \times \hat{\mathbf{P}}_{\nu}. \quad (1.4.15)$$

For later use, we already introduce the current dipole moment $\hat{\boldsymbol{\mu}}$

$$\hat{\boldsymbol{\mu}} = \hat{\boldsymbol{\mu}}^e + \hat{\boldsymbol{\mu}}^n = -\sum_{i=1}^{N_e} \frac{e}{m} \hat{\mathbf{p}}_i + \sum_{\nu=1}^{N_n} \frac{Z_{\nu}e}{M_{\nu}} \hat{\mathbf{P}}_{\nu}. \quad (1.4.16)$$

Here, e is the electronic charge, $Z_{\nu}e$ is the nuclear charge, m and M_{ν} are the electronic and nuclear masses and c is the speed of light. The position and momentum operators of the electronic subsystem are indicated as $\hat{\mathbf{r}}_i$ and $\hat{\mathbf{p}}_i$, respectively, and similar symbols are used for the nuclear operators, $\hat{\mathbf{R}}_{\nu}$ and $\hat{\mathbf{P}}_{\nu}$.

Using Fermi's golden rule, we can derive the leading term of the infrared absorption coefficient $\alpha(\omega)$ at frequency ω as^{41, 42, 48}

$$\alpha(\omega) = F(\omega)(1 - e^{-\beta\hbar\omega})I(\omega), \quad (1.4.17)$$

with a prefactor $F(\omega) = \frac{4\pi^2\omega}{3V\hbar cn'(\omega)}$ and a line shape function $I(\omega)$. Here, $\beta = (k_B T)^{-1}$ is the inverse temperature, k_B Boltzmann's constant, \hbar the reduced Planck constant, V the volume of the sample, c the speed of light and $n'(\omega)$ the frequency dependent real part of the refractive index.

The line shape function can be expressed in the Schrödinger picture (first equality) or in the Heisenberg picture (second equality)

$$I(\omega) = \sum_{f,i} \rho_i D_{if} \delta(\omega_{fi} - \omega) = \frac{1}{2\pi} \int_{-\infty}^{\infty} dt e^{-i\omega t} \langle \hat{\boldsymbol{\mu}}(0) \cdot \hat{\boldsymbol{\mu}}(t) \rangle. \quad (1.4.18)$$

Here, we have introduced the dipole strength $D_{if} = \left| \langle \Psi_f | \hat{\boldsymbol{\mu}} | \Psi_i \rangle \right|^2$ as the squared absolute value of the electric transition dipole moment between an initial and final state (i and f respectively) and the probability of occupation of the initial states ρ_i . In the second equality, we have used the Fourier transform of the equilibrium auto-correlation function of the electric dipole moment $\hat{\boldsymbol{\mu}}$.

The expressions of VCD in isotropic systems are very similar^{150, 151}

$$\Delta\alpha(\omega) = F(\omega)(1 - e^{-\beta\hbar\omega})\Delta I(\omega), \quad (1.4.19)$$

with the line shape function $\Delta I(\omega)$, in which the magnetic dipole moment $\hat{\mathbf{m}}$ enters

$$\Delta I(\omega) = 4 \sum_{f,i} \rho_i R_{if} \delta(\omega_{fi} - \omega) = \frac{4}{2\pi} \text{Im} \left[\int_{-\infty}^{\infty} dt e^{-i\omega t} \langle \hat{\boldsymbol{\mu}}(0) \cdot \hat{\mathbf{m}}(t) \rangle \right]. \quad (1.4.20)$$

In the Schrödinger picture, we find Rosenfeld's¹⁵² rotational strength

$$R_{if} = \text{Im} \left[\langle \Psi_i | \hat{\boldsymbol{\mu}} | \Psi_f \rangle \cdot \langle \Psi_f | \hat{\mathbf{m}} | \Psi_i \rangle \right] \quad (1.4.21)$$

and in the Heisenberg picture the Fourier transform of the equilibrium cross-correlation function of the electric and magnetic dipole moments.

The established approach to evaluate eqs. (1.4.18) and (1.4.20) is to invoke the double harmonic approximation to calculate the dipole D_{if} or rotational R_{if} strengths.¹⁷ In this work, we derive the time correlation function form of VCD first and subsequently recover the established results of the double harmonic approximations in section A.3.

1.4.3 TIME CORRELATION FUNCTION SPECTRA

The time correlation function (TCF) formalism relies on the evaluation of the time evolution of the corresponding operators. In a generalized notation we consider two operators \hat{A} and \hat{B} with vanishing equilibrium expectation values and their exact quantum TCF

$$C_{\hat{A}\hat{B}}(t) = \langle \hat{A}(0) \hat{B}(t) \rangle. \quad (1.4.22)$$

The TCF-based evaluation of vibrational spectra is possible in different approximations to the TCF.⁴⁸ We resort to AIMD with classical nuclei evolving on the quantum potential energy surface of the electronic degrees of freedom. This approach only provides the classical phase space evolution of the nuclear degrees of freedom, along which the required dipole moments can be calculated. The evaluation of the fully quantum TCF is therefore not possible. Instead, we approximate the exact quantum TCF by a classical one, scaled by a quantum correction factor to fulfill the detailed-balance condition.⁴⁸

It turns out that there is one particular transformation of the quantum TCF that naturally yields a consistent prefactor if approximated classically. This is the Kubo transformed TCF, which is used in its classical limit for IRA and VCD. The Kubo¹⁵³ transformed quantum TCF involves an integration in imaginary time

$$C_{\hat{A}\hat{B}}^K(t) = \left\langle \frac{1}{\beta} \int_0^\beta d\lambda \hat{A}(0) \hat{B}(t + i\hbar\lambda) \right\rangle \quad (1.4.23)$$

and by Fourier transform relates to the exact line shape function as

$$I_{\hat{A}\hat{B}}(\omega) = \frac{\beta\hbar\omega}{1 - e^{-\beta\hbar\omega}} \frac{1}{2\pi} \int_{-\infty}^{\infty} dt e^{-i\omega t} C_{\hat{A}\hat{B}}^K(t). \quad (1.4.24)$$

We approximate⁴⁸ the exact Kubo TCF $C_{\hat{A}\hat{B}}^K(t)$ by the classical TCF $C_{AB}^{cl}(t)$

$$C_{\hat{A}\hat{B}}^K(t) \approx C_{AB}^{cl}(t) = \langle A(0)B(t) \rangle \quad (1.4.25)$$

and obtain for IRA and VCD

$$\alpha(\omega) = F(\omega) \frac{\beta\hbar\omega}{2\pi} \int_{-\infty}^{\infty} dt e^{-i\omega t} \langle \boldsymbol{\mu}(0) \cdot \boldsymbol{\mu}(t) \rangle \quad (1.4.26)$$

$$\Delta\alpha(\omega) = F(\omega) \frac{4\beta\hbar\omega}{2\pi} \text{Im} \left[\int_{-\infty}^{\infty} dt e^{-i\omega t} \langle \boldsymbol{\mu}(0) \cdot \mathbf{m}(t) \rangle \right] \quad (1.4.27)$$

This “position form” is particularly useful if one only is interested in the IRA since eq. (1.4.26) has the advantage to contain only the electric dipole moments. In case of VCD, the evaluation of eq. (1.4.27) requires the additional knowledge of the magnetic dipole moment, which is not accessible in the BO scheme since it requires information on the electronic current density. In this work, we present a new perturbative scheme that allows to efficiently calculate the electronic currents and hence magnetic dipole moments along a molecular dynamics simulation. As a byproduct, this also gives access to the current dipole moment $\dot{\boldsymbol{\mu}}$ and hence enables us to work in the “velocity form”, which is obtained via partial integrations using the properties of the equilibrium TCFs

$$\alpha(\omega) = F(\omega) \frac{\beta\hbar}{2\pi\omega} \int_{-\infty}^{\infty} dt e^{-i\omega t} \langle \dot{\boldsymbol{\mu}}(0) \cdot \dot{\boldsymbol{\mu}}(t) \rangle \quad (1.4.28)$$

$$\Delta\alpha(\omega) = F(\omega) \frac{4\beta\hbar}{2\pi} \int_{-\infty}^{\infty} dt e^{-i\omega t} \langle \dot{\boldsymbol{\mu}}(0) \cdot \mathbf{m}(t) \rangle \quad (1.4.29)$$

where $\dot{\boldsymbol{\mu}}$ denotes the current dipole moment.

1.4.4 AB-INITIO THEORIES

After the first realizations of experimental VCD measurements,^{154–156} many theoretical descriptions of the modeling of VCD have been devised:¹⁷ The coupled oscillator model,^{31,157} the fixed partial charge model,^{30,158}

the localized molecular orbitals model,¹⁵⁹ the dynamic polarization model,¹⁶⁰ the charge flow model,^{161,162} the atomic polar tensor model¹⁶³ and the bond moment model.^{148,164} Quickly it became clear that an accurate description of the magnetic dipole moment is needed,³⁵ which is not accessible when working in the BO approximation. The current and magnetic dipole moment have a vanishing expectation value with the electronic BO wave functions. Formally, an incorporation of non-adiabatic effects can be achieved in a straightforward sum-over-excited-states approach that later also has been implemented.¹⁶⁵

More efficient and elegant routes have been proposed independently by Nafie^{32,33,166,167} and Stephens.^{34,168} Their perturbative description avoids the expensive sum-over-excited-states summation and keeps an adiabatic factorization of the wave function. Since that time, Stephens' magnetic field perturbation theory (MFPT) is the widely applied state of the art for the calculation of molecular VCD spectra.¹⁷ After the successful implementation of the MFPT by Stephens, the nuclear velocity perturbation theory (NVPT) proposed by Nafie has not been implemented until very recently in this work.¹³⁹ Both theories are equivalent formulations via a second derivative of the total energy, only the order of differentiation is reversed. However, in the following we point out that their implementation poses different complications that render the NVPT more suitable for a dynamical description in the condensed phase.¹⁶⁹

In the static picture, i.e. working only at the equilibrium geometry, also anharmonic corrections and more accurate electronic structure theories have been employed.^{39,40,170-173} Dynamical spectra, i.e. using the time correlation function formalism, are usually calculated employing a charge density-based description, either from partial charges^{49-51,151,174,175} or very recently from AIMD electronic densities.⁵² If the density and its time-derivative are known, it is possible to use the continuity equation to calculate the irrotational part of the electronic probability current density $\mathbf{j}(\mathbf{r})$, however the density does not determine its solenoidal part. In other words, the divergence of the current density $\mathbf{j}(\mathbf{r})$ can be uniquely determined, but not its curl.

$$\nabla \cdot \mathbf{j}(\mathbf{r}) + \partial_t n(\mathbf{r}) = 0 \quad \text{but} \quad \nabla \times \mathbf{j}(\mathbf{r}) = ? \quad (1.4.30)$$

A promising approach adopted from fluid dynamics has been proposed very recently by Thomas et al.⁵² They define the current via a conservative velocity field

$$\mathbf{j}(\mathbf{r}, t) = n(\mathbf{r}, t) \mathbf{v}(\mathbf{r}, t) \quad \text{with} \quad \mathbf{v}(\mathbf{r}, t) = -\nabla \alpha(\mathbf{r}, t). \quad (1.4.31)$$

This approach assures that the current density follows an irrotational vector field and, at the same time, flows only in spatial regions with non-vanishing electronic density. However, this ansatz assumes the absence of eddy currents, which cannot be determined from the density alone. Instead, our approach allows to directly calculate the full current density and hence also includes eddy currents. To which extent and in which systems these are relevant is an interesting question for future work.

MAGNETIC FIELD AND NUCLEAR VELOCITY PERTURBATION THEORIES

In the following, we present the connection between the MFPT and the NVPT and discuss the differences in an implementation in the condensed phase. The starting point of both theories is the solution of the BO electronic structure problem in a non-degenerate electronic ground state

$$\left[\hat{\mathcal{H}}_{BO} - \epsilon_{BO}^{(0)}(\mathbf{R}) \right] \varphi_{\mathbf{R}}^{(0)}(\mathbf{r}) = 0 \quad (1.4.32)$$

with the BO Hamiltonian $\hat{\mathcal{H}}_{BO}$, its real eigenfunctions $\varphi_{\mathbf{R}}^{(0)}(\mathbf{r})$ and eigenvalues $\epsilon_{BO}^{(0)}(\mathbf{R})$, which parametrically depend on the nuclear coordinates \mathbf{R} . We consider an electronic Hamiltonian including a magnetic field perturbation (MFP) and a nuclear velocity perturbation (NVP) due to vibronic couplings

$$\hat{\mathcal{H}}_{\mathbf{R},\dot{\mathbf{R}},\mathbf{H}}^e = \hat{\mathcal{H}}_{BO} - i\hbar\dot{\mathbf{R}} \cdot \frac{\partial}{\partial \mathbf{R}} - \hat{\mathbf{m}}^e \cdot \mathbf{H} \quad (1.4.33)$$

where the nuclear derivative only acts on the parametric dependence of the electronic wave function and not on the nuclear wave function. We do not further discuss Nafie's derivation^{*} of the NVPT and instead arrive at the same results via a rigorous approximation procedure starting from the exact factorization of the electron-nuclear wave function (c.p. sections 2.2 and 3.5). From this description of the electron-nuclear problem, the "back-conversion" of the nuclear position derivative to a classical nuclear velocity coordinate as a new parametric variable of the electronic wave function occurs naturally.

The linear order corrected electronic wave function of the Hamiltonian in eq. (1.4.33) has additional parametric dependences on the nuclear velocities and the magnetic field

$$|\varphi_{\mathbf{R},\dot{\mathbf{R}},\mathbf{H}}\rangle = |\varphi_{\mathbf{R}}^{(0)}\rangle + \dot{\mathbf{R}} \cdot |\varphi_{\mathbf{R}}^{(\dot{\mathbf{R}})}\rangle + \mathbf{H} \cdot |\varphi_{\mathbf{R}}^{(\mathbf{H})}\rangle. \quad (1.4.34)$$

The response orbitals are written in a compact notation where the superscript in parenthesis indicates the derivative. We are interested in the change of the expectation values of the electric and magnetic dipole moment due to nuclear displacements or velocities. These define the electronic atomic axial tensor (AAT) \mathcal{I} and the electronic atomic polar tensor (APT) \mathcal{E} in the position form (r). Alternatively, we can use the current dipole moment, i.e. the velocity form (v) of the electronic APT

$$\mathcal{I} = \frac{\partial \langle \hat{\mathbf{m}}^e \rangle}{\partial \dot{\mathbf{R}}}, \quad \mathcal{E}^r = \frac{\partial \langle \hat{\boldsymbol{\mu}}^e \rangle}{\partial \mathbf{R}} \quad \text{or} \quad \mathcal{E}^v = \frac{\partial \langle \hat{\boldsymbol{\mu}}^e \rangle}{\partial \dot{\mathbf{R}}}. \quad (1.4.35)$$

In the MFP and NVP, the corrections are purely imaginary. Therefore, the corresponding Sternheimer equations do not require self-consistent solutions and can be formally inverted to yield the response orbitals according to

$$|\varphi_{\mathbf{R}}^{(\mathbf{H})}\rangle = (\hat{\mathcal{H}}_{BO} - \epsilon_{BO}^{(0)}(\mathbf{R}))^{-1} \hat{\mathbf{m}}^e |\varphi_{\mathbf{R}}^{(0)}\rangle \quad (1.4.36)$$

$$|\varphi_{\mathbf{R}}^{(\dot{\mathbf{R}})}\rangle = (\hat{\mathcal{H}}_{BO} - \epsilon_{BO}^{(0)}(\mathbf{R}))^{-1} \hbar |\varphi_{\mathbf{R}}^{(\mathbf{R})}\rangle. \quad (1.4.37)$$

Using these relations, we can show the equivalence of both theories. The difference amounts to applying the Sternheimer formalism either to the left or to the right

$$\mathcal{I} \equiv 2\langle \varphi_{\mathbf{R}}^{(0)} | \hat{\mathbf{m}}^e | \varphi_{\mathbf{R}}^{(\dot{\mathbf{R}})} \rangle = 2\langle \varphi_{\mathbf{R}}^{(0)} | \hat{\mathbf{m}}^e (\hat{\mathcal{H}}_{BO} - \epsilon_{BO}^{(0)}(\mathbf{R}))^{-1} \hbar | \varphi_{\mathbf{R}}^{(\mathbf{R})} \rangle = 2\hbar \langle \varphi_{\mathbf{R}}^{(\mathbf{H})} | \varphi_{\mathbf{R}}^{(\mathbf{R})} \rangle \quad (1.4.38)$$

This equivalence motivates the interpretation of the MFPT and the NVPT as mixed second derivatives of the expectation values of the Hamiltonian in eq. (1.4.33) with the wave function in eq. (1.4.34), with changed order of differentiation. In the MFPT, the velocity derivative is taken analytically

$$\mathcal{I} = -\frac{\partial^2 \langle \hat{\mathcal{H}}_{\mathbf{R},\dot{\mathbf{R}},\mathbf{H}}^e \rangle}{\partial \mathbf{H} \partial \dot{\mathbf{R}}} = -i\hbar \frac{\partial}{\partial \mathbf{H}} \langle \varphi_{\mathbf{R},\dot{\mathbf{R}},\mathbf{H}} | \frac{\partial}{\partial \mathbf{R}} | \varphi_{\mathbf{R},\dot{\mathbf{R}},\mathbf{H}} \rangle = 2\hbar \text{Im} \left[\langle \varphi_{\mathbf{R}}^{(\mathbf{H})} | \varphi_{\mathbf{R}}^{(\mathbf{R})} \rangle \right]. \quad (1.4.39)$$

^{*} "As was first demonstrated in 1983, it is possible to retain the factorable, adiabatic nature of the molecular wavefunction by back-converting the derivative of the nuclear kinetic energy that operates on the nuclear wavefunction from a quantum mechanical operator to a classical nuclear velocity coordinate as a new parametric variable of the electronic wavefunction."^{27,33}

Here, we have used the orthogonality constraints due to the conservation of the norm. If the derivative is evaluated in the reversed order, we obtain the NVPT

$$\mathcal{I} = -\frac{\partial^2 \langle \hat{\mathcal{H}}_{\mathbf{R}, \dot{\mathbf{R}}, \mathbf{H}}^e \rangle}{\partial \dot{\mathbf{R}} \partial \mathbf{H}} = \frac{\partial}{\partial \dot{\mathbf{R}}} \langle \varphi_{\mathbf{R}, \dot{\mathbf{R}}, \mathbf{H}} | \hat{\mathbf{m}}^e | \varphi_{\mathbf{R}, \dot{\mathbf{R}}, \mathbf{H}} \rangle = 2 \langle \varphi_{\mathbf{R}}^{(0)} | \hat{\mathbf{m}}^e | \varphi_{\mathbf{R}}^{(\dot{\mathbf{R}})} \rangle. \quad (1.4.40)$$

Both formulations require the (purely real) response of the orbitals due to a nuclear displacement perturbation (NDP) $\varphi_{\mathbf{R}}^{(\mathbf{R})}$, the MFPT in the final projection, the NVPT as an intermediate result of the NVP calculation. This NDP response yields the electronic atomic polar tensor (APT) in the position form (r)

$$\mathcal{E}^r = -\frac{\partial^2 \langle \hat{\mathcal{H}}_{\mathbf{R}, \dot{\mathbf{R}}, \mathbf{H}}^e \rangle}{\partial \mathbf{R} \partial \mathbf{E}} = 2 \langle \varphi_{\mathbf{R}}^{(0)} | \hat{\boldsymbol{\mu}}^e | \varphi_{\mathbf{R}}^{(\mathbf{R})} \rangle \quad (1.4.41)$$

as mixed second derivative with respect to the electric field \mathbf{E} . In the NVPT also the velocity form can be used (the mixed second derivative with respect to the electro-magnetic vector potential \mathbf{A})

$$\mathcal{E}^v = -c \frac{\partial^2 \langle \hat{\mathcal{H}}_{\mathbf{R}, \dot{\mathbf{R}}, \mathbf{H}}^e \rangle}{\partial \dot{\mathbf{R}} \partial \mathbf{A}} = 2 \langle \varphi_{\mathbf{R}}^{(0)} | \hat{\boldsymbol{\mu}}^e | \varphi_{\mathbf{R}}^{(\dot{\mathbf{R}})} \rangle. \quad (1.4.42)$$

Both ways of calculation of the AAT are equivalent and also both forms of the APT are equivalent in the complete basis set limit.

The change of the magnetic moment due to a nuclear velocity can equivalently also be treated in a response function formalism.¹⁷⁶ This approach provides the intuitive picture of an electronic current response due to the changing electric field induced by nuclear motion. However, its merit rests rather conceptually, since no computationally more efficient implementation is devised.

ON THE IMPLEMENTATIONAL DIFFERENCES

The discussion of differences between the MFPT and the NVPT in terms of an implementation depends on the intended application. In a static picture, i.e. when working in the double harmonic approximation (c.p. section A.3), one is interested in the APT and the AAT. These give access to the change of the dipole moments caused by nuclear vibrations, which is in general not parallel to the mode displacements. In a molecule with N_n nuclei, the MFPT requires N_n calculations for the NDP and three calculations for the MFP. In the NVPT, one also needs N_n calculations for the NDP and additionally N_n calculations for the NVP. The computational costs of MFP and NVP calculations are comparable, since both do not require a self-consistent solution of the Sternheimer equations. That is, in isolated molecules and when working in the static picture, the MFPT is computationally more efficient than the NVPT.

This changes when a dynamical perspective is adopted. In the TCF description, only the dipole moments along a molecular dynamics are needed, i.e. one is interested in the perturbation along a particular nuclear velocity vector. This projection can be done a posteriori using the atomic tensors or a priori already in the setup of the perturbation calculation itself. The latter reduces the computational costs of the MFPT to one projected NDP and three MFP calculations. In contrast, the NVPT only requires one projected NDP and one projected NVP calculation. Even though the difference is by far smaller, here the NVPT is already more efficient than the MFP.

A further complication arises when working in the condensed phase. Due to the ill-definition of the position operator under periodic boundary conditions (c.p. section 1.3), the perturbation Hamiltonian of

the MFP is no longer well defined. When working with MLWO, the MFP can be also applied under periodic boundary conditions,^{14,138} but the number of perturbation calculations increases to ≥ 6 (c.p. section 1.1.4). Assuming grouped operator evaluations with molecular centers of mass as references, this requires $\geq 6 + N_{mol}$ perturbations. The NVPT is equally applicable in the condensed phase and outperforms the MFPT in terms of the number of required calculations.

This rather vague discussion applies only to plane wave codes, in which the basis function is independent of the nuclear position, velocity or external field.¹⁷ When working with atom centered basis functions or linear scaling techniques, other technical aspects might become important and the preferred choice might be different.

1.5 EXACT FACTORIZATION OF THE ELECTRON-NUCLEAR WAVE FUNCTION

In this section, we review the exact factorization of the electron-nuclear wave function^{177–179} (XF), which is used as a starting point to controlled approximations (c.p. sections 2.2 and 3.5). This presentation follows the already published introduction in ref.⁵⁴ as will be discussed in section 2.2. It has been proved that the full time-dependent electron-nuclear wave function $\Psi(\mathbf{r}, \mathbf{R}, t)$, which is the solution of the TDSE in eq. (1.1.2), can be exactly factorized to the product^{177–179}

$$\Psi(\mathbf{r}, \mathbf{R}, t) = \Phi_{\mathbf{R}}(\mathbf{r}, t)\chi(\mathbf{R}, t), \quad (1.5.1)$$

where

$$\int d\mathbf{r} |\Phi_{\mathbf{R}}(\mathbf{r}, t)|^2 = 1 \quad \forall \mathbf{R}, t. \quad (1.5.2)$$

Here, $\chi(\mathbf{R}, t)$ is the nuclear wave function and $\Phi_{\mathbf{R}}(\mathbf{r}, t)$ is the electronic wave function, which parametrically depends on the nuclear positions and satisfies the partial normalization condition (PNC) expressed in eq. (1.5.2). The PNC guarantees the interpretation of $|\chi(\mathbf{R}, t)|^2$ as the probability of finding the nuclear configuration \mathbf{R} at time t , and of $|\Phi_{\mathbf{R}}(\mathbf{r}, t)|^2$ itself as the conditional probability of finding the electronic configuration \mathbf{r} at time t , given the nuclear configuration \mathbf{R} . Further, the PNC makes the factorization (1.5.1) unique up to within a (\mathbf{R}, t) -dependent gauge transformation

$$\chi(\mathbf{R}, t) \rightarrow \tilde{\chi}(\mathbf{R}, t) = e^{-\frac{i}{\hbar}\theta(\mathbf{R}, t)}\chi(\mathbf{R}, t) \quad (1.5.3)$$

$$\Phi_{\mathbf{R}}(\mathbf{r}, t) \rightarrow \tilde{\Phi}_{\mathbf{R}}(\mathbf{r}, t) = e^{\frac{i}{\hbar}\theta(\mathbf{R}, t)}\Phi_{\mathbf{R}}(\mathbf{r}, t), \quad (1.5.4)$$

where $\theta(\mathbf{R}, t)$ is some real function of the nuclear coordinates and time.

As shown in section A.1, the stationary variations¹⁸⁰ of the quantum mechanical action

$$\mathcal{A}[\chi, \Phi_{\mathbf{R}}] = \int_{t_i}^{t_f} \langle \Psi | \hat{\mathcal{H}} - i\hbar\partial_t | \Psi \rangle dt \quad (1.5.5)$$

with respect to $\Phi_{\mathbf{R}}(\mathbf{r}, t)$ and $\chi(\mathbf{R}, t)$, inserting the PNC by means of Lagrange multipliers,^{181, 182} lead to the equations of motion

$$(\hat{\mathcal{H}}_e - \epsilon(\mathbf{R}, t)) \Phi_{\mathbf{R}}(\mathbf{r}, t) = i\hbar\partial_t \Phi_{\mathbf{R}}(\mathbf{r}, t) \quad (1.5.6)$$

$$\hat{\mathcal{H}}_n \chi(\mathbf{R}, t) = i\hbar\partial_t \chi(\mathbf{R}, t). \quad (1.5.7)$$

The electronic $\hat{\mathcal{H}}_e$ and nuclear $\hat{\mathcal{H}}_n$ Hamiltonians are defined as

$$\hat{\mathcal{H}}_e = \hat{\mathcal{H}}_{BO} + V_{e,ext}(\mathbf{r}, t) + \hat{U}_{en}^{coup}[\Phi_{\mathbf{R}}, \chi] \quad (1.5.8)$$

$$\hat{\mathcal{H}}_n = \sum_{\nu=1}^{N_n} \frac{[-i\hbar\nabla_{\nu} + \mathbf{A}_{\nu}(\mathbf{R}, t)]^2}{2M_{\nu}} + V_{n,ext}(\mathbf{R}, t) + \epsilon(\mathbf{R}, t), \quad (1.5.9)$$

respectively, with the “electron-nuclear coupling operator” (ENCO)

$$\begin{aligned} \hat{U}_{en}^{coup}[\Phi_{\mathbf{R}}, \chi] = & \sum_{\nu=1}^{N_n} \frac{1}{M_{\nu}} \left[\frac{[-i\hbar\nabla_{\nu} - \mathbf{A}_{\nu}(\mathbf{R}, t)]^2}{2} + \right. \\ & \left. \left(\frac{-i\hbar\nabla_{\nu}\chi}{\chi} + \mathbf{A}_{\nu}(\mathbf{R}, t) \right) (-i\hbar\nabla_{\nu} - \mathbf{A}_{\nu}(\mathbf{R}, t)) \right]. \end{aligned} \quad (1.5.10)$$

The time-dependent potentials are the time-dependent potential energy surface (TDPES), $\epsilon(\mathbf{R}, t)$, implicitly defined by eq. (1.5.6) as

$$\epsilon(\mathbf{R}, t) = \langle \Phi_{\mathbf{R}}(t) | \hat{\mathcal{H}}_e - i\hbar\partial_t | \Phi_{\mathbf{R}}(t) \rangle_{\mathbf{r}}, \quad (1.5.11)$$

and the time-dependent vector potential (TDVP), $\mathbf{A}_{\nu}(\mathbf{R}, t)$, defined as

$$\mathbf{A}_{\nu}(\mathbf{R}, t) = \langle \Phi_{\mathbf{R}}(t) | -i\hbar\nabla_{\nu} | \Phi_{\mathbf{R}}(t) \rangle_{\mathbf{r}}. \quad (1.5.12)$$

The symbol $\langle \cdot \rangle_{\mathbf{r}}$ indicates an integration over electronic coordinates only. Under the gauge transformation (1.5.3), the scalar potential and the vector potential transform as

$$\tilde{\epsilon}(\mathbf{R}, t) = \epsilon(\mathbf{R}, t) + \partial_t\theta(\mathbf{R}, t) \quad (1.5.13)$$

$$\tilde{\mathbf{A}}_{\nu}(\mathbf{R}, t) = \mathbf{A}_{\nu}(\mathbf{R}, t) + \nabla_{\nu}\theta(\mathbf{R}, t). \quad (1.5.14)$$

In eqs. (1.5.6) and (1.5.7), $\hat{U}_{en}^{coup}[\Phi_{\mathbf{R}}, \chi]$, $\epsilon(\mathbf{R}, t)$, and $\mathbf{A}_{\nu}(\mathbf{R}, t)$ are responsible for the coupling between electrons and nuclei in a formally exact way. It is worth noting that the ENCO, $\hat{U}_{en}^{coup}[\Phi_{\mathbf{R}}, \chi]$ in the electronic eq. (1.5.6) depends on the nuclear wave function and acts on the parametric dependence of $\Phi_{\mathbf{R}}(\mathbf{r}, t)$ as a differential operator. This “pseudo-operator” includes the coupling to the nuclear subsystem beyond the parametric dependence in the BO Hamiltonian $\hat{\mathcal{H}}_{BO}$.

The nuclear eq. (1.5.7) has the particularly appealing form of a Schrödinger equation that contains the TDPES (1.5.11) and the TDVP (1.5.12) governing nuclear dynamics and yielding the nuclear wave function. The scalar and vector potentials are uniquely determined up to within a gauge transformation, given by eqs. (1.5.13) and (1.5.14). As expected, the nuclear Hamiltonian in eq. (1.5.7) is form-invariant under such transformations. $\chi(\mathbf{R}, t)$ is interpreted as the nuclear wave function since it leads to an N -body nuclear density and an N -body current-density that reproduce the true nuclear N -body density and current-density¹⁷⁹ obtained from the full wave function $\Psi(\mathbf{r}, \mathbf{R}, t)$.

The exact factorization approach to the coupled dynamics of electrons and nuclei has been extensively investigated in the literature. The advantages of such a novel formulation of the quantum dynamical problem have been pointed out mainly focusing on the development of approximated numerical schemes to treat the effect of electronic excited-state (non-adiabatic) dynamics on nuclear motion.

Some purely theoretical works have proposed a new interpretation of non-adiabatic processes provided by the exact factorization framework. In refs.^{183–185} the TDPES has been analyzed. The aim of the analysis is to identify the important features that need to be accounted for when developing algorithms that treat in an approximate manner, e.g. quantum-classical, the coupled motion of electrons and nuclei. In particular, refs.^{183–185} have shown that the TDPES develops characteristic steps that bridge piecewise adiabatic shapes whenever the splitting of a nuclear wave packet is observed after its passage through an avoided crossing. Recently, further studies¹⁸⁶ have been devoted to the analysis of the properties of the TDPES when quantum interferences related to non-adiabatic effects arise. The common purpose of such investigations is to reproduce as accurately as possible the shape of the TDPES within the quantum-classical (approximate) description of the coupled electron-nuclear dynamics.

Further theoretical analysis has been devoted to the electronic equation, which describes the evolution of the electronic factor of the factorization. Such equation is a less standard evolution equation than the nuclear

time-dependent Schrödinger equation and it contains an electron-nuclear coupling operator (ENCO) which expresses the dynamical coupling to the nuclei. The peculiarity of the ENCO is that it explicitly depends on the nuclear wave function. Therefore, some work^{187,188} has been devoted to its analysis and approximation strategies within a classical and semi-classical treatment of the nuclear wave function. This analysis is also strictly related to the work presented in this thesis.⁵⁴

From the numerical perspective, the information collected from the theoretical analysis has led to the derivation of quantum-classical algorithms to solve the exact equations from the factorization in an approximate way. The main idea¹⁸⁹⁻¹⁹² is to derive the classical limit of the nuclear time-dependent Schrödinger equation via an asymptotic expansion in power of Planck's constant of the nuclear wave function. Classical (Newton) equations have been derived for trajectories that evolve of the TDPES generated by the electrons in their excited states. Depending on the approximations introduced to efficiently solve the electronic equation, an independent-trajectory^{189,190} and a coupled-trajectory^{191,192} schemes have been derived.

The work presented in this thesis is mainly related to the analysis performed on the electronic equation, as we have initiated the development of an approach to treat non-adiabatic effects based on perturbation theory and thus to efficiently solve the electronic equation of the factorization. Related to the work presented in this thesis,⁵⁴ additional applications of the approach have been proposed¹⁹³ to devise a strategy to compute electronic current densities beyond the BO approximation.

1.6 ELECTRONIC SUSCEPTIBILITY

When molecules are exposed to external or inter-molecular fields due to a polar chemical environment, their electrons respond to the change of the external potential and displace to minimize the energy. This change of the electronic structure gives rise to a polarization of the molecule that in turn can affect its environment. Accounting for polarization effects is a crucial aspect of classical or semi-empirical methods, which usually are employed when the size of the system is too large to apply first-principles approaches. In this chapter we deal with electronic polarization and introduce the electronic susceptibility.*

The electronic susceptibility is a very complex and rich object that finds applications in many domains, in particular due to its appearance in the adiabatic-connection fluctuation-dissipation theorem.^{194,195} It is a crucial ingredient to time-dependent density functional theory,^{196–199} symmetry adapted perturbation theory.^{68,69,78,200,201} and is also employed in G_0W_0 ,^{202–204} fluctuation-dissipation density functional theory,^{205–207} van-der-Waals^{208–213} or random phase approximation^{214–217} and beyond random phase approximation^{218–221} calculations. In a different spirit, it is employed in conceptual chemistry^{222,223} for interpretations of charge delocalization^{224,225} and aromaticity.²²⁶ Further applications involve the modeling of polarization effects in hybrid QM/MM free-energy calculations^{227–229} and of efficient alchemical derivative evaluations.^{230–232}

The response kernel can be obtained in different ways, via a sum-over-states expression,^{233–235} explicit time-dependent response calculations^{236–239} or iterative diagonalization schemes.^{90,240–243} However, its explicit non-local real-space representation has only been subject to few selected studies.^{90,240,244,245}

We first review the sum-over-states expression and the relation between the interacting and non-interacting case in section 1.6.1. An iterative method for the calculation of the static interacting electronic susceptibility is presented in section 1.6.2.

1.6.1 INTERACTING AND NON-INTERACTING RESPONSE FUNCTION

If the electronic ground state of a system of electrons is exposed to a time-dependent external potential $V_{ext}(\mathbf{r}, t)$

$$V_{ext}(\mathbf{r}, t) = V_{ext,0}(\mathbf{r}) + \delta V_{ext}(\mathbf{r}, t) \quad \text{with} \quad \delta V_{ext}(\mathbf{r}, t) = 0 \text{ at } t \leq 0, \quad (1.6.1)$$

its wave function and density respond to the changed potential and change over time. The linear density response

$$\delta n^{(1)}(\mathbf{r}, t) = \int_0^\infty dt' \int d^3r' \chi(\mathbf{r}, t, \mathbf{r}', t') \delta V_{ext}(\mathbf{r}', t'), \quad (1.6.2)$$

is related to the change of the potential $\delta V_{ext}(\mathbf{r}', t')$ via the the electronic susceptibility¹⁹⁷

$$\chi(\mathbf{r}, t, \mathbf{r}', t') = \left. \frac{\delta n(\mathbf{r}, t)}{\delta V_{ext}(\mathbf{r}', t')} \right|_{V_{ext,0}}. \quad (1.6.3)$$

*The electronic susceptibility is also denoted as the non-local electronic density susceptibility, density-density response function or screened electronic dielectric response function.

An explicit representation of the electronic susceptibility can be derived from time-dependent perturbation theory in the interaction picture^{197, 246, 247}

$$\chi(\mathbf{r}, t, \mathbf{r}', t') = -i\theta(t - t')\langle\varphi_0|[\hat{n}_I(\mathbf{r}, t), \hat{n}_I(\mathbf{r}', t')]| \varphi_0\rangle, \quad (1.6.4)$$

with $\hat{n}_I(\mathbf{r}, t) = e^{i\hat{\mathcal{H}}_0 t} \hat{n}(\mathbf{r}) e^{-i\hat{\mathcal{H}}_0 t}$ and $\hat{n}(\mathbf{r}) = \sum_i^{N_e} \delta(\mathbf{r} - \hat{\mathbf{r}}_i)$. A Fourier transform and a resolution of identity yields the Lehmann-representation of the electronic susceptibility^{233–235}

$$\chi(\mathbf{r}, \mathbf{r}', \omega) = \lim_{\eta \rightarrow 0^+} \sum_{j=0}^{\infty} \left(\frac{\langle\varphi_0|\hat{n}(\mathbf{r})|\varphi_j\rangle\langle\varphi_j|\hat{n}(\mathbf{r}')|\varphi_0\rangle}{\hbar\omega - \varepsilon_j + i\eta} - \frac{\langle\varphi_0|\hat{n}(\mathbf{r}')|\varphi_j\rangle\langle\varphi_j|\hat{n}(\mathbf{r})|\varphi_0\rangle}{\hbar\omega + \varepsilon_j + i\eta} \right), \quad (1.6.5)$$

with eigenvalues ε_j of the interacting states φ_j . In practice, a sum-over-states evaluation using interacting excited states is only practicable in model systems. Instead, we resort to the basis of KS states, in which we can define^{197, 248, 249}

$$\chi_0(\mathbf{r}, \mathbf{r}', \omega) = \lim_{\eta \rightarrow 0^+} \sum_{k,j=1} (f_k - f_j) \frac{\phi_k^{(0)*}(\mathbf{r})\phi_j^{(0)}(\mathbf{r})\phi_j^{(0)*}(\mathbf{r}')\phi_k^{(0)}(\mathbf{r}')}{\hbar\omega - (\epsilon_j - \epsilon_k) + i\eta}. \quad (1.6.6)$$

This expression has the advantage to involve the non-interacting reference system, however it only yields the non-interacting response function

$$\chi_0(\mathbf{r}, t, \mathbf{r}', t') = \left. \frac{\delta n(\mathbf{r}, t)}{\delta V_{KS}(\mathbf{r}', t')} \right|_{V_{KS,0}}. \quad (1.6.7)$$

The interacting χ response function is obtainable from the non-interacting χ_0 response function via a Dyson-like equation²⁴⁹

$$\chi = \chi_0 + \chi_0 \star f_{Hxc} \star \chi, \quad (1.6.8)$$

with the time-dependent non-local Hartree-exchange-correlation kernel f_{Hxc} and the convolution denoted by \star . The Hartree-exchange-correlation kernel f_{Hxc} is the time-dependent variant of the Kernel K introduced in section I.I.4. Since the exact exchange-correlation functional is not known, also f_{Hxc} is unknown. In practice one often uses the adiabatic approximation to f_{Hxc}

$$f_{xc}^{adia}(\mathbf{r}, \mathbf{r}', \omega) = \lim_{\omega \rightarrow 0} f_{xc}(\mathbf{r}, \mathbf{r}', \omega), \quad (1.6.9)$$

or the random-phase approximation^{195, 216, 250}

$$f_{Hxc}^{RPA}(\mathbf{r}, \mathbf{r}', \Delta t) = \frac{\delta(\Delta t)}{|\mathbf{r} - \mathbf{r}'|}. \quad (1.6.10)$$

In the latter case, it is possible to make use of the adiabatic connection to calculate the electronic correlation energy.^{251–254} Recently, an analytical expression for the direct analytical evaluation of the interacting response function has been derived,²⁵⁵ however, its practical usability is yet to be explored.

1.6.2 ITERATIVE SPECTRAL DECOMPOSITION

A different approach to the calculation of the electronic susceptibility is the iterative diagonalization of the static response function.^{90, 240–242} Since the electronic susceptibility has a bound eigenvalue spectrum, is real and symmetric

$$\chi(\mathbf{r}, \mathbf{r}') = \chi(\mathbf{r}', \mathbf{r}), \quad (1.6.11)$$

and its action on any given vector $V_{ext}(\mathbf{r}')$ (i.e. any valid perturbation potential)

$$n^{(1)}(\mathbf{r}) = \int d^3r' \chi(\mathbf{r}, \mathbf{r}') V_{ext}(\mathbf{r}'), \quad (1.6.12)$$

can be calculated via DFPT, it is possible to apply linear algebra techniques to iteratively diagonalize the full response function. The Hermitian Lanczos algorithm²⁵⁶ is such an iterative method to obtain approximate eigenvectors and the corresponding orthogonal projection $B_m \in \mathbb{C}^{m \times m}$ of a Hermitian matrix $A \in \mathbb{C}^{n \times n}$ with $m \ll n$ using Krylov subspaces \mathcal{K}^m . The algorithm works as follows: We choose a suitable initial vector $|\mathbf{v}_1| = 1$, set $\beta_1 = 0$, $\mathbf{v}_0 = 0$ and iterate for $j = 1, 2, \dots, m$:

$$\tilde{\mathbf{w}}_j = A \mathbf{v}_j \quad (1.6.13)$$

$$\alpha_j = \tilde{\mathbf{w}}_j \cdot \mathbf{v}_j \quad (1.6.14)$$

$$\mathbf{w}_j = \hat{P} \tilde{\mathbf{w}}_j \quad (1.6.15)$$

$$\beta_{j+1} = |\mathbf{w}_j| \quad (1.6.16)$$

$$\mathbf{v}_{j+1} = \mathbf{w}_j / \beta_{j+1} \quad (1.6.17)$$

where \hat{P} is an orthonormalization with respect to all vectors already found $\{\mathbf{v}_i | i \leq j\}$. The coefficients α_j and β_{j+1} are the diagonal and off-diagonal entries of the tridiagonal symmetric matrix B_m . Since $m \ll n$ it can be easily diagonalized $B_m = V_m^\dagger A V_m$. A suitable initial vector should have the same support as the density response and should span a large enough Krylov subspace. Both requirements are fulfilled by the normalized ground state density if its net charge is removed.

In practice, eqs. (1.6.13–1.6.17) correspond to the iterative solution of

$$(\hat{H}^{(0)} - \epsilon^{(0)})\phi_{[j]}^{(1)} = -V_{[j]}^{(1)}\phi^{(0)} \quad (1.6.18)$$

$$V_{[j+1]}^{(1)} = n^{(1)}[\phi_{[j]}^{(1)}]. \quad (1.6.19)$$

where eq. (1.6.18) is a self-consistent Sternheimer DFPT calculation.⁹⁰ The algorithm yields a decomposition of the full non-local interacting static response function in terms of eigenfunctions $\chi_i(\mathbf{r})$ and eigenvalues λ_i

$$\chi(\mathbf{r}, \mathbf{r}') \approx \sum_{i=0}^{N_{max}} \chi_i(\mathbf{r}) \lambda_i \chi_i(\mathbf{r}'). \quad (1.6.20)$$

The eigenfunctions $\chi_i(\mathbf{r})$ act as projectors on the relevant part of the perturbation potential and at the same time provide the shape of the response density. The eigenvalue gives the corresponding weight and is a measure of the physical significance of the corresponding eigenfunction.

At variance with the sum-over-states representation in eq. (1.6.6), the iterative diagonalization can yield the interacting response function, i.e. the self-consistent change of the electronic density due to an applied external potential. A recent variant of this approach using Wannier localization provides a promising decomposition procedure.²⁵⁷

The iterative spectral decomposition approach provides a basis for the representation of the full frequency dependent response function and can hence be used for efficient RPA^{203, 203, 217, 258, 259} and post-RPA calculations.²²¹

CHAPTER 2

ARTICLES PUBLISHED WITHIN THIS THESIS

2.1 OVERVIEW

This chapter presents the results obtained in this work that already have been published. The corresponding articles are reprinted with permissions from

- “A. Scherrer, F. Agostini, D. Sebastiani, E. K. U. Gross and R. Vuilleumier, *Nuclear velocity perturbation theory for vibrational circular dichroism: An approach based on the exact factorization of the electron-nuclear wave function*, J. Chem. Phys., 143(7): 074106, 2015” with the permission of AIP Publishing;⁵⁴
- “A. Scherrer, D. Sebastiani and R. Vuilleumier, *Nuclear velocity perturbation theory of vibrational circular dichroism*, J. Chem. Theory Comput., 9(12): 5305-5312, 2013”, copyright 2013 American Chemical Society;¹³⁹
- “A. Scherrer and D. Sebastiani, *Moment expansion of the linear density-density response function*, J. Comp. Chem., 37(7):665-674, 2016”, copyright 2015 Wiley Periodicals;⁹¹
- “A. Scherrer, C. Dreßler, P. Ahlert and D. Sebastiani, *Generalization of the electronic susceptibility for arbitrary molecular geometries*, J. Chem. Phys., 144(14):144111, 2016” with the permission of AIP Publishing.²⁶⁰

As pointed out in the introduction, this work extends the application range of density functional perturbation theory in two related, yet distinct directions: the efficient calculation

- (i) of electronic probability currents for spectroscopy and
- (ii) of electronic polarizability effects for the modeling of weak interactions,

both in the condensed phase.

The first direction (i) is pursued by the articles included in sections 2.2 and 2.3. They prepare our intended application of electronic currents, i.e. the calculation of accurate intensities for dynamical vibrational circular dichroism (VCD) spectra in the condensed phase. To realize this goal, it has been necessary to revisit the derivation of the nuclear velocity perturbation theory (NVPT) for a better theoretical understanding of its physical and mathematical properties. A rigorous derivation of the NVPT from the exact factorization of the electron-nuclear wave function (XF) has been obtained and is presented in section 2.2. The NVPT has already been proposed by Nafie³² but has so far not been implemented successfully. We have reported the first successful implementation of the NVPT within a large-scale electronic structure program package in this work as described in section 2.3. These results constitute the basis of the applications of the NVPT, presented in chapter 3.

Furthermore, the second direction (ii) is presented in sections 2.4 and 2.5. The starting point of this work is the spectral decomposition of the static interacting electronic susceptibility, as discussed in section 1.6. The spectral decomposition representation is a compact representation of the full information contained in the electronic susceptibility. Prior work in this direction has already shown that inter- as well as intra-molecular perturbations can be treated in this framework.^{90, 261} However, in certain applications, only a part of this full information is required and a more compact representation is desirable. This question has been addressed via the moment expansion presented in section 2.4. One long-term goal of this work is the use of the electronic susceptibility for a density-based modeling of inter-molecular interactions. To this end, the molecular geometry dependence of the very compact moment expanded representation is analyzed in section 2.5.

2.2 DERIVATION OF THE NUCLEAR VELOCITY PERTURBATION THEORY

One of the main results of this work is the rigorous derivation and successful implementation of the nuclear velocity perturbation theory (NVPT). As discussed in section 1.4.4, the NVPT has originally been proposed by Nafie^{32, 33, 166, 167} but has not been implemented until very recently in this work.¹³⁹ The implementation is discussed in section 2.3, whereas this section presents the derivation of the NVPT from the exact factorization of the electron-nuclear wave function (XF). This new formalism offers an exact starting point to include correction terms to the Born-Oppenheimer (BO) form of the molecular wave function, similar to the complete-adiabatic approximation of Nafie.

All authors contributed extensively to the work presented in this section.⁵⁴ F. Agostini, R. Vuilleumier and A. Scherrer derived the theory. F. Agostini and A. Scherrer wrote the manuscript. A. Scherrer implemented the theory and carried out the numerical calculations. D. Sebastiani and R. Vuilleumier supervised the project. E. K. U. Gross gave conceptual advice.

The main result of this work is the rigorous derivation of the NVPT, originally proposed by Nafie. The electronic BO ground state wave function is perturbatively corrected to contain non-adiabatic contributions that give rise to an electronic current density. The corrections depend on a small parameter that, in a classical treatment of the nuclei, is identified as the nuclear velocity. The potential energy is unchanged to first order, meaning that the time-dependent potential energy surface (TDPES) equals the BO ground state potential energy. Therefore, the ab-initio molecular dynamics can be performed on the TDPES of the clamped nuclei approximation, as presented in section 1.1. Apart from proposing a rigorous basis of the NVPT, the derivation shows that the rotational strengths, related to the intensity of the VCD signal, contain a new contribution beyond-BO (due to the time-dependent vector potential) that can be evaluated with the NVPT and that only arises when the XF approach is employed. Numerical results of chiral and non-chiral systems are presented to test the validity of the approach. The results show a very good agreement between the MFPT and the NVPT. Furthermore, the vector potential correction is shown to be small in the systems examined in this work. Even though the correction might be of relevance in case of amplified or enhanced VCD,^{262–266} we can safely ignore it in the intended applications in the liquid phase in section 3.2.

Nuclear velocity perturbation theory for vibrational circular dichroism: An approach based on the exact factorization of the electron-nuclear wave function

Arne Scherrer,^{1,2,3,a)} Federica Agostini,^{4,a)} Daniel Sebastiani,¹ E. K. U. Gross,⁴ and Rodolphe Vuilleumier^{2,3}

¹Martin-Luther-University Halle-Wittenberg, von-Danckelmann-Platz 4, D-06120 Halle, Germany

²UMR 8640 ENS-CNRS-UPMC, Département de Chimie, 24 rue Lhomond, École Normale Supérieure, 75005 Paris, France

³UPMC Université Paris 06, 4, Place Jussieu, 75005 Paris, France

⁴Max-Planck-Institute of Microstructure Physics, Weinberg 2, D-06120 Halle, Germany

(Received 19 May 2015; accepted 3 August 2015; published online 19 August 2015)

The nuclear velocity perturbation theory (NVPT) for vibrational circular dichroism (VCD) is derived from the exact factorization of the electron-nuclear wave function. This new formalism offers an *exact* starting point to include correction terms to the Born-Oppenheimer (BO) form of the molecular wave function, similar to the complete-adiabatic approximation. The corrections depend on a small parameter that, in a classical treatment of the nuclei, is identified as the nuclear velocity. Apart from proposing a rigorous basis for the NVPT, we show that the rotational strengths, related to the intensity of the VCD signal, contain a new contribution beyond-BO that can be evaluated with the NVPT and that only arises when the exact factorization approach is employed. Numerical results are presented for chiral and non-chiral systems to test the validity of the approach. © 2015 AIP Publishing LLC. [<http://dx.doi.org/10.1063/1.4928578>]

I. INTRODUCTION

Vibrational circular dichroism (VCD)^{1–3} in molecules refers to the difference in absorption of left and right circularly polarized light in the infrared region of the electromagnetic spectrum. In contrast to circular dichroism, which originates in electronic transitions, VCD is the difference in interaction of a molecule with radiation of opposite circular polarizations when it undergoes vibrational transitions. Experimentally, VCD is employed to probe the absolute configuration of chiral molecules in solution and provides detailed structural information, thus being a very sensitive form of vibrational spectroscopy.

From the theoretical point of view,^{4–21} the Born-Oppenheimer (BO),²² or adiabatic, treatment of the coupled motion of electrons and nuclei in molecular systems is inadequate for predicting VCD. Since the intensity of the VCD signal is proportional to the rotational strength for a transition between two vibrational states, the calculation of the electric current and of the magnetic dipole moment (and of their scalar product) is required. The electric current and the magnetic dipole moment contain both electronic and nuclear contributions, but when the BO approximation is employed, the electronic contributions identically vanish. This is due to the fact that the ground-state electronic wave function is real for a non-degenerate adiabatic state and therefore the expectation values of the purely imaginary (Hermitian) electric current^{23–28} and magnetic dipole moment operators vanish.¹⁸

Therefore, VCD appears a fundamentally non-adiabatic (beyond-BO) process, thus requiring a theoretical approach able to explicitly treat the dynamical coupling between electronic and nuclear degrees of freedom in molecules.

A practical question²⁹ arises at this point, as to whether such coupling can be accounted for within a standard *ab initio* molecular dynamics formulation. Among the most successful ideas are in fact those resorting to the treatment of beyond-BO effects as a perturbation to the BO problem, numerically less expensive than a full non-adiabatic calculation but indeed not consistent if strong non-adiabatic effects are expected, e.g., in the presence of conical intersections. Examples are the approaches proposed by Nafie,¹⁹ employing the complete-adiabatic expression of the electron-nuclear wave function, and by Stephens,²⁰ introducing the magnetic field perturbation theory. These methods allow to overcome the problems encountered in the BO calculation of VCD, while exploiting the advantages of the BO formalism like the product form of the electron-nuclear wave function. Recently, VCD has been calculated by developing and implementing a nuclear velocity perturbation theory (NVPT)³⁰ based on the complete-adiabatic approach of Nafie.¹⁹ In this formulation, non-adiabatic corrections to the electronic adiabatic ground-state are perturbatively taken into account and are induced by a “small” nuclear velocity.

In this paper, we propose a novel approach to NVPT, based on the exact factorization of the electron-nuclear wave function.^{31,32} The advantage of this formulation comes from using a product form, like in the BO approximation, of the wave function, which is not the result of an approximation but an *exact*

^{a)}A. Scherrer and F. Agostini contributed equally to this work.

starting point. The electron-nuclear wave function is written as a single product of an electronic many-body factor, parametrically depending on the nuclear positions, and a nuclear wave function. The latter can be interpreted as a proper nuclear wave function since it leads to the exact nuclear density and current-density. Moreover, when the product form is inserted into the time-dependent Schrödinger equation (TDSE), two coupled equations for the components of the full wave function are derived, with the nuclear equation being a TDSE where a time-dependent vector potential and a time-dependent scalar potential (or time-dependent potential energy surface, TD PES)^{33–37} represent the effect of the electrons on the nuclei beyond-BO. Therefore, in this context, the electronic equation generates the proper evolution expected when the coupling between electrons and nuclei is fully accounted for and it allows to recover the BO equation in a certain limit, as will be discussed in the paper.

Two major results will be reported: (i) NVPT³⁰ will be rigorously derived, using as starting point the exact electronic equation from the factorization rather than the complete-adiabatic approach¹⁹ and (ii) correction terms to the “standard” expression of the rotational strength will naturally appear in the new formulation due to the presence of the time-dependent vector potential of the theory. Throughout the paper, we will adopt a time-dependent picture, as this is crucial to introduce the concept of nuclear velocity and, thus, to make the connection with NVPT. In such a time-dependent picture, we will have access to the instantaneous expectation values of the electric current and of the magnetic dipole moment. The corrections to those expectation values, and therefore to the rotational strength, can be derived also in a static picture referring to the time-independent formulation³⁸ of the factorization, but the direct link to NVPT would then be missing.

The paper is organized as follows. In Section II A we review the linear response theory approach to VCD, showing the connection between rotational strength and intensity of the spectrum. In Section II B, we recall the exact factorization formalism. In Section III, we focus on the electronic equation from the exact factorization, showing how to recover the BO limit and introducing non-adiabatic effects as a perturbation to the adiabatic framework. The perturbation parameter is identified as the nuclear velocity, exactly as in NVPT, if the classical limit is considered. However, here we have access to the quantum electronic evolution equation, thus the perturbation parameter has a more general meaning since we are not restricted to a classical treatment of the nuclei. We derive the expressions of the quantities necessary to evaluate the VCD spectrum in Section IV A, while in Section IV B we discuss details on the practical calculation of the rotational strength by applying density functional perturbation theory (DFPT). In Section V A, we report numerical results for the calculation of rotational strengths and of their corrections for (S)-d₂-oxirane, a chiral system, in comparison to oxirane, a non-chiral molecule. We also report the comparison between the NVPT approach and the more standard magnetic field perturbation theory²⁰ in Section V B, for (S)-d₂-oxirane, (R)-propylene-oxide, and (R)-fluoro-oxirane. Our conclusions are stated in Section VI.

II. THEORETICAL BACKGROUND

A. Vibrational circular dichroism

Vibrational spectroscopy probes the coupling of the nuclear degrees of freedom to applied electro-magnetic fields. On the macroscopic level, the absorption process is described phenomenologically by the Beer-Lambert law,³⁹ where the material specific attenuation of the radiation per unit length is accounted for by the molar absorption coefficient ϵ . Microscopically, and within the linear response regime, the energy dissipated in the interaction between the medium and the radiation is expressed in terms of the observable that couples to the external field. In case of radiation in the infrared spectral range, the multipole approximation and the long wavelength limit can be applied^{39,40} to determine such coupling. The microscopic and the macroscopic perspectives can be connected in the framework of linear response theory.⁴¹ In the Heisenberg formulation, the frequency dependent absorption coefficient takes the form of the power spectrum of the dipole auto-correlation.^{42,43}

The specific feature of VCD is the different interaction of chiral systems with polarized light. Linearly polarized light encounters optical rotatory dispersion while circularly polarized light encounters different absorptions for the different handednesses of the radiation, VCD. Formally, this is accounted for by the dependence of the refractive index of a chiral system on the handedness of the radiation. While this effect is not relevant for the mean infrared absorption, the difference absorption gives rise to the VCD signal.

For the calculation of the absorption coefficient $\bar{\epsilon}(\omega)$ and the difference absorption $\Delta\epsilon(\omega)$,³ a common approach in the literature is to invoke the double harmonic approximation for nuclear motion and dipole moment. This leads to the expressions

$$\bar{\epsilon}(\omega) = \frac{8\pi^3}{3Vhcn(\omega)} \sum_k D_k \omega \delta(\omega - \omega_k) \quad (1)$$

and

$$\Delta\epsilon(\omega) = 4 \frac{8\pi^3}{3Vhcn(\omega)} \sum_k R_k \omega \delta(\omega - \omega_k). \quad (2)$$

The dipole strength D_k and rotational strength R_k of the vibrational mode k , with frequency ω_k , are evaluated as

$$D_k = \frac{\partial \langle \hat{\mu} \rangle}{\partial \dot{q}_k} \cdot \frac{\partial \langle \hat{\mu} \rangle}{\partial \dot{q}_k} \langle \dot{q}_k \rangle^2, \quad (3)$$

$$R_k = \frac{\partial \langle \hat{\mathbf{m}} \rangle}{\partial \dot{q}_k} \cdot \frac{\partial \langle \hat{\mu} \rangle}{\partial \dot{q}_k} \langle \dot{q}_k \rangle^2, \quad (4)$$

respectively, with the time derivative of the dipole moment $\hat{\mu}$, namely, the current, and the magnetic dipole moment $\hat{\mathbf{m}}$. In Eqs. (1) and (2), V indicates the volume occupied by the system, $h = 2\pi\hbar$ is the Planck constant, c is the speed of light, and $n(\omega)$ is the refractive index of the medium. Normal modes will be indicated throughout the paper as \mathbf{q} , with velocities $\dot{\mathbf{q}}$.

The linear variations of the expectation values (over the instantaneous state of the system) of the current and of the magnetic dipole moment with respect to (w.r.t.) the mode q_k

around their equilibrium values are calculated from the total (electronic and nuclear) atomic polar tensor \mathcal{P}^ν (APT) and atomic axial tensor \mathcal{M}^ν (AAT). The APT and AAT have electronic and nuclear contributions,^{3,30} namely,

$$\frac{\partial \langle \hat{\mu}_\beta \rangle}{\partial \dot{R}_\alpha^\nu} \equiv \mathcal{P}_{\alpha\beta}^\nu = \mathcal{E}_{\alpha\beta}^\nu + \mathcal{N}_{\alpha\beta}^\nu, \quad (5)$$

$$\frac{\partial \langle \hat{m}_\beta \rangle}{\partial \dot{R}_\alpha^\nu} \equiv \mathcal{M}_{\alpha\beta}^\nu = \mathcal{I}_{\alpha\beta}^\nu + \mathcal{J}_{\alpha\beta}^\nu, \quad (6)$$

with electronic parts \mathcal{E} and \mathcal{I} and nuclear parts \mathcal{N} and \mathcal{J} . Here, the indices α and β are used for the Cartesian coordinates, while ν labels the nuclei. The dipole and rotational strengths are related via the chain rule to the vibrational nuclear displacement vector $S_{\alpha k}^\nu$ which describes the displacement of nucleus ν in direction α due to the k th normal mode q_k ,

$$S_{\alpha k}^\nu = \left. \frac{\partial \dot{R}_\alpha^\nu}{\partial \dot{q}_k} \right|_{\dot{q}=0} = \left. \frac{\partial R_\alpha^\nu}{\partial q_k} \right|_{q=0}. \quad (7)$$

B. Exact factorization of the electron-nuclear wave function

The non-relativistic Hamiltonian describing a system of interacting electrons and nuclei, in the absence of a time-dependent external field, is

$$\hat{H} = \hat{T}_n + \hat{H}_{BO}, \quad (8)$$

where \hat{T}_n is the nuclear kinetic energy operator and

$$\hat{H}_{BO}(\mathbf{r}, \mathbf{R}) = \hat{T}_e(\mathbf{r}) + \hat{W}_{ee}(\mathbf{r}) + \hat{V}_{en}(\mathbf{r}, \mathbf{R}) + \hat{W}_{nn}(\mathbf{R}) \quad (9)$$

is the standard BO electronic Hamiltonian, with electronic kinetic energy $\hat{T}_e(\mathbf{r})$, and with potentials $\hat{W}_{ee}(\mathbf{r})$ for electron-electron, $\hat{W}_{nn}(\mathbf{R})$ for nucleus-nucleus, and $\hat{V}_{en}(\mathbf{r}, \mathbf{R})$ for electron-nucleus interaction. The symbols \mathbf{r} and \mathbf{R} are used to collectively indicate the coordinates of N_e electrons and N_n nuclei, respectively.

It has been proved^{31,32} that the full time-dependent electron-nuclear wave function $\Psi(\mathbf{r}, \mathbf{R}, t)$ which is the solution of the TDSE,

$$\hat{H}\Psi(\mathbf{r}, \mathbf{R}, t) = i\hbar\partial_t\Psi(\mathbf{r}, \mathbf{R}, t), \quad (10)$$

can be exactly factorized to the product

$$\Psi(\mathbf{r}, \mathbf{R}, t) = \Phi_{\mathbf{R}}(\mathbf{r}, t)\chi(\mathbf{R}, t), \quad (11)$$

where

$$\int d\mathbf{r} |\Phi_{\mathbf{R}}(\mathbf{r}, t)|^2 = 1 \quad \forall \mathbf{R}, t. \quad (12)$$

Here, $\chi(\mathbf{R}, t)$ is the nuclear wave function and $\Phi_{\mathbf{R}}(\mathbf{r}, t)$ is the electronic wave function which parametrically depends on the nuclear positions and satisfies the partial normalization condition (PNC) expressed in Eq. (12). The PNC guarantees the interpretation of $|\chi(\mathbf{R}, t)|^2$ as the probability of finding the nuclear configuration \mathbf{R} at time t , and of $|\Phi_{\mathbf{R}}(\mathbf{r}, t)|^2$ itself as the conditional probability of finding the electronic configuration \mathbf{r} at time t , given the nuclear configuration \mathbf{R} . Further, the PNC makes factorization (11) unique up to within a (\mathbf{R}, t) -dependent gauge transformation,

$$\chi(\mathbf{R}, t) \rightarrow \tilde{\chi}(\mathbf{R}, t) = e^{-\frac{i}{\hbar}\theta(\mathbf{R}, t)}\chi(\mathbf{R}, t), \quad (13)$$

$$\Phi_{\mathbf{R}}(\mathbf{r}, t) \rightarrow \tilde{\Phi}_{\mathbf{R}}(\mathbf{r}, t) = e^{\frac{i}{\hbar}\theta(\mathbf{R}, t)}\Phi_{\mathbf{R}}(\mathbf{r}, t),$$

where $\theta(\mathbf{R}, t)$ is some real function of the nuclear coordinates and time.

The stationary variations⁴⁴ of the quantum mechanical action w.r.t. $\Phi_{\mathbf{R}}(\mathbf{r}, t)$ and $\chi(\mathbf{R}, t)$ lead to the equations of motion

$$(\hat{H}_{el}(\mathbf{r}, \mathbf{R}) - \epsilon(\mathbf{R}, t))\Phi_{\mathbf{R}}(\mathbf{r}, t) = i\hbar\partial_t\Phi_{\mathbf{R}}(\mathbf{r}, t), \quad (14)$$

$$\hat{H}_n(\mathbf{R}, t)\chi(\mathbf{R}, t) = i\hbar\partial_t\chi(\mathbf{R}, t), \quad (15)$$

where the PNC is inserted by means of Lagrange multipliers.^{45,46} Here, the electronic and nuclear Hamiltonians are defined as

$$\hat{H}_{el}(\mathbf{r}, \mathbf{R}) = \hat{H}_{BO}(\mathbf{r}, \mathbf{R}) + \hat{U}_{en}^{coup}[\Phi_{\mathbf{R}}, \chi] \quad (16)$$

and

$$\hat{H}_n(\mathbf{R}, t) = \sum_{\nu=1}^{N_n} \frac{[-i\hbar\nabla_\nu + \mathbf{A}_\nu(\mathbf{R}, t)]^2}{2M_\nu} + \epsilon(\mathbf{R}, t), \quad (17)$$

respectively, with the “electron-nuclear coupling operator”

$$\begin{aligned} \hat{U}_{en}^{coup}[\Phi_{\mathbf{R}}, \chi] = & \sum_{\nu=1}^{N_n} \frac{1}{M_\nu} \left[\frac{[-i\hbar\nabla_\nu - \mathbf{A}_\nu(\mathbf{R}, t)]^2}{2} \right. \\ & + \left(\frac{-i\hbar\nabla_\nu\chi}{\chi} + \mathbf{A}_\nu(\mathbf{R}, t) \right) \\ & \left. \times (-i\hbar\nabla_\nu - \mathbf{A}_\nu(\mathbf{R}, t)) \right]. \end{aligned} \quad (18)$$

The time-dependent potentials are the TD PES, $\epsilon(\mathbf{R}, t)$, implicitly defined by Eq. (14) as

$$\epsilon(\mathbf{R}, t) = \langle \Phi_{\mathbf{R}}(t) | \hat{H}_{BO} + \hat{U}_{en}^{coup} - i\hbar\partial_t | \Phi_{\mathbf{R}}(t) \rangle_{\mathbf{r}}, \quad (19)$$

and the vector potential, $\mathbf{A}_\nu(\mathbf{R}, t)$, defined as

$$\mathbf{A}_\nu(\mathbf{R}, t) = \langle \Phi_{\mathbf{R}}(t) | -i\hbar\nabla_\nu | \Phi_{\mathbf{R}}(t) \rangle_{\mathbf{r}}. \quad (20)$$

The symbol $\langle \cdot \rangle_{\mathbf{r}}$ indicates an integration over electronic coordinates only. Under gauge transformation (13), the scalar potential and the vector potential transform as

$$\tilde{\epsilon}(\mathbf{R}, t) = \epsilon(\mathbf{R}, t) + \partial_t\theta(\mathbf{R}, t), \quad (21)$$

$$\tilde{\mathbf{A}}_\nu(\mathbf{R}, t) = \mathbf{A}_\nu(\mathbf{R}, t) + \nabla_\nu\theta(\mathbf{R}, t). \quad (22)$$

In Eqs. (14) and (15), $\hat{U}_{en}^{coup}[\Phi_{\mathbf{R}}, \chi]$, $\epsilon(\mathbf{R}, t)$ and $\mathbf{A}_\nu(\mathbf{R}, t)$ are responsible for the coupling between electrons and nuclei in a formally exact way. It is worth noting that the electron-nuclear coupling operator, $\hat{U}_{en}^{coup}[\Phi_{\mathbf{R}}, \chi]$ in electronic equation (14) depends on the nuclear wave function and acts on the parametric dependence of $\Phi_{\mathbf{R}}(\mathbf{r}, t)$ as a differential operator. This “pseudo-operator” includes the coupling to the nuclear subsystem beyond the parametric dependence in the BO Hamiltonian $\hat{H}_{BO}(\mathbf{r}, \mathbf{R})$.

Nuclear equation (15) has the particularly appealing form of a Schrödinger equation that contains TD PES (19) and vector potential (20) governing nuclear dynamics and yielding the nuclear wave function. The scalar and vector potentials are uniquely determined up to within a gauge transformation, given by Eqs. (21) and (22). As expected, the nuclear Hamiltonian in Eq. (15) is form-invariant under such transformations. $\chi(\mathbf{R}, t)$ is interpreted as the nuclear wave function since it leads

to an N -body nuclear density and an N -body current-density which reproduce the true nuclear N -body density and current-density³² obtained from the full wave function $\Psi(\mathbf{r}, \mathbf{R}, t)$. The uniqueness of $\epsilon(\mathbf{R}, t)$ and $\mathbf{A}_v(\mathbf{R}, t)$ can be straightforwardly proved by following the steps of the current-density version⁴⁷ of the Runge-Gross theorem,⁴⁸ or by referring to the theorems proved in Ref. 31.

III. NUCLEAR VELOCITY PERTURBATION THEORY

Before showing the derivation of the velocity-dependent corrections to the BO wave function within the exact factorization approach, let us present a procedure that allows us to recover the BO limit of electronic equation (14). Suppose first that the electron-nuclear wave function is given as a BO product,

$$\Psi(\mathbf{r}, \mathbf{R}, t) = \Phi_{\mathbf{R}}(\mathbf{r}, t) \chi(\mathbf{R}, t) = \varphi_{\mathbf{R}}^{(0)}(\mathbf{r}) \chi(\mathbf{R}, t). \quad (23)$$

Here, $\varphi_{\mathbf{R}}^{(0)}(\mathbf{r})$ indicates the real and not degenerate BO ground-state. Using Eq. (20), it follows that the vector potential vanishes identically, $\mathbf{A}_v(\mathbf{R}, t) \equiv 0$.⁴⁹ This can be interpreted as a choice of gauge.⁵⁰ With this assumption, the electron-nuclear coupling operator from Eq. (18) becomes

$$\hat{U}_{en}^{coup}[\Phi_{\mathbf{R}}, \chi] = \sum_{v=1}^{N_n} \frac{-\hbar^2 \nabla_v^2}{2M_v} + \frac{-i\hbar \nabla_v \chi(\mathbf{R}, t)}{M_v \chi(\mathbf{R}, t)} \cdot (-i\hbar \nabla_v). \quad (24)$$

The first term on the right hand side (RHS), containing the Laplacian^{51–53} w.r.t. nuclear coordinates, will be neglected from now on. It can be shown, as reported in Refs. 54–56, that this term contributes with second-order non-adiabatic couplings to the electronic equation, but being explicitly $O(M_v^{-1})$ its effect can be neglected if compared to the remaining (and leading) term. Following again Refs. 54–56, the term that depends on χ can be approximated to zero-th order in an \hbar -expansion⁵⁷ of the nuclear wave function as the classical nuclear velocity, namely,

$$\frac{1}{M_v} \frac{-i\hbar \nabla_v \chi(\mathbf{R}, t)}{\chi(\mathbf{R}, t)} = \frac{\mathbf{P}_v(\mathbf{R}, t)}{M_v} = \dot{\mathbf{R}}_v(t). \quad (25)$$

We have invoked here the classical limit in order to directly relate our results to the NVPT³⁰ and to justify the condition of “small nuclear velocity” that allows a treatment of effects beyond-BO within perturbation theory. The procedure, however, does not rely on the classical limit and the “small” perturbation parameter will be denoted as

$$\lambda_v(\mathbf{R}, t) = \frac{1}{M_v} \frac{-i\hbar \nabla_v \chi(\mathbf{R}, t)}{\chi(\mathbf{R}, t)}. \quad (26)$$

Eq. (26) contains the variations in space of the phase and of the modulus of the nuclear wave function,⁵⁸ and when both variations are “small” then the approach considered here can be applied. We have justified the former hypothesis (small variations of the phase) by employing the classical approximation and we are now assuming valid also the latter (small variations of the modulus).

The electronic Hamiltonian from Eq. (16) becomes

$$\hat{H}_{el}(\mathbf{r}, \mathbf{R}) = \hat{H}_{BO} + \sum_{v=1}^{N_n} \lambda_v(\mathbf{R}, t) \cdot (-i\hbar \nabla_v) \quad (27)$$

and the TDPES reads

$$\begin{aligned} \epsilon(\mathbf{R}, t) &= \langle \varphi_{\mathbf{R}}^{(0)} | \hat{H}_{BO} + \sum_{v=1}^{N_n} \lambda_v(\mathbf{R}, t) \cdot (-i\hbar \nabla_v) | \varphi_{\mathbf{R}}^{(0)} \rangle_{\mathbf{r}} \\ &= \epsilon_{BO}^{(0)}(\mathbf{R}), \end{aligned} \quad (28)$$

i.e., only the \hat{H}_{BO} term survives, since the second term does not contribute to the TDPES. Notice that here the term $\langle \Phi_{\mathbf{R}}(t) | -i\hbar \partial_t | \Phi_{\mathbf{R}}(t) \rangle_{\mathbf{r}}$ identically vanishes, because the electronic wave function is the time-independent BO wave function. In order to recover from Eq. (27) the electronic equation within the BO approximation, one should impose $\lambda_v(\mathbf{R}, t) = 0$, or similarly $\dot{\mathbf{R}}_v(t) = 0 \forall v$ as the electronic equation in BO is solved for fixed nuclei (meaning that their velocity is zero).

To summarize, in order to construct the Hamiltonian in Eq. (27), (i) we treat the nuclei classically, thus we consider the nuclear wave function up to within $O(\hbar^0)$ terms, (ii) we derive corrections to the BO Hamiltonian that are proportional to the nuclear velocity, thus recovering the BO electronic equation if the nuclear velocity is zero (condition of fixed nuclei), (iii) we “relax” the hypothesis of classical nuclei by introducing $\lambda_v(\mathbf{R}, t)$ as the perturbation parameter.

Combining Eqs. (27) and (28) will provide the electronic equation within the new formulation of NVPT. In contrast to the formulation based on the complete-adiabatic approach,¹⁹ the perturbative scheme presented here directly applies to the electronic equation rather than to the full TDSE. Using perturbation theory,³⁰ where \hat{H}_{BO} is the unperturbed Hamiltonian and the second term on the RHS of Eq. (27) is the perturbation, we find the solutions of the equation

$$\left[\hat{H}_{BO} - \epsilon^{(1)} - i\hbar \sum_{v=1}^{N_n} \lambda_v(\mathbf{R}, t) \cdot \nabla_v \right] \varphi_{\mathbf{R}}(\mathbf{r}, t) = 0 \quad (29)$$

as

$$\begin{aligned} \varphi_{\mathbf{R}}(\mathbf{r}, t) &= \varphi_{\mathbf{R}}^{(0)}(\mathbf{r}) \\ &+ \sum_{e \neq 0} \frac{\langle \varphi_{\mathbf{R}}^{(e)} | -i\hbar \sum_{v,\alpha} \lambda_{v\alpha}^v(\mathbf{R}, t) \partial_{\alpha}^v \varphi_{\mathbf{R}}^{(0)} \rangle_{\mathbf{r}}}{\epsilon_{BO}^{(0)}(\mathbf{R}) - \epsilon_{BO}^{(e)}(\mathbf{R})} \varphi_{\mathbf{R}}^{(e)}(\mathbf{r}) \end{aligned} \quad (30)$$

up to within linear-order in the perturbation, with the index v running over the N_n nuclei and with α running over the three Cartesian coordinates. The symbol ∂_{α}^v is used to indicate a spatial derivative along the α direction of the position of the v th nucleus and e labels the (unperturbed) adiabatic excited states. The TDPES, up to within first-order terms, is labeled $\epsilon^{(1)}$. It is worth noting that in writing Eq. (29), we are discarding the variations in time of the first-order correction to the BO wave function, adopting a previously assumed³⁰ hypothesis that these variations are smaller than the perturbation itself, thus negligible at the given order. We re-write Eq. (30) as

$$\varphi_{\mathbf{R}}(\mathbf{r}, t) = \varphi_{\mathbf{R}}^{(0)}(\mathbf{r}) + \sum_{v,\alpha} i\lambda_{v\alpha}^v(\mathbf{R}, t) \varphi_{\mathbf{R},v\alpha}^{(1)}(\mathbf{r}), \quad (31)$$

introducing the definition of the first-order perturbation to the BO ground-state

$$\varphi_{\mathbf{R},\nu\alpha}^{(1)}(\mathbf{r}) = \sum_{e \neq 0} \frac{d_{e0,\nu\alpha}(\mathbf{R})}{\omega_{e0}(\mathbf{R})} \varphi_{\mathbf{R}}^{(e)}(\mathbf{r}). \quad (32)$$

Here, $d_{e0,\nu\alpha}(\mathbf{R})$ is the α th Cartesian component of the non-adiabatic coupling vector, corresponding to the ν -th nucleus, between the unperturbed ground-state and the excited state e , whereas the frequency $\omega_{e0}(\mathbf{R})$ is the energy difference (divided by \hbar) between the excited (e) and the ground (0) states. When the adiabatic states are real, Eq. (32) is real as well and the second term in Eq. (31) is purely imaginary. Moreover, the correction term in Eq. (31) depends on time only implicitly, via its dependence on $\lambda_\nu(\mathbf{R},t)$, and $\varphi_{\mathbf{R},\nu\alpha}^{(1)}(\mathbf{r})$ is orthogonal to $\varphi_{\mathbf{R}}^{(0)}(\mathbf{r})$. This last property can be interpreted as a choice of gauge. For instance, by imposing the condition that $\langle \varphi_{\mathbf{R}}^{(0)} | \varphi_{\mathbf{R}}(t) \rangle_{\mathbf{r}}$ is real $\forall \mathbf{R}, t$, which is allowed as gauge condition, we imply the orthogonality of $\varphi_{\mathbf{R},\nu\alpha}^{(1)}(\mathbf{r})$ and $\varphi_{\mathbf{R}}^{(0)}(\mathbf{r})$, namely, $\langle \varphi_{\mathbf{R}}^{(0)} | \varphi_{\mathbf{R},\nu\alpha}^{(1)} \rangle_{\mathbf{r}} = 0$. It is easy to prove that the PNC remains valid up to within $O(\lambda_\nu^2)$, using the orthogonality of $\varphi_{\mathbf{R}}^{(0)}(\mathbf{r})$ and $\varphi_{\mathbf{R},\nu\alpha}^{(1)}(\mathbf{r})$.

The first-order approximation to the TD PES is

$$\epsilon^{(1)}(\mathbf{R},t) = \epsilon_{BO}^{(0)}(\mathbf{R}) - i \sum_{\nu} O(\lambda_\nu(\mathbf{R},t)) \quad (33)$$

but the second term on the RHS is identically zero, as can be proved by either inserting Eq. (31) in the definition of the TD PES given in Eq. (19) or by considering the fact that $\epsilon^{(1)}(\mathbf{R},t)$ must be real while the correction is purely imaginary.

As in the NVPT approach based on the complete-adiabatic form of the electron-nuclear wave function,¹⁹ the first-order perturbation to the electronic wave function represents the effect of the non-adiabatic coupling between the ground and the excited electronic states. Within a fully non-adiabatic approach,^{59–68} it would be possible to compute Eq. (32). However, it has been shown in Ref. 30 that within DFPT the perturbation can be determined by the knowledge of only ground-state properties. Eq. (29) is solved by inserting the chosen expression for electronic wave function (31) and by solving for each order in the perturbation $\lambda_\nu(\mathbf{R},t)$. At the zeroth order, we obtain

$$[\hat{H}_{BO} - \epsilon_{BO}^{(0)}(\mathbf{R})] \varphi_{\mathbf{R}}^{(0)}(\mathbf{r}) = 0, \quad (34)$$

and at the first-order,

$$[\hat{H}_{BO} - \epsilon_{BO}^{(0)}(\mathbf{R})] \varphi_{\mathbf{R},\nu\alpha}^{(1)}(\mathbf{r}) = \hbar \partial_\alpha^\nu \varphi_{\mathbf{R}}^{(0)}(\mathbf{r}) \quad \forall \nu, \alpha. \quad (35)$$

Eq. (34) is simply the eigenvalue problem associated to the BO Hamiltonian; Eq. (35) is solved in the framework of DFPT as illustrated in the Section IV B.

The TD PES of the theory based on the exact factorization remains unaffected if compared to the BO case, up to within the first-order perturbation, as shown in Eq. (33). The vector potential, which is identically zero in the adiabatic treatment, becomes

$$\mathbf{A}_\nu(\mathbf{R},t) = -2\hbar \sum_{\nu',\alpha} \lambda_{\nu'}^{\nu'}(\mathbf{R},t) \langle \nabla_{\nu'} \varphi_{\mathbf{R}}^{(0)} | \varphi_{\mathbf{R},\nu'\alpha}^{(1)} \rangle_{\mathbf{r}}. \quad (36)$$

This expression is obtained by using Eq. (31) in the definition of the vector potential given in Eq. (20). Using Eq. (35) in Eq. (36), an alternative expression is derived, which is used

in actual calculations, namely,

$$\begin{aligned} A_\alpha^\nu(\mathbf{R},t) &= - \sum_{\nu',\beta} \lambda_{\nu'}^{\nu'}(\mathbf{R},t) \mathcal{A}_{\alpha\beta}^{\nu\nu'}(\mathbf{R}) \\ &= -2 \sum_{\nu',\beta} \lambda_{\nu'}^{\nu'}(\mathbf{R},t) \langle \varphi_{\mathbf{R},\nu'\beta}^{(1)} | \hat{H}_{BO} - \epsilon_{BO}(\mathbf{R}) | \varphi_{\mathbf{R},\nu\alpha}^{(1)} \rangle_{\mathbf{r}}, \end{aligned} \quad (37)$$

(38)

where we have introduced the definition of the matrix $\mathcal{A}_{\alpha\beta}^{\nu\nu'}(\mathbf{R})$ and the symbol A_α^ν stands for the α Cartesian coordinate of the vector potential corresponding to the ν -th nucleus. It is instructive to give an alternative formula for the evaluation of the vector potential matrix in Eq. (37), namely,

$$\mathcal{A}_{\alpha\beta}^{\nu\nu'}(\mathbf{R}) = 2\hbar \sum_{e \neq 0} \frac{d_{e0,\nu'\beta}(\mathbf{R}) d_{e0,\nu\alpha}(\mathbf{R})}{\omega_{e0}(\mathbf{R})}, \quad (39)$$

which is obtained by using Eq. (32) in Eq. (38) and acting with the BO Hamiltonian on its eigenstates. This expression is useful to determine the vector potential by combining the NVPT with (explicit) non-adiabatic calculations. In general, evaluating the vector potential from the full electronic wave function in Eq. (11) is difficult because the exact electronic state is not known, thus approximations have to be invoked. Here, we have derived an expression that can instead be used in actual calculations. However, in the present paper we focus on Eq. (38) and we estimate it within DFPT.

IV. OBSERVABLES

A. Current and magnetic dipole moment

In a time-dependent picture, the expectation values of the current and of the magnetic dipole moment on the instantaneous state of the system are employed to evaluate the rotational strength giving access to the VCD spectrum in the linear response regime. We will derive their expressions employing the factorized form of the full wave function when calculating explicitly the expectation values.

The current and magnetic dipole moment operators are defined as

$$\hat{\boldsymbol{\mu}} = \hat{\boldsymbol{\mu}}^e + \hat{\boldsymbol{\mu}}^n = - \sum_{i=1}^{N_e} \frac{e}{m} \hat{\mathbf{p}}_i + \sum_{\nu=1}^{N_n} \frac{Z_\nu e}{M_\nu} \hat{\mathbf{p}}_\nu \quad (40)$$

and

$$\hat{\mathbf{m}} = \hat{\mathbf{m}}^e + \hat{\mathbf{m}}^n = - \sum_{i=1}^{N_e} \frac{e}{2mc} \hat{\mathbf{r}}_i \times \hat{\mathbf{p}}_i + \sum_{\nu=1}^{N_n} \frac{Z_\nu e}{2M_\nu c} \hat{\mathbf{R}}_\nu \times \hat{\mathbf{p}}_\nu, \quad (41)$$

respectively. Here, $-e$ is the electronic charge, $Z_\nu e$ is the nuclear charge, m and M_ν are the electronic and nuclear masses, and c is the speed of light. The position and momentum operators for the electronic subsystem are indicated as $\hat{\mathbf{r}}_i$ and $\hat{\mathbf{p}}_i$, respectively, and similar symbols are used for the nuclear operators, $\hat{\mathbf{R}}_\nu$ and $\hat{\mathbf{p}}_\nu$. As expected, the vector potential does not appear in Eqs. (40) and (41) since we are not yet calculating an expectation value. However, since the nuclear momentum operator in position representation acts as a derivative w.r.t. the nuclear coordinates \mathbf{R} , the vector potential appears (only)

when the derivative acts on the parametric dependence of the electronic wave function. Indeed, if the factorization is not introduced, such vector potential will never be present.

The expectation values of the operators in Eqs. (40) and (41) on $\Psi(\mathbf{r}, \mathbf{R}, t)$ are indicated with the symbol $\langle \cdot \rangle_\Psi$,

$$\langle \hat{\mu} \rangle_\Psi = \int d\mathbf{R} \chi^*(\mathbf{R}, t) \left[\langle \Phi_{\mathbf{R}}(t) | \hat{\mu}^e | \Phi_{\mathbf{R}}(t) \rangle_{\mathbf{r}} + \hat{\mu}^n + \sum_{\nu=1}^{N_n} \frac{Z_\nu e}{M_\nu} \mathbf{A}_\nu(\mathbf{R}, t) \right] \chi(\mathbf{R}, t) \quad (42)$$

and

$$\langle \hat{\mathbf{m}} \rangle_\Psi = \int d\mathbf{R} \chi^*(\mathbf{R}, t) \left[\langle \Phi_{\mathbf{R}}(t) | \hat{\mathbf{m}}^e | \Phi_{\mathbf{R}}(t) \rangle_{\mathbf{r}} + \hat{\mathbf{m}}^n + \sum_{\nu=1}^{N_n} \frac{Z_\nu e}{2M_\nu c} \hat{\mathbf{R}}_\nu \times \mathbf{A}_\nu(\mathbf{R}, t) \right] \chi(\mathbf{R}, t). \quad (43)$$

We will now introduce the following symbols for the expectation values of the electronic contributions to the current and magnetic dipole moment on the (exact) electronic wave function:

$$\dot{\mu}_{\mathbf{R}}^e(t) = \langle \Phi_{\mathbf{R}}(t) | \dot{\mu}^e | \Phi_{\mathbf{R}}(t) \rangle_{\mathbf{r}}, \quad (44)$$

$$\mathbf{m}_{\mathbf{R}}^e(t) = \langle \Phi_{\mathbf{R}}(t) | \hat{\mathbf{m}}^e | \Phi_{\mathbf{R}}(t) \rangle_{\mathbf{r}}. \quad (45)$$

If the BO electronic wave function is used to approximate $\Phi_{\mathbf{R}}(\mathbf{r}, t)$, both equations, i.e., the electronic contributions to the expectation values, vanish, as well as the vector potential in Eqs. (42) and (43), as mentioned above. It is, however, now possible to insert the NVPT approximation to the electronic wave function, Eq. (31), and this leads to the following expressions for the expectation values:

$$\langle \hat{\mu} \rangle_\Psi \simeq \langle \dot{\mu}_{\mathbf{R}}^{e,(1)}(t) \rangle_\chi + \sum_{\nu=1}^{N_n} \frac{Z_\nu e}{M_\nu} \langle \hat{\mathbf{P}}_\nu + \mathbf{A}_\nu(\mathbf{R}, t) \rangle_\chi, \quad (46)$$

$$\langle \hat{\mathbf{m}} \rangle_\Psi \simeq \langle \mathbf{m}_{\mathbf{R}}^{e,(1)}(t) \rangle_\chi + \sum_{\nu=1}^{N_n} \frac{Z_\nu e}{2M_\nu c} \langle \hat{\mathbf{R}}_\nu \times [\hat{\mathbf{P}}_\nu + \mathbf{A}_\nu(\mathbf{R}, t)] \rangle_\chi. \quad (47)$$

Here, we have written the expectation values (on the left hand sides) on Ψ , the full electron-nuclear wave function, in terms of expectation values of new observables on χ , the nuclear wave function only. Therefore, the vector potential naturally appears in the equations. In addition, since the electronic wave function has been approximated, as stated above, by using Eq. (31), we obtain that the current and the magnetic dipole moment contain an electronic contribution that is first-order (1) in the perturbation. The second terms in both equations, containing the vector potential, correct the nuclear contribution to both expectation values and these corrections shall be considered within NVPT since they are first-order in the perturbation parameter $\lambda_\nu(\mathbf{R}, t)$ (see Eq. (37)). Standard approaches do not consider these correction terms, because the vector potential is a quantity that has been introduced only in the context of the exact factorization. We will compute explicitly these corrections in Section V, but we can already anticipate that while the first (standard) term is $O(\lambda_\nu)$, because of the $\hat{\mathbf{P}}_\nu/M_\nu$ term, the correction is $O(\lambda_\nu/M_\nu)$ since the vector

potential itself has a linear dependence on the perturbation parameter.

It is worth mentioning here that the advantage of introducing expectation values on the nuclear wave function, rather than on the full wave function, becomes clear when the classical approximation for the nuclear subsystem is considered. In this case, due to the properties of the nuclear wave function in the factorization framework (χ is a proper wave function, as it evolves according to a TDSE, and leads to the density and current-density calculated from the full wave function), the classical limit can be performed by imposing that the nuclear density infinitely localizes, at each time, at the classical position denoted by the trajectory. The second terms on the RHS of Eqs. (46) and (47) then become simply functions of phase-space variables. It is important to notice, however, that the vector potential has to be taken into account to appropriately relate the nuclear velocity and momentum.

B. Rotational strengths from density functional perturbation theory

The direct numerical solution of Eqs. (34) and (35) is very expansive for systems with more than a few degrees of freedom. Already, the calculation for small chiral molecules requires an approximate treatment of the electronic structure problem. In our implementation, we resort to standard Kohn-Sham (KS) density functional theory (DFT)^{69–71} with generalized gradient approximation to the exchange-correlation functional.^{72,73} For simplicity, we will limit our discussion to the case of spin saturated closed shell systems and drop the explicit notation of the parametric dependence on the nuclear positions.

In the framework of single determinant KS-DFT, Eq. (34) directly translates to the standard BO ground-state electronic structure problem

$$[\hat{H}_{KS}^{(0)} - \epsilon_o^{(0)}] \phi_o^{(0)}(\mathbf{r}) = 0, \quad (48)$$

with the unperturbed KS Hamiltonian $\hat{H}_{KS}^{(0)}$ and the unperturbed KS orbitals $\phi_o^{(0)}$ and KS energies $\epsilon_o^{(0)}$ of the occupied electronic states o . In DFPT,^{74–78} the calculation of the non-adiabatic correction to the ground-state orbitals can be done without explicit knowledge of the unoccupied states via a Sternheimer equation,⁷⁹

$$-\hat{P}_e [\hat{H}_{KS}^{(0)} - \epsilon_o^{(0)}] \hat{P}_e \phi_o^{(1)}(\mathbf{r}) = \hat{P}_e \hat{H}_{KS}^{(1)}[\{\phi_o\}] \phi_o^{(0)}(\mathbf{r}), \quad (49)$$

with a projector on the manifold of the unoccupied states $\hat{P}_e = 1 - \sum_o |\phi_o\rangle\langle\phi_o|$. The perturbation Hamiltonian on the RHS, $\hat{H}_{KS}^{(1)}[\{\phi_o\}]$, can depend on the electronic density response and hence implicitly on the perturbed orbitals on the left hand side. This is the case for electric field or nuclear displacement perturbations and requires a self-consistent solution. Explicitly, Eq. (49) for a nuclear displacement perturbation j reads

$$-\hat{P}_e [\hat{H}_{KS}^{(0)} - \epsilon_o^{(0)}] \hat{P}_e \frac{\partial \phi_o^{(0)}(\mathbf{r})}{\partial R_j} = \hat{P}_e \frac{\partial \hat{H}_{KS}}{\partial R_j}[\{\phi_o\}] \phi_o^{(0)}(\mathbf{r}). \quad (50)$$

The perturbed KS orbitals $\partial_{R_j} \phi_o^{(0)}(\mathbf{r})$ are the gradient of the KS orbitals $\phi_o^{(0)}(\mathbf{r})$ w.r.t. a nuclear displacement j . They can be

used for the calculation of the electronic APT in the position form.^{3,30}

The corresponding translation of Eq. (35) to DFPT reads

$$\hat{P}_e [\hat{H}_{KS}^{(0)} - \epsilon_o^{(0)}] \hat{P}_e \phi_{o,j}^{(1)}(\mathbf{r}) = \hat{P}_e \hbar \partial_{R_j} \phi_o^{(0)}(\mathbf{r}) \quad \forall j. \quad (51)$$

Also this equation is reminiscent of a Sternheimer equation. However, instead of an explicit perturbation Hamiltonian acting on the unperturbed KS orbitals, the RHS is proportional to the gradient of the ground-state wave function w.r.t. a nuclear displacement. As already discussed, this gradient is accessible via Eq. (50). This method requires two response calculations, a self-consistent one for the nuclear displacement perturbation and another for the nuclear velocity perturbation.

Recently, a related approach to the calculation of NVPT has been reported²⁹ which relies on an iterative finite-differences scheme for the construction of the intermediate nuclear gradient information.

With the imaginary correction to the BO electronic wave function in Eq. (31), it is possible to calculate the electronic APT \mathcal{E} in the velocity form,

$$\mathcal{E}_{\alpha\beta}^v = \frac{\partial \langle \hat{\mu}_\beta^e \rangle}{\partial \dot{R}_\alpha^v} = 2 \sum_o \langle \phi_o | \hat{\mu}_\beta^e | \phi_{o,(v,\alpha)}^{(1)} \rangle \quad (52)$$

and the electronic AAT \mathcal{I} ,

$$\mathcal{I}_{\alpha\beta}^v = \frac{\partial \langle \hat{m}_\beta^e \rangle}{\partial \dot{R}_\alpha^v} = 2 \sum_o \langle \phi_o | \hat{m}_\beta^e | \phi_{o,(v,\alpha)}^{(1)} \rangle. \quad (53)$$

For the calculation of the magnetic moment, a choice of the origin of the position operator has to be made. This poses additional complications for the calculation of observables in the condensed phase where periodic boundary conditions are used. For a detailed discussion, we refer to the literature^{3,30} and to the [Appendix](#).

The nuclear AAT \mathcal{J} is decomposed into its “conventional” contribution and the correction due to the presence of the vector potential

$$\mathcal{J}_{\alpha\beta}^v = \frac{Z_v e}{2c} \epsilon_{\alpha\beta\gamma} R_\gamma^v + \Delta \mathcal{J}_{\alpha\beta}^v, \quad (54)$$

where we used Einstein’s summation convention for repeated indices. The correction due to the additional term in the nuclear magnetic moment in Eq. (47) is given by the derivative of

$$\langle \Delta m_\beta^v \rangle = \frac{Z_v e}{2M_{\gamma C}} \epsilon_{\beta\gamma\delta} R_\gamma^v A_\delta^v = \frac{Z_v e}{2M_{\gamma C}} \epsilon_{\beta\gamma\delta} R_\gamma^v \mathcal{A}_{\delta\eta}^{v'v'} \lambda_{\eta'}^{v'} \quad (55)$$

w.r.t. \dot{R}_α^v . Written in this form, the correction to the magnetic moment depends linearly on the nuclear velocities, via the identification $\lambda_{\eta'}^{v'} = \dot{R}_{\eta'}^{v'}$. However, this dependence can be removed in the picture of the nuclear AAT. To see this, we evaluate the vector potential matrix of Eq. (38) as

$$\mathcal{A}_{\delta\eta}^{v'v'} = 2 \sum_o \langle \phi_{o,(v',\delta)}^{(1)} | \hat{H}_{KS}^{(0)} - \epsilon_o^{(0)} | \phi_{o,(v,\eta)}^{(1)} \rangle \quad (56)$$

and take the derivative of Eq. (55) w.r.t. a nuclear velocity. This gives the correction to the nuclear AAT as

$$\Delta \mathcal{J}_{\alpha\beta}^v = \frac{Z_v e}{2M_{\gamma C}} \epsilon_{\beta\gamma\delta} R_\gamma^v \mathcal{A}_{\delta\alpha}^{v'v'}. \quad (57)$$

This expression illustrates two features of the correction. First, it is non-local in the nuclear contributions, i.e., all nuclei contribute to the AAT of a single nucleus. Second, the prefactor contains the inverse nuclear mass, while the conventional contribution does not.

V. NUMERICAL RESULTS

The presented NVPT has been implemented in our development version of the CPMD^{30,80} electronic structure package. The calculations have been performed using DFPT^{76–78} with Troullier-Martins⁸¹ pseudo-potentials and the BLYP^{72,73} functional. We have employed a plane wave cutoff of 100 Ry. The fluorine pseudo-potential with a radius $r_c = 1.2$ has been used. The geometry optimizations, harmonic analysis, and magnetic field perturbation²⁰ calculations were done using the electronic structure program Gaussian 09 Revision D.01⁸² employing aug-cc-pVTZ basis set⁸³ and BLYP functional.

A. (S)-d₂-oxirane vs. oxirane

The vector potential from Eq. (37) has been calculated for a small rigid chiral molecule, (S)-d₂-oxirane shown in Fig. 1. As will be clear from the numerical results, the vector potential contributes only a small fraction to the rotational strengths R_k (with $k = 1, \dots, 15$ for the (S)-d₂-oxirane and oxirane), as it is computed within a perturbation theory approach. The vector potential is first-order in the perturbation parameter $\lambda_v(\mathbf{R}, t)$ and it appears as an explicit $O(M_v^{-1})$ term in the expressions of the current and of the magnetic dipole moment. Further analysis, currently under investigation, is focussing on the calculation of corrections due to the vector potential in explicit non-adiabatic molecular dynamics, in order to estimate the actual effect of the vector potential on observable properties as the VCD signal.

Before presenting the results for (S)-d₂-oxirane, let us first discuss the case of oxirane, a non-chiral molecule. Oxirane differs from (S)-d₂-oxirane in the deuterium atoms, which are replaced by hydrogen atoms. In Fig. 2, we draw as blue arrows⁸⁴ the velocities corresponding to normal modes at 1127 cm⁻¹ (upper panel) and at 1489 cm⁻¹ (lower panel), which have been selected as examples among the 15 total modes. Perturbations parallel to these velocities are used in Eq. (37) to construct the vector potential, which are shown as red arrows in the figure. It is very interesting to notice that in the case of a non-chiral system, the vector potential maintains the same symmetry of the vibrational modes and is nearly anti-parallel to the nuclear displacement: this is what one would expect, if

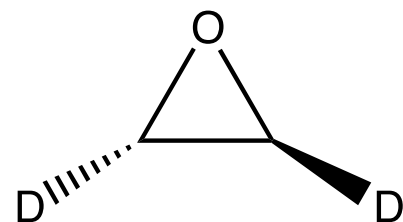


FIG. 1. (S)-d₂-oxirane.

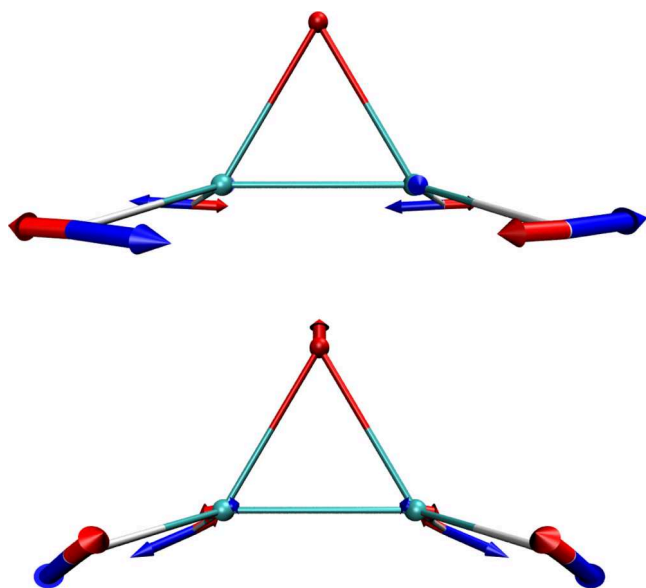


FIG. 2. Vibrational modes at 1127 cm^{-1} (upper panel) and at 1489 cm^{-1} (lower panel) for oxirane, with nuclear velocities indicated as blue arrows. The corresponding vector potential is shown as red arrows.

the vector potential is not to affect the VCD properties, i.e., current and magnetic dipole, and thus the rotational strength of the molecule.

In the case of (S)-d₂-oxirane, the results are quite different, as shown in Fig. 3. Again, the velocities corresponding to the normal modes are indicated as blue arrows, whereas the vector potential is drawn in red. The selected modes are at 896 cm^{-1} and at 1089 cm^{-1} . It is clear in this case that (i) a well-defined symmetry of the vector potential cannot be identified and, as a consequence, (ii) it is not simply (anti-)parallel to the normal mode velocities, as was the case for oxirane. This behavior

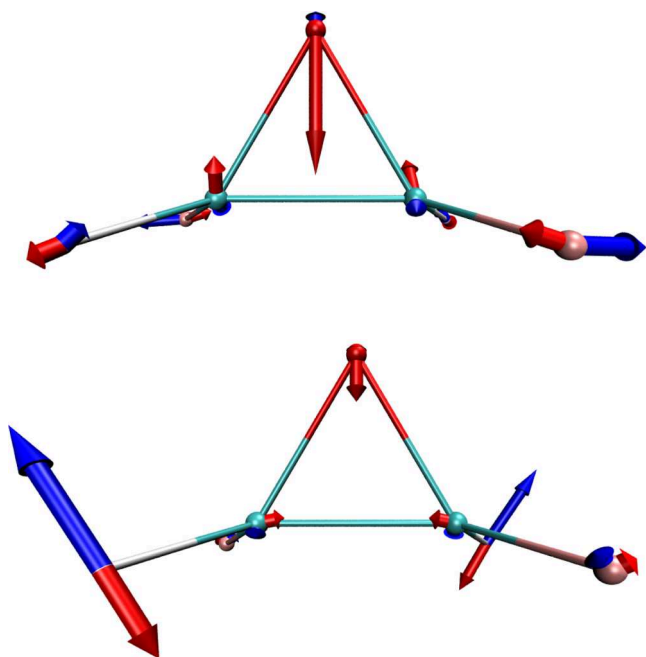


FIG. 3. Vibrational modes at 896 cm^{-1} (upper panel) and at 1089 cm^{-1} (lower panel) for (S)-d₂-oxirane, with nuclear velocities indicated as blue arrows. The corresponding vector potential is shown as red arrows.

TABLE I. Normal modes for (S)-d₂-oxirane. The frequencies of the modes are indicated in the first column, the rotational strengths R are listed in the second column, from Eq. (4), the corrections ΔR due to the vector potential are reported in the third (absolute value) and fourth (relative correction) columns.

$\tilde{\nu}$ (cm^{-1})	R ($10^{-44}\text{ esu}^2\text{ cm}^2$)	ΔR ($10^{-44}\text{ esu}^2\text{ cm}^2$)	$\Delta R/R$ (%)
647.50	-0.45	-0.003	0.67
733.42	10.54	0.016	0.15
769.76	3.29	0.001	0.05
856.38	2.70	0.002	0.09
894.67	-3.89	0.006	0.15
936.33	-20.26	0.001	0.01
1088.21	8.34	-0.027	0.32
1093.95	-4.97	0.004	0.09
1210.44	10.45	-0.029	0.28
1326.86	-0.76	0.0002	0.03
1377.38	-8.17	0.025	0.31
2235.16	-22.90	-0.010	0.04
2244.19	16.78	0.011	0.07
3047.68	-32.59	-0.063	0.19
3054.15	47.04	0.047	0.10

thus results in an actual contribution of the vector potential to the VCD properties of (S)-d₂-oxirane. Such contribution is quantitatively estimated by calculating the correction to the rotational strengths in Eq. (4) of (S)-d₂-oxirane, due to the vector potential terms in Eqs. (46) and (47). Table I lists, for all modes in the (S)-d₂-oxirane, these rotational strengths R_k and the corrections ΔR_k due to the presence of the vector potential in the current and in the magnetic dipole moment.

As discussed above, we notice from the results reported in Table I that, despite the fact that the vector potential is non-zero, its effect is quite small, being of the order $\mathcal{O}(M_v^{-1})$. In fact, while the M_v^{-1} dependence in Eqs. (46) and (47) is removed in the first contributions, being these first terms proportional to the momentum, the second terms are actually $\mathcal{O}(M_v^{-1})$. We recall, however, that in the procedure developed in this paper, the vector potential is evaluated within the NVPT, thus being first-order in the perturbation. In a situation where the electronic wave function has a strong non-adiabatic character, namely, where the correction to a BO-type wave function is not small in the nuclear velocity, a larger contribution may be expected. Moreover, in the cases where the vector potential is singular, e.g., for adiabatic states that are locally degenerate in \mathbf{R} -space, this correction may become very important. However, further studies are required to develop a scheme that allows for the calculation of the vector potential beyond the NVPT.

B. Comparison with magnetic field perturbation theory

Further molecular systems have been investigated, namely (R)-propylene-oxide and (R)-fluoro-oxirane shown in Figs. 4 and 5.

In this section, we report the dipole D and rotational R strengths calculated by employing NVPT, indicated with the symbols D_{NVPT} and R_{NVPT} in Tables II–IV, and we compare these results with the magnetic field perturbation (MFP) theory,²⁰

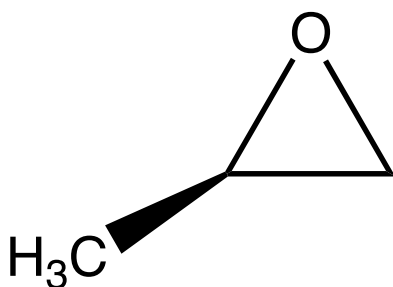


FIG. 4. (R)-propylene-oxide.

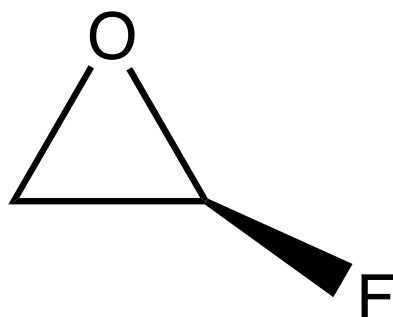


FIG. 5. (R)-fluoro-oxirane.

TABLE II. Normal modes, dipole and rotational strengths, for (S)-d₂-oxirane.

$\tilde{\nu}$ (cm ⁻¹)	D_{MFP} (10 ⁻⁴⁰ esu ² cm ²)	D_{NVP} (10 ⁻⁴⁰ esu ² cm ²)	R_{MFP} (10 ⁻⁴⁴ esu ² cm ²)	R_{NVP} (10 ⁻⁴⁴ esu ² cm ²)
647.50	0.55	0.85	-0.35	-0.45
733.42	123.35	124.88	8.73	10.54
769.76	53.44	51.77	3.17	3.29
856.38	145.31	145.55	4.31	2.70
894.67	9.78	10.24	-3.37	-3.89
936.33	39.73	39.24	-19.14	-20.26
1088.21	3.79	4.44	6.95	8.34
1093.95	1.41	1.71	-3.98	-4.97
1210.44	26.26	26.09	9.56	10.45
1326.86	0.34	0.37	-0.91	-0.76
1377.38	11.65	10.78	-7.50	-8.17
2235.16	49.17	50.88	-22.60	-22.90
2244.19	12.63	12.81	16.80	16.78
3047.68	11.43	11.66	-32.80	-32.59
3054.15	58.64	60.16	46.63	47.04

D_{MFP} and R_{MFP} in the tables. Such comparison has been carried out also for (S)-d₂-oxirane (Table II). Furthermore, Tables III and IV show the corrections ΔR to the rotational strengths due to the vector potential term in Eq. (37), as already presented for the case of (S)-d₂-oxirane in Section V A. In all tables the first column indicates the normal mode frequency, the second and third columns are the dipole strengths from MFP and NVP theories, the fourth and fifth columns show the rotational strengths from MFP and NVP theories. In Tables III and IV, the sixth and seventh columns are the corrections computed from (37), which in general are the same order of magnitude as the corrections reported in Table I for (S)-d₂-oxirane.

TABLE III. Normal modes, dipole and rotational strengths (with corrections), for (R)-propylene-oxide.

$\tilde{\nu}$ (cm ⁻¹)	D_{MFP} (10 ⁻⁴⁰ esu ² cm ²)	D_{NVP} (10 ⁻⁴⁰ esu ² cm ²)	R_{MFP} (10 ⁻⁴⁴ esu ² cm ²)	R_{NVP} (10 ⁻⁴⁴ esu ² cm ²)	ΔR (10 ⁻⁴⁴ esu ² cm ²)	$\Delta R/R$ (%)
202.12	6.91	7.12	3.54	3.47	-0.001	0.03
355.33	45.22	46.63	-12.84	-12.56	0.008	0.06
398.40	38.74	38.86	-3.72	-3.79	0.004	0.11
717.36	55.11	52.51	13.88	13.21	0.005	0.04
795.26	217.23	219.15	2.47	1.62	0.007	0.44
875.72	18.54	17.25	26.36	26.99	0.039	0.14
929.21	51.55	51.53	-35.52	-37.03	-0.049	0.13
1008.29	24.84	26.62	2.88	4.53	-0.004	0.09
1089.09	18.53	19.17	-6.03	-6.56	0.006	0.09
1112.88	7.92	7.79	6.65	7.50	0.023	0.31
1126.68	11.68	12.56	-13.44	-14.67	-0.034	0.23
1150.27	1.51	1.40	1.54	1.23	0.003	0.24
1246.96	19.77	19.85	-8.06	-8.01	-0.004	0.05
1371.08	10.35	9.83	3.30	3.53	0.007	0.19
1388.57	60.08	60.10	13.99	15.15	0.007	0.05
1447.69	13.15	14.16	1.34	1.45	0.005	0.32
1461.62	15.41	16.62	-1.69	-1.90	-0.008	0.42
1480.79	10.14	9.99	4.66	4.69	-0.005	0.11
2955.51	27.68	28.86	1.64	1.64	0.0002	0.01
3000.54	41.29	44.50	-0.29	0.20	-0.009	4.53
3005.59	22.70	24.14	5.13	6.04	-0.034	0.56
3007.28	22.57	22.86	-13.92	-15.14	0.053	0.35
3032.47	47.06	50.07	7.29	7.16	-0.019	0.27
3079.38	41.31	41.09	-7.19	-7.31	0.013	0.17

From the comparison between the two perturbation approaches, we notice an overall very good agreement not only in the absolute values of the dipole and rotational strengths, but also in the signs of the rotational strengths for the three systems investigated here. The MFP theory of Stephens²⁰ can be considered a “more standard” approach, nowadays implemented in most quantum-chemistry packages, thus it

TABLE IV. Normal modes, dipole and rotational strengths (with corrections), for (R)-fluoro-oxirane.

$\tilde{\nu}$ (cm ⁻¹)	D_{MFP} (10 ⁻⁴⁰ esu ² cm ²)	D_{NVP} (10 ⁻⁴⁰ esu ² cm ²)	R_{MFP} (10 ⁻⁴⁴ esu ² cm ²)	R_{NVP} (10 ⁻⁴⁴ esu ² cm ²)	ΔR (10 ⁻⁴⁴ esu ² cm ²)	$\Delta R/R$ (%)
411.61	52.63	53.11	9.48	9.80	-0.003	0.03
482.91	30.46	31.23	-3.10	-2.91	0.002	0.06
733.56	124.68	123.64	40.79	39.91	0.031	0.08
804.61	501.12	497.82	-12.79	-9.85	0.007	0.07
927.57	244.98	246.52	-27.57	-34.46	-0.052	0.15
1059.05	28.75	25.77	-9.38	-9.09	-0.019	0.21
1069.68	312.66	321.09	22.55	22.47	0.048	0.21
1106.47	5.52	4.95	-8.37	-8.84	-0.022	0.25
1125.52	11.52	11.28	4.11	4.77	0.005	0.10
1252.78	88.68	87.54	-0.07	1.73	0.006	0.32
1344.65	150.66	150.18	-6.39	-7.04	-0.016	0.23
1470.12	42.55	44.05	0.73	0.77	0.008	1.06
3024.87	20.22	21.53	1.64	1.53	0.003	0.16
3068.24	22.58	23.21	-1.07	-1.00	0.008	0.84
3115.60	14.50	14.02	0.34	0.37	-0.007	1.79

represents a suitable benchmark for the new approach introduced in Ref. 30 and discussed in the present work.

VI. CONCLUSIONS

One of the main goals of the paper has been to provide rigorous basis for the development of the NVPT approach to VCD. In this context, the complete adiabatic approach proposed by Nafie¹⁹ was adopted in previous study³⁰ as starting point, where the electron-nuclear wave function is approximated as a single product of a (nuclear) vibrational contribution and an electronic term. In particular, such electronic term contains corrections to the BO state which are first-order in the nuclear velocity. In the present work, we make this idea *exact*, in the sense that the starting point is not an approximate factorized form of the full wave function. The starting point is provided by the exact factorization of the electron-nuclear wave function, where approximations are inserted at a later stage in order to make numerical calculations feasible. The method outlined here can thus be seen as a rigorous basis for NVPT: at the first stage of the derivation, we describe how to recover the BO working equation from the exact electronic equation and at the second stage, a perturbation to BO is considered. Also, this perturbation does not rely on the use of the nuclear velocity as small parameter, in fact such parameter is, more generally, related to the spatial variations of the nuclear wave function from the factorization. Only in the classical limit, at $O(\hbar^0)$, these variations lead to an interpretation in terms of nuclear velocity. In the new approach presented here, a full quantum picture can be maintained, without invoking the classical approximation.

The second main result confirms the importance of using the exact factorization as starting point for the development of approximations. The time-dependent vector potential of the theory naturally appears in the observables, i.e., the current and the magnetic dipole moment, necessary for the calculation of the VCD spectrum. Therefore, within the perturbation approach presented in the paper, we have evaluated the vector potential using the harmonic approximation for the nuclear motion. In this case, the contribution has been shown to be small, but only further investigation, for instance in the context of non-adiabatic molecular dynamics, will clarify the actual extent of non-adiabatic corrections to the VCD signal. Also, situations where the non-adiabatic couplings are important shall be investigated, for instance for low-lying excited states,⁸⁵ where the exact factorization approach offers a strategy to overcome the limitations of BO approximation in a rigorous way.

According to the procedure presented in this work, NVPT is suitable for an implementation in any *ab initio* molecular dynamics code. Therefore, NVPT can be easily employed for the study of VCD properties of chiral molecules in solutions and for direct comparison with experimental data. Such procedure allows also to evaluate the corrections due the vector potential from the exact factorization approach. As it requires a DFPT calculation for each geometry sampled by the molecular dynamics trajectory, the numerical cost of a NVPT calculation is slightly larger than standard BO molecular dynamics but indeed feasible.

ACKNOWLEDGMENTS

The authors would like to thank Axel Schild for his help in improving the presentation of the paper. Partial support from the Deutsche Forschungsgemeinschaft (Grant No. SFB 762) and from the European Commission (Grant No. FP7-NMP-CRONOS) is gratefully acknowledged.

APPENDIX: INVARIANCE UNDER CHOICE OF THE ORIGIN

One of the main problems connected to the evaluation of molecular properties and spectroscopies depending on the magnetic field is to assure origin invariance of the final results. In case of VCD, this requires the evaluation of the electric and magnetic dipole moments, or accordingly, the APT and the AAT. While the APT shows no origin dependency, the exact AAT transforms under shifts of the origin $\mathbf{O} = \mathbf{O}' + \Delta$ as

$$\mathcal{M}_{\alpha\beta}^{vO} = \mathcal{M}_{\alpha\beta}^{vO'} - \sum_{\gamma\delta} \frac{1}{2c} \epsilon_{\beta\gamma\delta} \Delta_\gamma \mathcal{P}_{\alpha\delta}^v. \quad (\text{A1})$$

The rotational strength as a physical observable is gauge invariant,

$$R_k = \sum_{\alpha\alpha'\beta} \sum_{vv'} \mathcal{P}_{\alpha\beta}^v \mathcal{M}_{\alpha'\beta}^{v'O'} S_{\alpha'k}^{v'} S_{\alpha'k}^{v'} - \sum_{\alpha\alpha'\beta\gamma\delta} \sum_{vv'} \frac{1}{2c} \epsilon_{\beta\gamma\delta} \Delta_\gamma \mathcal{P}_{\alpha\beta}^v \mathcal{P}_{\alpha'\delta}^{v'} S_{\alpha'k}^{v'} S_{\alpha'k}^{v'}, \quad (\text{A2})$$

since the second terms constitute triple products containing two identical vectors.

The evaluation of origin dependent operators under periodic boundary conditions has been extensively discussed in the literature.^{86–88} A convenient approach is the combination of statewise origins with maximally localized Wannier orbitals, which has been applied successfully to the calculation of nuclear magnetic resonance chemical shifts.^{89,90} The canonical ϕ_o and localized φ_o states are mutually related via the unitary transformation for the unperturbed ground-state orbitals,

$$|\varphi_o\rangle = \sum_{o'} U_{oo'}^{(0)} |\phi_{o'}\rangle. \quad (\text{A3})$$

This approach is based on the natural assumption that the response orbitals are sufficiently localized in the region of their respective unperturbed ground-state orbitals. In the distributed origin (DO) gauge, the position operators are calculated with the corresponding Wannier center as its statewise origin,

$$\mathbf{r}_o = \langle \varphi_o | \hat{\mathbf{r}} | \varphi_o \rangle. \quad (\text{A4})$$

The electronic AAT in a statewise DO gauge then is given by

$$(I_{\alpha\beta}^v)_o = \frac{e}{mc} \langle \varphi_o | (\hat{\mathbf{r}}_\gamma - r_{o\gamma}) \hat{p}_\delta \epsilon_{\beta\gamma\delta} | \varphi_{o,(v,\alpha)}^{(1)} \rangle \quad (\text{A5})$$

and can be translated back to the common origin form via

$$I_{\alpha\beta}^{vO} = \sum_o (I_{\alpha\beta}^v)_o + \sum_{o\gamma\delta} \frac{1}{2c} \epsilon_{\beta\gamma\delta} (r_{o\gamma} - O_\gamma) \mathcal{E}_{\alpha\delta}^{vO}, \quad (\text{A6})$$

where $\mathcal{E}_{\alpha o}^{\nu o}$ is the contribution of the state o to the electronic APT. The numerical results in a supercell calculation are the same for canonical and Wannier orbitals.³⁰

- ¹L. A. Nafie, *Annu. Rev. Phys. Chem.* **48**, 357 (1997).
- ²G. Magyarfalvi, G. Tarczay, and E. Vass, *Wiley Interdiscip. Rev.: Comput. Mol. Sci.* **1**, 403 (2011).
- ³L. A. Nafie, *Vibrational Optical Activity. Principles and Applications*, 1st ed. (John Wiley & Sons Ltd., 2011).
- ⁴J. Bloino and V. Barone, *J. Chem. Phys.* **136**, 124108 (2012).
- ⁵C. Cappelli, J. Bloino, F. Lipparini, and V. Barone, *J. Phys. Chem. Lett.* **3**, 1766–1773 (2012).
- ⁶K. Ruud, *Comprehensive Chiroptical Spectroscopy: Instrumentation, Methodologies, and Theoretical Simulations* (John Wiley & Sons, 2012), Vol. 1, p. 699.
- ⁷G. Holzwarth and I. Chabay, *J. Chem. Phys.* **57**, 1632 (1972).
- ⁸P. Stephens and F. Devlin, *Chirality* **12**, 172 (2000).
- ⁹P. J. Stephens, F. J. Devlin, C. F. Chabalowski, and M. J. Frisch, *J. Phys. Chem.* **98**, 11623 (1994).
- ¹⁰J. A. Schellman, *J. Chem. Phys.* **58**, 2882 (1973); **60**, 343 (1974).
- ¹¹J. Snir, R. A. Frankel, and J. A. Schellman, *Biopolymers* **14**, 173 (1975).
- ¹²E. B. Wilson, Jr., J. C. Decius, and P. C. Cross, *Molecular Vibrations: The Theory of Infrared and Raman Vibrational Spectra*, 1st ed. (McGraw-Hill, New York, 1955).
- ¹³T. R. Faulkner, C. Marcott, A. Moscovitz, and J. Overend, *J. Am. Chem. Soc.* **99**, 8160 (1977).
- ¹⁴D. P. Craig and T. Thirunamachandran, *Mol. Phys.* **35**, 825 (1978).
- ¹⁵T. A. Keiderling and P. J. Stephens, *J. Am. Chem. Soc.* **99**, 8061 (1977).
- ¹⁶L. A. Nafie and T. H. Walnut, *Chem. Phys. Lett.* **49**, 441 (1977).
- ¹⁷A. D. Buckingham, P. W. Fowler, and P. A. Galwas, *Chem. Phys.* **112**, 1 (1978).
- ¹⁸L. A. Nafie and T. B. Freedman, *J. Chem. Phys.* **78**, 7108 (1983).
- ¹⁹L. A. Nafie, *J. Chem. Phys.* **79**, 4950 (1983).
- ²⁰P. J. Stephens, *J. Phys. Chem.* **89**, 748 (1985).
- ²¹L. A. Nafie, *J. Chem. Phys.* **96**, 5687 (1992).
- ²²M. Born and R. J. Oppenheimer, *Ann. Phys.* **389**, 457 (1927).
- ²³L. A. Nafie, *J. Phys. Chem. A* **101**, 7826 (1997).
- ²⁴T. B. Freedman, M.-L. Shih, E. Lee, and L. A. Nafie, *J. Am. Chem. Soc.* **119**, 10620 (1997).
- ²⁵T. B. Freedman, X. Gao, M.-L. Shih, and L. A. Nafie, *J. Phys. Chem. A* **102**, 3352 (1998).
- ²⁶I. Barth, H.-C. Hege, H. Ikeda, A. Kenfack, M. Koppitz, J. Manz, F. Marquardt, and G. K. Paramonov, *Chem. Phys. Lett.* **481**, 118 (2009).
- ²⁷H.-C. Hege, J. Manz, F. Marquardt, B. Paulus, and A. Schild, *Chem. Phys.* **376**, 46 (2010).
- ²⁸D. Andrae, I. Barth, T. Bredtmann, H.-C. Hege, J. Manz, F. Marquardt, and B. Paulus, *J. Phys. Chem. B* **115**, 5476 (2011).
- ²⁹S. Patchkovskii, *J. Chem. Phys.* **137**, 084109 (2012).
- ³⁰A. Scherrer, R. Vuilleumier, and D. Sebastiani, *J. Chem. Theory Comput.* **9**, 5305 (2013).
- ³¹A. Abedi, N. T. Maitra, and E. K. U. Gross, *Phys. Rev. Lett.* **105**, 123002 (2010).
- ³²A. Abedi, N. T. Maitra, and E. K. U. Gross, *J. Chem. Phys.* **137**, 22A530 (2012).
- ³³A. Abedi, F. Agostini, Y. Suzuki, and E. K. U. Gross, *Phys. Rev. Lett.* **110**, 263001 (2013).
- ³⁴F. Agostini, A. Abedi, Y. Suzuki, and E. K. U. Gross, *Mol. Phys.* **111**, 3625 (2013).
- ³⁵F. Agostini, A. Abedi, Y. Suzuki, S. K. Min, N. T. Maitra, and E. K. U. Gross, *J. Chem. Phys.* **142**, 084303 (2015).
- ³⁶Y. Suzuki, A. Abedi, N. T. Maitra, K. Yamashita, and E. K. U. Gross, *Phys. Rev. A* **89**, 040501(R) (2014).
- ³⁷Y. Suzuki, A. Abedi, N. T. Maitra, and E. K. U. Gross, e-print [arXiv:1506.04070](https://arxiv.org/abs/1506.04070) [physics.chem-ph].
- ³⁸N. I. Gidopoulos and E. K. U. Gross, *Philos. Trans. R. Soc., A* **372**, 20130059 (2014); e-print [arXiv:cond-mat/0502433](https://arxiv.org/abs/cond-mat/0502433) [cond-mat.mtrl-sci].
- ³⁹L. D. Barron, *Molecular Light Scattering and Optical Activity* (Cambridge University Press, 2004), Vol. 2, p. 443.
- ⁴⁰D. J. Caldwell and H. J. Eyring, *Theory of Optical Activity (Monographs on Chemistry)* (John Wiley & Sons, Inc., 1971), Vol. 1, p. 254.
- ⁴¹R. Kubo, M. Toda, and N. Hashitsume, *Statistical Physics II: Nonequilibrium Statistical Mechanics*, Springer Series in Solid-State Sciences Vol. 1 (Springer, 1985).
- ⁴²R. G. Gordon, *J. Chem. Phys.* **43**, 1307 (1965).
- ⁴³D. A. McQuarrie, *Statistical Mechanics* (University Science Books, 1976).
- ⁴⁴J. Frenkel, *Wave Mechanics* (Clarendon, Oxford, 1934).
- ⁴⁵J. L. Alonso, J. Clemente-Gallardo, P. Echeniche-Robba, and J. A. Jover-Galtier, *J. Chem. Phys.* **139**, 087101 (2013).
- ⁴⁶A. Abedi, N. T. Maitra, and E. K. U. Gross, *J. Chem. Phys.* **139**, 087102 (2013).
- ⁴⁷S. K. Ghosh and A. K. Dhara, *Phys. Rev. A* **38**, 1149 (1988).
- ⁴⁸E. Runge and E. K. U. Gross, *Phys. Rev. Lett.* **52**, 997 (1984).
- ⁴⁹S. K. Min, A. Abedi, K. S. Kim, and E. K. U. Gross, *Phys. Rev. Lett.* **113**, 263004 (2014).
- ⁵⁰This choice of gauge is in general not possible. For instance, when the electronic state is degenerate or when the electronic wave function has singularities in the parameter space, $\mathbf{R} \cdot \varphi_{\mathbf{R}}^{(0)}(\mathbf{r})$ cannot be real and thus the vector potential might be non-zero.
- ⁵¹N. C. Handy, Y. Yamaguchi, and H. F. Schaefer III, *J. Chem. Phys.* **84**, 4481 (1986).
- ⁵²E. F. Valeev and C. D. Sherrill, *J. Chem. Phys.* **118**, 3921 (2003).
- ⁵³A. Tajti, P. G. Szalay, and J. Gauss, *J. Chem. Phys.* **127**, 014102 (2007).
- ⁵⁴A. Abedi, F. Agostini, and E. K. U. Gross, *Europhys. Lett.* **106**, 33001 (2014).
- ⁵⁵F. Agostini, A. Abedi, and E. K. U. Gross, *J. Chem. Phys.* **141**, 214101 (2014).
- ⁵⁶S. K. Min, F. Agostini, and E. K. U. Gross, *Phys. Rev. Lett.* **115**, 073001 (2015).
- ⁵⁷J. H. van Vleck, *Proc. Natl. Acad. Sci. U. S. A.* **14**, 178 (1928).
- ⁵⁸F. Agostini, S. K. Min, and E. K. U. Gross, *Ann. Phys.* (published online 2015).
- ⁵⁹J. C. Tully, *J. Chem. Phys.* **93**, 1061 (1990).
- ⁶⁰N. L. Doltsinis and D. Marx, *Phys. Rev. Lett.* **88**, 166402 (2002).
- ⁶¹E. Tapavicza, I. Tavernelli, and U. Rothlisberger, *Phys. Rev. Lett.* **98**, 023001 (2007).
- ⁶²C. Hu, H. Hirai, and O. Sugino, *J. Chem. Phys.* **127**, 064103 (2007).
- ⁶³V. Chernyak and S. Mukamel, *J. Chem. Phys.* **112**, 3572 (2000).
- ⁶⁴R. Baer, *Chem. Phys. Lett.* **364**, 75 (2002).
- ⁶⁵I. Tavernelli, E. Tapavicza, and U. Rothlisberger, *J. Chem. Phys.* **130**, 124107 (2009).
- ⁶⁶I. Tavernelli, B. F. E. Curchod, and U. Rothlisberger, *J. Chem. Phys.* **131**, 196101 (2009).
- ⁶⁷I. Tavernelli, B. F. E. Curchod, A. Laktionov, and U. Rothlisberger, *J. Chem. Phys.* **133**, 194104 (2010).
- ⁶⁸Q. Ou, S. Fatehi, E. Alguire, Y. Shao, and J. E. Subotnik, *J. Chem. Phys.* **141**, 024114 (2014).
- ⁶⁹P. Hohenberg and W. Kohn, *Phys. Rev.* **136**, 864 (1964).
- ⁷⁰W. Kohn and L. J. Sham, *Phys. Rev.* **140**, 1133 (1965).
- ⁷¹R. O. Jones and O. Gunnarsson, *Rev. Mod. Phys.* **61**, 689 (1989).
- ⁷²A. D. Becke, *Phys. Rev. A* **38**, 3098 (1988).
- ⁷³C. Lee, W. Yang, and R. G. Parr, *Phys. Rev. B* **37**, 785 (1988).
- ⁷⁴X. Gonze, *Phys. Rev. A* **52**, 1086 (1995).
- ⁷⁵X. Gonze, *Phys. Rev. A* **52**, 1096 (1995).
- ⁷⁶A. Putrino, D. Sebastiani, and M. Parrinello, *J. Chem. Phys.* **113**, 7102 (2000).
- ⁷⁷S. Baroni, S. de Gironcoli, A. dal Corso, and P. Giannozzi, *Rev. Mod. Phys.* **73**, 515 (2001).
- ⁷⁸T. Watermann, A. Scherrer, and D. Sebastiani, in *Many-Electron Approaches in Physics, Chemistry and Mathematics*, Mathematical Physics Studies, edited by V. Bach and L. Delle Site (Springer International Publishing, 2014), pp. 97–110.
- ⁷⁹R. M. Sternheimer, *Phys. Rev.* **96**, 951 (1954).
- ⁸⁰See <http://www.cpmc.org/> for CPMD-3.15.3, Copyright IBM Corp. 1990–2008, Copyright MPI für Festkörperforschung Stuttgart 1997–2001.
- ⁸¹N. Troullier and J. L. Martins, *Phys. Rev. B* **43**, 1993 (1991).
- ⁸²M. J. Frisch, G. W. Trucks, H. B. Schlegel, G. E. Scuseria, M. A. Robb, J. R. Cheeseman, G. Scalmani, V. Barone, B. Mennucci, G. A. Petersson, H. Nakatsuji, M. Caricato, X. Li, H. P. Hratchian, A. F. Izmaylov, J. Bloino, G. Zheng, J. L. Sonnenberg, M. Hada, M. Ehara, K. Toyota, R. Fukuda, J. Hasegawa, M. Ishida, T. Nakajima, Y. Honda, O. Kitao, H. Nakai, T. Vreven, J. A. Montgomery, Jr., J. E. Peralta, F. Ogliaro, M. Bearpark, J. J. Heyd, E. Brothers, K. N. Kudin, V. N. Staroverov, R. Kobayashi, J. Normand, K. Raghavachari, A. Rendell, J. C. Burant, S. S. Iyengar, J. Tomasi, M. Cossi, N. Rega, J. M. Millam, M. Klene, J. E. Knox, J. B. Cross, V. Bakken, C. Adamo, J. Jaramillo, R. Gomperts, R. E. Stratmann, O. Yazyev, A. J. Austin,

- R. Cammi, C. Pomelli, J. W. Ochterski, R. L. Martin, K. Morokuma, V. G. Zakrzewski, G. A. Voth, P. Salvador, J. J. Dannenberg, S. Dapprich, A. D. Daniels, Ö. Farkas, J. B. Foresman, J. V. Ortiz, J. Cioslowski, and D. J. Fox, GAUSSIAN 09, Revision D.01, Gaussian, Inc., Wallingford, CT, 2009.
- ⁸³R. A. Kendall, T. H. Dunning, and R. J. Harrison, *J. Chem. Phys.* **96**, 6796 (1992).
- ⁸⁴The blue arrows are the velocities of the corresponding modes, i.e., removing the mass weighting of the eigenvectors.
- ⁸⁵L. A. Nafie, *J. Phys. Chem. A* **108**, 7222 (2004).
- ⁸⁶R. Resta, *Rev. Mod. Phys.* **66**, 899 (1994).
- ⁸⁷R. Resta, *J. Phys.: Condens. Matter* **22**, 123201 (2010).
- ⁸⁸L. A. Nafie, *Vibrational Optical Activity: Principles and Applications* (Wiley, 2011), pp. 105–108.
- ⁸⁹G. Berghold, C. J. Mundy, A. H. Romero, J. Hutter, and M. Parrinello, *Phys. Rev. B* **61**, 1049611 (2000).
- ⁹⁰D. Sebastiani and M. Parrinello, *J. Phys. Chem. A* **105**, 1951 (2001).

2.3 IMPLEMENTATION OF THE NUCLEAR VELOCITY PERTURBATION THEORY

Apart from the rigorous derivation of the nuclear velocity perturbation theory (NVPT), also the first successful implementation of the NVPT within a large-scale electronic structure program package has been reported in the course of this work.¹³⁹

We have chosen a plane wave electronic structure code (CPMD) in order to support vibrational circular dichroism (VCD) calculations in large-scale systems such as solvated (bio)molecules and supramolecular assemblies. Technical details of the implementation are discussed in section 1.2 and in the following. The starting point of the NVPT calculation is the Born-Oppenheimer wave function $\varphi_{\mathbf{R}}^{(0)}(\mathbf{r})$ in eq. (2.2.34). Two different applications of VCD have to be distinguished, the static and the dynamical picture.

In the static picture, the calculation of the normal modes q_k requires to work at the equilibrium geometry \mathbf{R}_0 . The calculation of the NVPT does not require to be at the equilibrium geometry. This allows to combine normal mode calculations of other programs or levels of theory, e.g. using the CP2K package.^{267,268} The NVPT then provides the atomic polar and atomic axial tensor, which together with the normal modes yield the dipole D_k and rotational R_k strengths in the double harmonic approximation.

The calculation of dynamical, ab-initio molecular dynamics based spectra is discussed in section 3.2. In this case, only the current $\dot{\boldsymbol{\mu}}(t)$ and magnetic $\mathbf{m}(t)$ dipole moments are needed. These can be obtained by projection of the nuclear velocity on the atomic polar and axial tensors. However, this projection on the nuclear velocity $\dot{\mathbf{R}}(t)$ can also be done already before the NVPT calculation, as discussed in section 3.2.

The calculation of the NVPT correction requires two subsequent perturbation calculations. First, the gradient of the electronic wave function $\phi_o^{(\mathbf{R})}(\mathbf{r})$ with respect to the nuclear positions \mathbf{R} has to be calculated for all nuclei that are to be moved. This nuclear nuclear displacement perturbation (NDP) is described in section 1.1.4. For a calculation of the atomic tensors, this has to be done for one nucleus ν and one Cartesian component α at a time, resulting in altogether $3N_n$ self-consistent response calculations R_{α}^{ν} . If the projection is already done before the perturbation calculation at the level of the perturbation Hamiltonian, only one self-consistent perturbation calculation is required. As discussed in section 1.4.4, this is one of the main advantages of the NVPT over the magnetic field perturbation theory.

The gradient of the BO electronic wave function $\phi_o^{(\mathbf{R})}(\mathbf{r})$, obtained via the NDP calculations, is used as the right hand side of eq. (2.2.35) in the second non self-consistent Sternheimer calculation of the nuclear velocity perturbation (NVP) correction $\varphi_o^{(1)}(\mathbf{r})$. Since the NVP correction is purely imaginary, the linear order density response vanishes analytically and there is no need to solve the Sternheimer equation self-consistently. On the implementational level, the wave function gradient is passed as the non-local part of the perturbation Hamiltonian whereas the local part is set to zero.

Since both, the NDP and the NVP, are well defined also under periodic boundary conditions, the perturbation calculation can be done in the canonical Kohn-Sham (KS) basis. As described in section 1.3, only the calculation of the expectation values requires a change of representation to maximally localized Wannier orbitals (MLWO). The transformation matrix $U^{(0)}$ is calculated from the unperturbed KS orbitals and is applied to the unperturbed-, the NDP- and the NVP wave functions. With the localized wave functions, it is possible to take the expectation values of the electric dipole moment operator $\hat{\boldsymbol{\mu}}$ with the NDP wave function and of the current $\hat{\boldsymbol{\mu}}$ and magnetic $\hat{\mathbf{m}}$ dipole moment operators with the NVP wave function.

As described in section 1.4.4, the NDP yields the electric dipole moment derivative, i.e. the atomic polar tensor (APT) in the position form, and the NVP yields the current dipole moment and magnetic dipole moment derivatives, i.e. the APT in the velocity form and the atomic axial tensor (AAT). For the evaluation of the momentum operator $\hat{\mathbf{p}}$, occurring in both, the current and the magnetic dipole moment operator, it is necessary to explicitly evaluate the commutator of the position operator with the Hamiltonian. The commutator is split in its local part, which is evaluated as the electronic gradient in reciprocal space, and the non-local part, which is explicitly evaluated as a commutator.

The application of the position operator $\hat{\mathbf{r}}$ under periodic boundary conditions is done with respect to the corresponding Wannier centers \mathbf{r}_o as described in section 1.3. Using the translational relations of the magnetic dipole moment or the AAT, the state wise contributions to the expectation value of the origin dependent magnetic observables can be translated in a common origin gauge. In condensed phase systems, a common origin cannot be defined and strategies to circumvent this problem are discussed in sections 1.3, 3.2 and 3.3. For molecules that do not extend over the whole cell, it is always possible to translate the gauge of all contributing MLWO and nuclei to a common origin, e.g. the molecular center of mass.

The implementation has been tested extensively with small rigid molecules. As a reference, we have chosen an existing implementation^{34,168,269} of the magnetic field perturbation theory, which employs a Gaussian basis set. Both theories are found to be in excellent agreement. Regarding numerical aspects, the results are analyzed for their correct origin dependence and gauge invariance of the physical observables. A useful property for the comparison of the atomic tensors are the translational and rotational sum rule connections between them. We find the APT position and velocity form to be equivalent in the basis set limit. For a consistent transformation of gauge origins, the APT in the velocity form should be used. Further technical aspects concerning the use of non-local pseudopotentials with moving nuclei are treated in section 3.4.

Nuclear Velocity Perturbation Theory of Vibrational Circular Dichroism

A. Scherrer,^{†,‡,§} R. Vuilleumier,^{*,†,‡} and D. Sebastiani^{*,§}

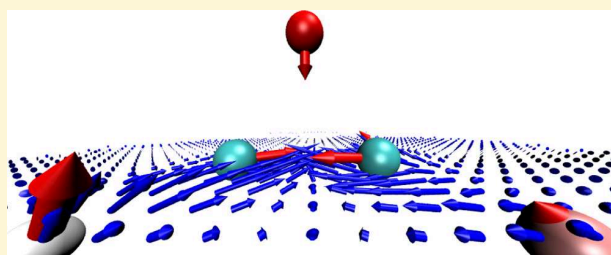
[†]UMR 8640 ENS-CNRS-UPMC, Département de Chimie, 24 rue Lhomond, École Normale Supérieure, 75005 Paris, France

[‡]UPMC Université Paris 06, 4, Place Jussieu, 75005 Paris, France

[§]Institute of Chemistry, Martin-Luther-Universität Halle-Wittenberg, von-Danckelmann-Platz 4, 06120 Halle (Saale), Germany

Supporting Information

ABSTRACT: We report the first implementation of vibrational circular dichroism (VCD) within density functional theory (DFT) using the nuclear velocity perturbation (NVP) theory. In order to support VCD calculations in large-scale systems such as solvated (bio)molecules and supramolecular assemblies, we have chosen a plane-wave electronic structure code (CPMD). This implementation allows the incorporation of fully anharmonic effects in VCD spectra on the basis of ab initio molecular dynamics simulations. On the conceptual level, we compare our NVP results for rigid molecules with an existing implementation based on the magnetic field perturbation (MFP) technique using a Gaussian basis set and find an excellent agreement. Regarding numerical aspects, we analyze our results for their correct origin dependence and gauge invariance of the physical observables. The correlation with experimental data is very satisfactory, with certain deviations mainly due to the level of electronic structure theory used.



1. INTRODUCTION

Vibrational circular dichroism (VCD) describes the response of chiral molecules to left and right circularly polarized radiation in the infrared (IR) range. For enantiomers, the VCD spectrum shows the same intensities but has opposite signs. VCD spectroscopy is a widely used tool for the determination of the absolute configuration of chiral molecules.^{1–4} Its application range comprises, in particular, most biomolecules (as, e.g., polypeptides). Because of its intrinsic connection to the underlying molecular structure, VCD is one of the most structurally sensitive spectroscopic techniques available.

The ab initio calculation of VCD has proven to successfully predict experimentally observable spectra.^{3–5} Its presently most applied form is the magnetic field perturbation theory (MFP),⁶ which is implemented in the Gaussian^{7,8} and, e.g., more recently, in the ADF⁹ packages.

An alternative theory of VCD was proposed theoretically by Nafie. He showed that the calculation of the required magnetic transition dipole moment needs non-Born–Oppenheimer contribution in the wave functions.^{10,11} In the nuclear velocity perturbation theory (NVP),^{12–14} this is achieved by the perturbative calculation of the complete adiabatic (CA) correction to the Born–Oppenheimer ground-state orbitals.^{15–18} This provides a closely related yet conceptually different route for the calculation of VCD spectra. In particular, this allows for an efficient calculation of molecular dynamics-based VCD spectra. However, to this day, no successful implementation of the NVP-theory of VCD has been reported.¹⁹

It is known that the VCD spectrum is highly sensitive to configurational changes and solvation effects.^{20–23} Theoretically, this has been addressed by incorporating anharmonicities and implicit or explicit solvent models.^{24–26} However, the influence of hydrogen bonding solvents is known to require the consideration of explicit solvents beyond the harmonic approximation.²⁷ Furthermore, the increasing interest in VCD spectra for large-scale systems such as biomolecules has given rise to various fragmentation based approaches.^{20,28–30} Both problems can naturally be addressed by our extension of the ab initio theory of VCD to extended systems.

In this work, we report the first implementation of the NVP theory of VCD. After revising the basic constituents of the harmonic VCD theory, we present a reformulation of Nafie's NVP theory within density functional theory (DFT)^{31–33} using linear order density functional perturbation theory (DFPT).^{34–39} The resulting expressions are implemented and numerically analyzed for their correct origin dependence and gauge invariance. The implementation is based on the plane-wave electronic structure code CPMD,⁴⁰ allowing for ab initio VCD calculations of extended systems such as solvated (bio)molecules and supramolecular assemblies. We compare our NVP results with an existing MFP implementation using Gaussian basis sets and find an excellent agreement of the harmonic spectra.

Received: August 7, 2013

Published: October 17, 2013

2. METHOD

2.1. Constituents of VCD Theory. The experimentally observable vibrational absorption intensities are theoretically accessible by the involved transition dipole moments. In the harmonic approximation, the dipole and rotational strengths for the $g_0 \rightarrow g_1$ vibrational transition in the electronic ground-state are given as

$$D_m^{(r)} = \text{Re}[\langle \hat{\mu} \rangle_m \cdot \langle \hat{\mu} \rangle_m] \quad (1)$$

$$R_m^{(r)} = \text{Im}[\langle \hat{\mu} \rangle_m \cdot \langle \hat{\mathbf{m}} \rangle_m] \quad (2)$$

$$D_m^{(v)} = \text{Re}[\langle \hat{\mu} \rangle_m \cdot \langle \hat{\mu} \rangle_m] \omega_m^{-2} \quad (3)$$

$$R_m^{(v)} = \text{Im}[\langle \hat{\mu} \rangle_m \cdot \langle \hat{\mathbf{m}} \rangle_m] \omega_m^{-1} \quad (4)$$

where (r) denotes the position and (v) the velocity form of the dipole and rotational strengths D and R , and the brackets $\langle \cdot \rangle$ represent the transition matrix element $g_0 \rightarrow g_1$ of the vibrational mode m with frequency ω_m . The electronic and magnetic dipole moments are composed of electronic and nuclear contributions:

$$\hat{\mu} = \hat{\mu}^e + \hat{\mu}^n \quad (5)$$

$$= -\sum_j e\hat{\mathbf{r}}_j + \sum_\lambda eZ^\lambda \hat{\mathbf{R}}^\lambda \quad (6)$$

$$\hat{\mathbf{m}} = \hat{\mathbf{m}}^e + \hat{\mathbf{m}}^n \quad (7)$$

$$= -\sum_j \frac{e}{2c} \hat{\mathbf{r}}_j \times \hat{\mathbf{r}}_j + \sum_\lambda \frac{eZ^\lambda}{2c} \hat{\mathbf{R}}^\lambda \times \hat{\mathbf{R}}^\lambda \quad (8)$$

where the summation runs over all electronic states (j) and atoms (λ). In eqs 3 and 4, $\langle \hat{\mu} \rangle$ represents the total current,

$$\hat{\mu} = \hat{\mu}^e + \hat{\mu}^n \quad (9)$$

$$= -\sum_j e\hat{\mathbf{r}}_j + \sum_\lambda eZ^\lambda \hat{\mathbf{R}}^\lambda \quad (10)$$

and eq 3 corresponds to a current–current correlation. Equations 1–4 are valid in the absence of quadrupole contributions. This condition is fulfilled in the isotropic rotational ensemble average.⁴¹ The meaning of the time derivatives $\hat{\mathbf{r}}$ and $\hat{\mathbf{R}}$, as well as derivations, with respect to $\hat{\mathbf{R}}$, will be clarified later.

The electronic and magnetic transition dipole moments arise due to the vibrational motion of the nuclei in the respective normal modes. They are related to the vibrational nuclear displacements via the total Atomic Polar Tensor \mathcal{P}^λ (APT) and the Atomic Axial Tensor \mathcal{M}^λ (AAT)

$$\mathcal{P}_{\alpha\beta}^\lambda = \mathcal{E}_{\alpha\beta}^\lambda + \mathcal{N}_{\alpha\beta}^\lambda \quad (11)$$

$$\mathcal{M}_{\alpha\beta}^\lambda = \mathcal{I}_{\alpha\beta}^\lambda + \mathcal{J}_{\alpha\beta}^\lambda \quad (12)$$

which have the following electronic (e) and nuclear (n) constituents:¹⁹

$$\mathcal{E}_{\alpha\beta}^{\lambda(r)} = \frac{\partial \langle \hat{\mu}_\beta^e \rangle}{\partial R_\alpha^\lambda} \quad (13)$$

$$\mathcal{E}_{\alpha\beta}^{\lambda(v)} = \frac{\partial \langle \hat{\mu}_\beta^e \rangle}{\partial \dot{R}_\alpha^\lambda} \quad (14)$$

$$\mathcal{I}_{\alpha\beta}^\lambda = \frac{\partial \langle \hat{m}_\beta^e \rangle}{\partial \dot{R}_\alpha^\lambda} \quad (15)$$

$$\mathcal{N}_{\alpha\beta}^{\lambda(r)} = \frac{\partial \langle \hat{\mu}_\beta^n \rangle}{\partial R_\alpha^\lambda} = eZ^\lambda \delta_{\alpha\beta} \quad (16)$$

$$\mathcal{N}_{\alpha\beta}^{\lambda(v)} = \frac{\partial \langle \hat{\mu}_\beta^n \rangle}{\partial \dot{R}_\alpha^\lambda} = eZ^\lambda \delta_{\alpha\beta} \quad (17)$$

$$\mathcal{J}_{\alpha\beta}^\lambda = \frac{\partial \langle \hat{m}_\beta^n \rangle}{\partial \dot{R}_\alpha^\lambda} = \frac{eZ^\lambda}{2c} \sum_\gamma \varepsilon_{\alpha\beta\gamma} R_\gamma^\lambda \quad (18)$$

In the harmonic approximation, the expectation value for the nuclear contributions is taken classically which yields the analytical expressions given in eqs 16–18. The electronic contributions require a quantum mechanical expectation value that must be computed numerically. The involved dipole operators for the electronic degrees of freedom are

$$\hat{\mu}^e = -e\hat{\mathbf{r}} \quad (19)$$

$$\hat{\mu}^n = -e\hat{\mathbf{r}} \quad (20)$$

$$\hat{\mathbf{m}}^e = -\frac{e}{2c} \hat{\mathbf{r}} \times \hat{\mathbf{r}} \quad (21)$$

where the velocity operator is

$$\hat{\mathbf{r}} = \frac{i}{\hbar} [\hat{\mathbf{H}}^e, \hat{\mathbf{r}}] \quad (22)$$

Using Einstein's summation convention for repeated Greek indices, the dipole and rotational strengths of the m th normal mode in the position and the velocity form are

$$D_m^{(r)} = \mathcal{P}_{\alpha\beta}^{\lambda(r)} \mathcal{P}_{\alpha'\beta}^{\lambda'(r)} S_{\alpha m}^\lambda S_{\alpha' m}^{\lambda'} \quad (23)$$

$$R_m^{(r)} = \mathcal{P}_{\alpha\beta}^{\lambda(r)} \mathcal{M}_{\alpha'\beta}^{\lambda'(r)} S_{\alpha m}^\lambda S_{\alpha' m}^{\lambda'} \quad (24)$$

$$D_m^{(v)} = \mathcal{P}_{\alpha\beta}^{\lambda(v)} \mathcal{P}_{\alpha'\beta}^{\lambda'(v)} S_{\alpha m}^\lambda S_{\alpha' m}^{\lambda'} \quad (25)$$

$$R_m^{(v)} = \mathcal{P}_{\alpha\beta}^{\lambda(v)} \mathcal{M}_{\alpha'\beta}^{\lambda'(v)} S_{\alpha m}^\lambda S_{\alpha' m}^{\lambda'} \quad (26)$$

The Cartesian displacement vector S_m^λ describes the displacement of nucleus λ in direction α due to the m th normal mode (Q_m):

$$S_{\alpha m}^\lambda = \left. \frac{\partial R_\alpha^\lambda}{\partial Q_m} \right|_{Q=0} = \left. \frac{\partial \dot{R}_\alpha^\lambda}{\partial \dot{Q}_m} \right|_{\dot{Q}=0} \quad (27)$$

2.2. Nuclear Velocity Perturbation in DFPT. By construction, the Born–Oppenheimer ground-state wave function does not contain the nuclear momentum information necessary for the calculation of electronic fluxes. This, in turn, is needed for the calculation of the magnetic transition dipole moment of a molecular system as required by the theory of VCD. In the literature, there are different perturbative approaches to address this problem, as outlined in the Introduction. In this work, the Nuclear Velocity Perturbation (NVP) approach, originally proposed theoretically by Nafie,¹³

is used. This requires the perturbative calculation of the complete adiabatic correction (CA) to the Born–Oppenheimer ground state. The following derivation of the NVP approach focuses on the implementation in the CPMD DFPT framework. For a detailed derivation, we refer the reader to the original theoretical works of Nafe or his recent book.^{10,11,13,19}

The idea of the NVP approach is to take into account the linear term of the adiabatic coupling, which can be formulated in condensed form as

$$\langle \Psi_k | [\hat{T}^n, \Psi_k] \rangle = \langle \Psi_k | \hat{T}^n | \Psi_k \rangle + \langle \Psi_k | -i\hbar \partial_{\mathbf{R}} | \Psi_k \rangle \cdot \dot{\mathbf{R}} \quad (28)$$

where \hat{T}^n is the nuclear kinetic energy operator, Ψ_k the total electronic wave function of state k . The linear term is taken as a perturbative correction to the electronic structure problem, i.e., a nuclear coordinate derivative is acting on the electronic degrees of freedom. This gives rise to an adiabatic imaginary correction to the Born–Oppenheimer ground-states, but leaves the electronic energy and, thus, the molecular dynamics unchanged. The resulting modified electronic structure problem is

$$(\mathcal{H}^e - E_k) |\Psi_k\rangle = i\hbar \dot{\mathbf{R}} \cdot \partial_{\mathbf{R}} |\Psi_k\rangle \quad (29)$$

which introduces a complex correction to the Born–Oppenheimer wave function. Separating real and imaginary part as adiabatic (A) and complete adiabatic (CA) contribution and developing to first order around \mathbf{R}_0 and $\dot{\mathbf{R}}_0 = 0$ gives the following Ansatz for the complex complete adiabatic wave function:

$$\tilde{\Psi}_k^{\text{CA}}(\mathbf{r}, \mathbf{R}, \dot{\mathbf{R}}) = \Psi_k^{\text{A}}(\mathbf{r}, \mathbf{R}) + i\Psi_k^{\text{CA}}(\mathbf{r}, \mathbf{R}, \dot{\mathbf{R}}) \quad (30)$$

$$= \Psi_k^{\text{A}}(\mathbf{r}, \mathbf{R}_0) + \Psi_k^{(\text{R})}(\mathbf{r}, \mathbf{R}_0) \cdot (\mathbf{R} - \mathbf{R}_0) + i\Psi_k^{(\text{R})}(\mathbf{r}, \mathbf{R}_0) \cdot \dot{\mathbf{R}} \quad (31)$$

where the superscripts in parentheses, (\mathbf{R}) and $(\dot{\mathbf{R}})$, denote partial derivatives with respect to the corresponding quantity, e.g., $\Psi_k^{(\text{R})} = \partial \Psi_k / \partial \mathbf{R}$. The real part of the adiabatic correction, i.e., the derivative with respect to a nuclear displacement \mathbf{R} , is accessible via DFPT calculation for a nuclear displacement perturbation.³⁸ As for the imaginary part, insertion of this Ansatz in eq 29 yields a Sternheimer-like equation, which can be solved iteratively:

$$(\mathcal{H}^e - E_k) \Psi_k^{(\text{R})} = \hbar \Psi_k^{(\text{R})} \quad (32)$$

In the framework of single-determinant theories such as DFT and DFPT,^{37,38} this relation directly translates to Kohn–Sham orbitals φ_o :

$$(\mathcal{H}_{\text{KS}}^{(0)} - \varepsilon_o^{(0)}) |\varphi_o^{(\text{R})}\rangle = \hbar |\varphi_o^{(\text{R})}\rangle \quad (33)$$

Since $i\varphi_o^{(\text{R})}$ is purely imaginary and does not change the electronic density, no self-consistent solution is required.

With this complete adiabatic correction (CA), it is possible to calculate the atomic tensors in the position and the velocity form. The electronic APT in the position and velocity form is

$$\begin{aligned} \mathcal{E}_{\alpha\beta}^{\lambda(r)} &= \sum_o \mathcal{E}_{\alpha\beta}^{\lambda o(r)} \\ &= \sum_o \partial_{\hat{\mathbf{R}}_a} \langle \varphi_o^{\text{CA}} | \hat{\mu}_\beta^e | \varphi_o^{\text{CA}} \rangle \\ &= -2e \sum_o \langle \varphi_o^{(0)} | \hat{r}_\beta | \varphi_o^{(\text{R}_a)} \rangle \end{aligned} \quad (34)$$

$$\begin{aligned} \mathcal{E}_{\alpha\beta}^{\lambda(v)} &= \sum_o \mathcal{E}_{\alpha\beta}^{\lambda o(v)} \\ &= \sum_o \partial_{\hat{\mathbf{R}}_a} \langle \varphi_o^{\text{CA}} | \hat{\mu}_\beta^e | \varphi_o^{\text{CA}} \rangle \\ &= -2e \sum_o \langle \varphi_o^{(0)} | \hat{r}_\beta | \varphi_o^{(\text{R}_a)} \rangle \end{aligned} \quad (35)$$

and the electronic AAT is

$$\begin{aligned} \mathcal{I}_{\alpha\beta}^{\lambda} &= \sum_o \mathcal{I}_{\alpha\beta}^{\lambda o} \\ &= \sum_o \partial_{\hat{\mathbf{R}}_a} \langle \varphi_o^{\text{CA}} | \hat{m}_\beta^e | \varphi_o^{\text{CA}} \rangle \\ &= -\frac{ie}{c} \sum_{o\gamma\delta} \varepsilon_{\beta\gamma\delta} \langle \varphi_o^{(0)} | \hat{r}_\gamma \hat{r}_\delta | \varphi_o^{(\text{R}_a)} \rangle \end{aligned} \quad (36)$$

For both the APT in the velocity form and the AAT, the accuracy and the gauge invariance of the results highly depends on how well the hypervirial relation is satisfied:

$$\langle \varphi_o^{\text{CA}} | \hat{\mu} | \varphi_o^{\text{CA}} \rangle = \frac{i}{\hbar} \langle \varphi_o^{\text{CA}} | [\hat{\mathcal{H}}^e, \hat{\mu}] | \varphi_o^{\text{CA}} \rangle \quad (37)$$

This provides an important criterion for the basis set convergence. For a plane-wave basis with nonlocal pseudopotentials, this requires the explicit calculation of the commutator in the velocity operator in eq 22:⁴²

$$\hat{\mathbf{r}} = \frac{i}{\hbar} [\hat{\mathcal{H}}^e, \hat{\mathbf{r}}] = \frac{-i\hbar}{m_e} \partial_{\mathbf{r}} + \frac{i}{\hbar} [\hat{V}_{\text{nlc}}, \hat{\mathbf{r}}] \quad (38)$$

2.3. Gauge Dependencies. The APT shows no origin dependency whereas the exact AAT transforms under shifts of the gauge origin $\mathcal{O} = \mathcal{O}' + \Delta\mathcal{O} = \mathcal{O}' + \Delta$ as

$$\mathcal{M}_{\alpha\beta}^{\lambda\mathcal{O}} = \mathcal{M}_{\alpha\beta}^{\lambda\mathcal{O}'} - \frac{1}{2c} \varepsilon_{\beta\gamma\delta} \Delta_\gamma \mathcal{P}_{\alpha\delta}^{\lambda(v)} \quad (39)$$

In the common origin (CO) gauge, the rotational strength as a physical observable is gauge invariant:

$$R_m^{(r)} = \mathcal{P}_{\alpha\beta}^{\lambda(r)} \mathcal{M}_{\alpha'\beta}^{\lambda'\mathcal{O}'} S_{\alpha m}^{\lambda'} S_{\alpha' m}^{\lambda'} - \frac{1}{2c} \varepsilon_{\beta\gamma\delta} \Delta_\gamma \mathcal{P}_{\alpha\beta}^{\lambda(r)} \mathcal{P}_{\alpha'\delta}^{\lambda'(v)} S_{\alpha m}^{\lambda'} S_{\alpha' m}^{\lambda'} \quad (40)$$

$$R_m^{(v)} = \mathcal{P}_{\alpha\beta}^{\lambda(v)} \mathcal{M}_{\alpha'\beta}^{\lambda'\mathcal{O}'} S_{\alpha m}^{\lambda'} S_{\alpha' m}^{\lambda'} - \frac{1}{2c} \varepsilon_{\beta\gamma\delta} \Delta_\gamma \mathcal{P}_{\alpha\beta}^{\lambda(v)} \mathcal{P}_{\alpha'\delta}^{\lambda'(v)} S_{\alpha m}^{\lambda'} S_{\alpha' m}^{\lambda'} \quad (41)$$

since the second terms constitute triple products containing two identical vectors. For the position form of the rotational strength, this is only true if position and velocity forms of the APT are identical.

Alternatively, the distributed origin (DO) gauge provides different choices for the gauge, which helps to reduce the gauge dependence of the results introduced by basis set incompleteness and discretization effects:

$$\mathcal{M}_{\alpha\beta}^{\lambda\mathcal{O}} = (\mathcal{M}_{\alpha\beta}^{\lambda})_{\text{DO}} + \frac{1}{2c} \varepsilon_{\beta\gamma\delta} (R_\gamma^{\lambda} - \mathcal{O}_\gamma) \mathcal{P}_{\alpha\delta}^{\lambda(v)} \quad (42)$$

In this nuclear DO gauge, each AAT is calculated with the nuclear position as the gauge origin. This reduces the magnitude of the position operator in eq 36 and thereby numerical instabilities.⁴³ The translation from the distributed origin to a common origin is achieved by the different

translation vectors and guarantees the required gauge invariance of the physical observable

$$R_m^{(v)} = \mathcal{P}_{\alpha\beta}^{\lambda(v)} (M_{\alpha'\beta}^{\lambda'} S_{\alpha m}^{\lambda'} S_{\alpha' m}^{\lambda'} + \frac{1}{2c} \varepsilon_{\beta\gamma\delta} R_\gamma^{\lambda'} \mathcal{P}_{\alpha\beta}^{\lambda(v)} \mathcal{P}_{\alpha'\delta}^{\lambda'} S_{\alpha m}^{\lambda'} S_{\alpha' m}^{\lambda'}) \quad (43)$$

The overall expression is again invariant under translations of the origin. However, the last term cannot be factored out to form a triple product, because of the dependency of $R_\gamma^{\lambda'}$ on λ' . Therefore, the DO gauge is invariant under common translations of the origins but still requires the choice of a particular set of distributed origins.

Using eq 39, it is always possible to translate a DO gauge form of the AAT to a CO gauge form. In particular, it is also possible to define different sets of distributed origins. One convenient possibility is a set of statewise origins for the electronic AAT

$$\mathcal{I}_{\alpha\beta}^{\lambda o} = (\mathcal{I}_{\alpha\beta}^{\lambda})^o + \frac{1}{2c} \varepsilon_{\beta\gamma\delta} (\Delta_\gamma^o - O_\gamma) \mathcal{E}_{\alpha\delta}^{\lambda o(v)} \quad (44)$$

where $\mathcal{E}_{\alpha\delta}^{\lambda o(v)}$ is the contribution of the state o to the electronic APT in eq 35.

3. IMPLEMENTATION AND RESULTS

We have implemented the generalized Sternheimer equation (eq 33) in the CPMD code.⁴⁰ It is solved via an iterative conjugate gradient minimization and does not require a self-consistent solution. As for the related perturbation calculations, this approach does not involve a sum over excited states. Since the occurring perturbations do not include an explicit position operator, these calculations can be done using canonical orbitals ϕ_o . Because of the use of a plane-wave basis, no orbital-dependent gauge factors are required. This is a major advantage of this implementation, compared to atom-centered basis sets. As mentioned above, the use of nonlocal pseudo-potentials requires the explicit calculation of the commutator in eq 38. However, origin-dependent operators under periodic boundary conditions pose additional complications. Similar to the implementation for NMR,⁴⁴ the expectation values of the operators are taken with respect to maximally localized Wannier orbitals φ_o .⁴⁵ The perturbed canonical and localized states are mutually related via the same unitary transformation as that for the unperturbed ground-state orbitals.

$$|\varphi_o\rangle = \sum_{o'} U_{oo'}^{(0)} |\phi_{o'}\rangle \quad (45)$$

With this procedure, no cross terms between different Wannier orbitals arise.⁴⁴ This approach is based on the natural assumption that the response orbitals are sufficiently localized in the region of their respective unperturbed ground-state orbital. In the distributed origin gauge, the position operators are calculated with the corresponding Wannier center as its statewise origin:

$$\mathbf{r}_o = \langle \varphi_o | \mathbf{r} | \varphi_o \rangle \quad (46)$$

We checked that the numerical results in a supercell calculation are the same for canonical and Wannier orbitals.

The established method to verify the accuracy of the numerical results is the comparison of the tensor sum rules for the APT and AAT.⁴³ They connect the magnetic property AAT with the electronic properties, i.e., the APT and the dipole moment. In particular, this allows to check for consistency of

the implementation. In the notation of this work, the translational and rotational APT sum rules and the translational AAT sum rules are given as

$$\Sigma_{\alpha\beta}^0 = \sum_{\lambda} \mathcal{P}_{\alpha\beta}^{\lambda} \quad (47)$$

$$\Sigma_{\alpha\beta}^1 = \sum_{\gamma} \varepsilon_{\alpha\beta\gamma} \mu_{\gamma}^G \quad (48)$$

$$\Sigma_{\alpha\beta}^2 = \sum_{\lambda\gamma\delta} \varepsilon_{\beta\gamma\delta} R_\gamma^{\lambda} \mathcal{P}_{\delta\alpha}^{\lambda} \quad (49)$$

$$\Sigma_{\alpha\beta}^3 = 2c \sum_{\gamma} M_{\alpha\beta}^{\lambda} \quad (50)$$

where μ^G is the ground-state electric dipole moment. Σ^0 is zero for neutral systems and $\Sigma^1 = \Sigma^2 = \Sigma^3$ for all electron calculations in the basis set limit.

To benchmark the implementation, it is convenient to analyze small rigid molecules in the gas phase. We use R- d_2 -oxirane for the different numerical benchmarks of the implementation (see Figure 1).



Figure 1. R- d_2 -oxirane.

For the Σ^0 sum rule, which is ideally zero in all its components, we calculate the Frobenius norm $|\Sigma^0|$ to quantify the charge conservation. This provides a reference for the expected accuracy of the remaining sum rules. The dipole moment of R- d_2 -oxirane lies along the C2 symmetry axis which is chosen to be the z-axis in our calculations. Therefore, only the xy - and the yx -components differ from zero and are opposite in sign and equal in magnitude. This is trivially fulfilled for Σ^1 . The remaining APT and AAT sums are decomposed in their mean absolute value (symmetric) and the mean difference (antisymmetric); e.g., for Σ^2 ,

$$\overline{\Sigma}_{xy}^2 = \frac{1}{2} \|\Sigma_{xy}^2\| + \|\Sigma_{yx}^2\| \quad (51)$$

$$\Delta \Sigma_{xy}^2 = \frac{1}{2} \|\Sigma_{xy}^2\| - \|\Sigma_{yx}^2\| \quad (52)$$

A proper benchmark of our implementation would require a separate comparison of NVP with MFP results on the one hand and the quantification of the effective core potential approximation (ECP) on the other hand. At present, however, this is not possible, since the MFP is not implemented in CPMD or plane-wave codes with comparable ECP. We choose the most commonly applied MFP implemented in the Gaussian package as a reference. Thereby, we directly compare our results to all electron (AE) ones. The basis set convergence for R- d_2 -oxirane for different plane-wave energy cutoffs and the results for the MFP calculation with Gaussian basis sets are shown in Table 1.

The mean absolute values of the electronic sum rules converge with relative errors of the order of $|\Sigma^0|$, i.e., <1% for a plane-wave energy cutoff of 200 Ry. A suitable criterion for the required basis set convergence is the difference between the position and velocity form of the APT sum rules. Their relative

Table 1. Basis Set Convergence of the Sum Rules of the Atomic Tensors for R-*d*₂-Oxirane for the Effective Core Potential (ECP) Nuclear Velocity Perturbation (NVP) Implementation^a

cutoff	$ \Sigma^0 $	Σ_{xy}^1	$\overline{\Sigma}_{xy}^{2(r)}$	$\Delta\Sigma_{xy}^{2(r)}$	$\overline{\Sigma}_{xy}^{2(v)}$	$\Delta\Sigma_{xy}^{2(v)}$	$\overline{\Sigma}_{xy}^3$	$\Delta\Sigma_{xy}^3$
050	0.0501	0.6700	0.6746	0.0058	0.7013	0.0066	0.6778	0.0911
100	0.0261	0.7577	0.7819	0.0039	0.7857	0.0040	0.7946	0.1095
150	0.0095	0.7570	0.7639	0.0040	0.7641	0.0040	0.7517	0.1005
200	0.0035	0.7572	0.7594	0.0003	0.7596	0.0004	0.7400	0.0921
250	0.0041	0.7571	0.7580	0.0008	0.7580	0.0008	0.7378	0.0935
AE MFP	0.0000	0.7547	0.7546	0.0000			0.7270	0.0037

^aThe all electron (AE) magnetic field perturbation (MFP) reference is calculated with the Gaussian 09 package. The atomic tensors are given in atomic units, and the plane-wave energy cutoff is given in Rydbergs. The computational details are appended as Supporting Information.

error is <1% already for a plane-wave energy cutoff of 100 Ry. Similarly, their mean differences is of the order 10^{-3} and reduces with increasing basis set completion. All electronic sum rules converge toward the MFP all-electron (AE) results with relative errors of $\sim 10^{-3}$ for 250 Ry.

The mean absolute values of the AAT translational sum rule $\overline{\Sigma}_{xy}^3$ shows parallel convergence to the electronic sum rules. Also here, the ECP results converge toward the AE results within a relative error of $\sim 10^{-2}$ for 250 Ry. Both the ECP NVP and the AE MFP results yield a systematically smaller AAT sum rule, with a relative deviation on the order of 10^{-2} , with respect to the electronic ones. However, the mean difference $\Delta\Sigma_{xy}^3$ shows a different behavior. For both, the ECP NVP and the AE MFP tensors, the difference $\Delta\Sigma_{xy}^3$ is larger than the electronic ones $\Delta\Sigma_{xy}^{2(r)}/\Delta\Sigma_{xy}^{2(v)}$. The ECP NVP difference is much larger than the AE MFP one and does not show any systematic dependence on the basis set. We attribute this shift of Σ_{xy}^3 to the ECP approximation, since it does not show any gauge dependence. This is evident due to its symmetry, i.e., the equal sign of both entries, which differs from numerical errors introduced by basis set incompleteness and the resulting gauge dependence which yields an antisymmetric contribution.

The calculation of magnetic properties such as the AAT requires the careful analysis of the gauge invariance of the resulting physical observables. This especially applies to the plane-wave basis with periodic boundary conditions. Even though the sum rules are not direct physical observables, they ideally are independent of the chosen origin and, hence, provide a handy way to check for the correct dependence of the intermediate results. Therefore, we compare the sum rules for distributed origin (DO) gauge calculations (Σ_{DO}) with common origin (CO) gauge calculations with different gauge origins (Σ_{CO}). For example, for the AAT sum rule, this reads as

$$(\Sigma^3)_{\text{DO}} = 2c \sum_{\lambda} (\mathcal{M}^{\lambda})_{\text{DO}}^{\lambda} \quad (53)$$

$$(\Sigma^3)_{\text{CO}}^0 = 2c \sum_{\lambda} \mathcal{M}^{\lambda} \quad (54)$$

Using the Frobenius norm, the relative error is

$$\epsilon(\Sigma^3) = \frac{|(\Sigma^3)_{\text{CO}}^0 - (\Sigma^3)_{\text{DO}}|}{|(\Sigma^3)_{\text{DO}}|} \quad (55)$$

The gauge dependence of the sum rules for different distances of the R-*d*₂-oxirane molecule from the gauge origin is shown in Figure 2. The zero position corresponds to the molecular nuclear center of charge located at the origin of the position operator. We apply a sawtooth-shaped position operator for the

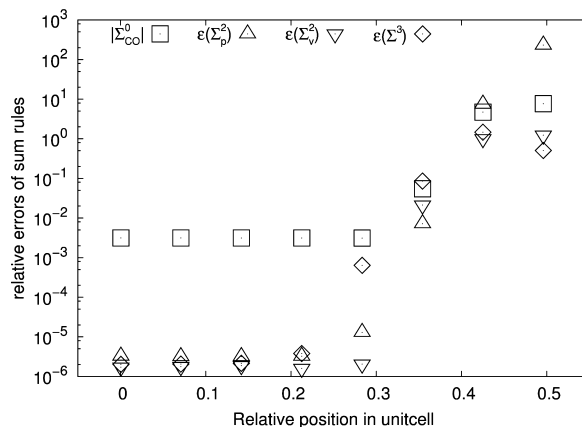


Figure 2. Relative errors of the atomic tensor sum rules using the common origin (CO) gauge and distributed origin (DO) gauge in the nuclear velocity perturbation (NVP). Dependence of the relative errors on the distance of the molecule to the box-centered gauge origin for a simulation supercell with a lattice size of 28 Å.

periodic boundaries that show a physically non-meaningful jump at the cell boundary (i.e., here at 0.5). The results for the CO and DO gauge calculations show a stable and gauge-independent behavior as long as the linear response orbitals do not extend to the ill-defined region of the jump in the position operator. For relative positions of the molecule from 0.0 to 0.25, the values are constant, indicating full gauge-invariance of our expressions. In particular, this allows for the translation of gauge origins in the distributed origin gauge. Note that the results in the distributed origin gauge are not affected by the jump of the sawtooth position operator. This holds as long as the orbitals are sufficiently localized in relation to the cell boundaries.

An interesting result is the different behavior of the position and velocity form of the APT. The velocity form does not show any systematic gauge dependence, not even on the logarithmic scale. The gauge dependence of the position form arises from numerical inaccuracies as, e.g., grid effects, which turn out to be of negligible absolute magnitude in our implementation (see Figure 2). This illustrates the potential of the NVP approach to obtain numerically gauge-invariant physical observables.

The calculation of isolated molecules using the supercell technique inherently introduces artificial interaction of the molecule with its periodic images. In particular, if the size of the supercell is insufficient, the molecule interacts with the dipole field of its mirror images. In order to quantify the relevance of this effect, we show the dependence of the sum rules on the cell

size in Figure 3. For all quantities, the decay perfectly follows the L^{-3} dipole contribution and, thus, can be controlled.

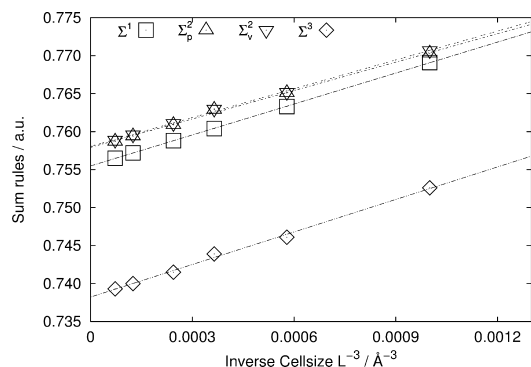


Figure 3. Dependence of the atomic tensor sum rules on the distance between the mirror images. The cell sizes are 10, 12, 14, 16, 20, and 24 Å.

Finally, the dipole- and rotational strengths as the desired physical observables must be benchmarked. Within the harmonic approximation, this requires the calculation of the normal modes at the respective equilibrium geometry. Again, we compare our ECP NVP results with the AE MFP results in the Gaussian framework. The dependence of the results on the similarity of the normal modes introduces another potential source of differences, which is known to be of the same order of magnitude as the inaccuracies of the actual atomic tensors.⁴⁶

As benchmark systems, we again use R-*d*₂-oxirane, the closely related R-propylene-oxide (Figure 4), S-norcamphor (Figure 5), and R- α -pinene (Figure 6).

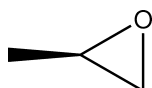


Figure 4. R-propylene-oxide.

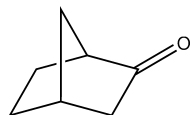


Figure 5. S-norcamphor.

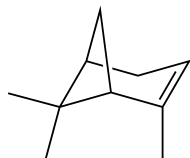


Figure 6. R- α -pinene.

The detailed table of the normal-mode frequencies and the dipole- and rotational strengths for R-*d*₂-oxirane is provided as Supporting Information. For visualization, we plot the correlation of the ECP NVP and the AE MFP results for the dipole- and rotational strengths in Figures 7–10).

The correlation with experimental data is very satisfactory, with virtually perfect agreement between our results (NVP) and the existing Gaussian-based implementation (MFP). There

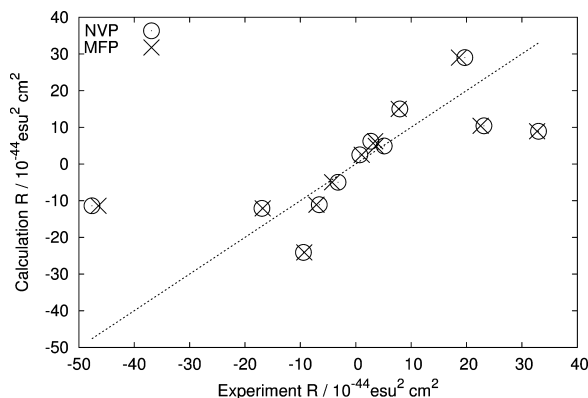


Figure 7. Correlation of experimental rotational strengths of R-*d*₂-oxirane with calculated ones using nuclear velocity perturbation (NVP) and magnetic field perturbation (MFP).

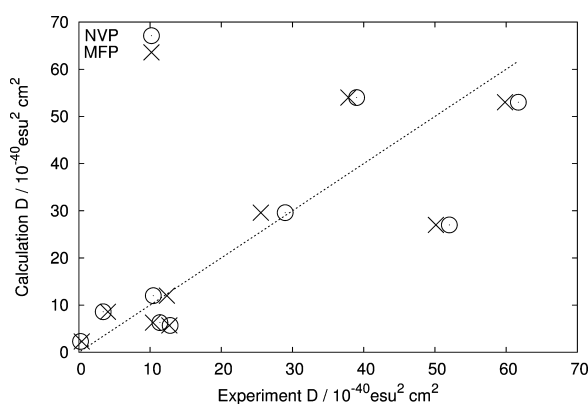


Figure 8. Correlation of experimental dipole strengths of R-*d*₂-oxirane with calculated ones using nuclear velocity perturbation (NVP) and magnetic field perturbation (MFP).

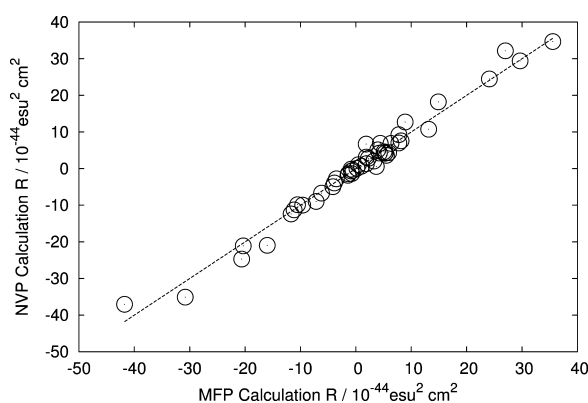


Figure 9. Correlation of rotational strengths of S-norcamphor calculated with magnetic field perturbation (MFP) and nuclear velocity perturbation (NVP).

are considerable numerical deviations of both methods with respect to the experiment, which have a variety of different reasons. Besides the level of theory (DFT, gradient-corrected xc-functional), the experimental values are mainly obtained in solution while the computed values represent gas-phase numbers. Here, the available experimental data for the enantiomer S-*d*₂-oxirane have been used.⁴⁷

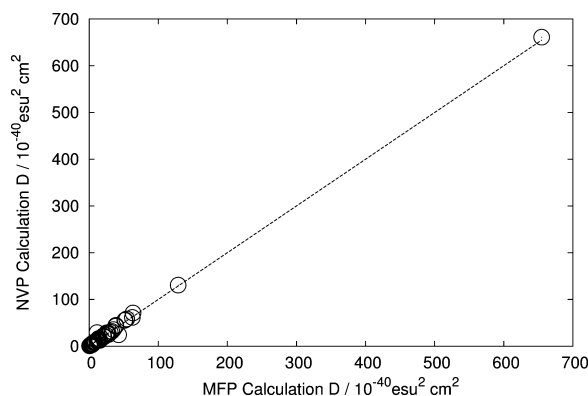


Figure 10. Correlation of dipole strengths of S-norcamphor calculated with magnetic field perturbation (MFP) and nuclear velocity perturbation (NVP).

In the bigger systems, such as α -pinene, the effect of mode degeneracies complicates the direct comparison. Some of the normal modes are degenerate and show a different symmetry, which strongly affects the sign of the individual contributions to the rotational strengths. However, this effect is a shortcoming of the harmonic analysis and not of the underlying atomic tensors. We have verified this qualitatively by taking the same normal modes for both calculations as is done for α -pinene (see the Supporting Information).

On the other hand, this subtle effect nicely illustrates the high sensitivity of VCD spectra on the molecular geometries, which represents one of the great strengths of this method and again highlights its suitability for structure determination.

4. CONCLUSION

We have presented the implementation of a reformulated nuclear velocity perturbation (NVP) theory of vibrational circular dichroism (VCD) within density functional perturbation theory (DFPT). Our results show the proper gauge invariance of the resulting physical observables. Our implementation in the plane-wave electronic structure code CPMD is the first successful NVP version of this theory. We have benchmarked our results against the popular magnetic field perturbation (MFP) theory implementation in the Gaussian 09 package and find them to be in remarkably good agreement. This work constitutes the basis for further application of ab initio calculation of VCD spectra for large biomolecular systems. In particular, NVP theory will allow for an efficient calculation of anharmonic VCD spectra based on ab initio molecular dynamics simulations.

■ ASSOCIATED CONTENT

Supporting Information

The Supporting Information gives additional data about computational details and MFP-NVP-correlation plots for the rotational strength and the dipole strength of R-propylene-oxide and R- α -pinene. This information is available free of charge via the Internet at <http://pubs.acs.org>.

■ AUTHOR INFORMATION

Corresponding Authors

*E-mail: rodolphe.vuilleumier@ens.fr.

*E-mail: daniel.sebastiani@chemie.uni-halle.de.

Notes

The authors declare no competing financial interest.

■ REFERENCES

- (1) Nafie, L. A. *Annu. Rev. Phys. Chem.* **1997**, *48*, 357–386.
- (2) Aamouche, A.; Devlin, F. J.; Stephens, P. J. *J. Am. Chem. Soc.* **2000**, *122*, 2346–2354.
- (3) Freedman, T. B.; Cao, X.; Dukor, R. K.; Nafie, L. A. *Chirality* **2003**, *15*, 743–758.
- (4) Magyarfalvi, G.; Tarczay, G.; Vass, E. *Wiley Interdiscip. Rev. Comput. Mol. Sci.* **2011**, *1*, 403–425.
- (5) Stephens, P. J.; Devlin, F. J.; Pan, J.-J. *Chirality* **2008**, *20*, 643–663.
- (6) Stephens, P. J. *J. Phys. Chem.* **1985**, *89*, 748–752.
- (7) Cheeseman, J. R.; Frisch, M. J.; Devlin, F. J.; Stephens, P. J. *Chem. Phys. Lett.* **1996**, *252*, 211–220.
- (8) Frisch, M. J.; Trucks, G. W.; Schlegel, H. B.; Scuseria, G. E.; Robb, M. A.; Cheeseman, J. R.; Scalmani, G.; Barone, V.; Mennucci, B.; Petersson, G. A.; Nakatsuji, H.; Caricato, M.; Li, X.; Hratchian, H. P.; Izmaylov, A. F.; Bloino, J.; Zheng, G.; Sonnenberg, J. L.; Hada, M.; Ehara, M.; Toyota, K.; Fukuda, R.; Hasegawa, J.; Ishida, M.; Nakajima, T.; Honda, Y.; Kitao, O.; Nakai, H.; Vreven, T.; Montgomery, J. A., Jr.; Peralta, J. E.; Ogliaro, F.; Bearpark, M.; Heyd, J. J.; Brothers, E.; Kudin, K. N.; Staroverov, V. N.; Kobayashi, R.; Normand, J.; Raghavachari, K.; Rendell, A.; Burant, J. C.; Iyengar, S. S.; Tomasi, J.; Cossi, M.; Rega, N.; Millam, J. M.; Klene, M.; Knox, J. E.; Cross, J. B.; Bakken, V.; Adamo, C.; Jaramillo, J.; Gomperts, R.; Stratmann, R. E.; Yazyev, O.; Austin, A. J.; Cammi, R.; Pomelli, C.; Ochterski, J. W.; Martin, R. L.; Morokuma, K.; Zakrzewski, V. G.; Voth, G. A.; Salvador, P.; Dannenberg, J. J.; Dapprich, S.; Daniels, A. D.; Farkas, O.; Foresman, J. B.; Ortiz, J. V.; Cioslowski, J.; Fox, D. J. *Gaussian 09, Revision A.02*, Gaussian, Inc.: Wallingford, CT, 2009.
- (9) Nicu, V. P.; Neugebauer, J.; Wolff, S. K.; Baerends, E. J. *Theor. Chem. Acc.* **2007**, *119*, 245–263.
- (10) Nafie, L. A.; Freedman, T. B. *J. Chem. Phys.* **1983**, *78*, 7108–7116.
- (11) Nafie, L. A. *J. Chem. Phys.* **1983**, *79*, 4950–4957.
- (12) Buckingham, A. D.; Fowler, P. W.; Galwas, P. A. *Chem. Phys.* **1987**, *112*, 1.
- (13) Nafie, L. A. *J. Chem. Phys.* **1992**, *96*, 5687–5702.
- (14) Nafie, L. A. *J. Phys. Chem. A* **2004**, *108*, 7222–7231.
- (15) Freedman, T. B.; Shih, M.-L.; Lee, E.; Nafie, L. A. *J. Am. Chem. Soc.* **1997**, *119*, 10620–10626.
- (16) Freedman, T. B.; Gao, X.; Shih, M.-L.; Nafie, L. A. *J. Phys. Chem. A* **1998**, *102*, 3352–3357.
- (17) Abedi, A.; Maitra, N. T.; Gross, E. K. U. *Phys. Rev. Lett.* **2010**, *105*, 123002.
- (18) Patchkovskii, S. *J. Chem. Phys.* **2012**, *137*, 084109.
- (19) Nafie, L. A. *Vibrational Optical Activity: Principles and Applications*; Wiley-VCH: Chichester, U.K., 2011; pp 95–130.
- (20) Bour, P.; Keiderling, T. A. *J. Phys. Chem. B* **2005**, *109*, 23687–23697.
- (21) Kubelka, J.; Huang, R.; Keiderling, T. A. *J. Phys. Chem. B* **2005**, *109*, 8231–8243.
- (22) Poopari, M. R.; Zhu, P.; Dezhahang, Z.; Xu, Y. *J. Chem. Phys.* **2012**, *137*, 194308.
- (23) Longhi, G.; Abbate, S.; Lebon, F.; Castellucci, N.; Sabatino, P.; Tomasini, C. *J. Org. Chem.* **2012**, *77*, 6033–6042.
- (24) Bak, K. L.; Bludský, O.; Jørgensen, P. *J. Chem. Phys.* **1995**, *103*, 10548–10555.
- (25) Cappelli, C.; Bloino, J.; Lipparini, F.; Barone, V. *J. Phys. Chem. Lett.* **2012**, *3*, 1766–1773.
- (26) Poopari, M. R.; Dezhahang, Z.; Yang, G.; Xu, Y. *ChemPhysChem* **2012**, *13*, 2310–2321.
- (27) Polavarapu, P. L. *Chirality* **2012**, *24*, 909–920.
- (28) Andrushchenko, V.; Tsankov, D.; Krasteva, M.; Wieser, H.; Bour, P. *J. Am. Chem. Soc.* **2011**, *133*, 15055–15064.
- (29) Jiang, N.; Tan, R. X.; Ma, J. *J. Phys. Chem. B* **2011**, *115*, 2801–2813.

- (30) Yamamoto, S.; Li, X.; Ruud, K.; Bour, P. *J. Chem. Theory Comput.* **2012**, *8*, 977–985.
- (31) Hohenberg, P.; Kohn, W. *Phys. Rev.* **1964**, *136*, 864–871.
- (32) Kohn, W.; Sham, L. J. *Phys. Rev.* **1965**, *140*, 1133–1138.
- (33) Jones, R. O.; Gunnarsson, O. *Rev. Mod. Phys.* **1989**, *61*, 689–746.
- (34) Gonze, X.; Vigneron, J.-P. *Phys. Rev. B* **1989**, *39*, 78112–13128.
- (35) Giannozzi, P.; de Gironcoli, S.; Pavone, P.; Baroni, S. *Phys. Rev. B* **1991**, *43*, 7231–7242.
- (36) Gonze, X.; Allan, D. C.; Teter, M. P. *Phys. Rev. Lett.* **1992**, *68*, 3603–3606.
- (37) Gonze, X. *Phys. Rev. A* **1995**, *52*, 1096–1114.
- (38) Putrino, A.; Sebastiani, D.; Parrinello, M. *J. Chem. Phys.* **2000**, *113*, 7102–7109.
- (39) Baroni, S.; de Gironcoli, S.; dal Corso, A.; Giannozzi, P. *Rev. Mod. Phys.* **2001**, *73*, 515–562.
- (40) CPMD-3.15.3, <http://www.cpmc.org/> (accessed Aug. 1, 2013), Copyright IBM Corp., 1990–2008; Copyright MPI für Festkörperforschung Stuttgart, 1997–2001.
- (41) Buckingham, A. D.; Dunn, M. B. *J. Chem. Soc.* **1971**, 1988.
- (42) Pickard, C. J.; Mauri, F. *Phys. Rev. Lett.* **2003**, *91*, 196401.
- (43) Stephens, P. J.; Jalkanen, K. J.; Amos, R. D.; Lazzeretti, P.; Zanasi, R. *J. Phys. Chem.* **1990**, *94*, 1811–1830.
- (44) Sebastiani, D.; Parrinello, M. *J. Phys. Chem. A* **2001**, *105*, 1951–1958.
- (45) Berghold, G.; Mundy, C. J.; Romero, A. H.; Hutter, J.; Parrinello, M. *Phys. Rev. B* **2000**, *61*, 1049611–1010048.
- (46) Stephens, P. J.; Ashvar, C. S.; Devlin, F. J.; Cheeseman, J. R.; Frisch, M. J. *Mol. Phys.* **1996**, *89*, 579–594.
- (47) Freedman, T. B.; Spencer, K. M.; Ragunathan, N.; Nafie, L. A.; Moore, J. A.; Schwab, J. M. *Can. J. Chem.* **1991**, *69*, 1619–1629.

2.4 MOMENT EXPANSION OF THE ELECTRONIC SUSCEPTIBILITY

The spectral decomposition representation of the electronic susceptibility, as discussed in section 1.6.2, is a compact representation of the full information contained in the electronic susceptibility. The full information allows e.g. to calculate responses to intra-molecular perturbations.^{203, 217, 261} For inter-molecular perturbations, only a small part of the full response function is required. We have shown in this work,⁹¹ that this part can be separated via a moment expansion transformation, yielding a very condensed representation of the response function for inter-molecular interactions. The derivation, analysis and benchmarking of this transformation has been established in this work.

In order to assess the physical relevance of the eigenfunctions, we introduce a multipolar expansion of the perturbing potential via a Laplace expansion in terms of real Racah normalized regular solid harmonic functions $R_l^m(\mathbf{r})$. We derive a unitary transformation in the space of the eigenfunctions, yielding subspaces with well-defined moments. This transformation generates the irreducible representations of the electronic susceptibility with respect to rotations within $SO(3)$ and allows to separate the contributions to the electronic response density from different multipole moments of the perturbation. The transformation maintains the form of an outer product of non-orthogonal transformed moment generating states. The moment expanded representation maximally condenses the physically relevant information of the electronic susceptibility required for inter-molecular interactions, yielding a considerable reduction in dimensionality. The performance and accuracy of this scheme is illustrated by computing the electronic response density of a water molecule to a complex interaction potential.

Moment Expansion of the Linear Density-Density Response Function

Arne Scherrer and Daniel Sebastiani*

We present a low rank moment expansion of the linear density-density response function. The general interacting (fully nonlocal) density-density response function is calculated by means of its spectral decomposition via an iterative Lanczos diagonalization technique within linear density functional perturbation theory. We derive a unitary transformation in the space of the eigenfunctions yielding subspaces with well-defined moments. This transformation generates the irreducible representations of the density-density response function with respect to rotations within SO(3). This allows to separate the contributions to the electronic response density from different

multipole moments of the perturbation. Our representation maximally condenses the physically relevant information of the density-density response function required for intermolecular interactions, yielding a considerable reduction in dimensionality. We illustrate the performance and accuracy of our scheme by computing the electronic response density of a water molecule to a complex interaction potential. © 2015 Wiley Periodicals, Inc.

DOI: 10.1002/jcc.24248

Introduction

The electronic response density is of paramount importance for many physical processes. Theoretically, the electronic response density is accessible from linear response theory which provides a powerful framework for linking experiment and theory.

A central quantity in this context is the linear density-density response function $\chi(\mathbf{r}, \mathbf{r}', \omega)$, which directly links an arbitrary external perturbation potential to its linear electronic density response

$$n_{\text{resp}}(\mathbf{r}, \omega) = \int \chi(\mathbf{r}, \mathbf{r}', \omega) V_{\text{pert}}(\mathbf{r}', \omega) d^3r'. \quad (1)$$

The frequency dependent density-density response function $\chi(\mathbf{r}, \mathbf{r}', \omega)$ is a crucial ingredient to time-dependent density functional theory^[1–4] as well as symmetry adapted perturbation theory.^[5–9] Via the adiabatic-connection fluctuation-dissipation theorem,^[10,11] also GW calculations,^[12–14] fluctuation-dissipation density functional theory,^[15–17] van-der-Waals^[18–23] or random phase approximation (RPA)^[24–26] and beyond-RPA^[27–29] calculations are based on it.

Most established applications of the density-density response function use its sum-over-states representation.^[30,31] In the Kohn-Sham (KS) formalism,^[32] this gives rise to the non-interacting density-density response function $\chi_s(\mathbf{r}, \mathbf{r}', \omega)$ ^[2]

$$\chi_s(\mathbf{r}, \mathbf{r}', \omega) = \lim_{\eta \rightarrow 0^+} \sum_o^{\text{occupied}} \sum_e^{\text{empty}} f_o \frac{\phi_o^*(\mathbf{r}) \phi_e(\mathbf{r}) \phi_e^*(\mathbf{r}') \phi_o(\mathbf{r}')}{\epsilon_o - \epsilon_e + \omega + i\eta} + \text{c.c.} \quad (2)$$

with KS-orbitals $\phi_o(\mathbf{r})$, KS-energies ϵ_o and occupancies f_o . The interacting response function $\chi(\mathbf{r}, \mathbf{r}', \omega)$ is obtained via a Dyson-like equation.^[2]

In the static limit ($\omega \rightarrow 0$), the spectral decomposition of the interacting density-density response function can be calculated

via Lanczos diagonalization techniques.^[33–36] Very recently, highly promising results for GW and RPA correlation energies have been achieved from explicit calculation of $\chi_s(\mathbf{r}, \mathbf{r}', \omega)$ using Lanczos chains.^[13,37] These techniques start from a diagonalization of the non-interacting static density-density response function, calculate its frequency dependence via Lanczos chains, and finally iterate the Dyson equation to obtain the interacting frequency dependent density-density response function.

The promising feature of this new Lanczos-based approach is the use of the eigenfunctions of the density-density response function as basis for subsequent calculations.^[13,37] The conventional route via the sum-over-states expression in eq. (2) employs auxiliary bases via density fitting techniques.^[7–9] Both ways of calculation yield a representation of the frequency dependent density-density response function as a weighted sum of auxiliary basis functions $\Phi_i(\mathbf{r})$. Due to the symmetry of the density-density response function, it is possible to diagonalize the expansion, yielding frequency dependent eigenfunctions $\chi_i(\mathbf{r}, \omega)$ and eigenvalues $\lambda_i(\omega)$

$$\chi(\mathbf{r}, \mathbf{r}', \omega) = \sum_{i,j=1}^{N_{\text{basis}}} \Phi_i(\mathbf{r}) \chi_{ij}(\omega) \Phi_j(\mathbf{r}') \quad (3)$$

$$= \sum_{i=1}^{N_{\text{basis}}} \chi_i(\mathbf{r}, \omega) \lambda_i(\omega) \chi_i(\mathbf{r}', \omega). \quad (4)$$

Using eq. (4) as our starting point, we present in this article a new representation of the density-density response function

A. Scherrer, D. Sebastiani
Institute of Theoretical Chemistry, Martin-Luther-University Halle-Wittenberg,
Von-Danckelmann-Platz 4, 06120 Halle (Saale), Germany
E-mail: daniel.sebastiani@chemie.uni-halle.de

© 2015 Wiley Periodicals, Inc.

which is transformed in irreducible representations with respect to rotations within $SO(3)$. This allows to separate the contributions to the electronic response density from different multipole moments of the perturbation. Our representation maximally condenses the physically relevant information of the density-density response function required for intermolecular interactions, yielding a considerable reduction in dimensionality (N_{basis}). This is particularly appealing for the calculation of intermolecular interactions, because it will give access to intermolecular electrostatic energies with the accuracy of self-consistent perturbation theory calculations at a fraction of their computational costs.

The following derivation and our numerical validation is carried out for the static limit ($\omega \rightarrow 0$) of the interacting response function of isolated molecules $\chi(\mathbf{r}, \mathbf{r}')$.^[36] The results can be generalized for the frequency dependent case, leading to the perspective of simplifying the equations for the calculation of RPA correlation energies and van-der-Waals interactions. It should be noted that our expansion is well-defined for both isolated and periodic boundary conditions.

The article is structured as follows. We first motivate the need for a change of representation from the spectral decomposition via a multipole expansion of the perturbing potential. The desired new representation is obtained via an unitary transformation of the eigenfunctions. This transformation is first described indirectly by the properties of the resulting representation. The actual algorithm to obtain the desired transformation is derived afterwards. By construction, the properties of the multipole expansion depend on the choice of the multipole moments, for example, traced versus traceless multipole moments. We discuss the impact of this choice of multipole moments on the properties of the transformation and show the gauge invariance of the transformation under periodic boundary conditions. For the numerical illustration and validation of our approach, we discuss the analytical case of the dipole-dipole polarizability and the convergence of the electronic response for a complex intermolecular interaction.

Change of representation

In the spectral decomposition representation eq. (4), the eigenvalue λ_i gives a measure for the weight of its corresponding eigenfunction $\chi_i(\mathbf{r})$ in the expansion of the response density for any arbitrary perturbation potential. The decay of the eigenvalue spectrum motivates the truncation of the infinite sum.

However, the eigenvalue does not solely determine the physical relevance of an eigenfunction. The overlap of the eigenfunction with the (unknown) perturbation potential often has a more significant impact on the contribution of a given eigenfunction. For a systematical quantification of this relevance, we propose an expansion of the perturbing potential $V_{\text{pert}}(\mathbf{r}')$. We restrict ourselves to the case of a perturbing potential arising from a charge density $n_{\text{pert}}(\mathbf{r}'')$, which has a vanishing overlap with the underlying density of the system

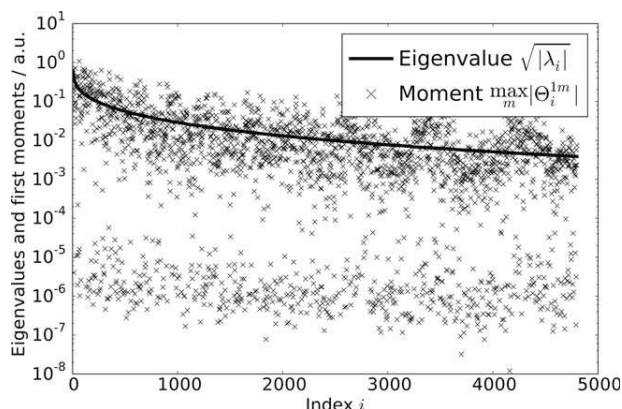


Figure 1. Moduli of eigenvalues and weighted first order moments according to eq. (9) of an isolated water molecule (note the logarithmic scale). The eigenvalue is a measure for the importance of the corresponding eigenfunction in the expansion of the response density for any arbitrary perturbation potential. Almost all eigenfunctions show a significant first order moment in at least one component.

$$V_{\text{pert}}(\mathbf{r}') = \int \frac{n_{\text{pert}}(\mathbf{r}'')}{|\mathbf{r}' - \mathbf{r}''|} d^3 r'' \quad (5)$$

Such a perturbation allows a multipole expansion of its Hartree potential via a Laplace expansion

$$V_{\text{pert}}(\mathbf{r}') = \sum_{l=0}^{\infty} \sum_{m=-l}^l V_l^m R_l^m(\mathbf{r}'), \quad (6)$$

in terms of real Racah normalized regular solid harmonic functions $R_l^m(\mathbf{r}')$. It is important to note that the more general case of a Taylor expansion including overlap effects is straightforward and will be discussed later on.

Combining eqs. (4) and (6) gives

$$n_{\text{resp}}(\mathbf{r}) = \sum_{i=1}^{\infty} \chi_i(\mathbf{r}) \left(\sqrt{\lambda_i} \sum_{l=1}^{\infty} \sum_{m=-l}^l V_l^m \Theta_i^{lm} \right), \quad (7)$$

with the traceless solid harmonic multipole moments of the weighted eigenfunctions

$$\Theta_i^{lm} = \sqrt{\lambda_i} \langle \chi_i | R_l^m \rangle. \quad (8)$$

The weight of an eigenfunction is given by the value of the parenthesis in eq. (7), which explicitly depends on the shape of the potential V_l^m .

The simplest case of a constant electric field perturbation is fully described by the $l=1$ terms, that is, $V_{l>1}^m=0$. For this case, the multipole moments for $l=1$ and $m \in \{-1, 0, 1\}$ according to eq. (8) determine the physical relevance of the corresponding eigenfunction. This expansion can be characterized by the decay of the maximum component of the modulus of the weighted eigenfunctions Θ_i^{1m}

$$\Theta_i^1 = \max_m |\Theta_i^{1m}|. \quad (9)$$

This decay of Θ_i^1 is depicted in Figure 1 for an isolated water molecule.

It is obvious that almost all eigenfunctions have a significant moment (in at least one component m , corresponding to at least one Cartesian direction). The decay is mainly due to the weighting of the eigenfunctions with their eigenvalues. This means that in the basis of the eigenfunctions, all eigenfunctions up to a chosen convergence threshold have to be considered to obtain converged results for observable quantities as e.g. the polarizability. This convergence requirement, in turn, renders a practical implementation and application of eq. (7) via eq. (8) computationally inefficient. This observation motivates a change of the representation via a multipole expansion.

The transformation

The spectral decomposition representation of the density-density response function reads

$$\chi(\mathbf{r}, \mathbf{r}') = \sum_{i=1}^{\infty} \chi_i(\mathbf{r}) \lambda_i \chi_i(\mathbf{r}') = \underline{Q} \underline{\Lambda} \underline{Q}^T, \quad (10)$$

with $\underline{Q} = [\chi_1(\mathbf{r}), \chi_2(\mathbf{r}), \dots]$ and $\underline{\Lambda} = \text{diag}[\lambda_1, \lambda_2, \dots]$. Due to the negative definiteness of the spectrum of real eigenvalues, it is always possible to find a decomposition as

$$\chi = \underline{Q} \underline{\Lambda}^{\frac{1}{2}} \underline{U} \underline{U}^T \underline{\Lambda}^{\frac{1}{2}} \underline{Q}^T = : \tilde{\underline{Q}} \tilde{\underline{Q}}^T, \quad (11)$$

with $\tilde{\underline{Q}} = \underline{Q} \underline{\Lambda}^{\frac{1}{2}} \underline{U}$, where \underline{U} is an arbitrary unitary transformation. With transformed states

$$\tilde{\chi}_i(\mathbf{r}) = \sum_{j=1}^{\infty} U_{ji} \sqrt{\lambda_j} \chi_j(\mathbf{r}), \quad (12)$$

this yields a new decomposition

$$\chi(\mathbf{r}, \mathbf{r}') = \sum_{i=1}^{\infty} \tilde{\chi}_i(\mathbf{r}) \tilde{\chi}_i(\mathbf{r}'). \quad (13)$$

It is important to note that no off-diagonal terms appear in the sum in eq. (13), even though the transformed states are no longer orthogonal. This implies that the response due to a transformed state $\tilde{\chi}_i(\mathbf{r})$ will have the same shape as the state itself. eq. (7) directly translates to

$$n_{\text{resp}}(\mathbf{r}) = \sum_{i=1}^{\infty} \tilde{\chi}_i(\mathbf{r}) \left(\sum_{l=1}^{\infty} \sum_{m=-l}^l v_l^m \tilde{\Theta}_i^{lm} \right), \quad (14)$$

with transformed weighted moments

$$\tilde{\Theta}_i^{lm} = \int \tilde{\chi}_i(\mathbf{r}') R_l^m(\mathbf{r}') d^3 r'. \quad (15)$$

Our goal is now to find a transformation \underline{U} , which concentrates the physically relevant moments in few moment generating states and thus improves the convergence of eq. (14). The transformed states (also during the iterative calculation of \underline{U}) are denoted with a tilde $\tilde{\chi}_i(\mathbf{r})$ to distinguish between orthonormal eigenfunctions $\chi_j(\mathbf{r})$ and non-orthogonal transformed states

$\tilde{\chi}_i(\mathbf{r})$. The final transformed states of the complete unitary transformation \underline{U} obey additional symmetry properties (which are to be explained in the following) and hence motivate a different nomenclature, that is, the state index i is replaced by the symmetry (l, m) . To facilitate the distinction between the auxiliary transformed states $\tilde{\chi}_i(\mathbf{r})$ and the final transformed states $\xi_l^m(\mathbf{r})$ we use a different letter of the Greek alphabet.

For most practical applications, the lower order moments in eq. (6) (i.e. for low l) are more important than the corrections due to higher order moment contributions. In the next section, we give a way to obtain a unitary transformation, which separates the contributions to the multipole moments in moment generating states $\xi_l^m(\mathbf{r})$, which fulfill

$$\int \xi_l^m(\mathbf{r}') R_{l'}^{m'}(\mathbf{r}') d^3 r' = \begin{cases} \Xi_{ll'}^{mm'} & \text{if } l \leq l' \\ 0 & \text{if } l > l' \end{cases} \quad (16)$$

In other words, the desired representation $\{\xi_l^m(\mathbf{r})\}$ yields states for which the subset $\{\xi_l^m(\mathbf{r}) | l \leq l_{\text{max}} \wedge m \in \{-l, \dots, l\}\}$ comprises the complete χ response up to an angular momentum channel of l_{max} .

The fulfillment of such a condition allows to partition the sum of the outer product of the transformed states in eq. (13) in orders of the angular momentum expansion

$$\chi(\mathbf{r}, \mathbf{r}') = \sum_{l=1}^{\infty} \chi^{(l)}(\mathbf{r}, \mathbf{r}') \quad (17)$$

$$\chi^{(l)}(\mathbf{r}, \mathbf{r}') = \sum_{m=-l}^l \xi_l^m(\mathbf{r}) \xi_l^m(\mathbf{r}'), \quad (18)$$

yielding a moment expansion of the whole tensor and hence of the induced density responses

$$n_{\text{resp}}(\mathbf{r}) = \sum_{l=1}^{\infty} n^{(l)}(\mathbf{r}) \quad (19)$$

$$n^{(l)}(\mathbf{r}) = \int \chi^{(l)}(\mathbf{r}, \mathbf{r}') V_{\text{pert}}(\mathbf{r}') d^3 r' \quad (20)$$

$$= \sum_{m=-l}^l \xi_l^m(\mathbf{r}) \langle \xi_l^m | V_{\text{pert}} \rangle. \quad (21)$$

Each set $\{\xi_l^m(\mathbf{r}) | m \in \{-l, \dots, l\}\}$ is an irreducible representation with respect to rotations in $SO(3)$, that is, eq. (17) is an expansion of the density-density response function in terms of irreducible representations.

The insertion of the expansion of the potential according to eq. (6) yields

$$n_{\text{resp}}(\mathbf{r}) = \sum_{l'=1}^{\infty} \sum_{l=1}^{\infty} \sum_{m'=-l'}^{l'} \sum_{m=-l}^l \xi_l^m(\mathbf{r}) \Xi_{ll'}^{mm'} V_{l'}^{m'} \quad (22)$$

$$= \sum_{l'=1}^{\infty} \sum_{l=1}^{l'} \sum_{m'=-l'}^{l'} \sum_{m=-l}^l \xi_l^m(\mathbf{r}) \Xi_{ll'}^{mm'} V_{l'}^{m'}, \quad (23)$$

where the double infinite sum in eq. (22) collapses to a sum up to l' using eq. (16). This dimensionality reduction illustrates the notion of a "maximally condensed" representation.

For the example of a constant electric field (with $V_{\nu}^{m'} = 0$ for $l' > 1$), the quadrupole sum in eq. (23) collapses, since only 3 states are required to obtain the full response

$$n_{\text{resp}}(\mathbf{r}) = \sum_{m'=-1}^1 \sum_{m=-1}^1 V_1^{m'} \Xi_{11}^{mm'} \zeta_1^m(\mathbf{r}). \quad (24)$$

In contrast to the in principle infinite sum in eq. (22), these 3 states contain the full information of density-density response function for this perturbation which illustrates the tremendous reduction in dimensionality.

Thus, it remains to find a suitable transformation U , which satisfies eq. (16).

The algorithm

The moment expansion can be done with respect to different sets of multipole moments. For simplicity of the notation, we present the case of real traceless spherical multipole moments. Alternative choices will be discussed later on. The real multipole moment with symmetry (l, m) of the weighted eigenfunction $\sqrt{\lambda_i} \chi_i(\mathbf{r})$ is given as

$$\Theta_i^{lm} = \int \sqrt{\lambda_i} \chi_i(\mathbf{r}) R_l^m(\mathbf{r}) d^3r. \quad (25)$$

We obtain the desired unitary transformation iteratively for each moment (l, m) with ascending l and m . The effect of the transformation for a given multipole moment (l, m) should be to concentrate all contributions to this multipole in one state. We illustrate the procedure by explicitly discussing the first transformation for $l = 1, m = -1$. Since this is the first multipole moment, the result of the transformation should be that only the first transformed state has a non-vanishing moment $\tilde{\Theta}_1^{1-1}$ and all the other $N - 1$ states are moment free for $l = 1, m = -1$ (with $N \rightarrow \infty$).

The necessary transformation is obtained by iterative Givens-rotations^[38] for each state

$$U^{1-1} = \prod_{j>1} \tilde{U}(\varphi_{1j}^{1-1}). \quad (26)$$

with elementary rotations determined by the angle φ_{1j}^{1-1}

$$\tan \varphi_{1j}^{1-1} = \frac{\Theta_j^{1-1}}{\Theta_1^{1-1}}. \quad (27)$$

which is chosen such that the transformed moment $\tilde{\Theta}_j^{1-1}$ vanishes after the Givens-rotation. After this transformation, the remaining $N - 1$ states have a vanishing first moment for $l = 1, m = -1$. The transformation for the second moment $l = 1, m = 0$ is obtained by rotating the transformed moments of the $N - 2$ remaining states into the second state.

We will now give a more compact and generalized notation for this algorithm. The unitary transformation for an expansion to order l_{max} is obtained by iterative rotations for each moment (l, m)

$$U = \prod_{l=1}^{l_{\text{max}}} U^l = \prod_{l=1}^{l_{\text{max}}} \prod_{m=-l}^l U^{lm}. \quad (28)$$

This requires an ordering of the moments, which naturally is given by increasing order l with ascending m within a given order. For spherical harmonics (l, m) , the most consistent realization can be achieved by means of a joint index f

$$f(l, m) = l^2 + l + m. \quad (29)$$

The transformation U for a given moment (l, m) transforms the original states $\chi_i(\mathbf{r})$ such that

- all preceding states $\tilde{\chi}_i(\mathbf{r})$ ($i < f(l, m)$) are left invariant
- the current state $\tilde{\chi}_i(\mathbf{r})$ ($i = f(l, m)$) comprises the moments for (l, m) of all subsequent states.
- all subsequent states $\tilde{\chi}_i(\mathbf{r})$ ($i > f(l, m)$) are moment free w.r.t. $R_l^m(\mathbf{r})$

The rotation for each moment [the generalization of eqs. (26) and (27)] is obtained by iterative Givens-rotations for each state, leaving the already expanded states invariant, that is, starting from $i_{\text{min}} = f(l, m)$

$$U^{lm} = \prod_{j>i_{\text{min}}} \tilde{U}(\varphi_{ij}^{lm}). \quad (30)$$

The elementary rotations are determined by the angle φ_{ij}^{lm}

$$\tan \varphi_{ij}^{lm} = \frac{\tilde{\Theta}_j^{lm}}{\tilde{\Theta}_i^{lm}}. \quad (31)$$

which is chosen such that the moment $\tilde{\Theta}_j^{lm}$ vanishes after the Givens-rotation. The computation of the moments $\tilde{\Theta}^{lm}$

$$\tilde{\Theta}_i^{lm} = \sum_{j=1}^{\infty} U_{ji} \Theta_j^{lm}. \quad (32)$$

is done with respect to the already rotated states at order $l - 1$. The calculation of φ^{lm} requires only states transformed by $U^{l'm'}$ with $f(l', m') < f(l, m)$, that is, the first transformation is done for the original weighted eigenfunctions.

The actual iterative calculation of the transformation U can be performed working only on moments, that is, the states are only used for the initial calculation of the weighted moments. All subsequent steps are carried out on transformed moments.

This procedure is a rotation of the moment generating components of the higher states on the current state $\tilde{\chi}_{i_{\text{min}}}(\mathbf{r})$, that is, the current expanded state has a maximum contribution to the current moment (l, m) and fulfills eq. (16). It can naturally be labeled by its corresponding moment since it is not changed by subsequent transformations

$$\xi_l^m(\mathbf{r}) \equiv \tilde{\chi}_{i_{\text{min}}}(\mathbf{r}). \quad (33)$$

The infinite number of eigenfunctions raises the question of the convergence of this transformation. In principle, there are

infinitely many eigenfunctions and their corresponding multipole moments, which have to be taken into account. However, due to the scaling with the eigenvalue their contributions will decay and asymptotically for $\tilde{\Theta}_j^{lm} \rightarrow 0$ we obtain $\phi_{ij}^{lm} = 0$, that is, the transformation for noncontributing eigenfunctions approaches the identity matrix. In practice, we have to truncate the spectral decomposition after a given number of N eigenfunctions, which determines the dimension of the transformation matrices.

The moment expansion requires the choice of a coordinate system as well as the specification of the used multipole moments. We show in the following that the decomposition in $\chi^{(l)}(\mathbf{r}, \mathbf{r}')$ in eq. (17) is uniquely defined for each order l .

Choice of multipole moments

In the preceding sections, we have presented the theory of the moment expansion for the choice of real traceless spherical multipole moments. This choice is always possible for non-overlapping charge distributions and allows to write the formalism in a closed form using the completeness of the Y_l^m basis. It is straightforward to adapt the presented equations for the case of complex or Cartesian multipole moments. These kind of choices real/complex or Cartesian/spherical multipole moments give the same results for the overall decomposition $\chi^{(l)}(\mathbf{r}, \mathbf{r}')$ in eq. (17) and can be inter-converted by simple transformations after the moment expansion.

A fundamental conceptual difference arises for the choice of traceless respectively traced multipole moments. While traceless multipoles are sufficient for the case of nonoverlapping charge distributions, overlap effects require the additional trace information. To illustrate this and to introduce the Cartesian notation for subsequent discussion, we resort to a Taylor expansion of the perturbing potential in terms of Cartesian coordinates. We do not impose further requirements on the potential other than being analytical. This is a generalization of the Laplace expansion in eq. (6)

$$V_{\text{pert}}(\mathbf{r}') = \sum_{k=0}^{\infty} \frac{(\mathbf{r}' \cdot \nabla_{\mathbf{r}''})^k}{k!} V_{\text{pert}}(\mathbf{r}'') \Big|_{\mathbf{r}''=0} \quad (34)$$

$$= \sum_{k=0}^{\infty} M_k^{\alpha\beta\ldots}(\mathbf{r}') V_k^{\alpha\beta\ldots} \quad (35)$$

Here, $\alpha, \beta, \ldots \in x, y, z$ denote Cartesian directions and $M_k^{\alpha\beta\ldots}(\mathbf{r}')$ are traced Cartesian multipole moment polynomials at order k

$$M_k^{\alpha\beta\ldots}(\mathbf{r}') = r'_{\alpha} r'_{\beta} \ldots \quad (36)$$

$$V_k^{\alpha\beta\ldots} = \frac{1}{k!} \frac{\partial^k}{\partial_{\alpha} \partial_{\beta} \ldots} V(\mathbf{r}) \Big|_{\mathbf{r}=0} \quad (37)$$

While there are $2k+1 =: \kappa_{\text{max}}^{\text{traceless}}(k)$ linear independent components at order k for traceless multipole moments, the additional $k(k-1)/2$ trace elements yield $(k+1)(k+2)/2 =: \kappa_{\text{max}}^{\text{traced}}(k)$ distinct elements for the traced multipole moments at order k , which have to be considered.^[39]

We denote the index of the distinct elements at order k by κ with $\kappa \in \{1, \ldots, \kappa_{\text{max}}^{\text{traced}}(k)\}$ at which a suitable equivalent of

the order in eq. (29) has to be chosen. With these choices, the whole formalism translates straightforwardly and all presented results apply here as well.

The gauge independence of the moment expansion is again guaranteed by including the transformation for the trace elements at their respective order, that is, the iterative transformation has to be carried out also for all trace elements at the present order before starting the transformation of the next order.

The additional trace elements give rise to additional trace terms in the moment expansion such that eq. (38) transforms to

$$\chi(\mathbf{r}, \mathbf{r}') = \sum_{k=1}^{\infty} \chi^{(k)}(\mathbf{r}, \mathbf{r}') \quad (38)$$

$$\chi^{(k)}(\mathbf{r}, \mathbf{r}') = \sum_{\kappa=1}^{\kappa_{\text{max}}^{\text{traced}}(k)} \zeta_{\kappa}^{\kappa}(\mathbf{r}) \zeta_{\kappa}^{\kappa}(\mathbf{r}'), \quad (39)$$

with new moment expanded states $\zeta_{\kappa}^{\kappa}(\mathbf{r})$. For traced spherical multipole moments, the additional trace elements belong to different irreducible representations and hence transform under rotation only within their subspace. For Cartesian multipole moments (traced and traceless), the rotational properties are more complicated. It is, however, always possible to transform from traceless Cartesian to traceless spherical multipole moments and vice versa. In addition, the transformation from traced Cartesian to traceless and traced spherical multipole moments is straightforward. Therefore, the moment expansion in eq. (38) is again uniquely defined for each order $\chi^{(k)}(\mathbf{r}, \mathbf{r}')$.

In Cartesian notation, we obtain the equivalent relation of eq. (23)

$$n_{\text{resp}}(\mathbf{r}) = \sum_{k'=1}^{\infty} \sum_{k=1}^{k'} \sum_{\kappa'=1}^{\kappa_{\text{max}}^{\text{traced}}(k')} \sum_{\kappa=1}^{\kappa_{\text{max}}^{\text{traced}}(k)} V_{k'}^{\kappa'} M_{kk'}^{\kappa\kappa'} \zeta_{\kappa}^{\kappa}(\mathbf{r}), \quad (40)$$

where the Cartesian moment matrix $M_{kk'}^{\kappa\kappa'}$ is the equivalent to the spherical moment matrix in eq. (16)

$$\int \zeta_{\kappa}^{\kappa}(\mathbf{r}') M_{kk'}^{\kappa\kappa'}(\mathbf{r}') d^3 r' = \begin{cases} M_{kk'}^{\kappa\kappa'} & \text{if } k \leq k' \\ 0 & \text{if } k > k' \end{cases} \quad (41)$$

This expansion allows the incorporation of overlap effects into the moment expanded response formalism, which will be necessary for the treatment of intermolecular interactions.

Gauge invariance

By construction, the rotated states $\tilde{\chi}_j(\mathbf{r})$ for $j > f(l, m)$ have vanishing moments $\tilde{\Theta}_j^{l'm'}$ for $l' \leq l, m' \leq m$. Here, we will show that this property guarantees the invariance of the transformation under shifts of the origin \mathbf{R} . The translational properties of regular solid harmonics under a translation $\mathbf{r}' = \mathbf{r} + \mathbf{R}$ can be expressed via the addition theorem^[40,41]

$$R_l^m(\mathbf{r} + \mathbf{R}) = \sum_{l_1=0}^l \sum_{\substack{m_1=-l_1 \\ l_2=l-l_1 \\ m_2=m-m_1}}^{l_1} \frac{A_{l_1}^m}{A_{l_1}^{m_1} A_{l_2}^{m_2}} R_{l_1}^{m_1}(\mathbf{r}) R_{l_2}^{m_2}(\mathbf{R}), \quad (42)$$

with $A_l^m = \sqrt{(l+m)!(l-m)!}$. Since no higher order terms appear, the calculation of the moments Θ_j^{lm} at order l for states $\tilde{\chi}_j(\mathbf{r})$ with $j > f(l, m)$ is independent of the choice of the origin. Hence, the gauge independence of the transformation is guaranteed by performing the iterative transformation in eq. (28) with increasing f . In other words, while the higher order moments depend on the choice of the origin, the transformation does not. Here, it should be noted that the order of transformations U^l is important, since U^l depends on all $U^{l' < l}$. In particular, since the eigenfunctions have vanishing moments for $l = 0$, also the expansion to first order is independent of the choice of origin. To illustrate this, we include the explicit dependence of the multipole moments on the chosen origin \mathbf{R} in eq. (25)

$$\Theta_i^{lm}(\mathbf{R}) = \int \sqrt{\lambda_i} \chi_i(\mathbf{r}) R_l^m(\mathbf{r} - \mathbf{R}) d^3r. \quad (43)$$

Since the eigenfunctions have vanishing moments for $l = 0$, their dipole moments $l = 1$ do not depend on the choice of the origin. After the moment expansion to first order $l = 1$, the remaining $N - 3$ states have vanishing dipole moments. Therefore, their quadrupole moment is independent of the choice of the origin and gives rise to a well defined second order moment expansion. This iterates to higher orders. We would like to stress here, that the procedure does not require to calculate the higher order multipole moments of the transformed states during the transformation. Instead, the higher order multipole moments of the eigenfunctions can be transformed according to eq. (32) and give rise to the same transformation.

We have numerically verified the gauge independence of the moment expansion up to fifth order and find an excellent fulfillment within the numerical accuracy. This result is also valid for the case of traced multipole moments, both analytically and numerically.

For each maximum order l_{\max} , the moment expansion is uniquely defined up to a rotation of the states in the three spacial dimensions. However, since the order of the labeling within an order l is arbitrary, each order l yields an upper diagonal moment matrix [cp. eq. (16)], shown here for order $l = 1$

$$\left(\Xi_{11}^{-1m'}, \Xi_{11}^{0m'}, \Xi_{11}^{1m'} \right) = \begin{pmatrix} \Xi_{11}^{-1-1} & \Xi_{11}^{0-1} & \Xi_{11}^{1-1} \\ 0 & \Xi_{11}^{00} & \Xi_{11}^{10} \\ 0 & 0 & \Xi_{11}^{11} \end{pmatrix} \quad (44)$$

Under rotation in $SO(3)$, the different irreducible representations do not mix, that is, the solid harmonic functions at order l rotate within their subspace

$$R_l^{m'}(\mathbf{r}) = \sum_{m''=-l}^l D_l^{m'm''} R_l^{m''}(\mathbf{r}'). \quad (45)$$

Here, D_l is the Wigner D-matrix at order l .^[42] Accordingly, also the moment matrix transforms as

$$\Xi_{ll}^{mm'} = \sum_{m''=-l}^l \Xi_{ll}^{mm''} D_l^{m'm''}. \quad (46)$$

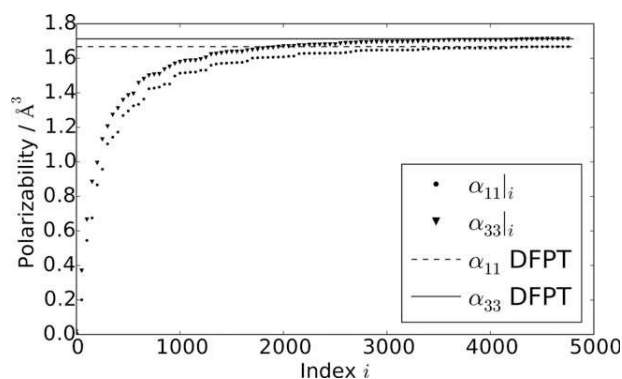


Figure 2. Convergence of the polarizability calculated with the eigenfunctions of the electronic susceptibility tensor, that is, $\alpha_{11|i}$ is polarization due to eigenstates up to index i . Here we only present the elements α_{11} and α_{33} since α_{22} shows a very similar convergence to α_{11} and would be superimposed in the plot. The direct DFPT reference calculations of the corresponding matrix elements are shown as black lines.

In the new coordinate system, $\Xi_{ll}^{mm''}$ is no longer upper-diagonal for the original moment expanded states $\xi_l^m(\mathbf{r})$. To obtain the same upper-diagonal form in the rotated frame, a simple unitary transformation of the states at order l is necessary.

In other words, while the moment expanded states $\xi_l^m(\mathbf{r}')$ at order l depend on the choice of the coordinate system (and on the ordering in m), the angular momentum decomposition $\chi^{(l)}(\mathbf{r}, \mathbf{r}')$ in eq. (17) does not. This is of great importance, because it guarantees the uniqueness of the decomposition. It is possible, however, to change the choice of coordinate system even after the transformation by using eq. (46).

Results

Dipole-dipole polarizability

The concept of our moment expansion can be illustrated and verified for the perturbation due to a homogeneous external field. In this case, the general response is given through the static polarizability tensor α . In our formulation, α can be represented as^[36]

$$\alpha_{\alpha\beta} = \sum_{i=1}^{\infty} \underbrace{\int \sqrt{\lambda_i} \chi_i(\mathbf{r}) r_{\alpha} d^3r}_{M_i^{\alpha}} \underbrace{\int \sqrt{\lambda_i} \chi_i(\mathbf{r}') r'_{\beta} d^3r'}_{M_i^{\beta}} \quad (47)$$

$$= \sum_{i=1}^{\infty} M_i^{\alpha} M_i^{\beta}. \quad (48)$$

The slow convergence of the first order multipole moments of the weighted eigenfunctions $\max_{\alpha} |M_i^{\alpha}|$ in Figure 1 entails a similarly slow convergence of the polarizability. This is illustrated in Figure 2, where we show the convergence of the polarizability tensor calculated from the spectral decomposition representation for an isolated water molecule.

In our moment expansion, the polarizability is straightforwardly obtained as

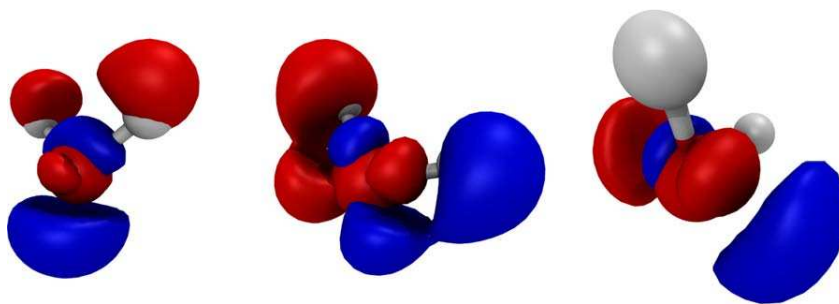


Figure 3. First order moment expanded states of H_2O , from left to right $\xi_1^x(\mathbf{r})$, $\xi_1^y(\mathbf{r})$, and $\xi_1^z(\mathbf{r})$.

$$\alpha_{\alpha\beta} = \sum_{\kappa=1}^3 M_{11}^{\beta\kappa} M_{11}^{\alpha\kappa}, \quad (49)$$

since $V_{k>1}^{\kappa} = 0$ for a homogeneous field. The sum runs over the moments of the 3 first order expanded states $\xi_1^{\kappa}(\mathbf{r})$. In contrast to the in principle infinite sum in eq. (48), these 3 states contain the *full* information of the polarizability tensor. This illustrates the tremendous reduction in dimensionality on the one hand, while on the other hand providing a simple mean for validation of the moment expansion [eqs. (38) and (40)] as such. We have verified the equivalence of eqs. (48) and (49) and find numerically identical results.

The only three contributing states are depicted in Figure 3 for a symmetry aligned coordinate system.

Molecular interaction from higher order expansion

For arbitrary perturbation potentials, also higher order terms $V_{k'}^{\kappa'}$ contribute. The relative importance of the different orders k' depends on the strength and the shape of the perturbing potential and cannot be quantified in a general way as for the homogeneous field ($k'=1$). We aim here at the perturbative treatment of molecular interactions. Therefore we choose a water dimer as a benchmark system (see Fig. 4, donor on the left, acceptor on the right) and analyze the convergence of the moment expanded response of one molecule due to the perturbation potential of the respective other molecule.

As the perturbation we choose the Hartree potential of the partial charges of a TIP3P^[43] water $Q_{\lambda}^{\text{partial}}$

$$V_{\text{TIP3P}}^{\text{frag}}(\mathbf{r}) = \sum_{\lambda=1}^{N_n} \frac{Q_{\lambda}^{\text{partial}}}{|\mathbf{r} - \mathbf{R}_{\lambda}|} \text{erf}\left(\frac{|\mathbf{r} - \mathbf{R}_{\lambda}|}{\sqrt{2}\sigma}\right), \quad (50)$$

where λ runs over the N_n atoms of the respective fragment.

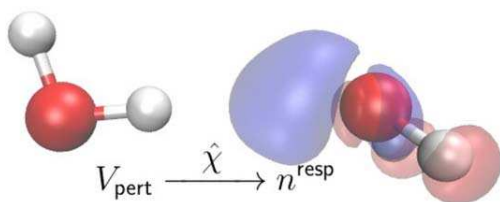


Figure 4. Water dimer with density response of the hydrogen bond acceptor (right) molecule due to the perturbation from the donor molecule (left).

The property of interest is the convergence of the response density in eq. (40). We show the profile of the response density along the $O - O$ axis at the equilibrium distance of the water dimer for different k_{max} and the full response (black line) in Figure 5. We find that great parts of the response even in this overlapping regime can be described by a moment expansion with respect to traced moments up to fourth order.

This can be quantified via the projection of the moment expanded response onto the full response $\langle n_{\text{resp}}^{\text{full}} | n^{(k_{\text{max}})} \rangle$. The completeness of the moment expansion up to order k_{max} then is quantified via the projection of its cumulated response

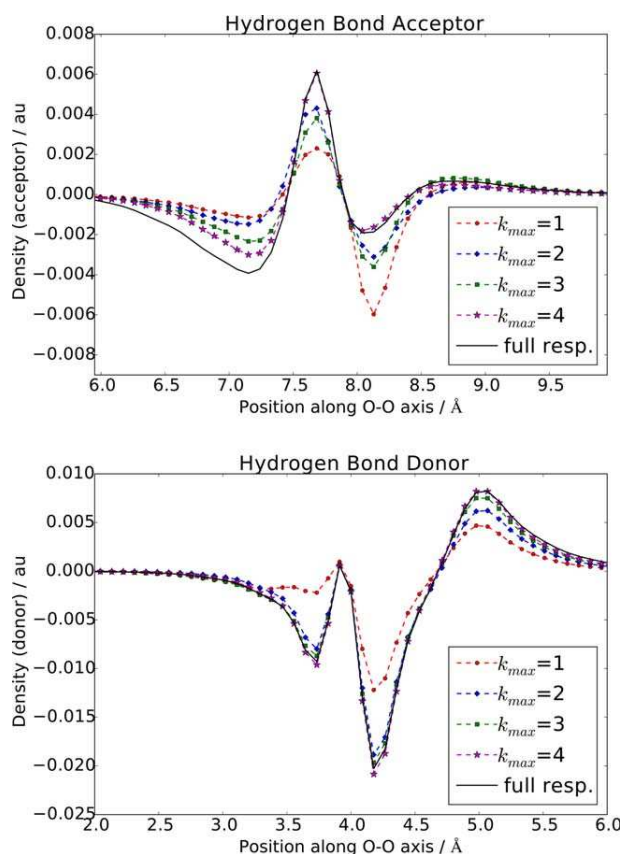


Figure 5. Profile of the response density along the $O - O$ axis at the equilibrium distance of the water dimer for different k_{max} . The full response is shown as a black line. [Color figure can be viewed in the online issue, which is available at wileyonlinelibrary.com.]

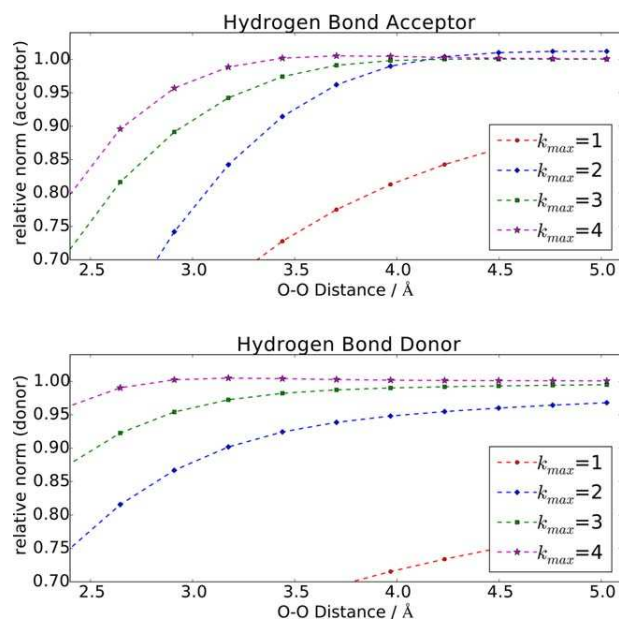


Figure 6. Cumulative response projections $\langle n_{\text{resp}}^{\text{full}} | n_{\text{cum}}^{(k_{\text{max}})} \rangle$ in dependence of the distance to the dipole moment. [Color figure can be viewed in the online issue, which is available at wileyonlinelibrary.com.]

$$\langle n_{\text{resp}}^{\text{full}} | n_{\text{cum}}^{(k_{\text{max}})} \rangle = \sum_{k=1}^{k_{\text{max}}} \langle n_{\text{resp}}^{\text{full}} | n^{(k)} \rangle. \quad (51)$$

In Figure 6, we show the relative norm of the cumulated response according to eq. (51) for different distances of the fragments. The traced multipole expansion up to fourth order allows to accurately describe over 90% of the density response, even in the repelling regime of the Hydrogen bond.

Computational details

The presented theory has been implemented in our development version of the CPMD^[44] electronic structure package. The calculations have been performed using Density Functional Perturbation Theory^[32,45–49] with Troullier-Martins^[50] pseudo potentials in the Becke^[51] Lee-Yang-Parr^[52] approximation for the exchange correlation kernel. We have employed a plane wave cutoff of 100 Ry and use the optimized geometry of an isolated water at this level of theory for all our calculations. The geometry of the water dimer is not relaxed, instead the fragments are held at their equilibrium geometry with fixed orientation and only the distance between the centers of masses is varied. In practice, the infinite space of the eigenfunctions is restricted to a subspace of $N_{\text{eig}} = 4800$ converged eigenfunctions calculated via an iterative Lanczos diagonalization of the static interacting density-density response function.^[36] We use a plane wave basis for all involved quantities, be it the electronic density, the perturbing potentials or the eigenfunctions and their transformations. The real space representation naturally gives rise to a regular grid. For our chosen parameters, the grid increment is about 0.08 Angstroms whereas the spread of the Gaussians in eq. (50) is chosen as $\sigma = 0.5a_0$.

Discussion

The moment expansion derived in this article yields a new representation of the density-density response function, which separates the contributions to the electronic response density from different multipole moments of the perturbation. This new representation maximally condenses the physically relevant information of the density-density response function required for intermolecular interactions, yielding a considerable reduction in dimensionality. This reduction is effective at two distinct yet related algorithmic steps: the number of functions to represent the response function as such [eqs. (3) and (4)] and the number of projections on the perturbing potential which have to be evaluated for an actual application of eq. (7).

At this stage, our transformation is applied after the spectral decomposition of the whole response function is known. The computational costs of the transformation are negligible compared to the numerical effort for the calculation of the spectral decomposition of the response function. It should be noted that at the present stage, the main computational effort for a single application of eq. (7) is the calculation of the spectral decomposition, that is, the response functions (as opposed to their application onto the perturbation potential or their consolidation into correlation energies). The presented change of representation reduces the computational costs for storage and application of the response function by a factor of $N_{\text{eig}}/N_{\text{me}}$, that is for the systems considered so far by about two orders of magnitude (with the number of eigenfunctions N_{eig} and the number of moment expanded states N_{me}). We refer to ref. [37] for a discussion of the computational scaling of the Lanczos-Sternheimer method compared to the conventional sum over states calculations.

This new mathematical property of the widely used response function is by virtue of its own an interesting property which might be of value to simplify the expressions used for the calculation of RPA correlation energies and van-der-Waals interactions. The solution of the Dyson-like equation in the reduced dimension space of the moment expanded response function in analogy to ref. [37] is a possible extension of the presented change of representation. The shape of the Hartree exchange correlation Kernel, that is, an intramolecular interaction, might require high angular momentum contributions, which reduces the advantage of the moment expanded representation. However, the response function gives access to the self-consistent response density independent of the perturbing potential. Therefore, aiming at intermolecular interactions, the costly spectral decomposition has to be done just once for each type of molecule (e.g., an isolated water molecule), whereas the actual application to intermolecular interactions is repeated many times. A condensed representation of the response function for this purpose reduces the computational cost of the frequent evaluation of the actual response density by several orders of magnitude.

This application of the response function is in principle only valid for a single molecular geometry. The explicit geometry dependence of the response functions is nontrivial. However, preliminary results indicate that an adequate expansion in

terms of normal coordinates may be able to yield accurate response functions for variable molecular geometries. In a previous work, we have already shown that the density-density response function is capable of describing the change of the ground-state density due to a variation of the molecular geometry.^[53] The actual dependence of the response function on the molecular geometry itself is currently under investigation.

An interesting question is the efficiency of our approach for the modeling of intermolecular interactions of larger molecules. The single multipole expansion of a strongly inhomogeneous perturbation potential requires higher multipole contributions, which diminishes the computational efficiency of our method. This also applies to extended systems exhibiting extremely nonlocal polarization waves.^[54] Both aspects might be addressed via a generalization to a distributed multipole expansion in the spirit of refs. [55–57].

Conclusions

We derive a unique representation of the density-density response function, which has the lowest possible rank in terms of its multipole moments. This expansion in moment generating contributions can be obtained by a unitary transformation from the spectral decomposition representation.

The expansion in multipole moments maximizes the information density per moment allowing a maximally efficient response calculation for perturbations of a given angular momentum. The analytical and numerical properties of our new scheme are greatly improved with respect to the straightforward representation in actual eigenfunctions.

We show explicitly that the density response of a water molecule due to the perturbation induced by a second water is already chemically converged at an order $k_{\text{max}} = 4$. This corresponds to a total of 34 functions compared to a requirement of about 2000 eigenfunctions in the conventional formulation.

We aim for a fragmentation based approach to molecular modeling that combines first principles derived response densities with favorable scaling properties with respect to the system size. Our maximally condensed formulation of the density-density response function for molecular systems will pave the way for a new generation of first principles based modeling of molecular interactions, combining low computational cost with near *ab initio* accuracy. Further development might allow a generalization of the method to distributed multipoles, RPA correlation energies, and van-der-Waals interactions.

Keywords: density-density response function • multipoles • molecular interaction • density functional perturbation theory

How to cite this article: A. Scherrer, D. Sebastiani. *J. Comput. Chem.* **2015**, DOI: 10.1002/jcc.24248

- [2] E. Gross, N. Maitra, In *Fundamentals of Time-Dependent Density Functional Theory*, Vol. 837; M. A. Marques, N. T. Maitra, F. M. Nogueira, E. Gross, A. Rubio, Eds.; Springer: Berlin, Heidelberg, **2012**; pp. 53–99.
- [3] N. Doltsinis, In *Many-Electron Approaches in Physics, Chemistry and Mathematics*; V. Bach, L. Delle Site, Eds.; Springer International Publishing: Switzerland, **2014**; pp. 135–151.
- [4] T. Olsen, K. S. Thygesen, *Phys. Rev. Lett.* **2014**, *112*, 203001.
- [5] A. Heßelmann, G. Jansen, *Chem. Phys. Lett.* **2003**, *367*, 778.
- [6] A. J. Misquitta, B. Jeziorski, K. Szalewicz, *Phys. Rev. Lett.* **2003**, *91*, 033201.
- [7] A. Heßelmann, G. Jansen, M. Schütz, *J. Chem. Phys.* **2005**, *122*, 014103.
- [8] R. Bukowski, R. Podeszwa, K. Szalewicz, *Chem. Phys. Lett.* **2005**, *414*, 111.
- [9] A. J. Misquitta, A. J. Stone, *J. Chem. Phys.* **2006**, *124*, 024111.
- [10] D. C. Langreth, J. P. Perdew, *Solid State Commun.* **1975**, *17*, 1425.
- [11] D. C. Langreth, J. P. Perdew, *Phys. Rev. B* **1977**, *15*, 2884.
- [12] H. V. Nguyen, T. A. Pham, D. Rocca, G. Galli, *Phys. Rev. B* **2012**, *85*, 81101.
- [13] T. A. Pham, H. V. Nguyen, D. Rocca, G. Galli, *Phys. Rev. B* **2013**, *87*, 155148.
- [14] F. Caruso, P. Rinke, X. Ren, A. Rubio, M. Scheffler, *Phys. Rev. B* **2013**, *88*, 075105.
- [15] M. Fuchs, X. Gonze, *Phys. Rev. B* **2002**, *65*, 235109.
- [16] F. Furche, T. Van Voorhis, *J. Chem. Phys.* **2005**, *122*, 164106.
- [17] J. Toulouse, I. C. Gerber, G. Jansen, A. Savin, J. G. Ángyán, *Phys. Rev. Lett.* **2009**, *102*, 096404.
- [18] J. F. Dobson, J. Wang, *Phys. Rev. Lett.* **1999**, *82*, 2123.
- [19] M. Dion, H. Rydberg, E. Schröder, D. C. Langreth, B. I. Lundqvist, *Phys. Rev. Lett.* **2004**, *92*, 246401.
- [20] D. Lu, Y. Li, D. Rocca, G. Galli, *Phys. Rev. Lett.* **2009**, *102*, 206411.
- [21] J. F. Dobson, T. Gould, *J. Phys. Condens. Matter* **2012**, *24*, 073201.
- [22] A. Tkatchenko, A. Ambrosetti, R. A. DiStasio, *J. Chem. Phys.* **2013**, *138*, 074106.
- [23] A. Ambrosetti, A. M. Reilly, R. A. DiStasio, A. Tkatchenko, *J. Chem. Phys.* **2014**, *140*, 18A508.
- [24] F. Furche, *Phys. Rev. B* **2001**, *64*, 195120.
- [25] F. Furche, *J. Chem. Phys.* **2008**, *129*, 114105.
- [26] X. Ren, P. Rinke, V. Blum, J. Wieferink, A. Tkatchenko, A. Sanfilippo, K. Reuter, M. Scheffler, *New J. Phys.* **2012**, *14*, 3020.
- [27] X. Ren, P. Rinke, G. E. Scuseria, M. Scheffler, *Phys. Rev. B* **2013**, *88*, 035120.
- [28] J. E. Bates, F. Furche, *J. Chem. Phys.* **2013**, *139*, 171103.
- [29] N. Colonna, M. Hellgren, S. de Gironcoli, *Phys. Rev. B* **2014**, *90*, 035105.
- [30] S. L. Adler, *Phys. Rev.* **1962**, *126*, 413.
- [31] N. Wiser, *Phys. Rev.* **1963**, *129*, 62.
- [32] W. Kohn, L. J. Sham, *Phys. Rev.* **1965**, *140*, 1133.
- [33] S. Hamel, A. J. Williamson, H. F. Wilson, F. Gygi, G. Galli, E. Ratner, D. Wack, *Appl. Phys. Lett.* **2008**, *92*, 3115.
- [34] D. Lu, F. Gygi, G. Galli, *Phys. Rev. Lett.* **2008**, *100*, 147601.
- [35] H. F. Wilson, D. Lu, F. Gygi, G. Galli, *Phys. Rev. B* **2009**, *79*, 245106.
- [36] A. Scherrer, V. Verschinin, D. Sebastiani, *J. Chem. Theory Comput.* **2012**, *8*, 106.
- [37] D. Rocca, *J. Chem. Phys.* **2014**, *140*, 18A501.
- [38] W. H. Press, S. A. Teukolsky, W. T. Vetterling, and B. P. Flannery, *Numerical Recipes: The Art of Scientific Computing*, 3rd ed.; Cambridge University Press: New York, **2007**.
- [39] J. D. Jackson, *Classical Electrodynamics*, 3rd ed.; Wiley: New Jersey, **1998**.
- [40] R. J. A. Tough, A. J. Stone, *J. Phys. A* **1977**, *10*, 1261.
- [41] S. Chakrabarti, D. P. Dewangan, *J. Phys. B: At. Mol. Opt. Phys.* **1995**, *28*, L769.
- [42] E. Wigner, *Gruppentheorie und ihre Anwendung auf die Quantenmechanik der Atomspektren*; Vieweg und Teubner Verlag: Wiesbaden, **1933**.
- [43] W. L. Jorgensen, J. Chandrasekhar, J. D. Madura, R. W. Impey, M. L. Klein, *J. Chem. Phys.* **1983**, *79*, 926.
- [44] CPMD-3.15.3, Available at: <http://www.cpmid.org/>, Copyright IBM Corp 1990–2008, Copyright MPI für Festkörperforschung Stuttgart 1997–2001.
- [45] P. Hohenberg, W. Kohn, *Phys. Rev.* **1964**, *136*, 864.
- [46] X. Gonze, *Phys. Rev. A* **1995**, *52*, 1096.
- [47] A. Putrino, D. Sebastiani, M. Parrinello, *J. Chem. Phys.* **2000**, *113*, 7102.

[1] E. Runge, E. K. U. Gross, *Phys. Rev. Lett.* **1984**, *52*, 997.

- [48] S. Baroni, S. de Gironcoli, A. dal Corso, P. Giannozzi, *Rev. Mod. Phys.* **2001**, 73, 515.
- [49] T. Watermann, A. Scherrer, D. Sebastiani, In *Many-Electron Approaches in Physics, Chemistry and Mathematics*; V. Bach, L. Delle Site, Eds.; Springer International Publishing, **2014**; pp. 97–110.
- [50] N. Troullier, J. L. Martins, *Phys. Rev. B* **1991**, 43, 1993.
- [51] A. D. Becke, *Phys. Rev. A* **1988**, 38, 3098.
- [52] C. Lee, W. Yang, R. G. Parr, *Phys. Rev. B* **1988**, 37, 785.
- [53] A. C. Ihrig, A. Scherrer, D. Sebastiani, *J. Chem. Phys.* **2013**, 139, 094102.
- [54] V. V. Gobre, A. Tkatchenko, *Nat. Commun.* **2013**, 4, 2341.
- [55] A. Stone, *Chem. Phys. Lett.* **1981**, 83, 233.
- [56] J. G. Ángyán, G. Jansen, M. Loss, C. Hättig, B. A. Heß, *Chem. Phys. Lett.* **1994**, 219, 267.
- [57] G. Naray-Szabo, G. G. Ferenczy, *Chem. Rev.* **1995**, 95, 829.

Received: 25 August 2015

Revised: 19 October 2015

Accepted: 21 October 2015

Published online on 00 Month 2015

2.5 MOLECULAR GEOMETRY DEPENDENCE OF THE ELECTRONIC SUSCEPTIBILITY

One long-term goal of this work is the use of the electronic susceptibility for a density-based modeling of inter-molecular interactions for molecular dynamics applications.

Wave function and density functional theory based perturbation theories are very successful in providing chemically accurate inter-molecular interaction energies, yielding instructive energy decomposition schemes.^{10,67-69} However, their power comes at the price of a high computational complexity. In view of their application to molecular dynamics simulations, the dependence of the involved quantities on the atomic configuration $\mathbf{R} = \{\mathbf{R}_i\}$ has to be considered explicitly.

Density-based methods promise more favorable scaling properties than wave function-based methods, especially since the molecular geometry and inter-molecular orientations are constantly changing in the course of the molecular dynamics. During a molecular dynamics simulation, an orbital-based evaluation of the electronic response corresponds to solving the unperturbed ground state electronic structure $H_{KS}^{(0)}(\mathbf{R})$, $\epsilon_o^{(0)}(\mathbf{R})$, $\phi_{[R]o}^{(0)}(\mathbf{r})$ for each fragment and configuration \mathbf{R} and subsequently a series of self-consistent solutions of the perturbation equations $\phi_{[R]o}^{(1)}(\mathbf{r})$, $n_{[R]}^{\text{resp}}(\mathbf{r})$ for each pairwise interaction $V_{\text{pert}}(\mathbf{r})$ of the fragments. This is evidently a very costly undertaking, limiting its applicability to comparatively small system sizes.

In order to use the electronic susceptibility for inter-molecular interactions at changing molecular geometries, we need to study its dependence on the molecular geometry changes. In this work, we generalize the explicit representation of the susceptibility at arbitrary molecular geometries \mathbf{R} . The results have been obtained in cooperation with Christian Dreßler and Paul Ahlert and have been published as a regular article in the Journal of Chemical Physics in ref.²⁶⁰ with the title “*Generalization of the electronic susceptibility for arbitrary molecular geometries*”, which is included at the end of this section.

All authors contributed extensively to the work presented in this section.²⁶⁰ A. Scherrer derived the theory. C. Dreßler and P. Ahlert and A. Scherrer implemented the theory and carried out the numerical calculations. C. Dreßler and A. Scherrer wrote the manuscript. D. Sebastiani supervised the project and gave conceptual advice.

The explicit representation of the molecular geometry dependence is achieved by means of a Taylor expansion in the nuclear coordinates. In order to obtain an efficient representation of the gradient of the full non-local response function, we use the moment expanded representation. This representation has the advantage that its finite difference derivation is possible. We illustrate the performance and accuracy of our scheme by computing the vibrationally induced variations of the response function of a water molecule and its resulting Raman spectrum.

Generalization of the electronic susceptibility for arbitrary molecular geometries

Arne Scherrer, Christian Dreßler, Paul Ahlert, and Daniel Sebastiani^{a)}

Institute of Chemistry, Martin-Luther-University Halle-Wittenberg, Von-Danckelmann-Platz 4, 06120 Halle (Saale), Germany

(Received 12 January 2016; accepted 7 March 2016; published online 14 April 2016)

We generalize the explicit representation of the electronic susceptibility $\chi_{[\mathbf{R}]}(\mathbf{r}, \mathbf{r}')$ for arbitrary molecular geometries \mathbf{R} . The electronic susceptibility is a response function that yields the response of the molecular electronic charge density at linear order to an arbitrary external perturbation. We address the dependence of this response function on the molecular geometry. The explicit representation of the molecular geometry dependence is achieved by means of a Taylor expansion in the nuclear coordinates. Our approach relies on a recently developed low-rank representation of the response function $\chi_{[\mathbf{R}]}(\mathbf{r}, \mathbf{r}')$ which allows a highly condensed storage of the expansion and an efficient application within dynamical chemical environments. We illustrate the performance and accuracy of our scheme by computing the vibrationally induced variations of the response function of a water molecule and its resulting Raman spectrum. © 2016 AIP Publishing LLC. [<http://dx.doi.org/10.1063/1.4945372>]

I. INTRODUCTION

The accurate evaluation of intermolecular electrostatic interactions is of great importance for large scale molecular dynamics simulations. In many cases a fragmentation approach can be used to increase the efficiency of such calculations. Common methods employed are based on multipole expansions,^{1–6} density fitting,^{7–9} or perturbation theories.^{10–13} Provided that polarization effects are taken into account, this involves the calculation of *response* properties of the fragments, e.g., in the simplest case the dipole-dipole-polarizability α .

Wave function and density functional theory based perturbation theories are very successful in providing chemically accurate intermolecular interaction energies yielding instructive energy decomposition schemes.^{10–13} However, their power comes at the price of a high computational complexity. In view of their application to molecular dynamics simulations, the dependence of the involved quantities on the atomic configuration $\mathbf{R} = \{\mathbf{R}_i\}$ has to be considered explicitly.

The orbital based calculation of the linear electronic response density via density functional perturbation theory^{14–18} (DFPT) requires a self-consistent solution of the Sternheimer equation

$$-\left[\hat{H}_{KS}^{(0)}(\mathbf{R}) - \epsilon_o^{(0)}(\mathbf{R})\right] \hat{P}_{[\mathbf{R}]e} \left|\phi_{[\mathbf{R}]o}^{(1)}\right\rangle = \hat{P}_{[\mathbf{R}]e} \hat{H}_{KS}^{(1)}[\{\phi_o\}] \left|\phi_{[\mathbf{R}]o}^{(0)}\right\rangle, \quad \text{for } o = 1 \dots N, \quad (1)$$

$$n_{[\mathbf{R}]}^{\text{resp}}(\mathbf{r}) = 2 \sum_{o=1}^{N_e} \text{Re} \left[\phi_{[\mathbf{R}]o}^{(0)*}(\mathbf{r}) \phi_{[\mathbf{R}]o}^{(1)}(\mathbf{r}) \right], \quad (2)$$

where $\hat{P}_{[\mathbf{R}]e} = 1 - \sum_{o=1}^{N_e} |\phi_{[\mathbf{R}]o}\rangle \langle \phi_{[\mathbf{R}]o}|$ is a projector on the manifold of unoccupied states.

We have explicitly included the parametric dependence of the involved operators and orbitals on the molecular geometry

\mathbf{R} . The perturbation Hamiltonian on the right hand side $\hat{H}_{KS}^{(1)}[\{\phi_o\}]$ depends on the electronic density response and hence implicitly on the perturbed orbitals on the left hand side, which necessitates a self-consistent solution of the equations.

During a molecular dynamics simulation, an orbital-based evaluation of the electronic response corresponds to solving the unperturbed ground state electronic structure $H_{KS}^{(0)}(\mathbf{R})$, $\epsilon_o^{(0)}(\mathbf{R})$, $\phi_{[\mathbf{R}]o}^{(0)}(\mathbf{r})$ for each fragment and configuration \mathbf{R} and subsequently a series of self-consistent solutions of the perturbation equations $\phi_{[\mathbf{R}]o}^{(1)}(\mathbf{r})$, $n_{[\mathbf{R}]}^{\text{resp}}(\mathbf{r})$ for each pairwise interaction $V_{\text{pert}}(\mathbf{r})$ of the fragments. This is evidently a very costly undertaking, limiting its applicability to comparatively small system sizes.

Density based methods provide a considerable reduction of dimensionality. The long-range regime of the electrostatic interaction is elegantly described by the (distributed) point multipole approximation, which drastically simplifies the interaction.^{1–4,19,20} For larger molecules, distributed point multipoles have proven to work even if the single point multipole approximation diverges.^{19,21} A further generalization allowing for polarization effects is the distributed polarizability method which attributes multipole polarizabilities to different sites of the molecules.^{22–25} By construction, point multipoles give a poor description of the short range regime of the interaction.²⁶ Strategies to overcome this problem employ a spatial representation of the electronic density via Gaussian charge distributions^{27,28} or Gaussian multipoles.^{6,29–31}

Our work aims to push this approach to the next level, combining the advantages of a reduced computational complexity for the evaluation of the response density while keeping the response density in its full non-local spatial dependence and not only its multipole moments. In analogy to Gaussian multipole moments^{6,31} (as a generalization of point multipoles), our representation of the electronic susceptibility $\chi(\mathbf{r}, \mathbf{r}')$ provides a generalization of the multipole-multipole-polarizabilities.^{22–25,32,33}

^{a)}Electronic mail: daniel.sebastiani@chemie.uni-halle.de

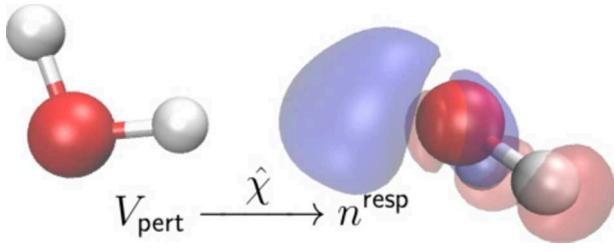


FIG. 1. Density response $n^{\text{resp}}(\mathbf{r})$ of a water molecule (right) due to the perturbation potential $V_{\text{pert}}(\mathbf{r})$ generated by the electrostatic potential of a hydrogen bond donor (left water molecule).

Here, we make a step towards a higher usability of the approach without the need of solving Eqs. (1) and (2) self-consistently for each

- (a) novel external perturbation potential and
- (b) new molecular conformation \mathbf{R} .

The first aspect (a) is achieved by our recently developed explicit representation of the electronic susceptibility $\chi_{[\mathbf{R}]}(\mathbf{r}, \mathbf{r}')$ within a low-rank approximation.^{32–37} The electronic linear response density $n_{[\mathbf{R}]}^{\text{resp}}(\mathbf{r})$ due to a perturbation potential $V_{\text{pert}}(\mathbf{r}')$ then is determined by the linear electronic susceptibility $\chi_{[\mathbf{R}]}(\mathbf{r}, \mathbf{r}')$ via

$$n_{[\mathbf{R}]}^{\text{resp}}(\mathbf{r}) = \int \chi_{[\mathbf{R}]}(\mathbf{r}, \mathbf{r}') V_{\text{pert}}(\mathbf{r}') d^3 r'. \quad (3)$$

The specific example of the density response $n_{[\mathbf{R}]}^{\text{resp}}(\mathbf{r})$ within a water molecule due to a hydrogen bond is illustrated in Fig. 1. Here, the specific perturbation potential $V_{\text{pert}}(\mathbf{r}) = \int \frac{n_{\text{left}}^{\text{H}_2\text{O}}(\mathbf{r}')}{|\mathbf{r} - \mathbf{r}'|} d^3 r'$ was used to compute $n_{[\mathbf{R}]}^{\text{resp}}(\mathbf{r})$ via Eq. (3). In principle, however, Eq. (3) defines a response function which is formally *independent* of the perturbation potential. The simultaneous incorporation of the implicit geometry dependence (b) requires in principle an explicit representation of the susceptibility $\chi_{[\mathbf{R}]}(\mathbf{r}, \mathbf{r}')$ on the nuclear coordinates \mathbf{R} which is nontrivial. In this article we show that this explicit representation of the full non-local response function on the molecular geometry can be achieved by means of a Taylor expansion in the nuclear coordinates. Our approach relies on the very condensed representations^{32,33} of the full response function which provides an efficient way to address this problem.

II. MOLECULAR GEOMETRY EXPANSION

Formally, there is no obstacle to explicitly calculate the response function $\chi_{[\mathbf{R}]}(\mathbf{r}, \mathbf{r}')$ for different configurations \mathbf{R} . This allows to analyze the dependencies of the electronic susceptibility on the molecular geometry and it will be used for comparison in the following. However, its brute force tabulation for all relevant configurations is no practicable way to approach problem (b).

An obvious approach to explicitly express the geometry dependence of the response function is a multi-dimensional Taylor expansion around the geometry of interest, e.g., the

equilibrium geometry \mathbf{R}_0

$$\chi_{[\mathbf{R}]}(\mathbf{r}, \mathbf{r}') = \sum_{|a| \geq 0} \frac{(\mathbf{R} - \mathbf{R}_0)^a}{a!} \partial^a \chi_{[\mathbf{R}_0]}(\mathbf{r}, \mathbf{r}'), \quad (4)$$

where we have used multi-index notation. This involves the calculation of derivatives of the high-dimensional response function, i.e., for the displacement of nucleus ν in Cartesian direction k we obtain

$$\chi_{[\mathbf{R}_0]}^{(\nu k)}(\mathbf{r}, \mathbf{r}') = \left. \frac{\partial \chi_{[\mathbf{R}]}(\mathbf{r}, \mathbf{r}')}{\partial R_k^\nu} \right|_{\mathbf{R}=\mathbf{R}_0}, \quad (5)$$

where the superscripts in parenthesis (νk) denote the derivative. Its direct calculation, i.e., an explicit diagonalization of the analytical derivative $\chi_{[\mathbf{R}_0]}^{(\nu k)}(\mathbf{r}, \mathbf{r}')$ might be possible. Prior work on the non-local polarizability density has expressed its analytical derivative in terms of the non-local hyperpolarizability density.^{38,39} This nicely illustrates the physics underlying the derivative of the response function but barely provides a numerically practical scheme for its computation.

An evident way to calculate the derivatives in Eq. (4) is the numerical derivative of the response function via finite differences, e.g., via forward difference for the first order. For a geometry \mathbf{R}_k^ν with nucleus ν displaced in direction k , i.e., $R_l^{\nu'} = R_{l,0}^{\nu'} + \Delta \delta_{kl} \delta_{\nu\nu'}$, this gives

$$\chi_{[\mathbf{R}_0]}^{(\nu k)}(\mathbf{r}, \mathbf{r}') = \frac{\chi_{[\mathbf{R}_k^\nu]}(\mathbf{r}, \mathbf{r}') - \chi_{[\mathbf{R}_0]}(\mathbf{r}, \mathbf{r}')}{\Delta}. \quad (6)$$

However, this operation is computationally very inconvenient due to the extremely high dimensionality of the involved objects. Therefore, the direct difference of the response function will not be used in this work. In order to obtain a feasible expression for the derivative of the total response function, its spectral decomposition is used^{32,34}

$$\chi_{[\mathbf{R}]}(\mathbf{r}, \mathbf{r}') = \sum_{i=1}^{\infty} \chi_{[\mathbf{R}]}(\mathbf{r}) \chi_{[\mathbf{R}]}(\mathbf{r}'). \quad (7)$$

The full response function is represented as a weighted outer product over eigenvalues $\chi_{[\mathbf{R}]}(\mathbf{r})$ and eigenfunctions $\chi_{[\mathbf{R}]}(\mathbf{r}')$.

The direct derivation of Eq. (7) gives via the product rule

$$\begin{aligned} \chi_{[\mathbf{R}_0]}^{(\nu k)}(\mathbf{r}, \mathbf{r}') &= \sum_i \left(\chi_{[\mathbf{R}_0]}^{(\nu k)}(\mathbf{r}) \chi_{[\mathbf{R}_0]}(\mathbf{r}') \right. \\ &\quad + \chi_{[\mathbf{R}_0]}(\mathbf{r}) \chi_{[\mathbf{R}_0]}^{(\nu k)}(\mathbf{r}') \\ &\quad \left. + \chi_{[\mathbf{R}_0]}(\mathbf{r}) \chi_{[\mathbf{R}_0]}^{(\nu k)}(\mathbf{r}') \right), \end{aligned} \quad (8)$$

where derivatives are taken at $\mathbf{R} = \mathbf{R}_0$.

This suggests that the numerical derivative can be performed on the eigenstates $\chi_{[\mathbf{R}_0]}(\mathbf{r})$ and eigenvalues $\chi_{[\mathbf{R}_0]}(\mathbf{r}')$ of the spectral decomposition

$$\chi_{[\mathbf{R}_0]}^{(\nu k)}(\mathbf{r}) = \frac{\chi_{[\mathbf{R}_k^\nu]}(\mathbf{r}) - \chi_{[\mathbf{R}_0]}(\mathbf{r})}{\Delta}, \quad (9)$$

$$\chi_{[\mathbf{R}_0]}^{(\nu k)}(\mathbf{r}') = \frac{\chi_{[\mathbf{R}_k^\nu]}(\mathbf{r}') - \chi_{[\mathbf{R}_0]}(\mathbf{r}')}{\Delta}. \quad (10)$$

At first glance, this appears to solve the problem. In particular, the representation and the subtraction of the states are technically feasible.

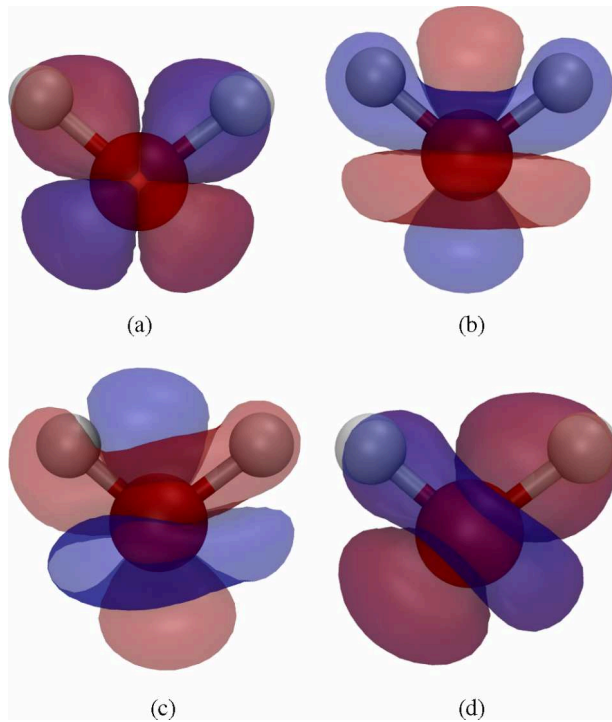


FIG. 2. Eigenstates 13 and 14 for H_2O in equilibrium geometry ((a) and (b)) and in slightly displaced geometry ((c) and (d)). The sign and order of the states have changed. This illustrates that small changes of the system can lead to completely different eigenstates. (a) $\chi_{[\mathbf{R}_0]13}(\mathbf{r})$, (b) $\chi_{[\mathbf{R}_0]14}(\mathbf{r})$, (c) $\chi_{[\mathbf{R}_k]13}(\mathbf{r})$, (d) $\chi_{[\mathbf{R}_k]14}(\mathbf{r})$.

However, a closer look at the eigenstates for different geometries reveals an additional complication. In Fig. 2 we show the eigenstates $\chi_{[\mathbf{R}]13}(\mathbf{r})$ and $\chi_{[\mathbf{R}]14}(\mathbf{r})$ of an isolated water molecule for different geometries.

The change of symmetry of the eigenstates stems from the intermixing of near degenerate eigenstates. If the system changes gradually, e.g., due to a different configuration, some eigenstates shift their eigenvalues. This reveals itself via a change of the ordering eigenvalues and eigenstates. If two states have near degenerate eigenvalues, this change can lead to an intermixing or swap of the eigenstates. The eigenstates with the same index i for different configurations may, even if the displacement is very small, have completely different symmetry. This applies in particular if the displacement breaks a molecular symmetry. Furthermore, only the absolute values of the eigenstates are well defined, their signs have no physical relevance since they cancel themselves in the symmetric outer product in Eq. (7). This means that eigenstates are in general not continuously differentiable and Eq. (8) provides no feasible way for the calculation of the derivative. Hence, an additional theoretical step is necessary.

III. DIFFERENTIABILITY THANKS TO SYMMETRY DECOMPOSITION

We look for a decomposition of the response function in states that are generally continuously differentiable and hence suited for finite differences. That is, the states should be continuously differentiable in the nuclear coordinates.

For electronic systems far from conical intersections, the overall response function should fulfill this property. For the eigenstates, this condition is not fulfilled. Therefore, a change of representation is needed that yields transformed states with the desired properties.

We have very recently derived a new representation of the full electronic susceptibility via a moment expansion.³³ In this very condensed representation, the total response function is given as a sum of the outer products of transformed states, partitioned in orders of the angular momentum expansion

$$\chi_{[\mathbf{R}]}(\mathbf{r}, \mathbf{r}') = \sum_{l=1}^{\infty} \chi_{[\mathbf{R}]}^l(\mathbf{r}, \mathbf{r}'), \quad (11)$$

$$\chi_{[\mathbf{R}]}^l(\mathbf{r}, \mathbf{r}') = \sum_{m=-l}^l \xi_{[\mathbf{R}]}^m(\mathbf{r}) \xi_{[\mathbf{R}]}^m(\mathbf{r}'). \quad (12)$$

The transformed states $\xi_{[\mathbf{R}]}^m(\mathbf{r})$ are labeled by their corresponding multipole moment and fulfill the property

$$\langle \xi_{[\mathbf{R}]}^m | R_{l'}^{m'} \rangle = \begin{cases} \Xi_{[\mathbf{R}]}^{mm'} & \text{if } l \leq l' \\ 0 & \text{if } l > l' \end{cases}, \quad (13)$$

where $R_{l'}^{m'}(\mathbf{r})$ are real Racah normalized regular solid harmonic functions and $\Xi_{[\mathbf{R}]}^{mm'}$ are multipole moments of the states and in general non-zero. In other words, the new representation $\{\xi_{[\mathbf{R}]}^m(\mathbf{r})\}$ yields states for which the subset $\{\xi_{[\mathbf{R}]}^m(\mathbf{r}) | l \leq l_{\max} \wedge m \in \{-l, \dots, l\}\}$ comprises the *complete* χ response up to an angular momentum channel of l_{\max} .

The derivation of the change of representation as well as its properties is not in the scope of this article and is discussed extensively elsewhere.³³ Important for this work are the new properties of the moment expanded states $\xi_{[\mathbf{R}]}^m(\mathbf{r})$. For each angular momentum channel l of the moment expansion $\chi_{[\mathbf{R}]}^l(\mathbf{r}, \mathbf{r}')$, the new decomposition in Eq. (11) is uniquely defined, i.e., the derivative of the whole response function can be split into a sum of derivatives of angular momentum contributions

$$\chi_{[\mathbf{R}_0]}^{(\nu k)}(\mathbf{r}, \mathbf{r}') = \sum_{l=1}^{\infty} \chi_{[\mathbf{R}_0]}^{l(\nu k)}(\mathbf{r}, \mathbf{r}'). \quad (14)$$

For a given choice of the coordinate system, also the decomposition of each angular momentum contribution $\chi_{[\mathbf{R}]}^l(\mathbf{r}, \mathbf{r}')$ in moment expanded states $\xi_{[\mathbf{R}]}^m(\mathbf{r})$ according to Eq. (12) is well defined. Therefore, the physically observable contribution of one transformed state to the total response is uniquely determined by its symmetry

$$n_{[\mathbf{R}]}^{\text{resp}}(\mathbf{r}) = \sum_{l=1}^{\infty} n_{[\mathbf{R}]}^l(\mathbf{r}), \quad (15)$$

$$n_{[\mathbf{R}]}^l(\mathbf{r}) = \int \chi_{[\mathbf{R}]}^l(\mathbf{r}, \mathbf{r}') V_{\text{pert}}(\mathbf{r}') d^3 r' \quad (16)$$

$$= \sum_{m=-l}^l \xi_{[\mathbf{R}]}^m(\mathbf{r}) \langle \xi_{[\mathbf{R}]}^m | V_{\text{pert}} \rangle. \quad (17)$$

This property is the key difference to the eigenstates: the partition of the total response into physically observable contributions of distinct symmetry guarantees that the underlying states are also continuously differentiable. It is this property that prohibits a discontinuous intermixing of

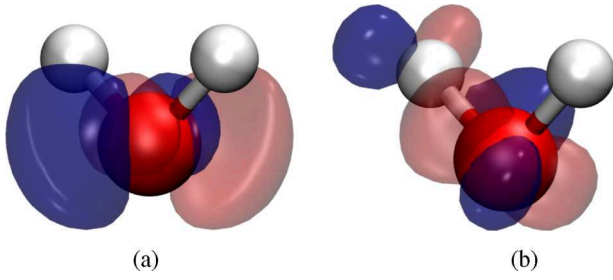


FIG. 3. (a) First moment-expanded state $\xi_{[\mathbf{R}_0]l}^{-1}(\mathbf{r})$ for H₂O in equilibrium geometry. (b) Derivative state $\xi_{[\mathbf{R}_0]l}^{-1(\nu k)}(\mathbf{r})$ for OH-bond elongation.

different states and hence guarantees that the finite-difference method gives well-defined derivatives

$$\chi_{[\mathbf{R}_0]l}^{l(\nu k)}(\mathbf{r}, \mathbf{r}') = \sum_{m=-l}^l \left(\xi_{[\mathbf{R}_0]l}^{m(\nu k)}(\mathbf{r}) \xi_{[\mathbf{R}_0]l}^m(\mathbf{r}') + \xi_{[\mathbf{R}_0]l}^m(\mathbf{r}) \xi_{[\mathbf{R}_0]l}^{m(\nu k)}(\mathbf{r}') \right). \quad (18)$$

In contrast to Eq. (8) where only the total sum is continuously differentiable, in Eq. (18) all single terms in the sum are continuously differentiable on their own.

Therefore, the numerical finite difference calculation of the derivatives of moment expanded states is possible

$$\xi_{[\mathbf{R}_0]l}^{m(\nu k)}(\mathbf{r}) = \frac{\xi_{[\mathbf{R}_k]l}^m(\mathbf{r}) - \xi_{[\mathbf{R}_0]l}^m(\mathbf{r})}{\Delta}. \quad (19)$$

In Fig. 3 we show a moment expanded state $\xi_{[\mathbf{R}_0]l}^m(\mathbf{r})$ and its corresponding bond-elongation derivative state $\xi_{[\mathbf{R}_0]l}^{m(\nu k)}(\mathbf{r})$.

IV. NUMERICAL VERIFICATION

The theoretical implication of continuous differentiability of the moment expanded states can be verified numerically. We have calculated the spectral decomposition and the corresponding moment expanded representation for different nuclear configurations \mathbf{R} . As a benchmark system we use an isolated water molecule and vary the nuclear configuration. For the time being we truncate the Taylor expansion in Eq. (4) after the second order and restrict ourselves to the first two angular momentum channels of the moment expansion $l = 1, 2$,

$$\begin{aligned} \chi_{[\mathbf{q}]l}(\mathbf{r}, \mathbf{r}') \approx & \sum_{l=1}^2 \left(\chi_{[\mathbf{q}_0]l}^l(\mathbf{r}, \mathbf{r}') + \sum_{n=1}^{N_{\text{int}}} \chi_{[\mathbf{q}_0]l}^{l(n)}(\mathbf{r}, \mathbf{r}') \Delta q_n \right. \\ & \left. + \frac{1}{2} \sum_{n, n'=1}^{N_{\text{int}}} \chi_{[\mathbf{q}_0]l}^{l(nn')}(\mathbf{r}, \mathbf{r}') \Delta q_n \Delta q_{n'} \right), \end{aligned} \quad (20)$$

with $\Delta q_n = q_n - q_{n0}$. The superscript (n) denotes the derivatives with respect to the internal coordinate q_n and N_{int} is the number of internal coordinates, $N_{\text{int}} = 3N - 6$ for a nonlinear isolated molecule. It is important to note that the systematic extension of this approach to higher orders in the Taylor expansion or the moment expansion poses no conceptual difficulties. For the second order traced moment expansion altogether 9 states have to be considered, 3 for the linear order and 5 + 1 for the second order.³³

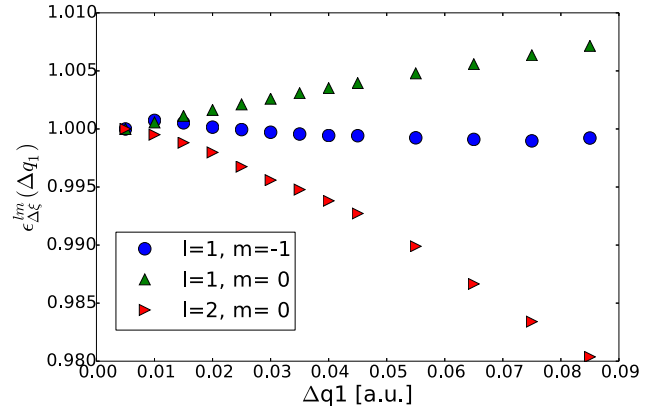


FIG. 4. Overlap between the explicitly calculated and the extrapolated states ξ_l^m for a single water molecule according to Eq. (22). The displacements roughly correspond to temperatures of 2000 K. Also the second order states show a well defined dependence on the nuclear displacement (a.u. refers to atomic units).

To quantify the errors of the expansion for finite displacements $q_{n'} = q_{n'0} + \delta_{nn'} \Delta q_n$ we can compare the extrapolated states with the exact explicitly calculated state at the displaced geometry $\xi_{[\mathbf{q}]}^m$ by means of their overlap

$$\epsilon_{\xi}^{lm}(\Delta q_n) = \frac{\langle \xi_{[\mathbf{q}]}^m | \xi_{[\mathbf{q}_0]l}^m + \xi_{[\mathbf{q}_0]l}^{m(n)} \Delta q_n \rangle}{\langle \xi_{[\mathbf{q}]}^m | \xi_{[\mathbf{q}]}^m \rangle}, \quad (21)$$

where ideally $\epsilon_{\xi}^{lm}(\Delta q_n) = 1$ for an exact finite order expansion. As a more significant measure, we look at the corresponding relative errors for the displacement induced changes of the states

$$\epsilon_{\Delta\xi}^{lm}(\Delta q_n) = \frac{\langle \xi_{[\mathbf{q}]}^m - \xi_{[\mathbf{q}_0]l}^m | \xi_{[\mathbf{q}_0]l}^{m(n)} \Delta q_n \rangle}{\langle \xi_{[\mathbf{q}]}^m - \xi_{[\mathbf{q}_0]l}^m | \xi_{[\mathbf{q}]}^m - \xi_{[\mathbf{q}_0]l}^m \rangle}. \quad (22)$$

The relative errors of the moment expanded states for different nuclear displacements are shown in Fig. 4. The deviation of the extrapolated states from the explicitly diagonalized states shows a smooth and continuous behavior. Its relative error is of the order of a few percent in the displacement range typical for nuclear vibrations. (Also the relative error of the change of the state is at most two percent over the relevant range.) These results confirm the validity of the first order expansion of the molecular geometry dependence of the electronic susceptibility for geometries expected within an ambient temperature MD trajectory ($\Delta q = 0.045$ Å).

V. FINITE TEMPERATURE RAMAN SIGNATURE OF A WATER MOLECULE

A first important application of the geometry dependence of the molecular polarizability tensor $\alpha_{[\mathbf{R}]}$ is the calculation of an anharmonic Raman spectra.^{40–46} By construction of the moment expanded representation, the full polarizability can be determined from the first order $l = 1$ angular moment contribution $\chi_{[\mathbf{q}]}^{l=1}(\mathbf{r}, \mathbf{r}')$ of the susceptibility. This requires only three moment expanded states for $m \in \{-1, 0, 1\}$

$$\alpha_{[q]ij} = \sum_{m=-1}^1 M_{[q]i}^m M_{[q]j}^m, \quad (23)$$

where $M_{[q]i}^m = \int r_i \xi_{[q]1}^m(\mathbf{r}) d^3r$ is the linear order Cartesian multipole moment in direction i of state $l = 1, m$.^{32,33} In analogy to Eq. (20) the polarizability tensor can be expanded in terms of derivatives of the first moments

$$\alpha_{[q]ij} \approx \alpha_{[q_0]ij} + \sum_{n=1}^{N_{\text{int}}} \alpha_{[q_0]ij}^{(n)} \Delta q_n + \frac{1}{2} \sum_{n,n'=1}^{N_{\text{int}}} \alpha_{[q_0]ij}^{(nn')} \Delta q_n \Delta q_{n'}. \quad (24)$$

Plugging Eq. (23) into Eq. (24) yields for the first and second order,

$$\alpha_{[q_0]ij}^{(n)} = \sum_{m=-1}^1 (M_{[q_0]i}^{m(n)} M_{[q_0]j}^m + M_{[q_0]i}^m M_{[q_0]j}^{m(n)}), \quad (25)$$

$$\alpha_{[q_0]ij}^{(nn')} = \sum_{m=-1}^1 (M_{[q_0]i}^{m(nn')} M_{[q_0]j}^m + M_{[q_0]i}^{m(n)} M_{[q_0]j}^{m(n')} + M_{[q_0]i}^{m(n')} M_{[q_0]j}^{m(n)} + M_{[q_0]i}^m M_{[q_0]j}^{m(nn')}). \quad (26)$$

The evaluation of the moment derivatives can be done either via calculation of the moments of the derivative state or equivalently via finite difference derivative of the moments for the different geometries.

In Fig. 5 we show the correlation of the first and second order moments for nuclear displacements along an internal coordinate (O–H distance). The first and second order moments, derived from extrapolated values and explicit calculations, are in excellent agreement.

We can calculate the change of the polarizability tensor from the change of the linear moments of the moment expanded states according to Eq. (25) or Eq. (26). This change of the polarizability for nuclear displacements along different internal coordinates is shown in Fig. 6. We would like to stress that these results are a verification and benchmark of our method, that is, the explicit geometry dependence of the general response function. Of course, a simple interpolation

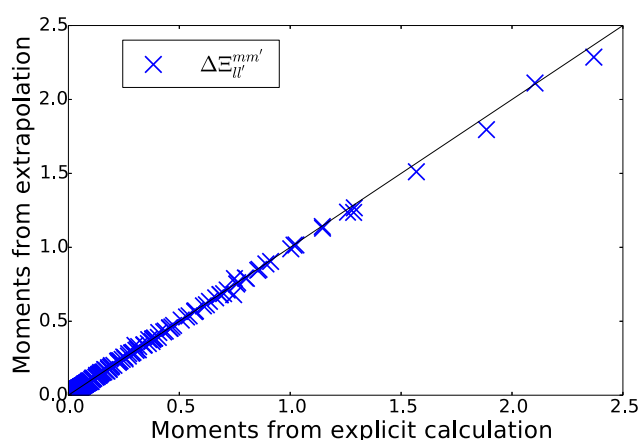


FIG. 5. Correlation of the vibrationally induced variations of $\Delta \Xi_{ll'}^{mm'}$ obtained from explicit calculation and extrapolation. The $\Delta \Xi_{ll'}^{mm'}$ are depicted for all moments up to $\Xi_{2,2}^{2,2}$ over a representative range. The displacements correspond to temperatures of 2000 K.

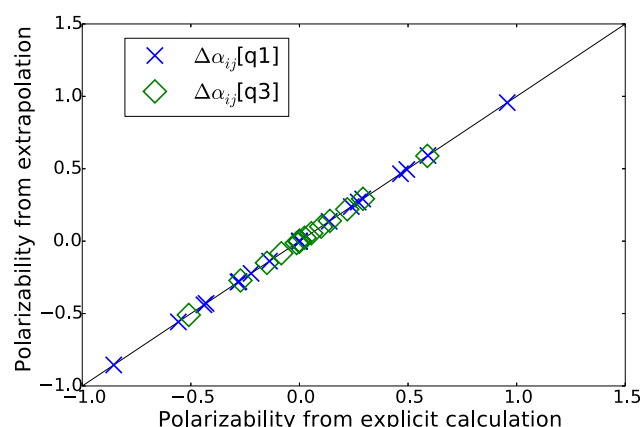


FIG. 6. Correlation of the geometry dependence of the polarizability for nuclear displacements along the O–H-bond q_1 and the H–O–H-angle q_3 . Explicit calculations for the corresponding geometry are correlated with interpolated values via second order Taylor expansion Eq. (26).

and tabulation of the polarizability tensor is much easier to achieve, this is however not our primary goal.

In order to obtain an estimate for the deviation of our approach from the exact calculation we have so far resorted to the comparison with the explicitly calculated susceptibility at the displaced geometry of interest. By construction, the deviation is zero for the equilibrium geometry and increases for larger displacements, especially if individual Cartesian coordinates are far from equilibrium.

For the application we are aiming at, i.e., spectroscopic sampling along molecular dynamics simulations or molecular dynamics simulations via fragmentation, the actual error of our method has to be weighted with the probability of the corresponding configuration during the simulation under ambient conditions. An explicit calculation of the polarizability via diagonalization of the non-local electronic susceptibility for many configurations along a molecular dynamics is far to expensive, which is the motivation for this work after all. We therefore compare the polarizability changes in our approach to direct DFPT calculations of the polarizability.

We have determined an average deviation of our method from direct DFPT calculations for the change of the polarizability along a molecular dynamic simulation. As a benchmark system we choose again a water molecule at 350 K. The average relative error of the induced changes of the polarizability using a first order Taylor expansion is 4.43% for the trace and 7.47% for the full tensor. Correcting with second order terms including mixed derivatives we obtain a mean relative deviation of 1.69% for the trace and 3.74% for the full tensor. These results nicely confirm our idea that the explicit geometry dependence for relevant vibrational displacements can be obtained via first- or second order Taylor expansion of the electronic susceptibility.

A direct illustration of the applicability of these results is the calculation of a Raman spectrum, which is obtained by Fourier-transform autocorrelation of the vibrationally induced polarizability changes.^{47,48} In Fig. 7 we show the Raman spectrum of an isolated water molecule at 350 K. Our explicit geometry dependence of the electronic susceptibility can

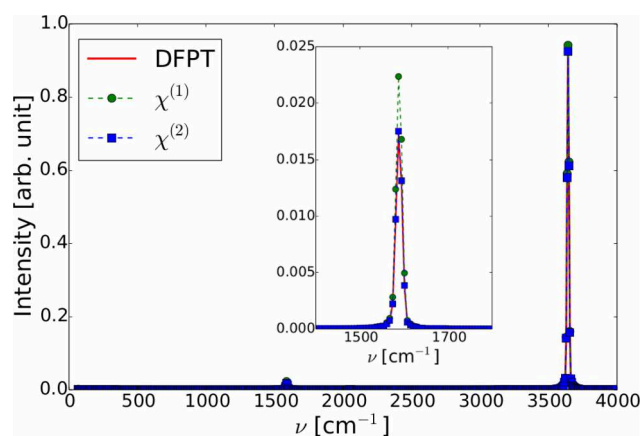


FIG. 7. Raman scattering intensities from vibrationally induced polarizability changes. The red line shows the explicit DFPT calculation as a reference. The first order (green) and second order (blue) Taylor expansion of the electronic susceptibility can reproduce all the features of the spectrum with systematic convergence to the reference.

reproduce all the features of the total spectrum and show only minor deviations of the intensity at the bending peak.

VI. CONCLUSION

In this work we validate the accuracy of a first and second order Taylor expansion of the molecular geometry dependence of the full non-local electronic susceptibility. Our long-term motivation is to work towards a new generation of fragmentation based molecular dynamics, which requires an efficient calculation of electronic response properties. The calculation of electronic response properties requires a much higher initial (once for all) effort but has a considerable better scaling for repeated application (e.g., along an AIMD trajectory) compared to trajectory sampling with an explicit DFPT approach. The key step enabling a Taylor expansion of the geometry dependence of the susceptibility is to resort to an explicit representation via a spectral decomposition of the response function. Combined with our recently developed moment expanded representation, this yields an efficiently differentiable representation of the response function. We validated our method numerically for an isolated water molecule, yielding a quantitative agreement for the Raman spectrum of water in the gas phase. We could show that a first order Taylor expansion is sufficient to reproduce moments and states within an error of two percent for molecular displacements corresponding to ambient temperatures.

VII. COMPUTATIONAL DETAILS

The presented theory was implemented in our development version of the CPMD⁴⁹ electronic structure package. The calculations have been performed using density functional perturbation theory^{15–18,50,51} with Troullier-Martins⁵² pseudo potentials in the Becke⁵³ Lee-Yang-Parr⁵⁴ approximation for the exchange correlation kernel. We have employed a plane wave cutoff of 70 Ry and used the optimized geometry of an isolated water at this level of theory for all our calculations. In practice, the infinite space of the eigenfunctions is restricted

to a subspace of 5000 converged eigenstates. The molecular dynamics was generated with the CP2K^{55,56} program package using the TZV2P-MOLOPT-GTH basis⁵⁷ and GTH pseudo potentials^{58–60} with a 0.5 fs time step. The temperature was set to 350 K by a Nosé-Hoover chain thermostat.^{61,62} For the comparison of polarizability tensors we employ the Frobenius norm, i.e., $\epsilon = |\alpha_{\text{ref}} - \alpha|_F / |\alpha_{\text{ref}}|_F$.

- ¹A. D. Buckingham, *Adv. Chem. Phys.* **12**, 107 (1967).
- ²A. J. Stone, *Chem. Phys. Lett.* **83**, 233 (1981).
- ³G. Naray-Szabo and G. G. Ferenczy, *Chem. Rev.* **95**, 829 (1995).
- ⁴J. G. Ángyán, C. Chipot, F. Dehez, C. Hättig, G. Jansen, and C. Millot, *J. Comput. Chem.* **24**, 997 (2003).
- ⁵D. Elking, T. Darden, and R. J. Woods, *J. Comput. Chem.* **28**, 1261 (2007).
- ⁶R. J. Wheatley, *Mol. Phys.* **79**, 597 (1993).
- ⁷G. G. Hall and C. M. Smith, *Int. J. Quantum. Chem.* **25**, 881 (1984).
- ⁸K. Eichkorn, O. Treutler, H. Öhm, M. Häser, and R. Ahlrichs, *Chem. Phys. Lett.* **240**, 283 (1995).
- ⁹G. A. Cisneros, J.-P. Piquemal, and T. A. Darden, *J. Chem. Phys.* **123**, 044109 (2005).
- ¹⁰B. Jeziorski, R. Moszynski, and K. Szalewicz, *Chem. Rev.* **94**, 1887 (1994).
- ¹¹D. M. Benoit, D. Sebastiani, and M. Parrinello, *Phys. Rev. Lett.* **87**, 226401 (2001).
- ¹²A. Heßelmann and G. Jansen, *Chem. Phys. Lett.* **367**, 778 (2003).
- ¹³A. J. Misquitta, B. Jeziorski, and K. Szalewicz, *Phys. Rev. Lett.* **91**, 033201 (2003).
- ¹⁴X. Gonze, *Phys. Rev. A* **52**, 1086 (1995).
- ¹⁵X. Gonze, *Phys. Rev. A* **52**, 1096 (1995).
- ¹⁶A. Putrino, D. Sebastiani, and M. Parrinello, *J. Chem. Phys.* **113**, 7102 (2000).
- ¹⁷S. Baroni, S. de Gironcoli, A. dal Corso, and P. Giannozzi, *Rev. Mod. Phys.* **73**, 515 (2001).
- ¹⁸T. Watermann, A. Scherrer, and D. Sebastiani, in *Many-Electron Approaches in Physics, Chemistry and Mathematics*, edited by V. Bach and L. Delle Site, Mathematical Physics Studies (Springer International Publishing, 2014), pp. 97–110.
- ¹⁹A. J. Stone and M. Alderton, *Mol. Phys.* **56**, 1047 (1985).
- ²⁰J. D. Jackson, *Classical Electrodynamics*, 3rd ed. (Wiley, 1998), pp. 145–151.
- ²¹A. J. Misquitta, A. J. Stone, and F. Fazeli, *J. Chem. Theory Comput.* **10**, 5405 (2014).
- ²²A. J. Stone, *Mol. Phys.* **56**, 1065 (1985).
- ²³C. R. L. Sueur and A. J. Stone, *Mol. Phys.* **78**, 1267 (1993).
- ²⁴C. R. L. Sueur and A. J. Stone, *Mol. Phys.* **83**, 293 (1994).
- ²⁵A. J. Misquitta and A. J. Stone, *J. Chem. Phys.* **124**, 024111 (2006).
- ²⁶A. Stone, *The Theory of Intermolecular Forces*, 2nd ed. (Oxford University Press, 2013).
- ²⁷R. Chelli, R. Righini, S. Califano, and P. Procacci, *J. Mol. Liq.* **96–97**, 87 (2002).
- ²⁸P. Paricaud, M. Predota, A. A. Chialvo, and P. T. Cummings, *J. Chem. Phys.* **122**, 244511 (2005).
- ²⁹D. Martin and G. G. Hall, *Theor. Chem. Acc.* **59**, 281 (1981).
- ³⁰R. J. Wheatley and J. B. O. Mitchell, *J. Comput. Chem.* **15**, 1187 (1994).
- ³¹D. M. Elking, G. A. Cisneros, J.-P. Piquemal, T. A. Darden, and L. G. Pedersen, *J. Chem. Theory Comput.* **6**, 190 (2010).
- ³²A. Scherrer, V. Verschinin, and D. Sebastiani, *J. Chem. Theory Comput.* **8**, 106 (2012).
- ³³A. Scherrer and D. Sebastiani, *J. Comput. Chem.* **37**, 665 (2016).
- ³⁴S. Hamel, A. J. Williamson, H. F. Wilson, F. Gygi, G. Galli, E. Ratner, and D. Wack, *Appl. Phys. Lett.* **92**, 3115 (2008).
- ³⁵D. Lu, F. Gygi, and G. Galli, *Phys. Rev. Lett.* **100**, 147601 (2008).
- ³⁶H. F. Wilson, D. Lu, F. Gygi, and G. Galli, *Phys. Rev. B* **79**, 245106 (2009).
- ³⁷A. C. Ihrig, A. Scherrer, and D. Sebastiani, *J. Chem. Phys.* **139**, 094102 (2013).
- ³⁸K. L. C. Hunt, *J. Chem. Phys.* **90**, 4909 (1989).
- ³⁹K. L. C. Hunt, Y. Q. Liang, R. Nimalakirithi, and R. A. Harris, *J. Chem. Phys.* **91**, 5251 (1989).
- ⁴⁰J. S. Bader and B. J. Berne, *J. Chem. Phys.* **100**, 8359 (1994).
- ⁴¹J. Borysow, M. Moraldi, and L. Frommhold, *Mol. Phys.* **56**, 913 (1985).
- ⁴²P. L. Silvestrelli, M. Bernasconi, and M. Parrinello, *Chem. Phys. Lett.* **277**, 478 (1997).
- ⁴³R. Ifimie and M. E. Tuckerman, *J. Chem. Phys.* **122**, 214508 (2005).
- ⁴⁴M.-P. Gaigeot and M. Sprik, *J. Phys. Chem. B* **107**, 10344 (2003).

- ⁴⁵J. Neugebauer, M. Reiher, C. Kind, and B. A. Hess, *J. Comput. Chem.* **23**, 895 (2002).
- ⁴⁶D. A. A. McQuarrie, *Statistical Mechanics* (University Science Books, 2000).
- ⁴⁷M. Thomas, M. Brehm, R. Fligg, P. Vohringer, and B. Kirchner, *Phys. Chem. Chem. Phys.* **15**, 6608 (2013).
- ⁴⁸R. Futrelle and D. McGinty, *Chem. Phys. Lett.* **12**, 285 (1971).
- ⁴⁹CPMD, Computer code, <http://www.cpmc.org/>, 2016.
- ⁵⁰P. Hohenberg and W. Kohn, *Phys. Rev.* **136**, B864 (1964).
- ⁵¹W. Kohn and L. J. Sham, *Phys. Rev.* **140**, A1133 (1965).
- ⁵²N. Troullier and J. L. Martins, *Phys. Rev. B* **43**, 1993 (1991).
- ⁵³A. D. Becke, *Phys. Rev. A* **38**, 3098 (1988).
- ⁵⁴C. Lee, W. Yang, and R. G. Parr, *Phys. Rev. B* **37**, 785 (1988).
- ⁵⁵G. Lippert, J. Hutter, and M. Parrinello, *Mol. Phys.* **92**, 477 (1997).
- ⁵⁶J. VandeVondele, M. Krack, F. Mohamed, M. Parrinello, T. Chassaing, and J. Hutter, *Comput. Phys. Commun.* **167**, 103 (2005).
- ⁵⁷J. VandeVondele and J. Hutter, *J. Chem. Phys.* **127**, 114105 (2007).
- ⁵⁸S. Goedecker, M. Teter, and J. Hutter, *Phys. Rev. B* **54**, 1703 (1996).
- ⁵⁹C. Hartwigsen, S. Goedecker, and J. Hutter, *Phys. Rev. B* **58**, 3641 (1998).
- ⁶⁰M. Krack, *Theor. Chem. Acc.* **114**, 145 (2005).
- ⁶¹S. Nosé, *J. Chem. Phys.* **81**, 511 (1984).
- ⁶²W. G. Hoover, *Phys. Rev. A* **31**, 1695 (1985).

2.6 DISCUSSION

In this chapter, we have established the methodological basis for an efficient calculation of electronic probability currents in complex molecular systems. The rigorous derivation of the nuclear velocity perturbation theory and its successful implementation in the electronic structure package CPMD provide the necessary tools for the applications presented in chapter 3. These are the dynamical time correlation function formulation of vibrational circular dichroism in the condensed phase (c.p. section 3.2), the formulation of the modern theory of magnetization for the nuclear velocity perturbation theory (c.p. section 3.3), the analysis of gauge invariant non-local pseudopotentials (c.p. section 3.4) and the fundamental question, as to which masses rotate and vibrate in a molecule, discussed in section 3.5.

Furthermore, we devised a condensed representation of the electronic susceptibility that separates the relevant part for molecular interactions in a very compact way. However, the moment expansion not only yields a compact representation, it also provides a direct way to its calculation as shown in section 3.6. For the application of the electronic susceptibility to molecular dynamics simulations, it was necessary to study the molecular geometry dependence of the response function. This has been achieved by means of a Taylor expansion in terms of the nuclear coordinates and provides a starting point of further development in this direction.

CHAPTER 3

FURTHER RESULTS NOT YET PUBLISHED

3.1 OVERVIEW

Based on the rigorous derivation and successful implementation, we report the first fully ab-initio calculation of dynamical vibrational circular dichroism (VCD) spectra in the liquid phase from nuclear velocity perturbation theory (NVPT) derived electronic currents. This application of the NVPT to VCD spectra in the liquid phase, along with a discussion of the gauge problem in the liquid phase, is presented in section 3.2.

One direct follow-up question is the extension of the presented theory to the ordered condensed phase. Such an extension might allow applications to e.g. polypeptides or parts of protein crystal structures. We present first steps towards NVPT VCD in the ordered condensed phase via an adaption of the modern theory of magnetization in section 3.3.

This late realization of a NVPT implementation is partially due to technical complications posed by the use of atom centered basis functions in conventional quantum chemical program packages. In the CPMD program package chosen by us, these difficulties are replaced by technical difficulties due to the presence of non-local pseudopotentials. Their effect to moving nuclei is discussed in section 3.4.

The rigorous derivation of the NVPT from the exact factorization of the electron-nuclear wave function (XF) leads to the question on how exactly the NVPT is related to the Born-Oppenheimer (BO) approximation procedure. We have studied the adiabatic limit of the XF as perturbative expansion in terms of the electron-nuclear mass ratio. The NVPT correction is recovered as the first correction to the BO limit. The additional kinetic coupling mediated via the vector potential is shown to account for the electronic mass in the nuclear Hamiltonian. The resulting position dependent mass renormalization provides an answer to the question what masses rotate and vibrate in molecules while at the same time maintaining an adiabatic point of view. This theoretical development and first applications are presented in section 3.5.

Finally, we take a further step in the calculation of the moment expanded representation of the electronic susceptibility in section 3.6. Bypassing the expensive iterative diagonalization, we present a simple way of a direct calculation of the moment expanded representation.

3.2 GAUGE IN THE LIQUID PHASE AND FIRST APPLICATIONS

The main motivation for the theoretical development and implementation of the nuclear velocity perturbation theory (NVPT) is its intended application to dynamical vibrational circular dichroism (VCD) spectra in the liquid phase. In this work, we report the first fully ab-initio calculation of dynamical VCD spectra in the liquid phase using NVPT derived electronic currents. Our approach is rigorous and general at and thus capable of treating weak interactions of chiral molecules as e.g. chirality transfer from a chiral molecule to an achiral solvent. We use an implementation of the NVPT that is projected along the dynamics to obtain the current and magnetic dipole moments required for accurate intensities. The gauge problem in the liquid phase is resolved in a twofold approach. The electronic expectation values are evaluated in a distributed origin gauge, employing maximally localized Wannier orbitals (MLWO). In a second step, the gauge invariant spectrum is obtained in terms of a scaled molecular moments, which allows to systematically include solvent effects while keeping a significant signal-to-noise ratio. We give a thorough analysis and discussion of this choice of gauge in the liquid phase. At low temperatures, we recover the established double harmonic approximation. The methodology is applied to chiral molecules ((S)-d₂-oxirane and (R)-propylene-oxide) in the gas phase and in solution. We find an excellent agreement with the theoretical and experimental references, including the emergence of signals due to chirality transfer.

3.2.1 MOTIVATION

A natural extension of the theoretical description of VCD is the combination of perturbation theory based currents with ab-initio molecular dynamics (AIMD)-based time correlation function (TCF) spectra in the condensed phase. This combination not only provides a general and rigorous extension of the established methods, it is also capable of describing weak inter-molecular interactions, chirality transfer^{23, 24, 27} and conformational changes⁶ in solution at ambient conditions. In other words, it more closely describes what experimentalists actually measure.

The missing link to realize this goal is an efficient scheme to compute the magnetic moments along a molecular dynamics. The magnetic field perturbation theory (MFPT) is not particularly suited for a condensed phase implementation due to the ill-definition of the one-particle position operator under periodic boundary conditions.¹⁴ However, our recent implementation of the NVPT^{54, 139} provides the necessary means for this task.

In this work, we report for the first time fully AIMD-based dynamical VCD spectra in the liquid phase, with currents evaluated according to the NVPT. We use an implementation of the NVPT in the plane wave code CPMD^{54, 114, 139} that is projected along the dynamics and hence provides favorable scaling properties, allowing the treatment of molecules in solution. The gauge problem in the liquid phase is resolved in a twofold approach. The electronic expectation values are evaluated in a distributed origin gauge, employing MLWOs. In a second step, the gauge invariant spectrum is obtained in terms of a scaled molecular gauge in order to address the disorder induced signal-to-noise problem.

We give a thorough analysis and discussion of this solution of the gauge problem in the liquid phase. At low temperatures, we recover the established double harmonic approximation in a stepwise approximation procedure. Our methodology is applied to chiral molecules in the gas phase and in solution, yielding an

excellent agreement with the theoretical and experimental references.

3.2.2 ELECTRONIC CURRENT OBSERVABLES ALONG MOLECULAR DYNAMICS

As shown in sections I.4.2 and I.4.3, the evaluation of VCD spectra in the TCF formalism requires the knowledge of the fluctuations of the current and the magnetic dipole moments at thermal equilibrium. The purpose of our work is to apply this approach to systems in the liquid phase. In the following, we introduce a projected form of the already reported NVPT¹³⁹ that is well-defined under periodic boundary conditions and requires only one additional perturbation calculation.

PROJECTED NUCLEAR VELOCITY PERTURBATION THEORY

In the NVPT, the total perturbative correction to the electronic wave function $\Phi_{\mathbf{R}}^{(1)}(\mathbf{r}, t)$ is obtained as a weighted sum over the component wise corrections

$$\Phi_{\mathbf{R}}^{(1)}(\mathbf{r}, t) = \sum_{\nu=1}^{N_n} \sum_{\alpha=1}^3 \lambda_{\alpha}^{\nu}(\mathbf{R}, t) \Phi_{\mathbf{R}, \nu\alpha}^{(1)}(\mathbf{r}). \quad (3.2.1)$$

In our preceding works,^{54,139} we have used the linearity of the theory to calculate the component wise corrections separately. This is the natural choice if one works in the double harmonic approximation and if one is interested in the atomic polar or atomic axial tensors.²⁶⁹ For the calculation of the dipole moments along a molecular dynamics, we only are interested in the perturbation along a particular nuclear velocity vector $\lambda_{\nu}(\mathbf{R}, t)$. This projection can be done a posteriori, using the atomic tensors, or a priori already in the setup of the perturbation calculation itself. The latter is particularly suited for our purpose and is presented in the following.

We first recall the already established relations.⁵⁴ At zeroth order, we recover the standard Born-Oppenheimer (BO) problem in eq. (2.2.34). At first order, the component wise relation in eq.(2.2.35) requires the component wise solution of the nuclear displacement perturbation

$$-\left[\hat{\mathcal{H}}_{BO} - \epsilon_{BO}^{(0)}(\mathbf{R})\right] \partial_{\alpha}^{\nu} \Phi_{\mathbf{R}}^{(0)}(\mathbf{r}) = \frac{\partial \hat{\mathcal{H}}_{BO}}{\partial R_{\alpha}^{\nu}} \Phi_{\mathbf{R}}^{(0)}(\mathbf{r}) \quad \forall \nu, \alpha. \quad (3.2.2)$$

The projection of the NVPT equations on the nuclear velocity vector $\lambda_{\nu}(\mathbf{R}, t)$ is made in the setup of a projected nuclear displacement perturbation (PNDP) Hamiltonian $\hat{\mathcal{H}}_{BO}^{PNDP}(t)$

$$\hat{\mathcal{H}}_{BO}^{PNDP}(t) = \sum_{\nu=1}^{N_n} \sum_{\alpha=1}^3 \lambda_{\alpha}^{\nu}(\mathbf{R}, t) \frac{\partial \hat{\mathcal{H}}_{BO}}{\partial R_{\alpha}^{\nu}}. \quad (3.2.3)$$

The corresponding projected nuclear displacement perturbation correction to the electronic wave function $\Phi_{\mathbf{R}}^{PNDP}(\mathbf{r}, t)$ is obtained as a projected version of eq. (3.2.2)

$$-\left[\hat{\mathcal{H}}_{BO} - \epsilon_{BO}^{(0)}(\mathbf{R})\right] \Phi_{\mathbf{R}}^{PNDP}(\mathbf{r}, t) = \hat{\mathcal{H}}_{BO}^{PNDP}(t) \Phi_{\mathbf{R}}^{(0)}(\mathbf{r}), \quad (3.2.4)$$

with

$$\Phi_{\mathbf{R}}^{PNDP}(\mathbf{r}, t) = \sum_{\nu=1}^{N_n} \sum_{\alpha=1}^3 \lambda_{\alpha}^{\nu}(\mathbf{R}, t) \partial_{\alpha}^{\nu} \Phi_{\mathbf{R}}^{(0)}(\mathbf{r}). \quad (3.2.5)$$

The projected version of eq. (2.2.35) reads

$$\left[\hat{\mathcal{H}}_{BO} - \epsilon_{BO}^{(0)}(\mathbf{R}) \right] \Phi_{\mathbf{R}}^{(1)}(\mathbf{r}, t) = \hbar \Phi_{\mathbf{R}}^{PNDP}(\mathbf{r}, t). \quad (3.2.6)$$

Solving eqs. (3.2.4) and (3.2.6) requires only 2 perturbation calculations, whereas the straightforward solution of the non-projected version in eqs. (3.2.2) and (2.2.35) requires $6N_n$ perturbation calculations.

We have shown that the potential energy surface remains unaffected if compared to the BO case, up to within the first-order of the perturbation.⁵⁴ The second order correction gives rise to a position dependent mass renormalization for the nuclear motion, as shown in section 3.5, and is calculated by means of the \mathcal{A} -matrix (c.p. eqs. (37-39) in ref.⁵⁴). The \mathcal{A} -matrix is only accessible in terms of the $3N_n$ component wise electronic corrections. If one is interested in the vector potential $\mathbf{A}_\nu(\mathbf{R}, t)$ itself, the component wise expression

$$\mathbf{A}_\nu(\mathbf{R}, t) = -2\hbar \sum_{\nu'=1}^{N_n} \sum_{\alpha=1}^3 \lambda_{\alpha}^{\nu'}(\mathbf{R}, t) \left\langle \nabla_\nu \Phi_{\mathbf{R}}^{(0)} \left| \Phi_{\mathbf{R}, \nu' \alpha}^{(1)} \right. \right\rangle_{\mathbf{r}} \quad (3.2.7)$$

can be recast in a projected form using eq. (3.2.1)

$$\mathbf{A}_\nu(\mathbf{R}, t) = -2\hbar \left\langle \nabla_\nu \Phi_{\mathbf{R}}^{(0)} \left| \Phi_{\mathbf{R}}^{(1)}(t) \right. \right\rangle_{\mathbf{r}}. \quad (3.2.8)$$

Instead of $6N_n$ perturbation calculations for the evaluation of eq. (3.2.7), only $N_n + 1$ calculations are needed for the solution of eq. (3.2.8).

OBSERVABLES

In a time-dependent picture, the expectation values of the current and of the magnetic dipole moment on the instantaneous state of the system are employed to evaluate eqs. (1.4.28) and (1.4.29). The expectation values of the electronic contributions to the current and magnetic dipole moment on the NVPT electronic wave function are

$$\dot{\boldsymbol{\mu}}_{\mathbf{R}}^e(t) = \left\langle \Phi_{\mathbf{R}}(t) \left| \hat{\boldsymbol{\mu}}^e \right| \Phi_{\mathbf{R}}(t) \right\rangle_{\mathbf{r}} \quad (3.2.9)$$

$$\mathbf{m}_{\mathbf{R}}^e(t) = \left\langle \Phi_{\mathbf{R}}(t) \left| \hat{\mathbf{m}}^e \right| \Phi_{\mathbf{R}}(t) \right\rangle_{\mathbf{r}}. \quad (3.2.10)$$

If the BO electronic wave function is used to approximate $\Phi_{\mathbf{R}}(\mathbf{r}, t)$, both equations are zero, i.e. the electronic contributions to the expectation values vanish. Within the NVPT, we obtain

$$\left\langle \hat{\boldsymbol{\mu}} \right\rangle_{\Psi} = \left\langle \dot{\boldsymbol{\mu}}_{\mathbf{R}}^{e,(1)}(t) \right\rangle_{\chi} + \sum_{\nu=1}^{N_n} \frac{Z_{\nu} e}{M_{\nu}} \left\langle \tilde{\mathbf{P}}_{\nu}(\mathbf{R}, t) \right\rangle_{\chi} \quad (3.2.11)$$

$$\left\langle \hat{\mathbf{m}} \right\rangle_{\Psi} = \left\langle \mathbf{m}_{\mathbf{R}}^{e,(1)}(t) \right\rangle_{\chi} + \sum_{\nu=1}^{N_n} \frac{Z_{\nu} e}{2M_{\nu} c} \left\langle \hat{\mathbf{R}}_{\nu} \times \tilde{\mathbf{P}}_{\nu}(\mathbf{R}, t) \right\rangle_{\chi}, \quad (3.2.12)$$

with $\tilde{\mathbf{P}}_{\nu}(\mathbf{R}, t) = \hat{\mathbf{P}}_{\nu} + \mathbf{A}_{\nu}(\mathbf{R}, t)$. Here, we have written the expectation values (on the left hand sides) on Ψ , the full electron-nuclear wave function in the NVPT approximation, in terms of expectation values of observables on χ , the nuclear wave function only. The vector potential appearing in the equations is of

the order $\mathcal{O}(\lambda_\nu/M_\nu)$. We have already shown that its contribution to the dipole moments is small⁵⁴ in the systems to be considered here, such that it is omitted in the following.

We consider the classical approximation of the nuclear subsystem by imposing that the nuclear density localizes infinitely at each time at the classical position denoted by the trajectory. The second terms on the right hand side of eqs. (3.2.11) and (3.2.12) then become simply functions of phase-space variables.⁵⁴

3.2.3 GAUGE IN THE LIQUID PHASE

The calculation of magnetic observables in the liquid phase poses two major conceptual difficulties. First, the electronic expectation values in the condensed phase have to be calculated under periodic boundary conditions. This is a well known problem also when working in the double harmonic approximation and has been addressed successfully in various ways.^{14,52,132,170} We resort to a combination of a distributed origin gauge with maximally localized Wannier orbitals^{14,112,139,270} (MLWO).

Furthermore, the VCD spectrum, as a physical observable, has to be gauge invariant. Working in a distributed origin gauge, the total spectrum is given by the sum of a molecular and a gauge transport term that will be introduced in the following. Due to the disorder inherent in the liquid phase, we observe that the gauge transport term is very sensitive to insufficient sampling of phase space and hence is likely to cover the actual signal, introducing a poor signal to noise ratio.

This especially applies to the case of a very dilute solution of a chiral solute in an achiral solvent. In this case, the dominant contribution to the spectrum turns out to be the noise on the infrared absorbance (IRA) from the solvent, since the amplitude of the IRA is about four orders of magnitude larger than the one of the VCD.

We need to extract a robust, gauge invariant dynamical VCD spectrum from the finite AIMD sampling of phase space. To do so, we adopt a previously introduced^{47,271} local correlation that enforces the expected, yet numerically hard to achieve decorrelation at long distances.

ELECTRONIC EXPECTATION VALUES: WANNIER GAUGE

We turn our attention to the first problem, the operator evaluation of the electronic magnetic dipole moment under periodic boundary conditions. It is known that the atomic axial tensor (AAT) $\mathcal{M}_{\alpha\beta}^{\nu\mathcal{O}}$ with respect to the origin \mathcal{O} transforms under shifts of the gauge origin $\mathcal{O} = \mathcal{O}' + \Delta$ as²⁷²

$$\mathcal{M}_{\alpha\beta}^{\nu\mathcal{O}} = \mathcal{M}_{\alpha\beta}^{\nu\mathcal{O}'} - \frac{1}{2c} \sum_{\gamma,\delta=1}^3 \epsilon_{\beta\gamma\delta} \Delta_\gamma \mathcal{P}_{\alpha\delta}^\nu. \quad (3.2.13)$$

The gauge is transported by the atomic polar tensor (APT) $\mathcal{P}_{\alpha\delta}^\nu$. In the projected form, the magnetic moment $m_\beta^\mathcal{O}$ with respect to the origin \mathcal{O} transforms correspondingly

$$m_\beta^\mathcal{O} = m_\beta^{\mathcal{O}'}(t) - \frac{1}{2c} \sum_{\gamma,\delta=1}^3 \epsilon_{\beta\gamma\delta} \Delta_\gamma \dot{\mu}_\delta \quad (3.2.14)$$

and the gauge is transported by the current dipole moment $\dot{\mu}_\delta$. This property can be used to evaluate the position operator in a state wise distributed origin.^{14,273}

This approach, a combination of state wise origins with MLWOs, has already been applied successfully to the calculation of nuclear magnetic resonance chemical shifts.^{14,270} The canonical ϕ_o and localized φ_o states are mutually related via the unitary transformation of the unperturbed ground-state orbitals

$$|\varphi_o\rangle = \sum_{o'} U_{oo'}^{(0)} |\phi_{o'}\rangle. \quad (3.2.15)$$

This assumes that the response orbitals are sufficiently localized in the region of their respective unperturbed ground-state orbitals. In the distributed origin gauge, the position operators are calculated with the corresponding Wannier center as their state wise origins

$$\langle \hat{\mathbf{r}} \rangle_o = \langle \varphi_o | \hat{\mathbf{r}} | \varphi_o \rangle. \quad (3.2.16)$$

This state wise origin is introduced in the electronic magnetic dipole moment operator

$$\hat{\mathbf{m}} = -\frac{e}{2mc} \left[(\hat{\mathbf{r}} - \langle \hat{\mathbf{r}} \rangle_o) \times \hat{\mathbf{p}} + \langle \hat{\mathbf{r}} \rangle_o \times \hat{\mathbf{p}} \right], \quad (3.2.17)$$

where we define an orbital-dependent operator in which the position operator is centered around the corresponding Wannier center

$$\hat{\mathbf{m}}_{|\langle \hat{\mathbf{r}} \rangle_o} = -\frac{e}{2mc} (\hat{\mathbf{r}} - \langle \hat{\mathbf{r}} \rangle_o) \times \hat{\mathbf{p}}. \quad (3.2.18)$$

In insulating systems, the MLWOs decay exponentially such that the non-physical jump of the sawtooth position operator under periodic boundary conditions occurs in a region where the orbitals are practically zero.^{14,137} This assures the well-definition of eq. (3.2.18). The total expectation value is a sum over well defined expectation values and is given by

$$\mathbf{m}^e(t) = \sum_o \left[\langle \varphi_o | \hat{\mathbf{m}}_{|\langle \hat{\mathbf{r}} \rangle_o} | \varphi_o^{(1)}(t) \rangle_{\mathbf{r}} + \frac{1}{2c} \langle \hat{\mathbf{r}} \rangle_o \times \langle \varphi_o | \hat{\boldsymbol{\mu}} | \varphi_o^{(1)}(t) \rangle_{\mathbf{r}} + \text{c.c.} \right]. \quad (3.2.19)$$

Before the final evaluation of the VCD spectra, the state wise electronic contributions are attributed to their corresponding molecules, based on the localization of their Wannier centers. Both, the electronic and the classical nuclear contributions, are translated to the center of mass \mathbf{R}_I of the corresponding molecule I , which allows to introduce well defined molecular current $\boldsymbol{\mu}_I$ and magnetic dipole moments $\mathbf{m}_I \equiv \mathbf{m}_I|_{\mathbf{R}_I}$. The total magnetic moment with respect to the common origin \mathcal{O} is

$$\mathbf{m}|_{\mathcal{O}}(t) = \sum_{I=1}^{N_{\text{mols}}} \mathbf{m}_I|_{\mathbf{R}_I}(t) + \frac{1}{2c} (\mathbf{R}_I(t) - \mathcal{O}) \times \boldsymbol{\mu}_I(t). \quad (3.2.20)$$

In a pseudo isolated system, i.e. working in the super cell approach with a large enough simulation box, the VCD spectrum of a chiral molecule in an achiral solution is proportional to

$$\langle \boldsymbol{\mu} \cdot \mathbf{m}|_{\mathcal{O}}(t) \rangle = \sum_{I,J=1}^{N_{\text{mols}}} \langle \mathbf{m}_I|_{\mathbf{R}_I}(t) \cdot \boldsymbol{\mu}_J \rangle + \frac{1}{2c} \langle (\mathbf{R}_I(t) - \mathcal{O}) \times \boldsymbol{\mu}_I(t) \cdot \boldsymbol{\mu}_J \rangle. \quad (3.2.21)$$

The first term contains only molecular moments and is invariant under shifts of the origin. We denote it as the “molecular term” in the following. In contrast, the second term depends on the distance of the molecules from the gauge origin and hence on the chosen origin. We denote it as the “gauge transport term” in the following.

ANALYSIS OF THE GAUGE TRANSPORT TERM

With well-defined molecular dipole moments in a distributed molecular origin gauge, the gauge invariance of the physical observable is not yet assured. The final observable, the VCD spectrum or the rotational strength, is only gauge invariant if working in a common origin gauge. In a common origin gauge, according to eq. (3.2.21), any further translation of the gauge origin $\mathcal{O} = \mathcal{O}' + \Delta$ does not change the spectrum

$$\langle \dot{\boldsymbol{\mu}} \cdot \mathbf{m} |_{\mathcal{O}}(t) \rangle = \langle \dot{\boldsymbol{\mu}} \cdot \mathbf{m} |_{\mathcal{O}'}(t) \rangle - \frac{1}{2c} \langle \dot{\boldsymbol{\mu}}(t) \times \dot{\boldsymbol{\mu}} \rangle \cdot \Delta. \quad (3.2.22)$$

To obtain eq. (3.2.22), the summation in eq. (3.2.21) has been carried out, yielding a triple product of the translation vector with the total current dipole moment TCF. This term vanishes due to the stationarity and time reversal symmetry of the TCFs

$$\langle \dot{\mu}_\alpha(t) \dot{\mu}_\beta \rangle = \langle \dot{\mu}_\alpha \dot{\mu}_\beta(t) \rangle. \quad (3.2.23)$$

In a molecular dynamics simulation under periodic boundary conditions, this common origin is not well defined. One approach to address this problem is provided by the modern theory of magnetization,^{132,141} in which the sample magnetization can be calculated from bulk properties only. This is important if working in the ordered condensed phase, since the itinerary current can contribute significantly to the total magnetization. At variance, if working in the liquid phase, we expect the itinerary contribution to be small due to the finite correlation length and the total cell magnetization to be dominated by the gauge transport term. In particular, if we look at the case of a dilute chiral solute in an achiral solvent, the desired signal is only due to a single molecule and its near surrounding.

We rely on an alternative approach to address the gauge problem in the liquid phase. We can assume that the time correlation of the molecular motion in the liquid phase decays with increasing inter-molecular distances. In the limit of a large enough solvation cell, the molecular motions of two distant molecules are on average decorrelated. To which extent this is the case in our finite size and finite length simulations is analyzed in the following.

In our analysis, we choose (R)-propylene-oxide as a neat liquid and as a solute in water. Adapting the regularized decomposition of the IRA spectrum proposed by Heyden et al.,^{47,271} we quantify the magnitude of the relevant terms in the molecular and the gauge transport term. The mathematical procedure is described in section B.2 of the appendix.

The main result is a symmetry decomposition of the VCD spectrum in terms of the inter-molecular distance $\mathbf{r}_{12}(t) = \mathbf{R}_{IJ}(t) = \mathbf{R}_I(0) - \mathbf{R}_J(t)$. In the isotropic average, we can decompose the total spectrum in terms of a spatially resolved TCF between the molecular magnetic dipole moments in the molecular gauge \mathbf{m} and the molecular current dipole moments $\dot{\boldsymbol{\mu}}$. In the decomposition, we identify the molecular term $\Theta_0^{\dot{\boldsymbol{\mu}}\mathbf{m}}(r, t)$ and a second term proportional to $r\Theta_1^{\dot{\boldsymbol{\mu}}\dot{\boldsymbol{\mu}}}(r, t)$ that arises from the gauge transport term

$$\frac{1}{3} \text{Tr} \left[\int \frac{d\Omega}{4\pi} \left\langle \left(\dot{\boldsymbol{\mu}}\mathbf{m}(t) + \frac{1}{2c} \dot{\boldsymbol{\mu}}(\mathbf{r}_{12}(t) \times \dot{\boldsymbol{\mu}}(t)) \right) \delta(\mathbf{r} - \mathbf{r}_{12}(t)) \right\rangle \right] = \Theta_0^{\dot{\boldsymbol{\mu}}\mathbf{m}}(r, t) + \frac{1}{3c} r \Theta_1^{\dot{\boldsymbol{\mu}}\dot{\boldsymbol{\mu}}}(r, t). \quad (3.2.24)$$

This second term is scaled by the inter-molecular distance and it is this additional scaling, which introduces a slower convergence compared to the bare IRA.

In fig. 3.1, we show the two contributions to the dynamical VCD spectrum of bulk (R)-propylene-oxide solution, along with the IRA contribution $\Theta_0^{\dot{\mu}\dot{\mu}}(r, \tilde{\nu})$. The corresponding decompositions in a solvated system of (R)-propylene-oxide in water are depicted in fig. 3.2. In section B.2.3 of the appendix, we provide an additional discussion of the decomposed spectra of bulk water and a single (R)-propylene-oxide molecule solvated in water.

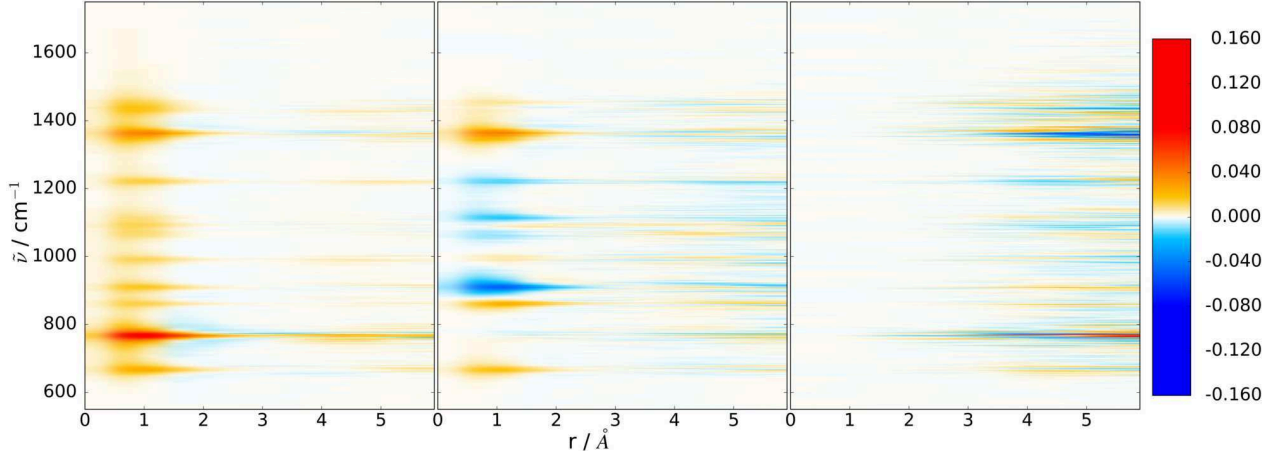


Figure 3.1: Isotropic radial decompositions of the vibrational IRA and VCD spectra of bulk (R)-propylene-oxide: 1. IRA spectrum $\Theta_0^{\dot{\mu}\dot{\mu}}(r, \tilde{\nu}) \cdot 10^{-4}$. 2. Molecular VCD term $\Theta_0^{\dot{\mu}\mathbf{m}}(r, \tilde{\nu})$. 3. Gauge transport VCD term $\frac{1}{3c} r \Theta_1^{\dot{\mu}\dot{\mu}}(r, \tilde{\nu})$. Intensities in $\text{\AA}^{-1} \text{cm}^{-1}$. The spatial extension of the molecular signals range up to about 2 \AA ; the features around 5 \AA correspond to its nearest neighbor molecules.

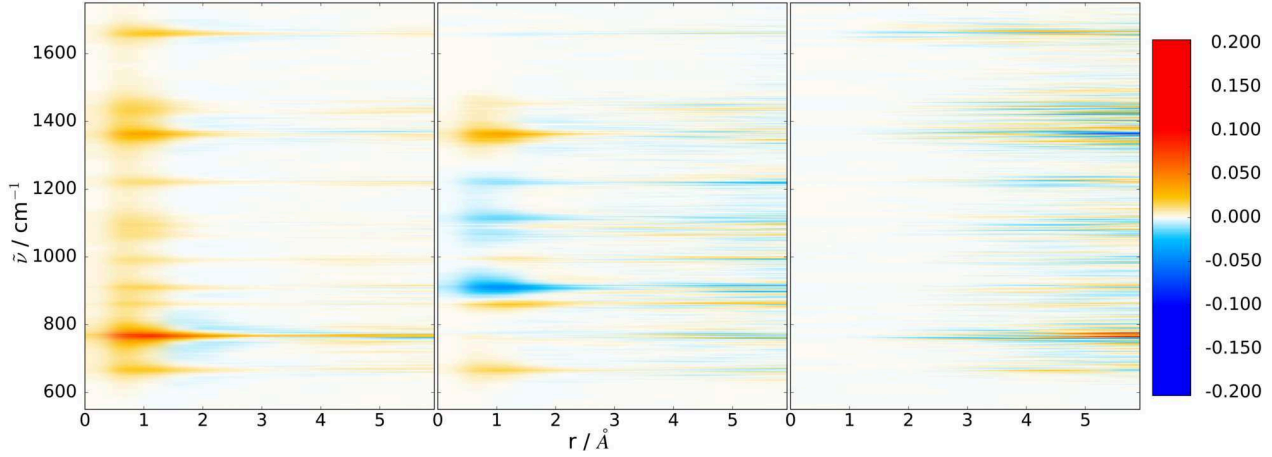


Figure 3.2: Isotropic radial decompositions of the vibrational IRA and VCD spectra of (R)-propylene-oxide solvated in water (7M concentration): 1. $\Theta_0^{\dot{\mu}\dot{\mu}}(r, \tilde{\nu}) \cdot 10^{-4}$. 2. $\Theta_0^{\dot{\mu}\mathbf{m}}(r, \tilde{\nu})$. 3. $\frac{1}{3c} r \Theta_1^{\dot{\mu}\dot{\mu}}(r, \tilde{\nu})$. Intensity in $\text{\AA}^{-1} \text{cm}^{-1}$.

Our analysis shows that the signals (in IRA and VCD) due to the molecular terms Θ_0 predominantly originate from small distances, i.e. from the intra molecular correlation itself. These contributions show the expected spectral features, with the additional sign fingerprint in case of the VCD. At larger distances, also the gauge transport term contributes to the spectrum, with amplitudes similar to the spectral intensities of the molecular signals. These contributions are highly fluctuating and, if integrated, yield a very noisy background to the spectrum, which covers the spectral features at smaller distances. The additional scaling by the distance further increases this noise. As discussed in the appendix, we attribute these highly oscillatory

contributions to the fluctuations of instantaneous chirality that only vanish on average, i.e. with improved sampling.

In the (R)-propylene-oxide water solution, we observe additional spectral features, most prominently at the water bending mode (1650 cm^{-1}), that also show up in the molecular and gauge transport term of the VCD. These originate from a) electronic polarization effects and b) changed molecular dynamics, e.g. due to hydrogen-bond formation. The decomposition does not provide a clear cut separation of the two effects but it allows to visualize their spatial distribution. In the following analysis, we make use of the fact that this solvation feature begins already at smaller distances than the other noisy contributions to the VCD spectrum.

In view of the gauge problem in the liquid phase, we observe that the dominant contributions to the spectrum are located within the first solvation shell. This result has already been established in the IRA case by Heyden and coworkers.^{47,271} In our case, the gauge transport, with the additional scaling by the distance r , results in an increased computational requirement of the sampling as compared to the IRA case, which renders the application of the TCF formalism to VCD in solution more difficult than for conventional IRA. However, with a finite correlation depth in the frequency range of interest, the gauge problem could be solved naturally by using a sufficiently large super cell and simulation time.

LOCAL CHIRALITY - LOCAL CORRELATION

From the results of the previous section, we know that the relevant contributions to the spectrum originate within the first solvation shells of the molecules. In order to localize the correlation to the relevant part and to discard the noisy part of the environment, we introduce scaled molecular moments that contain only the molecular moments in a finite region around a chosen center. Again, along the lines of ref.,⁴⁷ we adapt the concept of local correlation. For a chiral molecule K , we include the effect of the surrounding molecules J

$$\dot{\mathbf{m}}_K^s(t) = N_K^s(t) \left(\dot{\mathbf{m}}_K(t) + \sum_{J(\neq K)} P_{KJ}(t) \dot{\mathbf{m}}_J(t) \right) \quad (3.2.25)$$

$$\mathbf{m}_K^s(t) = N_K^s(t) \left(\mathbf{m}_K(t) + \sum_{J(\neq K)} P_{KJ}(t) \mathbf{m}_J(t) \right), \quad (3.2.26)$$

with a damping function for inter-molecular contributions $P_{KJ}(t) = (1 + \exp\{(|\mathbf{R}_{KJ}(t)| - R_0)/D\})^{-1}$ and normalization $N_K^s(t) = (1 + \sum_{J(\neq K)} P_{KJ}^2(t))^{-1/2}$. The correlation depth is controlled by the parameter R_0 and the slope of the cutoff by the sharpness parameter D .

We have to distinguish between two different situations. If we consider a single chiral molecule K in an achiral solvent, the chirality of the system is well localized and we expect the spectrum to originate from the vicinity of the chiral center. In this case the normalization has to be omitted to avoid downscaling the molecular contribution. In a chiral bulk liquid, the surrounding molecules J equally contribute and we have to normalize the scaled moments to obtain a normalized spectrum. In practice, each molecule can then be considered as solute and solvent and the local correlation can be calculated for each chiral center in the simulation cell.

3.2.4 NUMERICAL RESULTS

Using our projected NVPT implementation, we have calculated AIMD-based dynamical VCD spectra of a series of systems. In the following discussion, we first present spectra of (S)-d₂-oxirane and (R)-propylene-oxide in the gas phase and subsequently invoke the harmonic limits using effective normal modes.^{46, 274} The mathematical procedure is reviewed in section A.3 of the appendix. Secondly, we show the spectrum of (R)-propylene-oxide as a bulk liquid and introduce the local correlation technique. Finally, we discuss the induced chirality of (R)-propylene-oxide solvated in water as an example for an achiral solvent. The used implementation of the projected NVPT is accessible for scientific use in the official version of the CPMD program package.

DYNAMIC AND STATIC SPECTRA IN THE GAS PHASE

For molecules in the gas phase, the double harmonic approximation, possibly including anharmonicity corrections, is the natural choice for the calculation of VCD spectra. The use of the TCF formalism can be of interest if the molecule has conformational degrees of freedom.^{56, 275} At the present stage, we wish to benchmark our method and to subsequently recover the double harmonic approximation to assign the spectral features to molecular motion. To start with, we look at the small rigid chiral molecule (S)-d₂-oxirane.

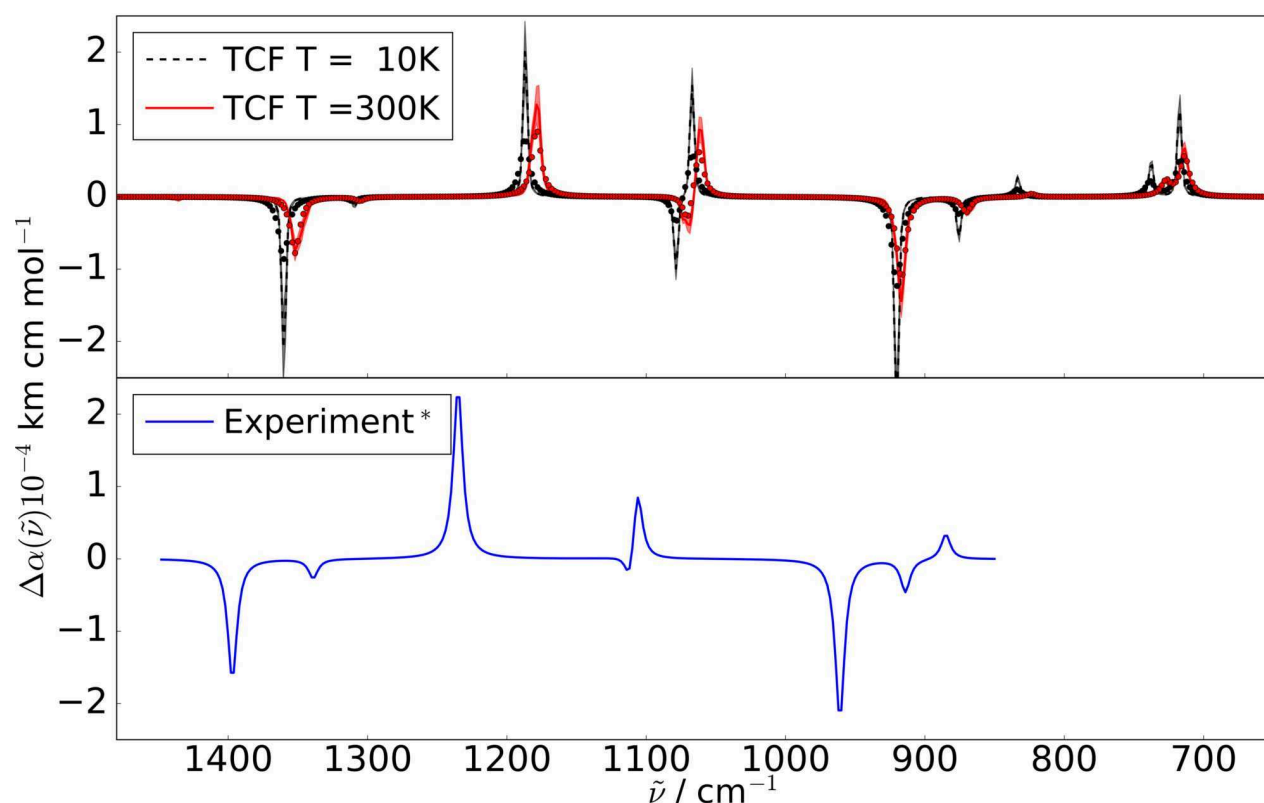


Figure 3.3: Dynamical VCD spectrum of an isolated (S)-d₂-oxirane molecule at 10K and 300K. The dots are the effective mode intensities according to eq. (A.3.8). The experimental data are reconstructed from the reported²⁷⁶ band intensities employing a Lorentzian line shape function.

In fig. 3.3, we show the dynamical VCD spectra of this system, both at 10K and 300K. To indicate our statistical error, we have included the standard deviation $\sigma(\omega)$ as shaded areas to our plots. This statistical

uncertainty manifests itself mainly at the high intensity peaks. We employ a Lorentzian line shape for the reconstruction of the experimental data from ref.²⁷⁶ and the effective modes. We find that the TCF spectra show all the features of the experimental spectrum and also provide the correct sign information for all intensity bands. The harmonic limit of the molecular motion is taken by extracting effective modes (EM) from the AIMD, as described in the appendix. The intensities of the EM are shown with dots in the corresponding color and show a very close match to the TCF spectrum.

Furthermore, we have also calculated the VCD spectrum in the double harmonic approximation. The intensities of the normal mode (NM) bands are so close to the EMs at 10K that they would be indistinguishable in the figure. We therefore provide the summary of frequencies, dipole and rotational strengths at the different levels of approximation in table 3.1. The results show that NMs are in very good agreement with the EMs and thus with the TCF spectrum. At higher temperature, we observe a broadening of the line shape of the peaks, together with slightly changed peak positions.

To benchmark dynamical VCD spectra in the liquid phase, we have chosen the (R)-propylene-oxide molecule. As a preliminary analysis, we have calculated dynamical VCD spectra of this molecule in the gas phase at 340K. The results, along with the experimental reference and the NM analysis, are shown in fig. 3.4. Also here, all features of the experimental spectrum are well represented in the TCF spectrum. Similar to the (S)-d₂-oxirane molecule, an EM analysis can provide a dissection of the spectrum in terms of vibrational modes. However, the resolution of the vibrational modes of the methyl-group introduces nearly degenerate modes that are hard to separate.

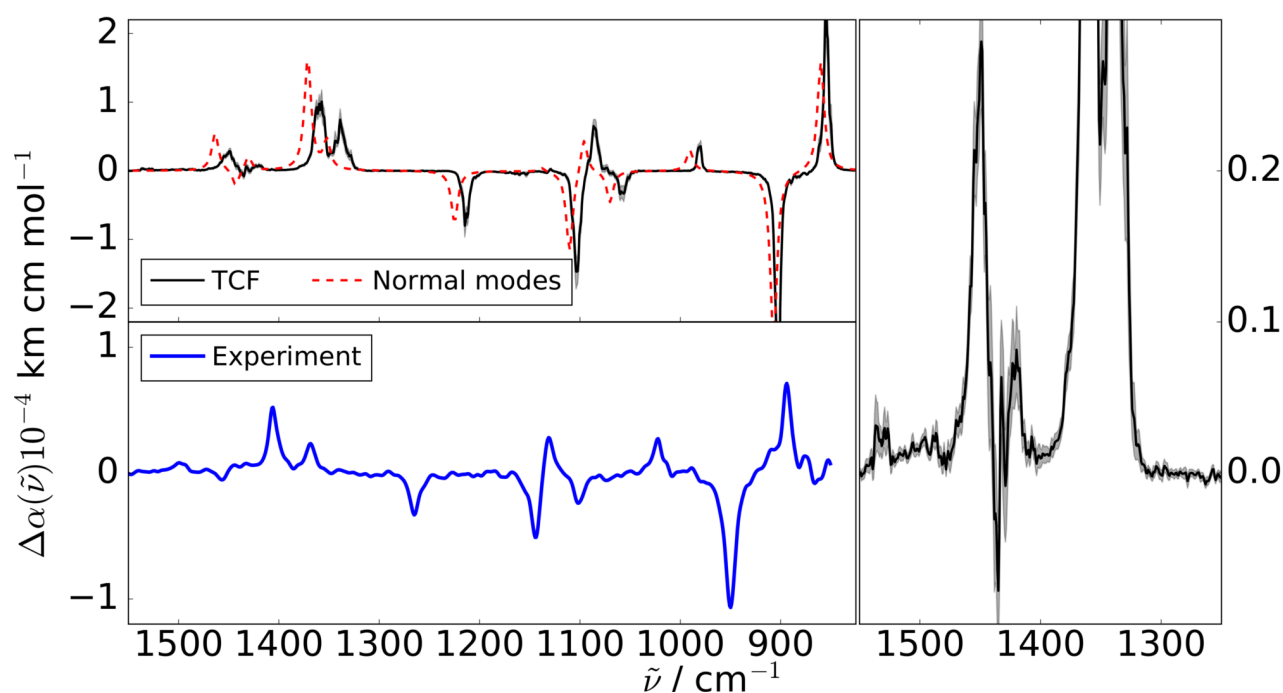


Figure 3.4: Dynamical VCD spectrum of an isolated (R)-propylene-oxide molecule at 340K. The TCF spectrum is consistent with the double harmonic approximation and shows all the features of the experimental spectrum. The enlarged view on the right shows the TCF spectrum in the region 1550-1250 cm^{-1} .

The presented results in figs. 3.3 and 3.4 show that the AIMD-based dynamical VCD spectra are consistent with the theoretical predictions in the double harmonic approximation and in very good agreement

with the experimental references, apart from a scaling factor usual in DFT studies of vibrational spectra. The VCD spectrum calculated in the TCF formalism shows additional spectral features due to anharmonic effects. In the enlarged view on the right of fig. 3.4 we see additional features at 1406 and 1530 cm^{-1} . These have been attributed to overtones and combination bands.²⁷⁷

Table 3.1: Vibrational frequencies, dipole and rotational strengths of (S)-d₂-oxirane from normal modes (NM) and effective modes (EM).

Experiment ²⁷⁶			NM			EM 10K			EM 300K		
$\tilde{\nu}$	D	R	$\tilde{\nu}$	D	R	$\tilde{\nu}$	D	R	$\tilde{\nu}$	D	R
673			635	1.0	-0.7	635	1.1	-1.0	634	1.0	-1.3
754			717	132.7	9.4	717	122.0	8.9	714	142.7	9.7
817			741	51.3	3.3	739	50.2	3.4	727	49.0	3.5
885		5.0	833	150.6	2.6	834	128.9	1.6	824	158.0	0.7
914	6.3	-6.2	872	9.7	-3.4	875	8.5	-3.4	870	7.5	-2.9
961	54.0	-29.0	918	32.4	-18.3	920	29.3	-16.8	917	22.3	-15.5
1106	8.6	11.1	1067	4.1	7.5	1067	4.0	7.4	1062	4.5	8.2
1112		-4.9	1079	2.1	-5.5	1079	2.0	-4.8	1070	2.2	-4.7
1235	29.6	24.1	1187	23.7	10.4	1187	20.0	8.6	1179	27.2	9.8
1339	2.3	-2.5	1310	0.2	-0.6	1310	0.2	-0.5	1305	0.3	-0.5
1397	12.0	-15.0	1361	10.0	-8.1	1360	10.0	-8.0	1352	8.0	-7.2
2240	27.0	-10.4	2213	49.5	-22.2	2217	54.9	-25.8	2199	49.7	-23.8
2254	5.7	12.1	2224	13.0	16.0	2227	15.9	20.7	2214	12.0	15.8
3015		-8.9	3016	11.2	-32.2	3029	11.0	-31.9	3009	10.3	-23.5
3028	53.0	11.4	3022	59.4	46.5	3034	61.0	49.5	3024	45.7	36.5
$\tilde{\nu}$ in cm^{-1} , D in $10^{-40} esu^2 cm^2$, R in $10^{-44} esu^2 cm^2$											

VIBRATIONAL CIRCULAR DICHROISM IN THE BULK

The principal application of our development is the calculation of VCD spectra in the liquid phase. We have chosen bulk (R)-propylene-oxide as a benchmark system and employ the normalized local correlation presented in section 3.2.3 to obtain a gauge invariant spectrum from our finite AIMD.

The results of the TCF calculations are given in fig. 3.5, where we show the dynamical IRA and VCD with an experimental reference. We employ two different cutoffs for the damping function, centered at the centers of mass of the (R)-propylene-oxide molecules. For the small cutoffs, we only observe the molecular contributions due to the chiral molecules themselves. In contrast, the cutoff $R_0 = 6\text{\AA}$ includes the first solvation shell, so that the total spectrum is mainly due to the molecular contributions of all molecules in the first solvation shell. As a main result, we find that in this system, the inter-molecular contributions do not significantly change the spectrum at the given statistical resolution.

To indicate our statistical error, we have again included the standard deviation $\sigma(\omega)$ as shaded areas to our plots. Compared to the isolated system, the two intensity bands at 1400 cm^{-1} are not as much resolved.

The broadening is due to environmental effects on the molecular spectra. Also in the double harmonic picture, the two band positions are much closer than in the experimental observation. The use of a more exact exchange correlation functional might yield better separated vibrational frequencies.

In view of the very recently published density derived dynamical VCD spectra,⁵² we think that a comparison of the two AIMD-based currents is an interesting question for future studies. We conclude that, in the systems analyzed in this work, the NVPT for VCD provides a rigorous thus robust theoretical approach.

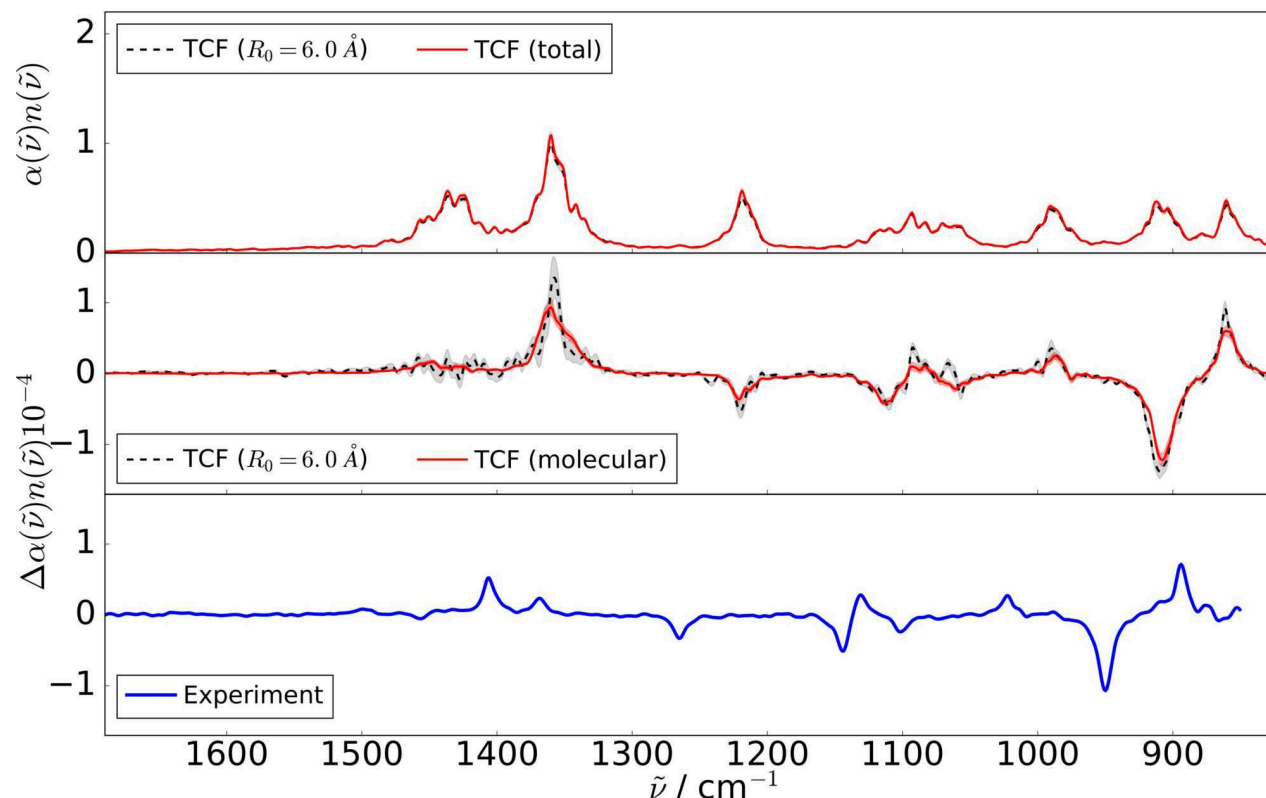


Figure 3.5: Dynamical IRA and VCD spectra of bulk (R)-propylene-oxide at 340K. The intensities are in units of km cm mol^{-1} . We show the molecular correlation and a damping cutoff $R_0 = 6\text{\AA}$, which includes the first solvation shell. The shaded areas indicate the standard deviation of the statistically independent microcanonical simulations. The experimental data are already divided by the refractive index and are in arbitrary units.*

CHIRALITY TRANSFER TO AN ACHIRAL SOLVENT

As a first application of dynamical VCD spectra, we look at the chiral solute (R)-propylene-oxide in an achiral solvent, in our case water. For this system, an additional VCD signal in the water bending region (1650 cm^{-1}) has been reported, which is not present in the bulk spectrum.^{23,24} The explanation for this effect has been a chirality transfer from the chiral solute to the achiral solvent, i.e. the on average achiral water molecules interact with the chiral molecule such that their average dynamics becomes chiral.

From the theoretical perspective, this effect has already been analyzed successfully, using a combination of classical molecular dynamics simulations and explicit solvent clusters in the double harmonic approximation.^{23,24} We expect that an AIMD-based TCF calculation of the VCD spectrum should naturally yield the chirality transfer signal and additionally provide an atomistic description of its origin.

We show the dynamical IRA and VCD spectra from our calculations in figs. 3.6 and 3.7, along with an experimental reference. Again, we employ the local correlation presented in section 3.2.3, this time however without the normalization.

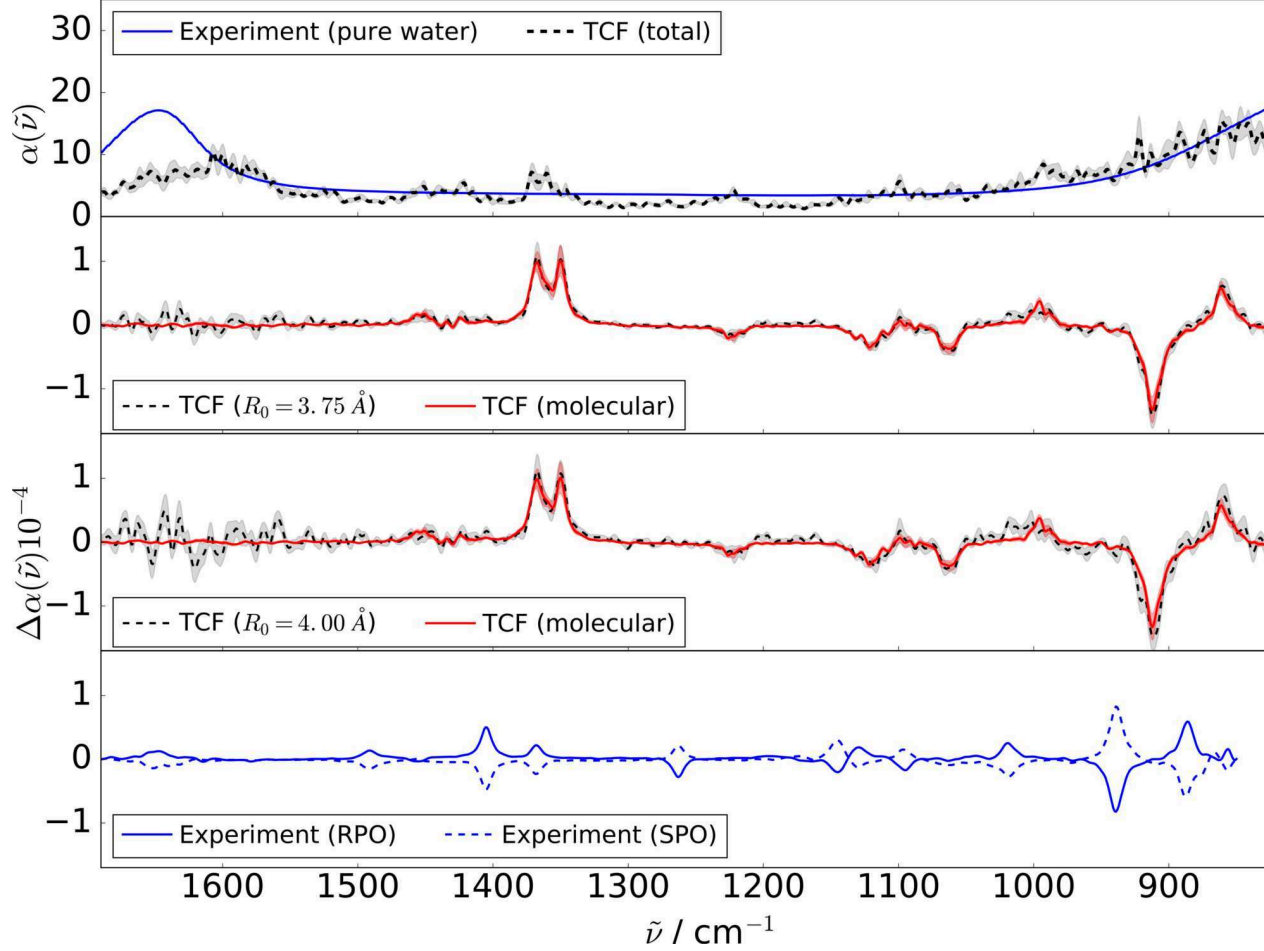


Figure 3.6: Dynamical IRA and VCD spectra of (R)-propylene-oxide solvated in water at 340K (7M concentration). The intensities are in units of km cm mol^{-1} . We show the molecular correlation and damping cutoffs of $R_0 = 3.75 \text{ \AA}$ and $R_0 = 4.0 \text{ \AA}$, which includes the hydrogen bonded water molecules. The shaded areas indicate the standard deviation of the statistically independent microcanonical simulations. The experimental data are taken from ref.²⁴ and are in arbitrary units. We have divided the computed spectra by the refractive index of bulk water²⁷⁸ to compare with the experiment.

As a first result, we find that the molecular VCD spectrum shows all the features of the experimental spectrum except at the signal in the water bending region (1650 cm^{-1}). This spectral feature is systematically included by increasing the scaling cutoff, i.e. the inclusion of the hydrogen bonded water molecules via the cutoff $R_0 \geq 3.75 \text{ \AA}$ leads to the emergence of the experimentally observed signal. This result is in line with the findings of ref.^{23,24} The signal due to the chirality transfer, despite the discussed signal-to-noise complications, naturally shows up in our AIMD TCF approach.

As a second step, we analyze the disorder induced signal-to-noise ratio in this system. In the IRA, we see that the solute signal is several orders of magnitude smaller than the solvent contribution. This manifests itself also in the VCD spectrum in terms of the dominant contribution of the solvent contribution to the gauge-term (c.p. section 3.2.3 and the appendix). We compare the cutoff dependence of the mean standard deviation $\bar{\sigma}(R_0)$ at the two different solute concentrations of (R)-propylene-oxide in water and bulk (R)-

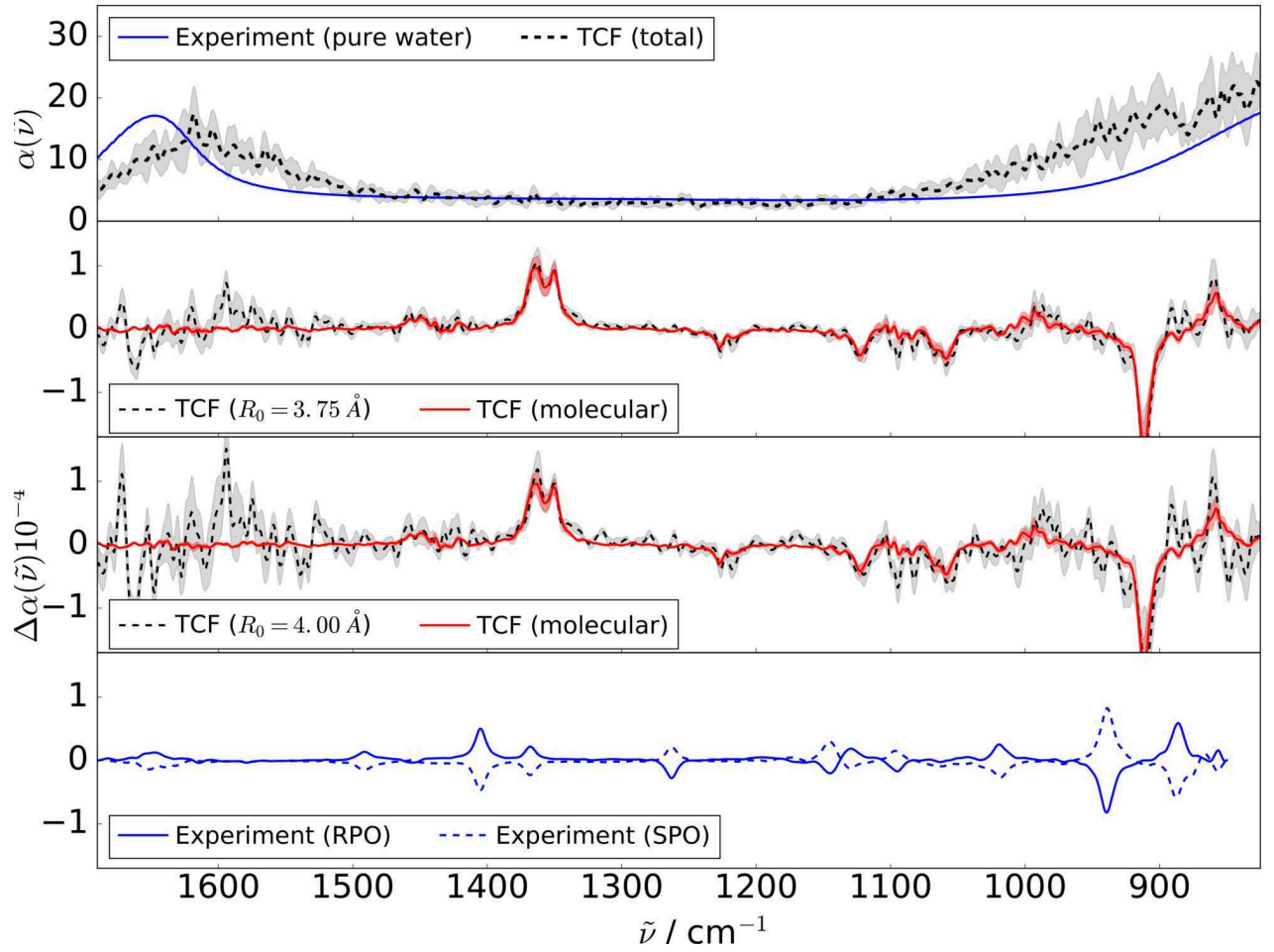


Figure 3.7: Dynamical IRA and VCD spectra of a (R)-propylene-oxide molecule solvated in water at 340K (infinite dilution). The intensities are in units of km cm mol^{-1} . We show the molecular correlation and damping cutoffs of $R_0 = 3.75\text{\AA}$ and $R_0 = 4.0\text{\AA}$, which includes the hydrogen bonded water molecules. The shaded areas indicate the standard deviation of the statistically independent microcanonical simulations. The experimental data are taken from ref.²⁴ and are in arbitrary units. We have divided the computed spectra by the refractive index of bulk water²⁷⁸ to compare with the experiment.

propylene-oxide in fig. (3.8). The graph illustrates the expected signal-to-noise at larger distances and shows that the chosen cutoffs are, given the available sampling, the best compromise. The cutoff $R_0 = 3.75\text{\AA}$ is the first cutoff that significantly includes solvent contributions while at the same time still having a significant signal-to-noise ratio.

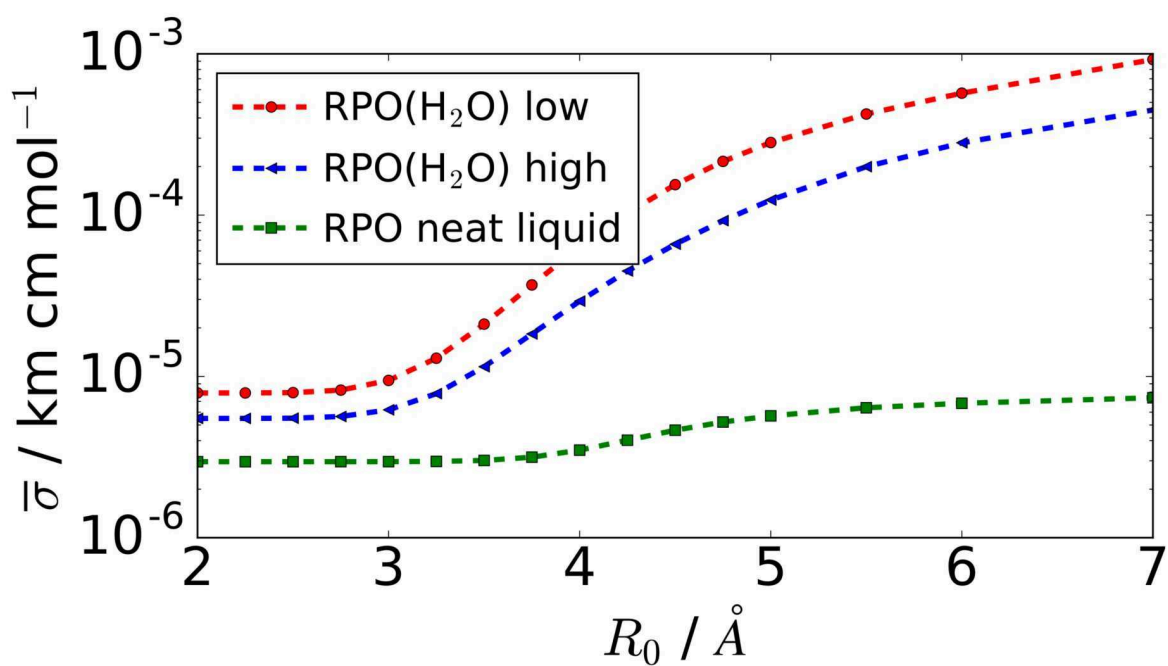


Figure 3.8: Cutoff dependence of the mean standard deviation of the VCD spectra. The magnitudes at the molecular level, i.e. at small distances, originate from the different quantity of sampling. However, the much larger relative changes at larger distances are system imminent.

3.3 MODERN THEORY OF MAGNETIZATION AND THE NUCLEAR VELOCITY PERTURBATION THEORY

The extension of the NVPT theory and implementation to the ordered condensed phase requires to take into account additional terms in the final observable. In oriented systems, also the quadrupole moment is contributing,^{149,279} even though in practice it is often neglected.^{280–283} However, the decorrelation at long distances, which is a reasonable assumption in the liquid state, can occur on much larger scales in the ordered condensed phase. An application to e.g. polypeptides or parts of protein crystal structures therefore needs a further analysis to assure gauge invariant spectra. As discussed in section 1.3, the modern theory of magnetization^{132,140,141} (MTM) provides a protocol to express the total magnetization of an extended sample in terms of properties of the bulk MLWOs. In this section we present an adaptation of the MTM in the NVPT framework for VCD.

In the following discussion we denote canonical KS orbitals with $|\Phi_o\rangle$, and MLWOs with $|w_o\rangle$. The calculation of the NVPT in the canonical representation

$$\hat{\mathcal{H}}|\Phi_o^{(0)}\rangle - \epsilon_o^{(0)}|\Phi_o^{(0)}\rangle = 0 \quad (3.3.1)$$

$$\hat{\mathcal{H}}|\Phi_o^{(1)}\rangle - \epsilon_o^{(0)}|\Phi_o^{(1)}\rangle = i\hbar\dot{\mathbf{R}} \cdot \frac{\partial}{\partial \mathbf{R}}|\Phi_o^{(0)}\rangle \quad (3.3.2)$$

is expressed in terms of MLWOs with cell translation vectors \mathbf{L}

$$|w_o^{(0)}(\mathbf{L})\rangle = \sum_{o'} U_{oo'}(\mathbf{L})|\Phi_{o'}^{(0)}\rangle \quad \text{and} \quad |\Phi_o^{(0)}\rangle = \sum_{\mathbf{L}} \sum_{o'} U_{oo'}^{-1}(\mathbf{L})|w_{o'}^{(0)}(\mathbf{L})\rangle \quad (3.3.3)$$

as

$$\hat{\mathcal{H}}|w_o^{(0)}(\mathbf{L})\rangle - \sum_{\mathbf{L}'} \sum_{o'} \Lambda_{oo'}(\mathbf{L}, \mathbf{L}')|w_{o'}^{(0)}(\mathbf{L}')\rangle = 0 \quad (3.3.4)$$

$$\hat{\mathcal{H}}|w_o^{(1)}(\mathbf{L})\rangle - \sum_{\mathbf{L}'} \sum_{o'} \Lambda_{oo'}(\mathbf{L}, \mathbf{L}')|w_{o'}^{(1)}(\mathbf{L}')\rangle = i\hbar\dot{\mathbf{R}} \cdot |w_o^{(0)}(\mathbf{L})\rangle \quad (3.3.5)$$

with

$$\Lambda_{oo'}(\mathbf{L}, \mathbf{L}') = \sum_{o''} U_{oo''}(\mathbf{L})\epsilon_{o''}^{(0)}U_{o''o'}^{-1}(\mathbf{L}') \quad \text{and} \quad w_o^{(0)}(\mathbf{L}) = U_{oo'}(\mathbf{L})\frac{\partial}{\partial \mathbf{R}}|\Phi_{o'}^{(0)}\rangle \quad (3.3.6)$$

and $w_o = w_o^{(0)} + w_o^{(1)}$, $\text{Re}[w_o^{(1)}] = 0$, $\text{Im}[w_o^{(0)}] = 0$, $\langle w_o^{(0)}(\mathbf{L})|w_{o'}^{(0)}(\mathbf{L}')\rangle = \delta_{oo'}\delta_{\mathbf{L}\mathbf{L}'}$. According to the MTM, the total magnetization is the sum of a local current (LC) and an itinerant current (IC) contribution (c.p. eq. (8) in ref.¹⁴¹)

$$\mathbf{M} = -\frac{e}{2Vc} \left[\sum_{\mathbf{L}} \sum_o \langle w_o(\mathbf{L})|(\hat{\mathbf{r}} - \mathbf{L}) \times \hat{\mathbf{r}}|w_o(\mathbf{L})\rangle + \mathbf{L} \times \langle w_o(\mathbf{L})|\hat{\mathbf{r}}|w_o(\mathbf{L})\rangle \right] = \mathbf{M}_{LC} + \mathbf{M}_{IC}. \quad (3.3.7)$$

The local current part is, within the bulk, translationally invariant. Similar to the procedure presented in section 1.3, it can be expressed in terms of the bulk properties only. Using its translational invariance, it is evaluated in a single unit cell with volume V_o , choosing the cell origin as a common origin

$$\mathbf{M}_{LC} = -\frac{e}{2V_o c} \sum_o \langle w_o(\mathbf{0})|(\hat{\mathbf{r}} - \mathbf{0}) \times \hat{\mathbf{r}}|w_o(\mathbf{0})\rangle. \quad (3.3.8)$$

The itinerary part is given by

$$\mathbf{M}_{IC} = -\frac{e}{2V_c} \sum_{\mathbf{L}} \sum_o \mathbf{L} \times \langle w_o(\mathbf{L}) | \hat{\mathbf{r}} | w_o(\mathbf{L}) \rangle. \quad (3.3.9)$$

We use $\hat{\mathbf{r}} = -\frac{i}{\hbar} [\hat{\mathbf{r}}, \hat{\mathcal{H}}]$ to write

$$\langle w_o(\mathbf{L}) | \hat{\mathbf{r}} | w_o(\mathbf{L}) \rangle = -\frac{i}{\hbar} \langle w_o(\mathbf{L}) | [\hat{\mathbf{r}}, \hat{\mathcal{H}}] | w_o(\mathbf{L}) \rangle \quad (3.3.10)$$

$$= -\frac{2i}{\hbar} \langle w_o^{(0)}(\mathbf{L}) | \hat{\mathbf{r}} \hat{\mathcal{H}} | w_o^{(1)}(\mathbf{L}) \rangle + \frac{2i}{\hbar} \langle w_o^{(0)}(\mathbf{L}) | \hat{\mathcal{H}} \hat{\mathbf{r}} | w_o^{(1)}(\mathbf{L}) \rangle \quad (3.3.11)$$

and use eqs. (3.3.4) and (3.3.5) to rewrite this as

$$\langle w_o^{(0)}(\mathbf{L}) | \hat{\mathbf{r}} \hat{\mathcal{H}} | w_o^{(1)}(\mathbf{L}) \rangle = \langle w_o^{(0)}(\mathbf{L}) | \hat{\mathbf{r}} \Lambda_{oo'}(\mathbf{L}, \mathbf{L}') | w_{o'}^{(1)}(\mathbf{L}') \rangle + i\hbar \langle w_o^{(0)}(\mathbf{L}) | \hat{\mathbf{r}} | \dot{\mathbf{R}} \cdot w_o'^{(0)}(\mathbf{L}) \rangle \quad (3.3.12)$$

$$\langle w_o^{(0)}(\mathbf{L}) | \hat{\mathcal{H}} \hat{\mathbf{r}} | w_o^{(1)}(\mathbf{L}) \rangle = \langle w_{o'}^{(0)}(\mathbf{L}') | \Lambda_{o'o}(\mathbf{L}', \mathbf{L}) \hat{\mathbf{r}} | w_o^{(1)}(\mathbf{L}) \rangle. \quad (3.3.13)$$

The two contributions can be split in a “rotational” and a “translational” part.

$$\mathbf{M}_{IC} = \mathbf{M}_{IC}^R + \mathbf{M}_{IC}^T \quad (3.3.14)$$

The “translational” contribution has no counter part in the conventional MTM. It involves the APT and does not contribute to the VCD spectrum since the triple product with current dipole moments vanishes

$$\mathbf{M}_{IC}^T = -\frac{e}{2V_c} \sum_{\mathbf{L}} \sum_o \mathbf{L} \times 2 \langle w_o^{(0)}(\mathbf{L}) | \hat{\mathbf{r}} | \dot{\mathbf{R}} \cdot w_o'^{(0)}(\mathbf{L}) \rangle \quad (3.3.15)$$

$$= \frac{1}{2V_c} \sum_{\mathbf{L}} \mathbf{L} \times \dot{\mathbf{R}} \cdot \frac{\partial}{\partial \mathbf{R}} \sum_o \langle w_o^{(0)}(\mathbf{L}) | -e \hat{\mathbf{r}} | w_o^{(0)}(\mathbf{L}) \rangle. \quad (3.3.16)$$

The “rotational” contribution reads

$$\begin{aligned} \mathbf{M}_{IC}^R = -\frac{e}{2V_c} \sum_{\mathbf{L}, \mathbf{L}'} \sum_{oo'} \mathbf{L} \times & \left[-\frac{2i}{\hbar} \langle w_o^{(0)}(\mathbf{L}) | \hat{\mathbf{r}} | w_{o'}^{(1)}(\mathbf{L}') \rangle \Lambda_{oo'}(\mathbf{L}, \mathbf{L}') \right. \\ & \left. + \frac{2i}{\hbar} \langle w_{o'}^{(0)}(\mathbf{L}') | \hat{\mathbf{r}} | w_o^{(1)}(\mathbf{L}) \rangle \Lambda_{o'o}(\mathbf{L}', \mathbf{L}) \right]. \end{aligned} \quad (3.3.17)$$

We use the symmetry in o, o' and \mathbf{L}, \mathbf{L}' to rewrite this as

$$\mathbf{M}_{IC}^R = -\frac{e}{2V_c} \sum_{\mathbf{L}, \mathbf{L}'} \sum_{oo'} (\mathbf{L} - \mathbf{L}') \times \left[-\frac{2i}{\hbar} \langle w_o^{(0)}(\mathbf{L}) | \hat{\mathbf{r}} | w_{o'}^{(1)}(\mathbf{L}') \rangle \Lambda_{oo'}(\mathbf{L}, \mathbf{L}') \right] \quad (3.3.18)$$

and use translational symmetry to reduce the double sum

$$\mathbf{M}_{IC}^R = \frac{e}{2V_{oc}} \sum_{\mathbf{L}'} \sum_{oo'} \mathbf{L}' \times \left[-\frac{2i}{\hbar} \langle w_o^{(0)}(\mathbf{0}) | \hat{\mathbf{r}} | w_{o'}^{(1)}(\mathbf{L}') \rangle \Lambda_{oo'}(\mathbf{0}, \mathbf{L}') \right]. \quad (3.3.19)$$

In the CPMD implementation within the Γ -point approximation, we only have access to

$$\Lambda_{oo'} = \sum_{\mathbf{L}} \Lambda_{oo'}(\mathbf{0}, \mathbf{L}), \quad (3.3.20)$$

i.e. the MLWOs are the same in all unit cells. However, we usually work with unit cells that are bigger than the MLWO-spread in insulating systems. Therefore, it is possible to attribute MLWOs at the cell boundary to neighboring cells, in other words, we manually construct the nearest neighbors via

$$\Lambda_{oo'}(\mathbf{0}, \mathbf{0}) = \Lambda_{oo'} \quad \text{if } \mathbf{r}_o - \mathbf{r}_{o'} < \frac{\mathbf{L}}{2} \text{ (nearest neighbor within same cell)} \quad (3.3.21)$$

$$\Lambda_{oo'}(\mathbf{0}, \mathbf{L}) = \Lambda_{oo'} \quad \text{if } \mathbf{r}_o - \mathbf{r}_{o'} > \frac{\mathbf{L}}{2} \text{ (nearest neighbor in neighboring cell),} \quad (3.3.22)$$

with $\Lambda_{oo'}(-\mathbf{L}, \mathbf{0}) = \Lambda_{oo'}(\mathbf{0}, \mathbf{L})$. For a pair of MLWOs o and o' , with o within the 0 unit cell, we check whether the nearest neighbor o' of o lies within the same cell or within a neighboring cell.

The evaluation of eq. (3.3.19) then involves the calculation of the following expressions of MLWOs of different unit cells

$$\mathbf{r}_{oo'k}^{(1)} = \langle w_o^{(0)} | \hat{r}_k | w_{o'}^{(1)} \rangle \quad \text{and} \quad \Lambda_{oo'}^{(0)} = \langle w_o^{(0)} | \hat{H} | w_{o'}^{(0)} \rangle = \Lambda_{o'o}^{(0)}. \quad (3.3.23)$$

We work with a unit cell that is sufficiently large in comparison to the spread of the MLWOs. Therefore, we only consider nearest neighbors in the overlaps of MLWOs. The position operator expectation value $\mathbf{r}_{oo'k}^{(0)}$ is taken with respect to the Wannier center of either of the involved states, e.g. state o with $\langle \hat{r}_k \rangle_o = \langle w_o^{(0)} | \hat{r}_k | w_o^{(0)} \rangle$

$$\mathbf{r}_{oo'k}^{(1)} \Big|_o = \langle w_o^{(0)} | \hat{r}_k - \langle \hat{r}_k \rangle_o | w_{o'}^{(1)} \rangle = \langle w_o^{(0)} | \hat{r}_k | w_{o'}^{(1)} \rangle. \quad (3.3.24)$$

The presented adaptation of the MTM for the NVPT has been implemented in the CPMD program package and first benchmarks are currently carried out. With a successful realization of this theory, the calculation of NVPT VCD spectra could be extended to anisotropic systems or extended molecules.

3.4 NON-LOCAL PSEUDOPOTENTIALS AND GALILEAN INVARIANCE

The use of a plane wave basis for the electronic wave function and density has the major advantage that the basis functions do not depend on the nuclear positions, nuclear velocities or external fields. It is therefore not necessary to consider Pulay terms^{m8} in the NDP calculation, to include velocity gauge factors in the atomic orbitals^{17,167} or gauge independent atomic orbitals in MFPs.²⁸⁴⁻²⁸⁶ The price to pay is the use of non-local pseudopotentials, which do not behave as regular local potentials. As discussed in sections 1.2 and 2.3, non-local pseudopotentials complicate several aspects of the calculation. They e.g. give rise to additional terms in the NDP perturbation Hamiltonian and require an explicit evaluation of the commutator of position operator with the unperturbed Hamiltonian. In presence of the vector potential of an external electromagnetic field, the GIPAW^{119,120} or ICL^{121,122} method have to be employed to obtain gauge invariant physical observables. However, also when the nuclei and their non-local pseudopotentials are moving, a correction is necessary, i.e. Hamiltonians with non-local potentials are not invariant under a Galilean transformation. The TDSE

$$\left(\frac{-\hbar^2}{2m}\hat{\nabla}^2 + \hat{V}_{loc} + \hat{V}_{nl}\right)|\phi_o(t)\rangle = \left(\hat{\mathcal{H}}_{loc}^{(0)} + \hat{V}_{nl}\right)|\phi_o(t)\rangle = i\hbar\frac{\partial}{\partial t}|\phi_o(t)\rangle \quad (3.4.1)$$

is form invariant under Galilean transformation²⁸⁷

$$\mathbf{r} \rightarrow \mathbf{r} - \mathbf{v}t \quad \text{and} \quad \phi_o(\mathbf{r}, t) \rightarrow \phi_o(\mathbf{r} - \mathbf{v}t, t) e^{i\frac{m}{\hbar}\mathbf{v}\cdot\mathbf{r}} e^{-i\frac{m}{2\hbar}|\mathbf{v}|^2 t} \quad (3.4.2)$$

only if $V_{nl} = 0$. Since the projectors of the non-local potential are still at rest

$$V_{nl}(\mathbf{r}, \mathbf{r}') = \sum_{\nu} V_{nl}^{\nu}(\mathbf{r} - \mathbf{R}^{\nu}, \mathbf{r}' - \mathbf{R}^{\nu}), \quad (3.4.3)$$

they introduce artificial sources and sinks of the probability current. In order to obtain a form invariant TDSE we have to evaluate the projection in the same reference frame, i.e. either by boosting the projector or with the opposite sign removing the boost of the orbitals. In the spirit of the ICL method, this corresponds to a transformation of the non-local potential with a linear transport between sources and sinks

$$V_{nl}(\mathbf{r}, \mathbf{r}') \rightarrow \sum_{\nu} V_{nl}^{\nu}(\mathbf{r} - \mathbf{R}^{\nu}, \mathbf{r}' - \mathbf{R}^{\nu}) \exp\left\{-i\frac{m}{\hbar}\dot{\mathbf{R}}^{\nu}(t) \cdot \int_{\mathbf{r}-\mathbf{R}^{\nu}}^{\mathbf{r}'-\mathbf{R}^{\nu}} d\mathbf{r}''\right\} \quad (3.4.4)$$

$$= \sum_{\nu} \langle \mathbf{r} | e^{i\frac{m}{\hbar}\dot{\mathbf{R}}^{\nu}(t) \cdot \hat{\mathbf{r}}} \hat{V}_{nl}^{\nu(0)} e^{-i\frac{m}{\hbar}\dot{\mathbf{R}}^{\nu}(t) \cdot \hat{\mathbf{r}}} | \mathbf{r}' \rangle \quad (3.4.5)$$

3.4.1 ONE DIMENSIONAL MODEL

We analyze this relation in a one dimensional model system, a harmonic oscillator with a non-local potential that shifts the energy of states depending on their symmetry via the parity operator $\hat{\Pi}$

$$\hat{V}_{loc}(\hat{x}) = \frac{1}{2}m\omega^2\hat{x}^2, \quad \hat{V}_{nl} = \Delta\hat{\Pi} \quad \text{and} \quad \hat{\Pi}(x, x')\phi(x', t) = \phi(-x, t). \quad (3.4.6)$$

At rest, the TDSE reads

$$\left(\frac{-\hbar^2}{2m}\hat{\nabla}^2 + V_{loc}(\hat{x})\right)\phi(x, t) + \Delta\hat{\Pi}(x, x')\phi(x', t) = i\hbar\frac{\partial}{\partial t}\phi(x, t). \quad (3.4.7)$$

After a Galilean transformation, i.e. from the point of view of an observer with velocity $-v$,

$$x \rightarrow \tilde{x}(t) = x - vt \quad \text{and} \quad \phi(x, t) \rightarrow \tilde{\phi}(\tilde{x}(t), t) = \phi(\tilde{x}(t), t) e^{\frac{i}{\hbar}(mv\tilde{x}(t) + \frac{mv^2}{2}t)} \quad (3.4.8)$$

we find the transformed TDSE

$$\left(\frac{-\hbar^2}{2m} \hat{\nabla}^2 + V_{loc}(\tilde{x}(t)) \right) \tilde{\phi}(\tilde{x}(t), t) + \Delta \hat{\Pi}(\tilde{x}(t), \tilde{x}'(t)) \tilde{\phi}(\tilde{x}'(t), t) = i\hbar \frac{\partial}{\partial t} \tilde{\phi}(\tilde{x}(t), t), \quad (3.4.9)$$

which simplifies to

$$\left(\frac{-\hbar^2}{2m} \hat{\nabla}^2 + V_{loc}(\tilde{x}) \right) \phi(\tilde{x}, t') + e^{-\frac{i}{\hbar}mv\tilde{x}} \Delta \hat{\Pi}(\tilde{x}, \tilde{x}') \phi(\tilde{x}', t') e^{\frac{i}{\hbar}mv\tilde{x}'} = i\hbar \frac{\partial}{\partial t'} \phi(\tilde{x}, t') \quad (3.4.10)$$

where the time derivative on the right hand side is not acting on the time dependence of $\tilde{x}(t)$ so that we can drop its time dependence. Without transformation of the non-local potential we obtain

$$\left(\frac{-\hbar^2}{2m} \hat{\nabla}^2 + V_{loc}(\tilde{x}) \right) \phi(\tilde{x}, t') + e^{-2\frac{i}{\hbar}mv\tilde{x}} \Delta \hat{\Pi}(\tilde{x}, \tilde{x}') \phi(\tilde{x}', t') = i\hbar \frac{\partial}{\partial t'} \phi(\tilde{x}, t') \quad (3.4.11)$$

and with correction we recover eq. (3.4.7)

$$\left(\frac{-\hbar^2}{2m} \hat{\nabla}^2 + V_{loc}(\tilde{x}) \right) \phi(\tilde{x}, t') + \Delta \hat{\Pi}(\tilde{x}, \tilde{x}') \phi(\tilde{x}', t') = i\hbar \frac{\partial}{\partial t'} \phi(\tilde{x}, t'). \quad (3.4.12)$$

In the basis of the harmonic oscillator eigenstates $|\phi_n\rangle$ eq. (3.4.11) reads

$$\langle \phi_m | \hat{\mathcal{H}}_{loc} + e^{-2\frac{i}{\hbar}mv\hat{x}} \Delta \hat{\Pi} | \phi_n \rangle = \epsilon_n \delta_{mn} + (-1)^n \Delta \langle \phi_m | e^{-2\frac{i}{\hbar}mv\hat{x}} | \phi_n \rangle, \quad (3.4.13)$$

which has been solved at different boost velocities using Gauss-Hermite quadrature²⁸⁸ with 2000 basis functions (and parameters $\hbar=1$, $m=1$ and $\omega=1$). The resulting stationary states $\phi_n(x)$ and eigenvalues ϵ_n of eq. (3.4.7) are depicted in fig. 3.9. Due to the parity dependent energy shift, the neighboring states with even and odd symmetry (or number n) switch.

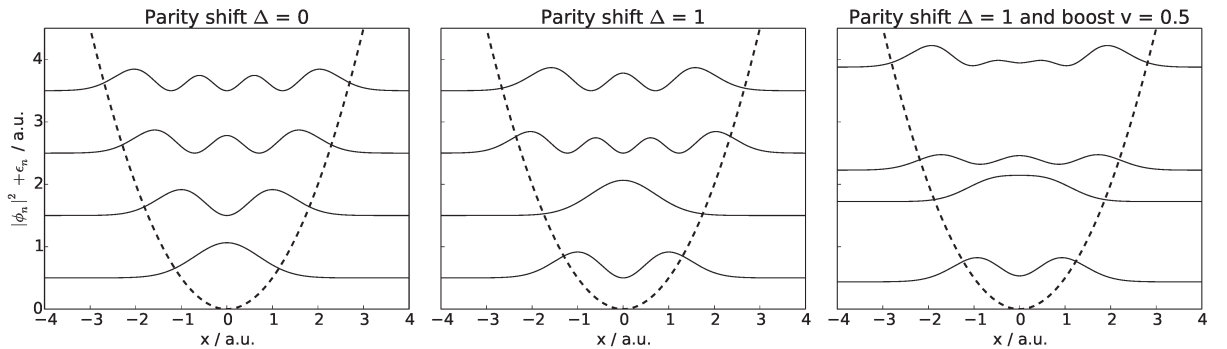


Figure 3.9: Stationary states with non-local potential. Left: Stationary states at rest without shift. Center: Stationary states at rest with shift. Right: Uncorrected stationary states with boost and shift.

The stationary solutions of eq. (3.4.13) at different boost velocities v are shown in fig. 3.10. The probability density of the stationary states changes and the switching of the states is reversed with increasing velocity. Furthermore, the stationary states carry a current.

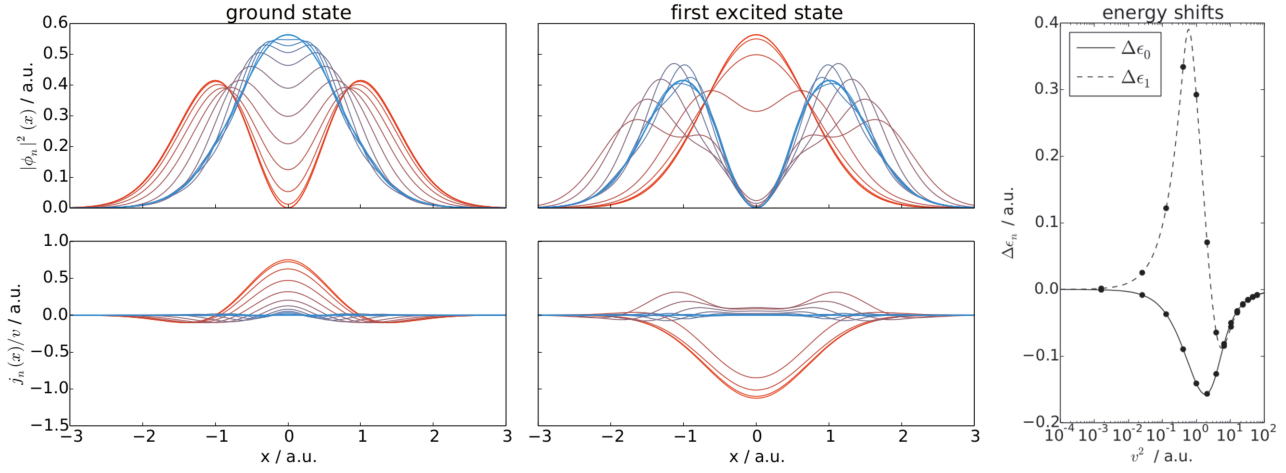


Figure 3.10: Left: Boosted non-corrected stationary states at different boosts. The color coding goes from zero velocity (red) to high velocity (blue) and the corresponding velocities are marked with points in the right panel. Right: Difference of the boosted eigenstate energy with respect to the correct value at different velocities.

We are interested in the time evolution of a wave packet, e.g. the correct ground or first excited state, in presence of the non-local potential. The wave packet can be expanded in terms of the stationary states of eq. (3.4.13) and shows a non-vanishing current dipole moment as well as an oscillation of the center of mass. These current dipole moments and the amplitude of the center of mass oscillation are depicted in fig. 3.11. We also include a linearized correction as discussed in the following section and see that the correction suppresses the unphysical effects up to about one per mill of the speed of light.

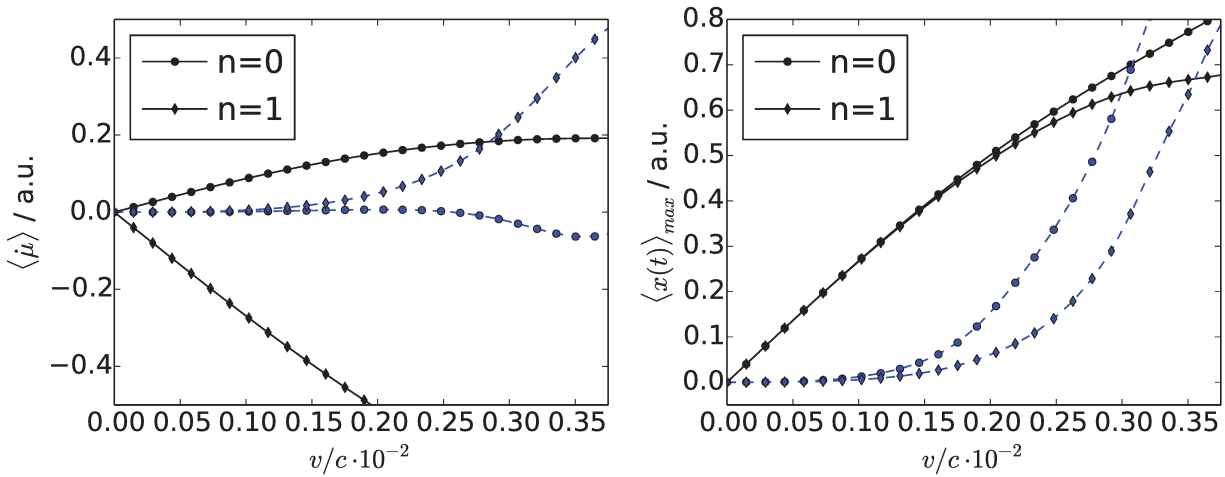


Figure 3.11: Current dipole moments and center of mass oscillations due to non-local potentials. The linearized correction yields the results colored in blue, which show a physical behavior up to about one per mill of the speed of light.

The results obtained with this model system give an estimate of the velocity range in which this effect is relevant. As long as the de Broglie wavelength of the electrons is much larger than the spatial extent of the non-local potential, the first order correction provided in the next section should suffice. At thermal velocities this condition is fulfilled and even scattering experiments might be treated with a linearized correction.

3.4.2 LINEARIZED CORRECTION

At small velocities, we can linearize the correction and find

$$\hat{V}_{nl}(\dot{\mathbf{R}}) \approx \sum_{\nu} \left(\hat{V}_{nl}^{\nu(0)} + \frac{im}{\hbar} [\dot{\mathbf{R}}^{\nu}(t) \cdot \hat{\mathbf{r}}, \hat{V}_{nl}^{\nu(0)}] \right) \quad (3.4.14)$$

In the NVPT, the electronic Hamiltonian changes to

$$\hat{\mathcal{H}}_e = \hat{\mathcal{H}}^{(0)} + \sum_{\nu} \left(-i\hbar \dot{\mathbf{R}}^{\nu}(t) \cdot \frac{\partial}{\partial \mathbf{R}^{\nu}} + \frac{im}{\hbar} [\dot{\mathbf{R}}^{\nu}(t) \cdot \hat{\mathbf{r}}, \hat{V}_{nl}^{\nu(0)}] \right) \quad (3.4.15)$$

and the corrected Sternheimer equation becomes

$$(\hat{\mathcal{H}}^{(0)} - \epsilon_o^{(0)})|\phi_o^{(1)}\rangle = \sum_{\nu} \left(i\hbar \dot{\mathbf{R}}^{\nu}(t) \cdot \frac{\partial}{\partial \mathbf{R}^{\nu}} - \frac{im}{\hbar} [\dot{\mathbf{R}}^{\nu}(t) \cdot \hat{\mathbf{r}}, \hat{V}_{nl}^{\nu(0)}] \right) |\phi_o^{(0)}\rangle, \quad (3.4.16)$$

giving rise to a different NVP wave function. However, also in the current operator, we have an additional term

$$\hat{\mathbf{r}} = \frac{1}{i\hbar} [\hat{\mathbf{r}}, \hat{\mathcal{H}}_e] = \frac{1}{i\hbar} [\hat{\mathbf{r}}, \hat{\mathcal{H}}^{(0)}] + \sum_{\nu} \frac{m}{\hbar^2} [\hat{\mathbf{r}}, [\dot{\mathbf{R}}^{\nu}(t) \cdot \hat{\mathbf{r}}, \hat{V}_{nl}^{\nu(0)}]] \quad (3.4.17)$$

and its NVPT expectation value turns out to be invariant

$$\begin{aligned} \langle \phi_o | \hat{\mathbf{r}} | \phi_o \rangle &= \langle \phi_o^{(0)} | \frac{1}{i\hbar} [\hat{\mathbf{r}}, \hat{\mathcal{H}}^{(0)}] | \phi_o^{(1)} \rangle + \langle \phi_o^{(1)} | \frac{1}{i\hbar} [\hat{\mathbf{r}}, \hat{\mathcal{H}}^{(0)}] | \phi_o^{(0)} \rangle \\ &+ \langle \phi_o^{(0)} | \sum_{\nu} \frac{m}{\hbar^2} [\hat{\mathbf{r}}, [\dot{\mathbf{R}}^{\nu}(t) \cdot \hat{\mathbf{r}}, \hat{V}_{nl}^{\nu(0)}]] | \phi_o^{(0)} \rangle \end{aligned} \quad (3.4.18)$$

$$= \sum_{\nu} \dot{\mathbf{R}}^{\nu}(t) \cdot \frac{\partial}{\partial \mathbf{R}^{\nu}} \langle \phi_o^{(0)} | \hat{\mathbf{r}} | \phi_o^{(0)} \rangle, \quad (3.4.19)$$

where we used

$$\langle \phi_o^{(0)} | \frac{1}{i\hbar} \hat{\mathbf{r}} (\hat{\mathcal{H}}^{(0)} - \epsilon_o^{(0)}) | \phi_o^{(1)} \rangle = \langle \phi_o^{(0)} | \sum_{\nu} \hat{\mathbf{r}} \left(\dot{\mathbf{R}}^{\nu}(t) \cdot \frac{\partial}{\partial \mathbf{R}^{\nu}} - \frac{m}{\hbar^2} [\dot{\mathbf{R}}^{\nu}(t) \cdot \hat{\mathbf{r}}, \hat{V}_{nl}^{\nu(0)}] \right) | \phi_o^{(0)} \rangle. \quad (3.4.20)$$

Using the linearity of the perturbation, we can show that the correction caused by the additional term in the NVPT perturbation Hamiltonian is not required for the calculation of current expectation values. To see this, we split eq. (3.4.16) in the local response $|\phi_{loc,o}^{(1)}\rangle$ and the non-local response $|\phi_{nl,o}^{(1)}\rangle$

$$(\hat{\mathcal{H}}^{(0)} - \epsilon_o^{(0)})|\phi_{loc,o}^{(1)}\rangle = \sum_{\nu} i\hbar \dot{\mathbf{R}}^{\nu}(t) \cdot \frac{\partial}{\partial \mathbf{R}^{\nu}} |\phi_o^{(0)}\rangle \quad (3.4.21)$$

$$(\hat{\mathcal{H}}^{(0)} - \epsilon_o^{(0)})|\phi_{nl,o}^{(1)}\rangle = \sum_{\nu} -\frac{im}{\hbar} [\dot{\mathbf{R}}^{\nu}(t) \cdot \hat{\mathbf{r}}, \hat{V}_{nl}^{\nu(0)}] |\phi_o^{(0)}\rangle \quad (3.4.22)$$

From eq. (3.4.18) we directly see

$$\langle \phi_o | \hat{\mathbf{r}} | \phi_o \rangle = \langle \phi_o^{(0)} | \frac{1}{i\hbar} [\hat{\mathbf{r}}, \hat{\mathcal{H}}^{(0)}] | \phi_{loc,o}^{(1)} \rangle + \langle \phi_{loc,o}^{(1)} | \frac{1}{i\hbar} [\hat{\mathbf{r}}, \hat{\mathcal{H}}^{(0)}] | \phi_o^{(0)} \rangle \quad (3.4.23)$$

That is, in presence of non-local pseudopotentials we can ignore the violation of the Galilean invariance in the calculation of current expectation values in boosted systems as long as the nuclear velocities are small. The results of section 3.4.1 indicate that this is the case at nuclear velocities at ambient conditions.

3.5 ON THE MASS OF ATOMS IN MOLECULES: BEYOND THE BORN-OPPENHEIMER APPROXIMATION

Describing the dynamics of nuclei in molecules requires a potential energy surface, which is traditionally provided by the Born-Oppenheimer or adiabatic approximation. However, we also need to assign masses to the nuclei. There, the Born-Oppenheimer picture does not account for the inertia of the electrons and only bare nuclear masses are considered. Nowadays, experimental accuracy challenges the theoretical predictions of rotational and vibrational spectra and requires to include the participation of electrons in the internal motion of the molecule. More than 80 years after the original work of Born and Oppenheimer,⁵³ this issue still is not solved in general. Here, we present a theoretical and numerical framework to address this problem in a general and rigorous way. Starting from the exact factorization of the electron-nuclear wave function, we include electronic effects beyond the Born-Oppenheimer regime in a perturbative way via position-dependent corrections to the bare nuclear masses. This maintains an adiabatic-like point of view: the nuclear degrees of freedom feel the presence of the electrons via a single potential energy surface, whereas the inertia of electrons is accounted for and the total mass of the system is recovered. This constitutes a general framework for describing the mass acquired by slow degrees of freedom due to the inertia of light, bounded particles. We illustrate it with a model of proton transfer, where the light particle is the proton, and with corrections to the vibrational spectra of molecules. Inclusion of the light particle inertia allows to gain orders of magnitude in accuracy.

All authors contributed extensively to the work presented in this section.²⁸⁹ F. Agostini, R. Vuilleumier and A. Scherrer derived the theory and wrote the manuscript. F. Agostini and R. Vuilleumier implemented the proton transfer model and carried out the numerical calculations. A. Scherrer implemented the corrections to the vibrational spectra of molecules and carried out the numerical calculations. F. Agostini, R. Vuilleumier and A. Scherrer analyzed and interpreted the results. D. Sebastiani and R. Vuilleumier supervised the project. E. K. U. Gross gave conceptual advice.

3.5.1 MOTIVATION

The Born-Oppenheimer⁵³ (BO), or adiabatic, treatment of the coupled motion of electrons and nuclei in molecular systems is among the most fundamental approximations in condensed matter physics and theoretical chemistry. Based on the hypothesis that part of the system, usually electrons or protons, evolves on a much shorter time-scale than the rest, i.e. (heavy) nuclei or ions, the BO approximation allows one to visualize molecules as a set of nuclei moving on a single potential energy surface that represents the effect of the electrons in a given eigenstate. Yet, it is an approximation, yielding the correct dynamics only in the limit of infinite nuclear masses. Consequently, when compared to highly accurate molecular spectroscopy measurements, theoretical predictions might deviate from experimentally observed behavior.

In those situations, the question of which *masses*^{290–295} are to be considered when calculating rotational and vibrational spectra of light molecules, for instance hydrogen-based,^{295–298} often appears in the literature to rationalize this problem. In the BO approximation, the electrons appear only implicitly in the dynamics, as a potential energy contribution to the Hamiltonian driving the motion of the nuclei. The kinetic energy arising from the molecular motion then involves only the bare nuclear masses. However, electrons are carried

along with the nuclei, thus how is their inertia accounted for? It has been proposed that more accurate results are obtained when employing *atomic masses* rather than bare nuclear masses; sometimes *fractional masses* are used to account for ionicity but there is no systematic way to do so.

One solution to the problem is to perform a full non-adiabatic treatment of the coupled electron-nuclear problem, but the numerical cost is much larger than a BO calculation. Also, from a fundamental point of view, this does not answer the question of what is the mechanism by which the inertia of the electrons affects the mass of the heavy degrees of freedom. An alternative approach, pioneered by Bunker and Moss,^{296,299} is to treat perturbatively non-adiabatic effects, but applications are still limited to di- and tri-atomic molecules.

In the present work, we examine this problem in the framework of the exact factorization of the electron-nuclear wave function.¹⁷⁸ This (non-adiabatic) reformulation of the quantum-mechanical problem is used as a starting point to develop a procedure that settles the issue described above in a rigorous way. The key point in the exact factorization is that the electronic effect on the nuclear system is taken into account by time-dependent vector and scalar potentials. These concepts are the generalization of similar, but static, quantities appearing also within the BO approximation. We show that non-adiabatic effects can be accounted for, by formulating a theory that treats these effects as a perturbation to the BO problem. Such a framework has been discussed in previous work⁵⁴ to derive the nuclear velocity perturbation theory¹³⁹ for vibrational circular dichroism.³³ Within the nuclear velocity perturbation theory, non-adiabatic effects can be included by taking into account corrections to the BO approximation up to within linear order in the classical nuclear velocity. We show here that this is equivalent to a perturbation approach where the small parameter is the electron-nuclear mass ratio.

The major achievement of such formulation is presented in this work: electronic non-adiabatic effects appear as a *position-dependent mass* correction^{292,294} to the bare nuclear mass, up to within linear order in the perturbation. From a fundamental perspective, we prove that it is possible to recover an adiabatic-like structure of the Hamiltonian governing the dynamics of the heavy degrees of freedom, with a kinetic energy contribution and a separate potential energy term. Since the mass correction can be fully identified with the electronic mass, totally missing in the BO approximation, we propose a theory able to restore a fundamental property, often overlooked, of the dynamical problem: the translational invariance of an isolated system with its physical mass, i.e. nuclear *and* electronic. If in the BO approximation, the nuclear masses are made position-dependent in the way proposed in this work, the center of mass can be separated from rotations and internal vibrations and evolves as a free particle with mass equal to the total mass of the system (expected from the Galilean invariance of the problem²⁹³). From an algorithmic perspective, the corrections to the mass involve only ground-state properties and can be calculated as a response to the nuclear motion, within standard perturbation theory.^{5,7,8} Therefore, we are able to perform numerical studies of molecular systems, pushing the applications beyond di- and tri-atomic molecules.

3.5.2 THE ADIABATIC LIMIT OF THE EXACT FACTORIZATION

The exact factorization of the electron-nuclear wave function has been already introduced and discussed in sections 1.5, 2.2 and A.1.

With this starting point, we observe that the electron nuclear coupling operator (ENCO) is inversely proportional to the nuclear masses M_ν and the BO limit³⁰⁰ corresponds to the solution of eqs. (1.5.6-1.5.7)

setting the ENCO to zero.⁵⁴ Formally, however, approaching this limit of large but finite nuclear masses depends on the physical situation considered.³⁰¹ In the time-dependent case, keeping fixed the kinetic energy, it has been shown³⁰¹ that the BO limit is recovered asymptotically in terms of a small expansion parameter μ^4 used to scale the nuclear mass, $M \rightarrow M^{(\mu)} \equiv M/\mu^4$. Making μ approach zero corresponds to the ratio of the nuclear mass over the electron mass $M^{(\mu)}/m_e$ going to infinity. This scaling factor will be used only to estimate perturbatively the order of the terms in the electronic equation, and will be set equal to unity to recover the values of the physical masses. The nuclear mass being made larger, their dynamics is slower such that time variable must then be scaled as well, by a factor μ^2 , i.e. $t \rightarrow t/\mu^2$,³⁰¹ increasing the separation of time-scales between the light and heavy particles. Similarly, following a simple scaling argument, the nuclear momentum behaves as μ^{-2} in the semi-classical limit (see Section C.1 of the appendix). Then, the ENCO from Eq. (1.5.10) scales with μ^4 as

$$\begin{aligned} \hat{U}_{en,\mu} [\Phi_{\mathbf{R}}, \chi] = & \sum_{\nu=1}^{N_n} \left[\frac{\mu^4}{M_\nu} \frac{[-i\hbar\nabla_\nu - \mathbf{A}_\nu(\mathbf{R}, t)]^2}{2} + \right. \\ & \left. \frac{\mu^2}{M_\nu} \left(\boldsymbol{\lambda}_\nu(\mathbf{R}, t) + \mu^2 \mathbf{A}_\nu(\mathbf{R}, t) \right) \left(-i\hbar\nabla_\nu - \mathbf{A}_\nu(\mathbf{R}, t) \right) \right], \end{aligned} \quad (3.5.1)$$

where $\boldsymbol{\lambda}_\nu(\mathbf{R}, t) = \mu^2 \frac{-i\hbar\nabla_\nu \chi(\mathbf{R}, t)}{\chi(\mathbf{R}, t)}$. $\boldsymbol{\lambda}_\nu(\mathbf{R}, t)$ tends towards a quantity independent of μ in the limit of small μ , since $-i\hbar\nabla_\nu \chi/\chi$ is related to the nuclear momentum^{54,187} and thus scales as μ^{-2} .

Using the definition in Eq. (1.5.11), we define the scaled time-dependent potential energy surface (TD-PES),

$$\begin{aligned} \epsilon_\mu(\mathbf{R}, t) = & \langle \Phi_{\mathbf{R}}(t) | \hat{\mathcal{H}}_{BO} | \Phi_{\mathbf{R}}(t) \rangle_{\mathbf{r}} + \mu^2 \langle \Phi_{\mathbf{R}}(t) | -i\hbar\partial_t | \Phi_{\mathbf{R}}(t) \rangle_{\mathbf{r}} \\ & + \mu^4 \sum_{\nu=1}^{N_n} \frac{1}{2M_\nu} \langle \Phi_{\mathbf{R}}(t) | [-i\hbar\nabla_\nu - \mathbf{A}_\nu(\mathbf{R}, t)]^2 | \Phi_{\mathbf{R}}(t) \rangle_{\mathbf{r}}, \end{aligned} \quad (3.5.2)$$

noting the second term in Eq. (3.5.1) does not contribute (by construction) to the TD-PES. The electronic equation thus obtained,

$$\left[\hat{\mathcal{H}}_{BO} + \hat{U}_{en,\mu} [\Phi_{\mathbf{R}}, \chi] - \epsilon_\mu(\mathbf{R}, t) \right] \Phi_{\mathbf{R}}(\mathbf{r}, t) = i\hbar\mu^2 \partial_t \Phi_{\mathbf{R}}(\mathbf{r}, t), \quad (3.5.3)$$

can be solved perturbatively in powers of μ^4 , with its solution of the form $\Phi_{\mathbf{R}}(\mathbf{r}, t) = \Phi_{\mathbf{R}}^{(0)}(\mathbf{r}, t) + \mu^2 \Phi_{\mathbf{R}}^{(1)}(\mathbf{r}, t) + \dots$ ^{53,302}

The time dependence appears only at order μ^2 , as it is clear from Eqs. (3.5.2) and (3.5.3). Therefore the time dependence of $\Phi_{\mathbf{R}}^{(0)}(\mathbf{r}, t) = \varphi_{\mathbf{R}}^{(0)}(\mathbf{r})$ can be dropped out and it satisfies the zeroth order equation

$$\left[\hat{\mathcal{H}}_{BO} - \epsilon^{(0)}(\mathbf{R}) \right] \varphi_{\mathbf{R}}^{(0)} = 0, \quad (3.5.4)$$

with $\epsilon^{(0)}(\mathbf{R})$ the first term on the right-hand-side of Eq. (3.5.2). Here, $\varphi_{\mathbf{R}}^{(0)}$ is an eigenstate of the BO Hamiltonian with eigenvalue $\epsilon^{(0)}(\mathbf{R}) = \epsilon_{BO}^{(0)}(\mathbf{R})$, chosen to be the ground state.

At the zeroth order:

- (i) the time dependent vector potential identically vanishes, $\mathbf{A}_\nu^{(0)}(\mathbf{R}, t) = 0$, as in the absence of a magnetic field $\varphi_{\mathbf{R}}^{(0)}(\mathbf{r})$ can be real;

- (ii) the evolution of the nuclear wave function is determined by the usual BO equation;
- (iii) the electronic wave function is used to fix the gauge freedom at all orders, by imposing $\langle \varphi_{\mathbf{R}}^{(0)} | \Phi_{\mathbf{R}}(t) \rangle \in \mathbb{R}$.

3.5.3 RECOVERING THE NUCLEAR VELOCITY PERTURBATION THEORY

The electronic equation eq. (3.5.3) at the next order yields

$$\left[\hat{\mathcal{H}}_{BO} - \epsilon_{BO}^{(0)}(\mathbf{R}) \right] \Phi_{\mathbf{R}}^{(1)} = i \sum_{\nu=1}^{N_n} \boldsymbol{\lambda}'_{\nu}(\mathbf{R}, t) \cdot \left(\hbar \nabla_{\nu} \varphi_{\mathbf{R}}^{(0)} \right), \quad (3.5.5)$$

where

$$\boldsymbol{\lambda}'_{\nu}(\mathbf{R}, t) = \frac{1}{M_{\nu}} \left[\boldsymbol{\lambda}_{\nu}(\mathbf{R}, t) + \mu^2 \mathbf{A}_{\nu}(\mathbf{R}, t) \right] \quad (3.5.6)$$

from eq. (1.5.10). We neglected the time-dependent vector potential (TDVP) from the second term in parenthesis since $\mathbf{A}_{\nu}(\mathbf{R}, t)$ is $\mathcal{O}(\mu^2)$. Furthermore, $\boldsymbol{\lambda}'_{\nu}$ contains a term $\mathcal{O}(\mu^2)$, which is analyzed below along with the TDVP.

In the following, we present the connection between eq. (3.5.5) and the nuclear velocity perturbation theory, thus providing a numerical scheme⁵⁴ to compute $\Phi_{\mathbf{R}}^{(1)}(\mathbf{r}, t)$ within perturbation theory.¹³⁹ The electronic wave function up to within $\mathcal{O}(\mu^2)$ is

$$\Phi_{\mathbf{R}}(\mathbf{r}, t) = \varphi_{\mathbf{R}}^{(0)}(\mathbf{r}) + \mu^2 i \sum_{\nu=1}^{N_n} \boldsymbol{\lambda}'_{\nu}(\mathbf{R}, t) \cdot \boldsymbol{\varphi}_{\mathbf{R},\nu}^{(1)}(\mathbf{r}), \quad (3.5.7)$$

where $\boldsymbol{\varphi}_{\mathbf{R},\nu}^{(1)}(\mathbf{r})$ is implicitly defined by eq. (3.5.5). Eq. (3.5.7) is valid also as initial condition, i.e. the correction is included if at the initial time the nuclear velocity (the classical limit of $\boldsymbol{\lambda}'_{\nu}(\mathbf{R}, t)$) is non-zero.³⁰³ $\Phi_{\mathbf{R}}(\mathbf{r}, t)$ is complex and can thus sustain an electronic current density^{193,304} induced by the nuclear motion.

We now show the relation between the μ^4 -expansion and the nuclear velocity perturbation theory (NVPT). In the framework of NVPT, we have used $\boldsymbol{\lambda}'_{\nu}(\mathbf{R}, t)$ in eq. (2.2.26) as the perturbation parameters that controls the degree of non-adiabaticity of the problem. The electronic equation (3.5.3) can be written using $\boldsymbol{\lambda}'_{\nu}(\mathbf{R}, t)$ as

$$\begin{aligned} \left[\hat{\mathcal{H}}_{BO} - \epsilon_{BO}^{(0)}(\mathbf{R}) \right] \left(\varphi_{\mathbf{R}}^{(0)}(\mathbf{r}) + \mu^2 \Phi_{\mathbf{R}}^{(1)}(\mathbf{r}, t) \right) = \\ \mu^2 \sum_{\nu=1}^{N_n} \boldsymbol{\lambda}'_{\nu}(\mathbf{R}, t) \cdot [i \hbar \nabla_{\nu} + \mathbf{A}_{\nu}(\mathbf{R}, t)] \varphi_{\mathbf{R}}^{(0)}(\mathbf{r}). \end{aligned} \quad (3.5.8)$$

Also, as proved in section 3.5.4, the TDVP is itself $\mathcal{O}(\mu^2)$, thus it will be neglected from the term in square brackets on the right-hand-side. If we solve this equation order by order, Eqs. (3.5.4) and (3.5.5) are easily obtained. In particular, we recall here Eq. (3.5.5) whose solution yields $\Phi_{\mathbf{R}}^{(1)}(\mathbf{r}, t)$,

$$\left[\hat{\mathcal{H}}_{BO} - \epsilon_{BO}^{(0)}(\mathbf{R}) \right] \Phi_{\mathbf{R}}^{(1)}(\mathbf{r}, t) = i \sum_{\nu=1}^{N_n} \boldsymbol{\lambda}'_{\nu}(\mathbf{R}, t) \cdot \left(\hbar \nabla_{\nu} \varphi_{\mathbf{R}}^{(0)}(\mathbf{r}) \right). \quad (3.5.9)$$

In section 2.2 we started from the electronic Hamiltonian eq. (2.2.27)

$$\hat{\mathcal{H}}_{el} = \hat{\mathcal{H}}_{BO} + \sum_{\nu=1}^{N_n} \boldsymbol{\lambda}'_{\nu}(\mathbf{R}, t) \cdot (-i\hbar \nabla_{\nu}), \quad (3.5.10)$$

and we have solved it perturbatively, using $\hat{\mathcal{H}}_{BO}$ as the unperturbed Hamiltonian. It is clear, as stated above, that $\boldsymbol{\lambda}'_{\nu}(\mathbf{R}, t)$ is the small parameter that controls the strength of the perturbation and that $-i\hbar \nabla_{\nu}$ is the (non-adiabatic) perturbation. In eq. (2.2.30), we have looked for the eigenstates of $\hat{\mathcal{H}}_{el}$ in the form

$$\Phi_{\mathbf{R}}(\mathbf{r}, t) = \varphi_{\mathbf{R}}^{(0)}(\mathbf{r}) + \sum_{e \neq 0} \frac{\langle \varphi_{\mathbf{R}}^{(e)} | -i\hbar \sum_{\nu} \boldsymbol{\lambda}'_{\nu}(\mathbf{R}, t) \cdot \nabla_{\nu} \varphi_{\mathbf{R}}^{(0)} \rangle_{\mathbf{r}}}{\epsilon_{BO}^{(0)}(\mathbf{R}) - \epsilon_{BO}^{(e)}(\mathbf{R})} \varphi_{\mathbf{R}}^{(e)}(\mathbf{r}) \quad (3.5.11)$$

as straightforwardly follows from the application of standard time-independent perturbation theory. The first order perturbation to BO ground state can be written as

$$i\varphi_{\mathbf{R}}^{(1)}(\mathbf{r}) = i \sum_{e \neq 0} \frac{\mathbf{d}_{\nu, e0}(\mathbf{R})}{\omega_{e0}(\mathbf{R})} \varphi_{\mathbf{R}}^{(e)}(\mathbf{r}), \quad (3.5.12)$$

with $\omega_{e0}(\mathbf{R}) = (\epsilon_{BO}^{(e)}(\mathbf{R}) - \epsilon_{BO}^{(0)}(\mathbf{R}))/\hbar$ and $\mathbf{d}_{\nu, e0}(\mathbf{R}) = \langle \varphi_{\mathbf{R}}^{(e)} | \nabla_{\nu} \varphi_{\mathbf{R}}^{(0)} \rangle_{\mathbf{r}}$, the non-adiabatic coupling vectors. This leads to a new expression for $\Phi_{\mathbf{R}}(\mathbf{r}, t)$,

$$\Phi_{\mathbf{R}}(\mathbf{r}, t) = \varphi_{\mathbf{R}}^{(0)}(\mathbf{r}) + i \sum_{\nu=1}^{N_n} \boldsymbol{\lambda}'_{\nu}(\mathbf{R}, t) \cdot \varphi_{\mathbf{R}}^{(1)}(\mathbf{r}), \quad (3.5.13)$$

which is exactly eq. (3.5.7) when setting $\mu^2 = 1$, to obtain the physical nuclear mass.

In the framework of NVPT, the perturbation parameter has been interpreted classically as the nuclear velocity.^{54, 187, 190} It is worth mentioning here that, when performing a numerical simulation, such dependence on the nuclear velocity shall be correctly accounted for also in the preparation of the initial electronic state. When using NVPT to perform the calculations, the electronic evolution is not explicit, in the sense that at each time the electronic wave function is simply reconstructed using ground state properties that are then inserted in Eq. (3.5.13). However, when NVPT results are (or can be) compared with quantum-mechanical fully non-adiabatic results, the initial electronic state cannot be simply prepared in the ground state, unless the initial nuclear velocity is zero. If this is not the case, then the first order contribution in Eq. (3.5.13), proportional to the finite value of the initial nuclear velocity, has to be included in the initial condition. Then NVPT and non-adiabatic results can be directly compared, as the same initial conditions are used in both.

Equating the first order corrections to the BO eigenstate, from the μ^4 - and the $\boldsymbol{\lambda}'_{\nu}(\mathbf{R}, t)$ -expansion, yields

$$\Phi_{\mathbf{R}}^{(1)}(\mathbf{r}, t) = i \sum_{\nu=1}^{N_n} \boldsymbol{\lambda}'_{\nu}(\mathbf{R}, t) \cdot \varphi_{\mathbf{R}}^{(1)}(\mathbf{r}). \quad (3.5.14)$$

The comparison between the μ^4 -expansion and NVPT allows, first of all, to derive an explicit expression of $\varphi_{\mathbf{R}}^{(1)}(\mathbf{r}, t)$ as given in Eq. (3.5.12), and, second, to decompose the perturbed state as a sum of independent (linear) responses to the non-adiabatic perturbations, thus leading to

$$[\hat{\mathcal{H}}_{BO} - \epsilon_{BO}^{(0)}(\mathbf{R})] \varphi_{\mathbf{R}, \nu\alpha}^{(1)}(\mathbf{r}) = \hbar \partial_{\nu\alpha} \varphi_{\mathbf{R}}^{(0)}(\mathbf{r}). \quad (3.5.15)$$

As above, the index ν is used to label the nuclei and α labels the Cartesian components of the gradient. This equation can now be easily solved by employing density functional perturbation theory as described in sections 1.1.4, 2.2 and 2.3.

3.5.4 ANALYSIS OF THE PERTURBATION PARAMETER

The TDVP, defined in eq. (1.5.12), is written using eq. (3.5.7) as

$$\mathbf{A}_\nu(\mathbf{R}, t) = \left\langle \varphi_{\mathbf{R}}^{(0)} + i\mu^2 \sum_{\nu'=1}^{N_n} \boldsymbol{\lambda}'_{\nu'}(\mathbf{R}, t) \cdot \boldsymbol{\varphi}_{\mathbf{R},\nu'}^{(1)} \right| \left| -i\hbar \nabla_\nu \varphi_{\mathbf{R}}^{(0)} + \mu^2 \hbar \nabla_\nu \sum_{\nu'=1}^{N_n} \boldsymbol{\lambda}'_{\nu'}(\mathbf{R}, t) \cdot \boldsymbol{\varphi}_{\mathbf{R},\nu'}^{(1)} \right\rangle_{\mathbf{r}}. \quad (3.5.16)$$

Up to within the linear order in μ^2 (or more precisely $\mu^2 \boldsymbol{\lambda}'_{\nu'}(\mathbf{R}, t)$), this expression is

$$\mathbf{A}_\nu(\mathbf{R}, t) = -2\hbar\mu^2 \int d\mathbf{r} \sum_{\nu'=1}^{N_n} [\boldsymbol{\lambda}'_{\nu'}(\mathbf{R}, t) \cdot \boldsymbol{\varphi}_{\mathbf{R},\nu'}^{(1)}(\mathbf{r})] \nabla_\nu \varphi_{\mathbf{R}}^{(BO)}(\mathbf{r}) \quad (3.5.17)$$

where we can use eq. (3.5.15) to identify the \mathcal{A} -matrix,

$$\underline{\underline{\mathcal{A}}}(\mathbf{R}) = 2 \left\langle \underline{\varphi}_{\mathbf{R}}^{(1)} \left| \hat{\mathcal{H}}_{BO} - \epsilon_{BO}^{(0)}(\mathbf{R}) \right| \underline{\varphi}_{\mathbf{R}}^{(1)} \right\rangle_{\mathbf{r}}. \quad (3.5.18)$$

We derive the following expression for the TDVP, namely

$$\underline{\underline{\mathcal{A}}}(\mathbf{R}, t) = -\mu^2 \underline{\underline{\mathcal{A}}}(\mathbf{R}) \underline{\lambda}'(\mathbf{R}, t). \quad (3.5.19)$$

Once again we keep the term $\mathcal{O}(\mu^2)$ in $\underline{\lambda}'$, but we show below how it is included in the definition of the small parameter $\underline{\lambda}$. $\underline{\underline{\mathcal{A}}}(\mathbf{R})$ is a matrix, thus the double-underlined notation, with $(3N_n \times 3N_n)$ elements, whereas $\underline{\varphi}_{\mathbf{R}}^{(1)}(\mathbf{r})$ is a vector with $(3N_n)$ components. We have written also the TDVP and the parameter in matrix notation, with $\underline{\underline{\mathcal{A}}}(\mathbf{R}, t)$ and $\underline{\lambda}'(\mathbf{R}, t)$ $(3N_n)$ -dimensional vectors. The elements of the \mathcal{A} -matrix are

$$\mathcal{A}_{\nu'\nu}^{ij}(\mathbf{R}) = \left\langle \varphi_{\mathbf{R},\nu'i}^{(1)} \left| \hat{\mathcal{H}}_{BO} - \epsilon_{BO}^{(0)}(\mathbf{R}) \right| \varphi_{\mathbf{R},\nu'j}^{(1)} \right\rangle_{\mathbf{r}}, \quad (3.5.20)$$

with i, j labeling the Cartesian components and ν', ν the nuclei. When using eq. (3.5.12), the elements of the \mathcal{A} -matrix can be written in terms of the non-adiabatic coupling vectors and of the BO eigenvalues as

$$\mathcal{A}_{\nu'\nu}^{ij}(\mathbf{R}) = 2\hbar \sum_{e \neq 0} \frac{\mathbf{d}_{\nu'i,e0}(\mathbf{R}) \mathbf{d}_{\nu'j,e0}(\mathbf{R})}{\omega_{e0}(\mathbf{R})} \quad (3.5.21)$$

from which it follows that the \mathcal{A} -matrix is symmetric. The \mathcal{A} -matrix is also positive definite* with positive diagonal elements, i.e.

$$\mathcal{A}_{\nu\nu}^{ii}(\mathbf{R}) = 2\hbar \sum_{e \neq 0} \frac{|\mathbf{d}_{\nu i,e0}(\mathbf{R})|^2}{\omega_{e0}(\mathbf{R})} \geq 0. \quad (3.5.22)$$

This property is essential for the interpretation of the \mathcal{A} -matrix as a position-dependent mass. The components of the TDVP can be expressed in terms of the components of the \mathcal{A} -matrix,

$$A_{\nu i}(\mathbf{R}, t) = -\mu^2 \sum_{\nu'=1}^{N_n} \sum_{j=x,y,z} \mathcal{A}_{\nu\nu'}^{ij}(\mathbf{R}) \lambda'_{\nu'j}(\mathbf{R}, t). \quad (3.5.23)$$

* For all non-zero real vectors \underline{v} , the relation $\underline{v}^T \underline{\underline{\mathcal{A}}} \underline{v} \geq 0$ holds.

This expression is used in the definition of the parameter $\lambda'_{\nu i}(\mathbf{R}, t)$, given in eq. (3.5.6),

$$\lambda'_{\nu i}(\mathbf{R}, t) = M_{\nu}^{-1} \lambda_{\nu i}(\mathbf{R}, t) - \mu^4 M_{\nu}^{-1} \sum_{\nu', j} \mathcal{A}_{\nu\nu'}^{ij}(\mathbf{R}) \lambda'_{\nu' j}(\mathbf{R}, t), \quad (3.5.24)$$

where

$$\lambda_{\nu i}(\mathbf{R}, t) = \mu^2 \frac{-i\hbar \partial_{\nu i} \chi(\mathbf{R}, t)}{\chi(\mathbf{R}, t)}, \quad (3.5.25)$$

which, we recall, tends towards a quantity independent of μ for $\mu \rightarrow 0$. Writing eq. (3.5.24) in matrix form and solving for $\underline{\lambda}(\mathbf{R}, t)$ we obtain

$$\underline{\lambda}(\mathbf{R}, t) = [\underline{M} + \mu^4 \underline{\mathcal{A}}(\mathbf{R})] \underline{\lambda}'(\mathbf{R}, t) = \underline{\mathcal{M}}(\mathbf{R}) \underline{\lambda}'(\mathbf{R}, t), \quad (3.5.26)$$

where \underline{M} is a diagonal $(3N_n \times 3N_n)$ matrix containing the masses of the nuclei and we have defined a position-dependent mass matrix $\underline{\mathcal{M}}(\mathbf{R})$. This equation can be inverted (by self-consistently summing up an infinite number of terms of order μ^{2n}) to obtain

$$\underline{\lambda}'(\mathbf{R}, t) = \underline{\mathcal{M}}^{-1}(\mathbf{R}) \underline{\lambda}(\mathbf{R}, t), \quad (3.5.27)$$

yielding the TDVP in the form

$$\underline{A}(\mathbf{R}, t) = -\underline{\mathcal{A}}(\mathbf{R}) \underline{\mathcal{M}}^{-1}(\mathbf{R}) \underline{\lambda}(\mathbf{R}, t), \quad \text{with} \quad \underline{\mathcal{M}}(\mathbf{R}) = \underline{M} + \mu^4 \underline{\mathcal{A}}(\mathbf{R}), \quad (3.5.28)$$

with $\mu^4 = 1$, where only $\underline{\lambda}$ appears.

Eq. (3.5.23) shows that the TDVP is at least first order in the perturbation parameter and this is the reason why it is not considered in the definition of the perturbed electronic Hamiltonian in eq. (3.5.10). Due to the explicit dependence of $\mathbf{A}_{\nu}(\mathbf{R}, t)$ on $\lambda'_{\nu}(\mathbf{R}, t)$, which is known via the \mathcal{A} -matrix, we have been able to isolate the “actual” small parameter, i.e. $\lambda(\mathbf{R}, t)$. In all expressions, however, we find $\lambda'(\mathbf{R}, t)$, the matrix product of $\underline{\mathcal{M}}^{-1}(\mathbf{R})$ and $\lambda(\mathbf{R}, t)$, which is a gauge-invariant quantity. If $\mu^4 = 1$, expressions where the physical masses appear are recovered. From eq. (3.5.18) it is evident that $\underline{\mathcal{A}}(\mathbf{R})$ is a purely electronic quantity, which affects the nuclear momentum through the TDVP. Such correction, however, also appears in the nuclear evolution equation (1.5.7).

3.5.5 NUCLEAR HAMILTONIAN

We show in this section the procedure leading to the appearance of the position-dependent mass $\underline{\mathcal{M}}(\mathbf{R})$ in the nuclear evolution equation (1.5.7) of the exact factorization. The nuclear time dependent Schrödinger equation, in matrix form, becomes

$$\left[\frac{1}{2} (-i\hbar \nabla)^T \underline{\mathcal{M}}^{-1}(\mathbf{R}) (-i\hbar \nabla) + E(\mathbf{R}) \right] \chi = i\hbar \partial_t \chi, \quad (3.5.29)$$

where the superscript T indicates the transpose vector and

$$E(\mathbf{R}) = \epsilon_{BO}^{(0)}(\mathbf{R}) + \sum_{\nu=1}^{N_n} (\hbar^2 / 2M_{\nu}) \langle \nabla_{\nu} \varphi_{\mathbf{R}}^{(0)} | \nabla_{\nu} \varphi_{\mathbf{R}}^{(0)} \rangle_{\mathbf{r}} \quad (3.5.30)$$

is the diagonal BO correction (DBOC). The kinetic energy term now involves dressed nuclear masses.

To derive this, we consider the action of the kinetic energy operator $\hat{T}_n = \sum_\nu [-i\hbar\nabla_\nu + \mathbf{A}_\nu]^2 / (2M_\nu)$ on the nuclear wave function $\chi(\mathbf{R}, t)$, which can be written in matrix form as

$$\hat{T}_n \chi = \frac{1}{2} \left[-i\hbar\nabla + \underline{\mathbf{A}} \right]^T \underline{\mathbf{M}}^{-1} \left[-i\hbar\nabla + \underline{\mathbf{A}} \right] \chi. \quad (3.5.31)$$

Using the expression (3.5.28) of the TDVP, we identify the following terms

$$\begin{aligned} \hat{T}_n \chi &= \frac{1}{2} (-i\hbar\nabla)^T \underline{\mathbf{M}}^{-1} (\underline{\mathcal{I}} - \underline{\mathcal{A}} \underline{\mathbf{M}}^{-1}) (-i\hbar\nabla) \chi \\ &\quad - \frac{1}{2} (\underline{\mathcal{A}} \underline{\mathbf{M}}^{-1} \underline{\lambda})^T \underline{\mathbf{M}}^{-1} \underline{\mathbf{M}} (\underline{\mathbf{M}}^{-1} \underline{\lambda}) \chi \\ &\quad + \frac{1}{2} (\underline{\mathcal{A}} \underline{\mathbf{M}}^{-1} \underline{\lambda})^T \underline{\mathbf{M}}^{-1} (\underline{\mathcal{A}} \underline{\mathbf{M}}^{-1} \underline{\lambda}) \chi. \end{aligned} \quad (3.5.32)$$

In the second term on the right-hand-side we have use the definition of $\underline{\lambda}$ to write $-i\hbar\nabla \chi = \underline{\lambda} \chi$ and we have inserted the definition of the identity matrix in the form $\underline{\mathcal{I}} = \underline{\mathbf{M}}^{-1} \underline{\mathbf{M}}$. We recall the expression of the position-dependent mass matrix, $\underline{\mathbf{M}} = \underline{\mathbf{M}} + \underline{\mathcal{A}}$, leading to the kinetic energy operator in the nuclear Hamiltonian in eq. (1.5.9)

$$\hat{T}_n \chi = \frac{1}{2} (-i\hbar\nabla)^T \underline{\mathbf{M}}^{-1} (-i\hbar\nabla) \chi - \frac{1}{2} (\underline{\mathbf{M}}^{-1} \underline{\lambda})^T \underline{\mathcal{A}} (\underline{\mathbf{M}}^{-1} \underline{\lambda}) \chi \quad (3.5.33)$$

where only the position-dependent mass appears. In the second term on the right-hand-side, we have used the property of the \mathcal{A} -matrix of being symmetric, thus $\underline{\mathcal{A}}^T = \underline{\mathcal{A}}$. We can now show that this second term is exactly canceled out by a second order contribution in the potential energy of the nuclear Hamiltonian. In fact, in the kinetic energy, the product of two factors containing $\underline{\lambda}' = \underline{\mathbf{M}}^{-1} \underline{\lambda}$ is fundamentally a second order quantity. Therefore, we analyze the potential energy up to within second order terms in the perturbation.

The nuclear Hamiltonian from the exact factorization, in eq. (1.5.9), contains $\epsilon(\mathbf{R}, t)$, the TDPEs. Therefore, we shall study its expression in order to identify a kinetic-like contribution to balance the second term in eq. (3.5.33). We write the expression of $\langle \Phi_{\mathbf{R}}(t) | \hat{\mathcal{H}}_{BO} | \Phi_{\mathbf{R}}(t) \rangle_{\mathbf{r}}$ up to within second order terms, when the electronic wave function is expanded as

$$\Phi_{\mathbf{R}}(\mathbf{r}, t) = \varphi_{\mathbf{R}}^{(0)}(\mathbf{r}) + \lambda'(t) \varphi_{\mathbf{R}}^{(1)}(\mathbf{r}) + \lambda'^2(t) \varphi_{\mathbf{R}}^{(2)}(\mathbf{r}). \quad (3.5.34)$$

We use here a simplified notation, also using the property that the only time-dependence in the electronic wave function appears via $\lambda'_\nu(\mathbf{R}, t)$. Using this form of the electronic wave function, we write

$$\begin{aligned} \langle \Phi_{\mathbf{R}}(t) | \hat{\mathcal{H}}_{BO} | \Phi_{\mathbf{R}}(t) \rangle_{\mathbf{r}} &= \epsilon_{BO}^{(0)}(\mathbf{R}) + \lambda'^2(t) \langle \varphi_{\mathbf{R}}^{(1)} | \hat{\mathcal{H}}_{BO} | \varphi_{\mathbf{R}}^{(1)} \rangle_{\mathbf{r}} \\ &\quad + \lambda'^2(t) \epsilon_{BO}^{(0)}(\mathbf{R}) \left[\langle \varphi_{\mathbf{R}}^{(2)} | \varphi_{\mathbf{R}}^{(0)} \rangle_{\mathbf{r}} + \langle \varphi_{\mathbf{R}}^{(0)} | \varphi_{\mathbf{R}}^{(2)} \rangle_{\mathbf{r}} \right] + \mathcal{O}(\lambda^3), \end{aligned} \quad (3.5.35)$$

and, by using the partial normalization condition up to within second order,

$$\langle \varphi_{\mathbf{R}}^{(0)} | \varphi_{\mathbf{R}}^{(0)} \rangle_{\mathbf{r}} + \lambda'^2(t) \left[\langle \varphi_{\mathbf{R}}^{(1)} | \varphi_{\mathbf{R}}^{(1)} \rangle_{\mathbf{r}} + \langle \varphi_{\mathbf{R}}^{(2)} | \varphi_{\mathbf{R}}^{(0)} \rangle_{\mathbf{r}} + \langle \varphi_{\mathbf{R}}^{(0)} | \varphi_{\mathbf{R}}^{(2)} \rangle_{\mathbf{r}} \right] = 1, \quad (3.5.36)$$

we find

$$\langle \varphi_{\mathbf{R}}^{(2)} | \varphi_{\mathbf{R}}^{(0)} \rangle_{\mathbf{r}} + \langle \varphi_{\mathbf{R}}^{(0)} | \varphi_{\mathbf{R}}^{(2)} \rangle_{\mathbf{r}} = - \langle \varphi_{\mathbf{R}}^{(1)} | \varphi_{\mathbf{R}}^{(1)} \rangle_{\mathbf{r}}, \quad (3.5.37)$$

since the normalization condition is already satisfied at zero-th order. We insert this result in eq. (3.5.35) to obtain

$$\begin{aligned} \langle \Phi_{\mathbf{R}}(t) | \hat{\mathcal{H}}_{BO} | \Phi_{\mathbf{R}}(t) \rangle_{\mathbf{r}} &= \epsilon_{BO}^{(0)}(\mathbf{R}) \\ &+ \lambda'^2(t) \langle \varphi_{\mathbf{R}}^{(1)} | \hat{\mathcal{H}}_{BO} - \epsilon_{BO}^{(0)}(\mathbf{R}) | \varphi_{\mathbf{R}}^{(1)} \rangle_{\mathbf{r}} + \mathcal{O}(\lambda'^3). \end{aligned} \quad (3.5.38)$$

In the second term on the right-hand-side we identify the \mathcal{A} -matrix and we thus write

$$\langle \Phi_{\mathbf{R}}(t) | \hat{\mathcal{H}}_{BO} | \Phi_{\mathbf{R}}(t) \rangle_{\mathbf{r}} = \epsilon_{BO}^{(0)}(\mathbf{R}) + \sum_{\nu, \nu'} \sum_{i, j} \frac{1}{2} \lambda'_{\nu i}(\mathbf{R}, t) \mathcal{A}_{\nu \nu'}^{ij}(\mathbf{R}) \lambda'_{\nu' j}(\mathbf{R}, t) \quad (3.5.39)$$

$$= \epsilon_{BO}^{(0)}(\mathbf{R}) + \frac{1}{2} \underline{\lambda}'^T(\mathbf{R}, t) \underline{\mathcal{A}}(\mathbf{R}) \underline{\lambda}'(\mathbf{R}, t), \quad (3.5.40)$$

where eq. (3.5.40) is a rewriting of eq. (3.5.39) in matrix form. Inserting the expression of $\underline{\lambda}'(\mathbf{R}, t)$ in terms of $\underline{\lambda}(\mathbf{R}, t)$ given in eq. (3.5.27), we can express the second term of eq. (3.5.40) as

$$\underline{\lambda}'^T(\mathbf{R}, t) \underline{\mathcal{A}}(\mathbf{R}) \underline{\lambda}'(\mathbf{R}, t) = \left[\underline{\mathcal{M}}^{-1}(\mathbf{R}) \underline{\lambda}(\mathbf{R}, t) \right]^T \underline{\mathcal{A}}(\mathbf{R}) \left[\underline{\mathcal{M}}^{-1}(\mathbf{R}) \underline{\lambda}(\mathbf{R}, t) \right], \quad (3.5.41)$$

which exactly cancels the second term on the right-hand-side of eq. (3.5.33). The nuclear Hamiltonian is thus derived as

$$\hat{\mathcal{H}}_n = \frac{1}{2} (-i\hbar \underline{\nabla})^T \underline{\mathcal{M}}^{-1}(\mathbf{R}) (-i\hbar \underline{\nabla}) + E(\mathbf{R}). \quad (3.5.42)$$

The potential energy is time-independent and contains the BO energy, from the first term in eq. (3.5.40), and an additional contribution, according to

$$E(\mathbf{R}) = \epsilon_{BO}^{(0)}(\mathbf{R}) + \sum_{\nu=1}^{N_n} \frac{\hbar^2}{2M_{\nu}} \langle \nabla_{\nu} \varphi_{\mathbf{R}}^{(0)} | \nabla_{\nu} \varphi_{\mathbf{R}}^{(0)} \rangle_{\mathbf{r}}. \quad (3.5.43)$$

It is worth noting that the first order contribution to the time-dependent potential $\epsilon(\mathbf{R}, t)$ is zero, thus only $\epsilon^{(0)}(\mathbf{R})$, the zeroth order term, appears as potential energy in the nuclear Hamiltonian of eq. (3.5.42). This statement has been already proven in ref.⁵⁴ using the definition in eq. (1.5.11) and the expression of the electronic wave function up to within first order terms in the perturbation. The second term on the right-hand-side is referred to as diagonal BO correction (DBOC) in the applications proposed in this chapter. Among the second order contributions to the potential energy (it appears at the order μ^4 in eq. (3.5.2)), only this term beyond $\epsilon_{BO}^{(0)}(\mathbf{R})$ is included in the calculations, due to the fact that at this stage the theory does not allow us to efficiently compute higher order terms.

The correspondence principle of quantum mechanics enables us to determine the classical nuclear Hamiltonian²⁹³ as

$$H_n = \frac{1}{2} \underline{P}^T \underline{\mathcal{M}}^{-1}(\mathbf{R}) \underline{P} + E(\mathbf{R}) \quad (3.5.44)$$

where $\underline{P} = \underline{\mathcal{M}}(\mathbf{R}) \dot{\underline{R}}$ is the nuclear momentum. This Hamiltonian contains both the nuclear and electronic contribution to the kinetic energy, in the forms $\dot{\underline{R}}^T \underline{\mathcal{M}} \dot{\underline{R}}/2$ and $\dot{\underline{R}}^T \underline{\mathcal{A}}(\mathbf{R}) \dot{\underline{R}}/2$, respectively.

The key result of the section is encoded in Eq. (3.5.29), where $\underline{\mathcal{M}}(\mathbf{R}) = \underline{M} + \underline{\mathcal{A}}(\mathbf{R})$ since we have taken $\mu^4 = 1$. Even in the presence of (weak) non-adiabatic effects, the dynamical problem can be expressed in

terms of nuclei moving on a single, static, potential energy surface – the electronic ground state (plus DBOC) – with masses that are corrected by the presence of the electrons. We have shown how, in a very simple and intuitive way, the electrons are carried along by the nuclei: $\underline{\mathcal{A}}(\mathbf{R})$, the \mathcal{A} -matrix, is a position-dependent mass that dresses the bare nuclear masses \underline{M} . The \mathcal{A} -matrix is a purely electronic quantity and is obtained by considering the lowest order corrections $\mathcal{O}(\mu^2)$ to the BO electronic wave function. It appears both in the definition of the TDVP and in the nuclear Hamiltonian, and can easily be computed by employing perturbation theory.⁵⁴

3.5.6 PROPERTIES OF THE POSITION-DEPENDENT MASS

When Cartesian coordinates are employed, as done here, the \mathcal{A} -matrix has the property of yielding the total electronic mass of the system when summed up over all nuclei,

$$\sum_{\nu, \nu'=1}^{N_n} \mathcal{A}_{\nu\nu'}^{ij}(\mathbf{R}) = m N_{el} \delta_{ij} \quad \forall \mathbf{R}, \quad (3.5.45)$$

supporting its interpretation as a correction term to the nuclear mass. This can be seen by using the property of the BO electronic wave function of being invariant under a translation of the coordinate reference system, namely $\varphi_{\mathbf{R}'}^{(0)}(\mathbf{r}') = \varphi_{\mathbf{R}}^{(0)}(\mathbf{r})$ with $\mathbf{R}' = \mathbf{R}_1', \dots, \mathbf{R}_{N_n}' = \mathbf{R}_1 + \eta \Delta, \dots, \mathbf{R}_{N_n} + \eta \Delta$ and analogously for \mathbf{r}' . Notice that Δ is a three-dimensional vector and that all positions, electronic and nuclear, are translated of the same amount $\eta \Delta$. Translational invariance^{293,305} means

$$\begin{aligned} 0 &= \frac{\partial \varphi_{\mathbf{R}'}^{(0)}(\mathbf{r}')}{\partial \eta} \\ &= \sum_{i=x,y,z} \left[\sum_{\nu=1}^{N_n} \frac{\partial \varphi_{\mathbf{R}'}^{(0)}(\mathbf{r}')}{\partial R'_{\nu i}} \frac{\partial R'_{\nu i}}{\partial \eta} + \sum_{k=1}^{N_{el}} \frac{\partial \varphi_{\mathbf{R}'}^{(0)}(\mathbf{r}')}{\partial r'_{ki}} \frac{\partial r'_{ki}}{\partial \eta} \right] \\ &= \sum_{i=x,y,z} \Delta_i \left[\sum_{\nu=1}^{N_n} \frac{\partial \varphi_{\mathbf{R}'}^{(0)}(\mathbf{r}')}{\partial R'_{\nu i}} + \sum_{k=1}^{N_{el}} \frac{\partial \varphi_{\mathbf{R}'}^{(0)}(\mathbf{r}')}{\partial r'_{ki}} \right] \\ &= \Delta \cdot \left[\sum_{\nu=1}^{N_n} \nabla_{\nu} \varphi_{\mathbf{R}'}^{(0)}(\mathbf{r}') + \sum_{k=1}^{N_{el}} \nabla_k \varphi_{\mathbf{R}'}^{(0)}(\mathbf{r}') \right], \end{aligned} \quad (3.5.46)$$

which is valid for all values of Δ . Identifying ∇_k as the position representation of the momentum operator $\hat{\mathbf{p}}_k$ corresponding to the k -th electron (divided by $-i\hbar$), which can be written also as

$$\hat{\mathbf{p}}_k = \frac{im}{\hbar} [\hat{\mathcal{H}}, \hat{\mathbf{r}}_k] = \frac{im}{\hbar} [\hat{\mathcal{H}}_{BO}, \hat{\mathbf{r}}_k], \quad (3.5.47)$$

and projecting the two terms in square brackets in eq. (3.5.46) onto $\varphi_{\mathbf{R}, \nu i}^{(1)}(\mathbf{r})$, from eq. (3.5.12),

$$\sum_{\nu=1}^{N_n} \langle \varphi_{\mathbf{R}, \nu i}^{(1)} | \hbar \nabla_{\nu} \varphi_{\mathbf{R}}^{(0)} \rangle_{\mathbf{r}} = \frac{m}{\hbar} \sum_{k=1}^{N_{el}} \langle \varphi_{\mathbf{R}, \nu i}^{(1)} | [\hat{\mathcal{H}}_{BO}, \hat{\mathbf{r}}_k] | \varphi_{\mathbf{R}}^{(0)} \rangle_{\mathbf{r}}, \quad (3.5.48)$$

we identify the \mathcal{A} -matrix on the left-hand-side and, for each Cartesian component j , we write

$$\sum_{\nu=1}^{N_n} \mathcal{A}_{\nu\nu'}^{ij}(\mathbf{R}) = -\frac{m}{\hbar} \sum_{k=1}^{N_{el}} \langle \varphi_{\mathbf{R}, \nu' i}^{(1)} | [\hat{\mathcal{H}}_{BO}, \hat{r}_{kj}] | \varphi_{\mathbf{R}}^{(0)} \rangle_{\mathbf{r}}. \quad (3.5.49)$$

From the term on the right-hand-side we derive the expression of the atomic polar tensor. First of all we write explicitly the commutator and we use eq. (3.5.15) to obtain

$$\begin{aligned} & \langle \varphi_{\mathbf{R},\nu'i}^{(1)} | [\hat{\mathcal{H}}_{BO}, \hat{r}_{kj}] | \varphi_{\mathbf{R}}^{(0)} \rangle_{\mathbf{r}} \\ &= \int d\mathbf{r} \varphi_{\mathbf{R},\nu'i}^{(1)}(\mathbf{r}) [\hat{\mathcal{H}}_{BO} - \epsilon_{BO}^{(0)}(\mathbf{R})] r_{kj} \varphi_{\mathbf{R}}^{(0)}(\mathbf{r}) \end{aligned} \quad (3.5.50)$$

$$= -\hbar \int d\mathbf{r} (\partial_{\nu'i} \varphi_{\mathbf{R}}^{(0)}(\mathbf{r})) r_{kj} \varphi_{\mathbf{R}}^{(0)}(\mathbf{r}), \quad (3.5.51)$$

then we identify the expectation value of the electronic dipole moment operator over the BO wave function in the following expression

$$\partial_{\nu'i} \sum_{k=1}^{N_{el}} \int d\mathbf{r} \varphi_{\mathbf{R}}^{(0)}(\mathbf{r}) r_{kj} \varphi_{\mathbf{R}}^{(0)}(\mathbf{r}) = \frac{1}{e} \partial_{\nu'i} \langle \hat{\mu}_j^{(el)}(\mathbf{R}) \rangle_{BO}. \quad (3.5.52)$$

The derivative with respect to the i -th Cartesian component, relative to the ν' -th nucleus, of the j -th Cartesian component of the electronic dipole moment is the definition of the electronic contribution to the atomic polar tensor³⁰⁶ $\mathcal{P}_{ij}^{\nu}(\mathbf{R})$. This leads to the relation^{36,305}

$$\sum_{\nu,\nu'=1}^{N_n} \mathcal{A}_{\nu'\nu}^{ij}(\mathbf{R}) = \sum_{\nu=1}^{N_n} \frac{m}{e} \mathcal{P}_{ij}^{\nu}(\mathbf{R}) = m N_{el} \delta_{ij}, \quad (3.5.53)$$

when we further sum over the index ν . This result states that when the \mathcal{A} -matrix is summed up over all nuclei it yields the total electronic mass of the complete system. In eq. (3.5.42) this means that the mass effect of the electrons is completely taken into account by the position-dependent mass corrections to the nuclear masses within the order of the perturbation considered here.

Eq. (3.5.53) is expressed in matrix form as

$$\sum_{\nu,\nu'=1}^{N_n} [\underline{\underline{\mathcal{A}}}(\mathbf{R})]_{\nu\nu'} = \frac{m}{e} \sum_{\nu=1}^{N_n} [\underline{\underline{\mathcal{P}}}(\mathbf{R})]_{\nu} = m N_{el} \underline{\underline{\mathcal{I}}}^{(3)}, \quad (3.5.54)$$

where $[\underline{\underline{\mathcal{A}}}(\mathbf{R})]_{\nu\nu'}$ and $[\underline{\underline{\mathcal{P}}}(\mathbf{R})]_{\nu}$ are (3×3) matrices (in Cartesian components) and $\underline{\underline{\mathcal{I}}}^{(3)}$ is the identity matrix. $[\underline{\underline{\mathcal{P}}}(\mathbf{R})]_{\nu} = \nabla_{\nu} \langle \hat{\mu}^{(el)}(\mathbf{R}) \rangle_{BO}$ is the electronic contribution to the atomic polar tensor, defined as the variation with respect to nuclear positions of the electronic dipole moment (here averaged over the BO state).³⁰⁶ The second equality in Eq. (3.5.54) is obtained using the known property of the atomic polar tensor of yielding the total electronic charge of the system when summed over all nuclei.^{36,305}

It is common to separate the center of mass (CoM) motion before introducing the BO approximation. Within the molecular frame, choosing coordinates in which the kinetic energy operator is the sum of two separated, nuclear and electronic terms, the procedure presented here can be straightforwardly applied. Using the above sum rule, Eq. (3.5.54), it is instead possible to separate of the CoM motion *a posteriori* and recover in that case the full mass of the system.

Starting from the Cartesian coordinates, we make the following change of coordinates

$$\begin{aligned} \mathbf{R}'_1 &= M_{tot}^{-1} \left(\sum_{\nu=1}^{N_n} M_{\nu} \mathbf{R}_{\nu} + m \sum_{k=1}^{N_{el}} \langle \hat{\mathbf{r}}_k \rangle_{BO} \right) \\ \mathbf{R}'_{\nu} &= \mathbf{R}_{\nu} - \mathbf{R}_1 \quad \text{with } \nu \geq 2, \end{aligned} \quad (3.5.55)$$

with $M_{tot} = \sum_{\nu} M_{\nu} + mN_{el}$. From the sum rule eq. (3.5.53), the nuclear Hamiltonian of eq. (3.5.42) becomes

$$\hat{\mathcal{H}}_n = \frac{\hat{P}_{\text{CoM}}^2}{2M_{tot}} + \frac{1}{2} (-i\hbar \underline{\nabla}')^T \underline{\mathcal{M}}'^{-1} (-i\hbar \underline{\nabla}') + E'. \quad (3.5.56)$$

\hat{P}_{CoM} is the momentum (operator) associated to the center of mass (CoM) coordinate in eq. (3.5.55), thus the first term accounts for the motion of the CoM as a free particle. The mass associated to the CoM is, correctly, the total mass of the system, i.e. nuclei and electrons, rather than the nuclear mass only, as in the BO approximation. The following terms are the kinetic and potential energies corresponding to the internal, rotational and vibrational, degrees of freedom. Section C.2 in the appendix provides a detailed description of the derivation.

3.5.7 APPLICATIONS

The formalism introduced above is employed to construct a numerical procedure that is (i) fundamentally adiabatic, namely only a single (static) potential energy surface is explicitly involved, but (ii) able to account for electronic effects beyond BO via the position-dependent corrections to the bare nuclear masses. The key quantity in the examples reported below is the nuclear Hamiltonian of eq. (3.5.42): quantum-mechanically, it is used to compute the spectrum of a model of a proton involved in a one-dimensional hydrogen bond;²⁷⁵ interpreted classically in the same model system, it is employed as the generator of the classical evolution of the oxygen atoms in the presence of a quantum proton. Transforming to internal coordinates and in the harmonic approximation, position-dependent corrections are included in the calculation of the vibrational spectra of H_2 , H_2O , NH_3 and H_3O^+ . Numerical details are given in section C.3 in the appendix.

NON-ADIABATIC PROTON TRANSFER

As a first application, we consider a model of a proton involved in a one-dimensional hydrogen bond $\text{O}-\text{H}-\text{O}$,²⁷⁵ in which non-adiabatic effects are known to be important.³⁰⁷ The light particle is the proton, assumed to be in its vibrational ground state. The mass ratio with the heavy particles, the two oxygens, is much larger than the electron-nuclear mass ratio, thus suggesting possible deviations from the BO approximation. We use an asymmetric potential mimicking a strong hydrogen bond (as shown in fig. 3.12): the proton is bonded to the oxygen atom O^- at large distances whereas at short distances it is shared by the two oxygen atoms and is localized around the center of the $\text{O}-\text{O}$ bond. The proton densities corresponding to the ground state is shown in Fig. 3.12.

At large distances we expect the effective mass of O^- to be close to 17 a.m.u. as it carries along the proton. This is clear in Fig. 3.13, where it is shown that the element $\mathcal{A}_{\text{O}^-\text{O}^-}(R)$ of the \mathcal{A} -matrix tends to a constant (equal to 1 a.m.u., the mass of the proton) at $R > 3 \text{ \AA}$, whereas all other components are zero, as expected from the sum rule of Eq. (3.5.54). We show this schematically in Fig. 3.13 where we plot the proton density along the $\text{O}-\text{O}$ bond. We also report an estimate of the amount of electronic mass associated to each oxygen, as the sum over the columns of the \mathcal{A} -matrix, e.g. $\mathcal{M}_{\text{O}^-}(R) = M_{\text{O}^-} + [\mathcal{A}_{\text{O}^-\text{O}^-}(R) + \mathcal{A}_{\text{O}^+\text{O}^-}(R)]$. At short distances instead the proton is shared by the oxygens: the elements of the \mathcal{A} -matrix are non-zero, but the O^- diagonal contribution remains dominant. Notice that it is not surprising that the off-diagonal elements

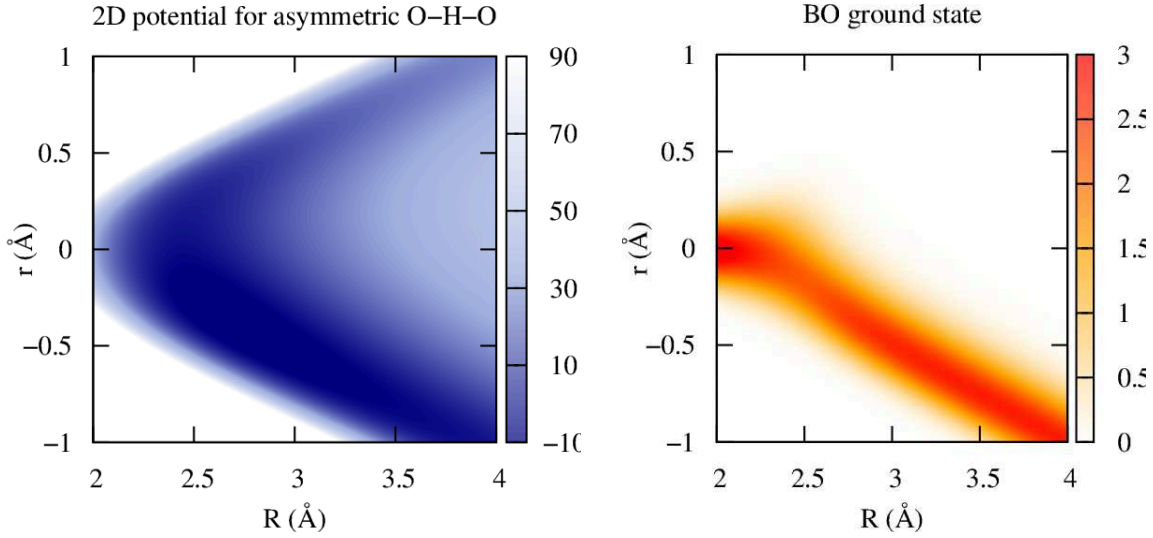


Figure 3.12: Left: Potential of the hydrogen bond model as a function of the O—O distance (R) and of the proton position (r). Right: proton density corresponding to the BO ground state.

of the \mathcal{A} -matrix are negative, as only two conditions are physically relevant: the diagonal elements must be non-negative, in a ground-state dynamics, and the sum of the elements must yield the electronic mass, in a translationally invariant system. As seen in Fig. 3.13, the two protons have then similar masses at very short distances.

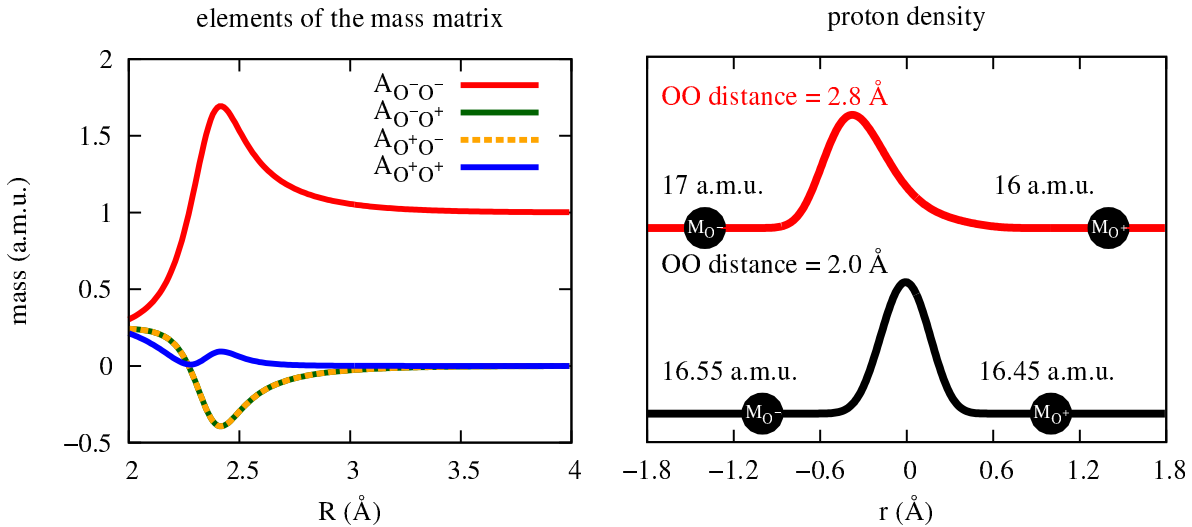


Figure 3.13: Left: Elements of the \mathcal{A} -matrix as functions of R . Right: Proton density at two values of the O—O distance (2.0 Å black and 2.8 Å red), where the masses of the oxygens (sum of columns of the matrix $\underline{\mathcal{M}}$, see text) \mathcal{M}_{O^+} and \mathcal{M}_{O^-} indicate the \mathcal{A} -matrix effect.

Fig. 3.14 shows the classical trajectories of the two oxygen atoms starting from a compressed O—O distance and zero velocity. Calculations have been performed both in the standard adiabatic approximation (BO) and with position-dependent corrections to the oxygen masses (BO+M). The two sets of calculations are compared with Ehrenfest dynamics, where non-adiabatic effects are included explicitly. The distance of the oxygens is plotted along with the mean position of the proton at the final steps of the dynamics. The masses are $\mathcal{M}_{O^+} = \mathcal{M}_{O^-} = 16$ a.m.u. and $\mathcal{M}_{H^+} = 1$ a.m.u. In Fig. 3.14(f) it is shown that the CoM of the system is perfectly fixed when position-dependent masses are employed, in contrast to the BO approximation.

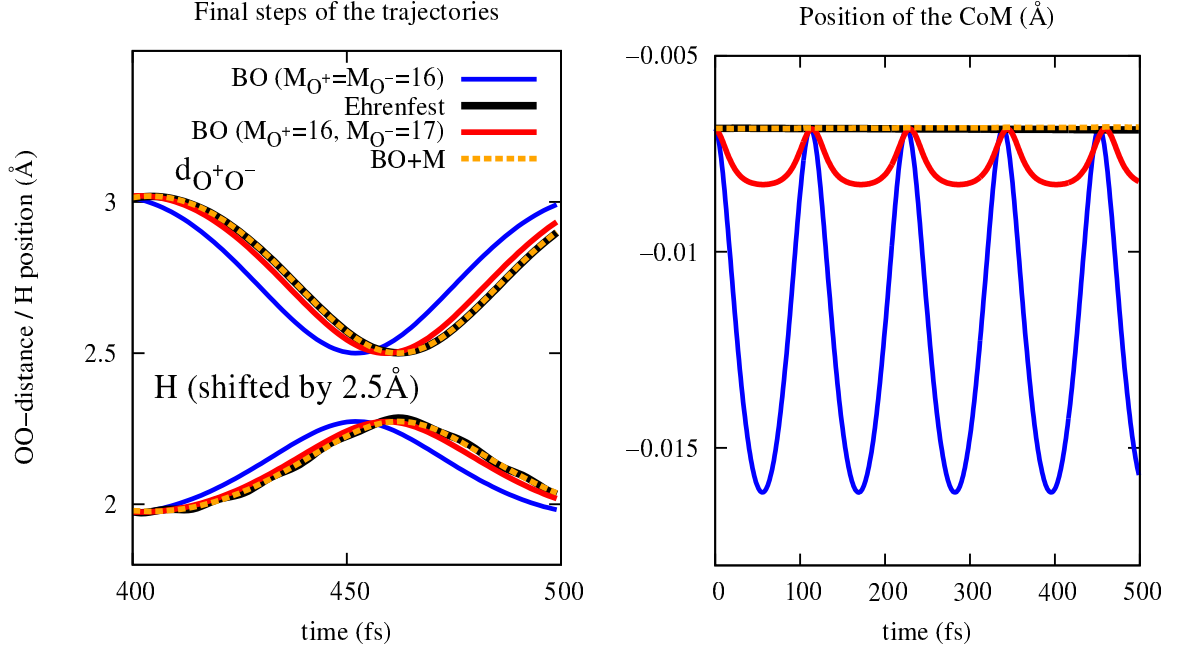


Figure 3.14: Left: Distance of the oxygens and position of the proton during the final steps of the dynamics: BO approximation with $M_{O+} = M_{O-} = 16$ a.m.u. (blue), BO approximation adding the proton mass $M_H = 1$ a.m.u. to the mass of M_{O-} (red), the BO approximation corrected by the position-dependent dressed mass (orange), Ehrenfest dynamics (black). Right: Position of the center of mass (CoM).

We have tested an *ad hoc* correction to the mass of the oxygen O^- , i.e. $M_{O-} = 17$ a.m.u. This improves the conservation of the CoM but does not fix it completely. BO dynamics is faster than the Ehrenfest dynamics because the heavy atoms have only the bare nuclear mass. Changing M_{O-} to 17 a.m.u. improves the result, but only including the position-dependent dressed mass leads to a systematic convergence to the Ehrenfest results. We have further compared the error with respect to Ehrenfest dynamics, of BO and BO+M dynamics, as function of the inverse mass ratio $\mu^{-4} = M_O/M_{H+}$. This is shown in Fig. 3.15 as the root-mean-square-deviation (RMSD) with respect to the reference Ehrenfest trajectory. The position-dependent dressed mass greatly improves the precision of the dynamics even at small values of μ^{-4} ($= 4$ is the smallest value used), and leads to an error four orders of magnitude smaller than BO at large mass ratios.

Further, we have computed the four lowest eigenstates of the full quantum Hamiltonian at different values of μ^{-4} . The diagonalization of the full Hamiltonian is compared to three approximations: BO, BO+DBOC, BO+DBOC+M (where we also include the position-dependent correction). Fig. 3.15 shows the error on the eigenvalues (the exact lowest eigenvalue is $-4127.08527 \text{ cm}^{-1}$ at $M_{O+} = M_{O-} = 16$ a.m.u.). At small μ^{-4} the BO approximation is expected to fail: the mass corrections allow to gain one order of magnitude in the eigenvalues, even if compared to the case where the DBOC is included. Overall, also in the static situation the mass correction leads to highly accurate results. At a mass ratio $\mu^{-4} = 1600$ an accuracy on the eigenvalues of about 10^{-5} cm^{-1} is reached whereas it is only 0.5 cm^{-1} using the BO approximation.

CORRECTIONS TO HARMONIC FREQUENCIES

Next, we consider non-adiabatic effects on vibrational frequencies and predict corrections to the harmonic frequencies of small molecules, i.e. H_2 , H_2O , NH_3 and H_3O^+ . The corrected frequencies $\nu + \Delta\nu$ have

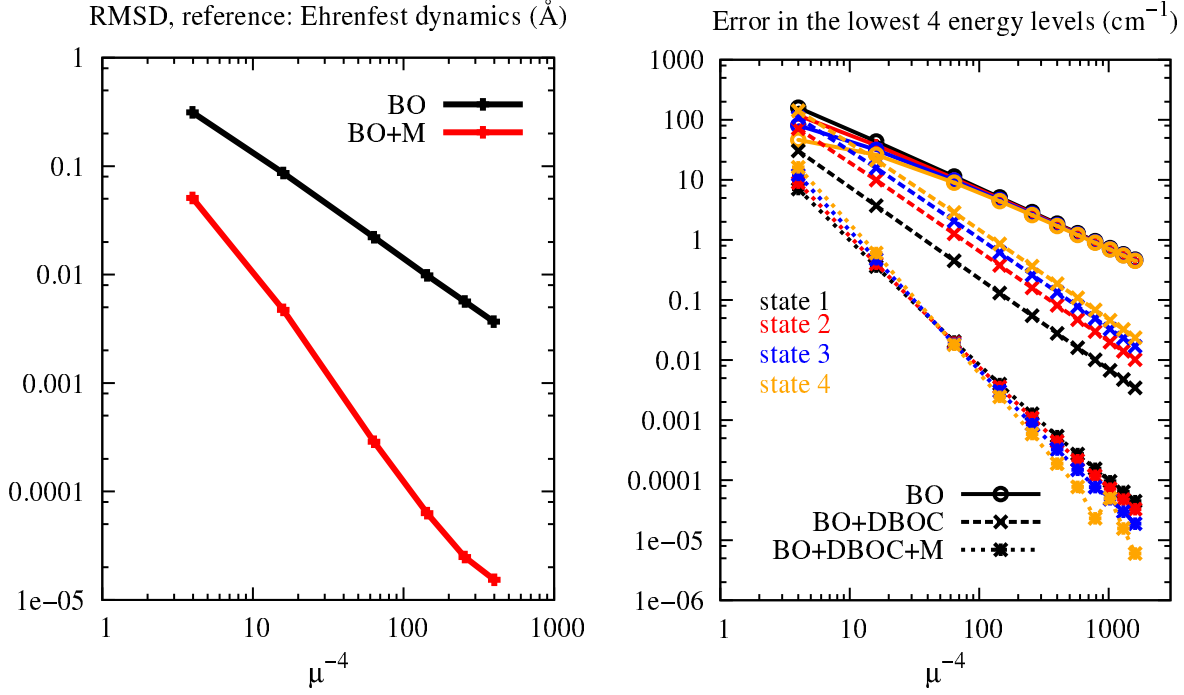


Figure 3.15: Left: RMSD between Ehrenfest results and the BO approximation (black) or the BO approximation corrected by the position-dependent dressed mass (red). Right: Error between the four lowest eigenvalues of the full Hamiltonian and BO (solid lines with circles), BO+DBOC (dashed lines with crosses), BO+DBOC+M (dotted lines with squares). Both panels show the results as functions of the inverse mass ratio μ^{-4} .

been computed by diagonalizing the matrix $[\underline{\mathcal{M}}^{-1}(\mathbf{R}_0)\underline{K}(\mathbf{R}_0)]$ at the equilibrium geometry \mathbf{R}_0 , where \underline{K} is the Hessian computed from the ground state adiabatic potential energy surface. Negative frequency shifts are expected, as shown in Table 3.2: non-adiabatic effects perturbing the ground-state dynamics tend to induce excitations of the light particles, and the energy necessary for the transition is “removed” from the heavy particles. Comparison with the literature,²⁹⁷ when available, shows that the theory is capable to predict accurate non-adiabatic corrections, even if working within the harmonic approximation and with the generalized gradient approximation to density functional theory. The approach can be easily applied to systems beyond di- and tri-atomic molecules^{296,297} and we provide the first predictions to the non-adiabatic corrections of vibrational frequencies of NH_3 and H_3O^+ . It can be seen that the shifts of the N-H stretch frequencies of NH_3 are larger than those of the O-H stretch frequencies of H_3O^+ , due to the fact that the N-H bonds are less ionic and as a result the mass carried along by the protons are larger in NH_3 than in H_3O^+ .

Table 3.2: Harmonic frequencies ν (in cm^{-1}) and their non-adiabatic corrections $\Delta\nu$. Benchmark values are taken from ref.²⁹⁷ when indicated.

molecule	H_2	H_2^{297}	H_2O	H_2O^{297}	NH_3	H_3O^+
$\nu, \Delta\nu$	4343.28, -0.89	-0.74	1594.93, -0.06	1597.60, -0.07	1016.73, -0.06	837.27, -0.03
			3656.19, -0.74	3661.00, -0.69	1628.30, -0.10	1639.25, -0.05
			3757.77, -0.59	3758.63, -0.77	3358.91, -0.82	3438.80, -0.36
					3471.93, -0.74	3522.10, -0.26

3.6 DIRECT MOMENT EXPANSION ALGORITHM

In section 2.4, we have devised a compact representation of the electronic susceptibility for inter-molecular interactions, the moment expanded representation. Using the properties of the derived transformation, it is possible to bypass the spectral decomposition of the response function and to directly calculate its moment expanded representation. We first outline the idea and then give a generalized closed form of the algorithm.. We start with a perturbing potential with only one symmetry contribution $V_1^{-1} = 1$, which gives rise to the electronic response via eq. (??)

$$n_{V_1^{-1}}^{\text{resp}}(\mathbf{r}) = \sum_{m=-l}^l \xi_l^m(\mathbf{r}) \Xi_{l1}^{m-1} = n_1^{-1}(\mathbf{r}) = \xi_1^{-1}(\mathbf{r}) \Xi_{11}^{-1-1}, \quad (3.6.1)$$

where eq. (??) has been used. This response can be obtained via conventional linear response perturbation theory. Via projection on the corresponding solid harmonic $R_1^{-1}(\mathbf{r}')$

$$\langle R_1^{-1} | n_1^{-1} \rangle = |\Xi_{11}^{-1-1}|^2, \quad (3.6.2)$$

the state of the corresponding symmetry $\xi_1^{-1}(\mathbf{r})$ can be extracted as

$$\xi_1^{-1}(\mathbf{r}) = \frac{n_1^{-1}(\mathbf{r})}{\sqrt{\langle R_1^{-1} | n_1^{-1} \rangle}}. \quad (3.6.3)$$

In the next higher symmetry, $V_1^0 = 1$, eq. (??) takes the form

$$n_{V_1^0}^{\text{resp}}(\mathbf{r}) = \xi_1^{-1}(\mathbf{r}) \Xi_{11}^{-10} + \xi_1^0(\mathbf{r}) \Xi_{11}^{00}. \quad (3.6.4)$$

Since the states and projections of symmetry with lower (l, m) are already known, in this case $\xi_1^{-1}(\mathbf{r})$ and Ξ_{11}^{-10} , we can determine the response density that has the desired symmetry only, namely

$$n_1^0(\mathbf{r}) = n_{V_1^0}^{\text{resp}}(\mathbf{r}) - \xi_1^{-1}(\mathbf{r}) \Xi_{11}^{-10} = \xi_1^0(\mathbf{r}) \Xi_{11}^{00}, \quad (3.6.5)$$

which gives access to the state of the corresponding symmetry using eq. (3.6.3), i.e.

$$\xi_1^0(\mathbf{r}) = \frac{n_1^0(\mathbf{r})}{\sqrt{\langle R_1^0 | n_1^0 \rangle}}. \quad (3.6.6)$$

Using the properties in eq. (??), this procedure can be iterated to higher angular momentum channels. In the following we give a generalized closed form of the algorithm.

This direct moment expansion requires one perturbation calculation per symmetry. The moment expansion thus not only yields a very compact form of the non-local response function for inter-molecular interactions, it also provides a straightforward way for its iterative calculation.

DIRECT MOMENT EXPANSION ALGORITHM

We iterate over all desired multipole symmetries (l, m) in increasing order in l and m , i.e. starting from $l = 1, m = -1$. At the given symmetry (l, m) , we calculate the linear response density $n_{V_l^m}^{\text{resp}}$ at the corresponding

symmetry ($V_l^m = 1$) via direct perturbation theory calculation or finite difference derivation of the density. Formally, we write this in terms of the full response function

$$n_{V_l^m}^{\text{resp}}(\mathbf{r}) = \int \chi(\mathbf{r}, \mathbf{r}') R_l^m(\mathbf{r}') d^3r'. \quad (3.6.7)$$

From eqs. (??) and (??), we know that the response is given by

$$n_{V_l^m}^{\text{resp}}(\mathbf{r}) = \sum_{l'=1}^l \sum_{m'=-l'}^{m'_{\max}(l')} \xi_{l'}^{m'}(\mathbf{r}) \Xi_{l'l}^{m'm}, \quad (3.6.8)$$

where we have defined an upper summation index

$$m'_{\max}(l') = \begin{cases} m & \text{if } l' = l \\ l' & \text{if } l' < l \end{cases}. \quad (3.6.9)$$

At $l = 1, m = -1$, the sum contains just one term. At higher moments, we assume to know the $\xi_{l'}^{m'}(\mathbf{r})$ of all preceding multipole moments. Therefore, we also know $\Xi_{l'l}^{m'm}$ and can subtract the response due to already known states.

$$n_l^m(\mathbf{r}) = n_{V_l^m}^{\text{resp}}(\mathbf{r}) - \sum_{l'=1}^l \sum_{\substack{m'=-l' \\ m' \neq m'_{\max}(l')}}^{m'_{\max}(l')} \xi_{l'}^{m'}(\mathbf{r}) \Xi_{l'l}^{m'm} = \xi_l^m(\mathbf{r}) \Xi_{ll}^{mm}. \quad (3.6.10)$$

This symmetry decomposition of the response $n_l^m(\mathbf{r})$ can be projected on the perturbation $R_l^m(\mathbf{r})$

$$\langle R_l^m | n_l^m \rangle = |\Xi_{ll}^{mm}|^2, \quad (3.6.11)$$

which gives access to the desired response states $\xi_l^m(\mathbf{r})$ via

$$\xi_l^m(\mathbf{r}) = \frac{n_l^m(\mathbf{r})}{\sqrt{\langle R_l^m | n_l^m \rangle}}. \quad (3.6.12)$$

The algorithm can be iterated until all desired states $\xi_l^m(\mathbf{r})$ are calculated and requires only one perturbation calculation per state.

The algorithm has been implemented in the CPMD program package. The resulting states converge systematically towards the results of the moment expansion after an explicit diagonalization. The two relevant convergence parameters are the number of eigenstates in the diagonalization and the plane wave cutoff of the representation of the sawtooth position operator in a plane wave basis. Increasing both parameters leads to a systematic convergence of the results. In a water molecule with 150 Ry plane wave energy cutoff and 5000 converged eigenfunctions we have relative errors of the moment matrices $\Xi_{ll}^{mm'}$ of 0.004 at $l = 1$ and 0.005 at $l = 2$.

This direct moment expansion also has been implemented in the Dalton program package³⁰⁸ via finite difference derivatives. This use of an atom centered basis allows to represent the states in an atom centered basis, which can be useful for applications with changing molecular geometry.

3.7 DISCUSSION

In section 3.2, we have reported the first fully ab-initio calculation of dynamical vibrational circular dichroism (VCD) spectra using nuclear velocity perturbation theory (NVPT) derived electronic currents. The employed combination of the time correlation function (TCF) formalism with ab-initio molecular dynamics (AIMD) and perturbation theory derived electronic currents provides a rigorous protocol for the calculation of VCD spectra in the liquid phase. It is naturally capable of describing weak inter-molecular interactions, chirality transfer and conformational changes in solution at ambient conditions, thereby more closely modeling what experimentalist actually measure. Our results show an excellent agreement with the theoretical and experimental references and are able to naturally describe weak interactions like chirality transfer from a chiral molecule to an achiral solvent.

A considerable effort has been devoted to the solution and analysis of the choice of gauge in the liquid phase. The electronic expectation values are evaluated in a distributed origin gauge, employing maximally localized Wannier orbitals. A gauge invariant spectrum is obtained in terms of a scaled molecular gauge, which allows to systematically include solvent effects while keeping a significant signal-to-noise ratio. Our analysis and discussion of this choice of gauge in the liquid phase shows that the application of TCF VCD spectra requires a higher computational effort than the infrared absorbance counterpart. However, the scaled molecular moments provide a systematic tool to extract statistically significant spectra also from finite time and finite size AIMDs.

One direct follow-up question is the extension of the presented methodology to the ordered condensed phase. This has been addressed in section 3.3, where the modern theory of magnetization has been formulated in the NVPT framework. This theoretical development justifies the procedure of section 3.2 for the liquid phase. Its implementation and benchmarking for the ordered condensed phase are still ongoing.

A further aspect that has to be considered in the calculation of the NVPT of real molecular systems is the basis set dependence on the nuclear velocity. In case of our plane wave implementation, this is translated to the Galilean invariance of Hamiltonians with non-local potentials. In section 3.4, we have devised a correction that cures this problem and verified that its linearization resolves this issue for our applications. Further analysis and benchmarking are still ongoing.

In section 3.5, we have developed a rigorous theory to include the effect of electronic motion on nuclear dynamics in molecules within the adiabatic framework. Nuclear masses are dressed by position-dependent corrections that are purely electronic quantities and a consequence of the fact that electrons do not follow rigidly the motion of the nuclei. Various applications are discussed, yielding in all cases striking agreements with the benchmarks, either exact or highly accurate quantum-mechanical calculations.

Conceptually, we have resolved a well-known³⁰⁹ fundamental inconsistency of the Born-Oppenheimer (BO) approximation. In a translationally invariant problem, the center of mass moves as a free particle with mass that equals the total mass of the systems, i.e. nuclei and electrons, not only the nuclear mass. This feature is naturally built in the theory and corrects for a deficiency of the BO approximation, providing exactly the missing mass of the electrons. From a more practical point of view, our approach is very general and can be applied whenever a “factorization” of the underlying physical problem is possible, e.g. in the case of proton and oxygen atoms or in the case of electrons and nuclei.

Further applications are indeed envisaged, since the perturbative incorporation of non-adiabatic effects greatly reduces the complexity of the fully coupled problem. For instance, the approximations can be applied to nuclear wave packet methods for the calculation of highly accurate vibrational spectra beyond the BO approximation.

Finally, we have taken a further step in the calculation of the moment expanded representation of the electronic susceptibility in section 3.6. Bypassing the expensive iterative diagonalization, we have devised a simple way of a direct calculation of the moment expanded representation. In view of the explicit molecular geometry dependence, presented in section 2.5, this greatly simplifies the calculation and improves the efficiency of the methodology.

CONCLUSION

The context of this work is the research and development of theoretical methods for the modeling of complex molecular systems and their spectroscopic responses, focusing on the condensed phase at ambient conditions. Foremost, we have worked on an improved interpretation and theoretical evaluation of experimental vibrational circular dichroism (VCD) spectra. Moreover, we have aimed for an efficient, density-based modeling scheme for inter-molecular interactions in the condensed phase. Both aspects will be summarized and concluded in the following.

ELECTRONIC PROBABILITY CURRENTS FOR VIBRATIONAL CIRCULAR DICHROISM

The calculation of VCD spectra of complex chemical systems in the condensed phase is a challenging task for which at present no satisfying first-principles theory has been reported. In this work, we have addressed this shortcoming by devising new theoretical and computational concepts for VCD spectra in the time correlation function (TCF) formalism.^{41,42} This dynamical approach had been successfully applied to infrared absorption (IRA) of bulk solutions and solvated molecules, based on ab-initio molecular dynamics (AIMD)⁴³⁻⁴⁷ or even more sophisticated methods.⁴⁸ However, even about 20 years after the milestone work of Silvestrelli,⁴³ a fully AIMD-based TCF VCD spectrum had never been reported. First attempts using partial charges or density-based reconstructed currents show the interest in this direction.⁴⁹⁻⁵²

This discrepancy between the IRA and VCD stems from the fact that for the calculation of VCD spectra, non-adiabatic electronic wave functions are required.^{32,33,54} The magnetic field perturbation theory³⁴ and the nuclear velocity perturbation theory³³ (NVPT) have provided perturbative formulations for the required electronic currents. The missing link to adopt the dynamic TCF approach for VCD is an efficient scheme to compute the electronic currents along a molecular dynamics. This has been accomplished in this work, in which we have developed the necessary theoretical and computational means for this task by deriving, implementing and benchmarking the NVPT in condensed phase systems.

At the beginning of this work stood the conceptual choice of how to approach this theoretical challenge. In view of the desired combination of AIMD in the condensed phase and linear response perturbation calculations, we have opted for a plane wave electronic structure program, the CPMD program package.² The use of plane waves has several advantages. It is particularly well suited for AIMD simulations in the condensed phase and at the same time facilitates the linear response calculation via the Sternheimer method, requiring ground state electronic structure information only and providing a large enough freedom for diffuse electronic responses. Based on this premise, we have decided to use the NVPT instead of the magnetic field perturbation theory due to its suitability for plane wave AIMD implementations. As discussed in section 1.4.4, this advantage is threefold. First, it results from the fact that the perturbation Hamiltonian is well defined also under periodic boundary conditions since no absolute position operator is involved. Second, the perturbation Hamiltonian can be projected along the dynamics, which greatly improves the computational efficiency for sampling along an AIMD. And third, the plane wave basis is independent of the nuclear positions, which reduces the computational complexity of the calculations since no additional Pulay-terms have to be considered.

The latter advantage is somewhat reduced if non-local potentials are employed, which typically is the case

in plane wave codes. The presence of atom centered projectors of the non-local pseudopotentials destroys the Galilean invariance of the solution to the Schrödinger equation. This is one of the prerequisites that we had to establish for a successful implementation. We have shown in section 3.4 that the Galilean invariance of the problem in presence of non-local potentials can be recovered by a suitable transformation of the non-local potentials. This correction is closely related to the widely used corrections for non-local potentials in presence of electro-magnetic vector potentials.^{119,122} Furthermore, we could show that for all relevant nuclear velocities, a linearized correction is sufficient to obtain Galilean gauge invariant results, and that the final current dipole and magnetic dipole operator expectation values are independent of this correction.

Having chosen the theoretical and the implementational framework, we have turned our attention to the foundations of the perturbative correction. The nuclear velocity perturbation theory (NVPT) has been proposed originally by Nafie.³³ His complete adiabatic correction yields the required non-adiabatic content for the calculation of electronic currents. However, while giving evidence for a deep physical intuition, the reported derivations of the NVPT still required a rigorous revision. One of the main results of this work is this rigorous derivation of the NVPT, which allows to study its physical properties and the limits of its applicability. To that extent, we have started from the exact factorization of the electron-nuclear wave function and derived the NVPT as a perturbative correction to the Born-Oppenheimer⁵³ approximation. The analysis in sections 2.2 and 3.5 have established that the NVPT actually is the lowest order correction to the Born-Oppenheimer approximation in the time-dependent case.³⁰¹ As long as the non-adiabatic couplings are small, i.e. the system is far away from avoided crossings, the electronic response due to the nuclear momenta can be accurately described by the NVPT.

This rigorous derivation has also provided further insights. We have shown that the perturbation parameter, which corresponds to the nuclear velocity in the semi-classical limit for the nuclei, can also be interpreted in a quantum mechanical way. The correction to the wave function can also be obtained from the non-adiabatic coupling vectors, which are accessible at various levels of theory in modern quantum chemistry codes.^{114, 310, 311} This sheds a new light on the NVPT as a more general yet efficient framework to obtain electronic probability density currents of complex chemical systems. Possible applications are e.g. the visualization of electronic currents during chemical reactions or the determination of electronic reordering processes. Again, the use of non-local pseudopotentials introduces artifacts in the form of additional sources and sinks of the electronic probability density currents. However, these are in principle only technical and no conceptual complications, which motivates further work in this direction.

Moreover, the derivation of the NVPT has revealed the existence of an additional term in the electronic expectation values of the current and magnetic dipole moment operators. This additional contribution is due to the vector potential occurring in the exact factorization formulation, which mediates the electron-nuclear coupling as a kinetic effect. We have been able to show that this correction to the NVPT VCD spectrum is very small for the systems that we have analyzed. However, we expect the correction to be relevant in case of amplified or enhanced VCD.^{262–266} Furthermore, we have been able to derive an expression for the calculation of the vector potential that is independent of the perturbation parameter, the vector potential matrix, short \mathcal{A} -matrix. This \mathcal{A} -matrix has been identified to account for the inertia of the electrons if the nuclei are moving and its sum rule is shown to yield the total electronic mass of the system. As a position dependent mass-renormalization, it cures the inconsistency of the Born-Oppenheimer approximation

in which only the bare nuclear masses are moving. With help of these results of section 3.5, we now can give an intuitive answer to the fundamental question as to which masses vibrate in a molecule. First applications to proton transfer and non-adiabatic vibrational frequency shifts of polyatomic molecules illustrate its far-reaching implications.

Based on this rigorous derivation, we have implemented the NVPT in the plane wave electronic structure program package CPMD. This is the first reported successful implementation of the NVPT and it is publicly accessible for scientific use. The implementation in the plane wave code uses density functional perturbation theory for the calculation of the electronic structure perturbation, as discussed in section 2.3. The use of plane waves facilitates the linear response calculation via the Sternheimer method and at the same time is particularly well suited for AIMD simulations in the condensed phase. However, at its present stage, it comes at the price of the use of non-local pseudopotentials and the limitation to the generalized gradient approximation as the electronic structure level of theory. We wish to point out that both limitations are merely technical compromises in order to achieve sufficiently long AIMD but pose no fundamental limitations to the developed theoretical framework, which is of a more general nature.

Two technical aspects of the plane wave implementation are worth mentioning. First, the magnetic dipole moment operator depends on the absolute position of the origin and is hence ill-defined under periodic boundary conditions. We have addressed this problem by adopting a previously realized combination of maximally localized Wannier orbitals in a state-wise distributed origin.¹⁴ This approach is applicable to insulating systems and can be efficiently realized in the disordered condensed phase, which commonly are treated in the Γ -point approximation. Second, the evaluation of the velocity operator in the current and magnetic dipole operators is complicated in presence of non-local pseudopotentials. The velocity operator is defined as the commutator of the position operator with the Hamiltonian. For Hamiltonians with local potentials, this commutator is proportional to the momentum operator. However, the non-local potentials do not commute with the position operator and yield an additional contribution to the momentum. Its evaluation requires the explicit calculation of the commutator of the position operator with the non-local potential.¹²⁰

After the successful realization, we have validated the results of our NVPT implementation. A first validation is given by the consistency of the sum rule relations between electronic dipole, electronic current dipole and magnetic dipole moments. In a second step, we have compared our results with the established magnetic field perturbation theory. The latter is implemented only in programs employing atom centered basis sets, which complicates the comparison. However, the benchmark for molecules in the gas phase, both in the double harmonic approximation, showed that both theories are in excellent agreement. This was an important intermediate result, since we were able to reproduce the state of the art of VCD spectra of isolated molecules in the double harmonic approximation and could now turn our attention to the envisaged generalizations of the theory.

For our intended application of dynamical VCD spectra in the condensed phase, we had to go beyond the static picture. We have implemented a projected version of the NVPT, which projects the perturbation Hamiltonian vector onto the nuclear velocity already before the perturbation calculation. This allows a very efficient evaluation of the electronic probability density along a molecular dynamics simulation in the condensed phase. From these, the cross-correlation between the current dipole and the magnetic dipole

moment evolution can be obtained. For dynamic VCD spectra in the TCF formalism, we have sampled several picoseconds of AIMD, both in the gas and in the condensed phase. Prior to this work, the evaluation of electronic current observables along molecular dynamics simulation in the condensed phase would not have been feasible at this time-scale. For the gas phase AIMD, we were able to extract effective normal modes as an intermediate step between fully dynamical TCF spectra and the double harmonic approximation: we found the resulting spectra to be in excellent agreement.

At this stage, having access to current related observables in the condensed phase, we faced the conceptual problem of the choice of gauge for the magnetic dipole moments. Given the magnetic dipole moments in a distributed Wannier origin gauge, we had to choose a consistent gauge of the magnetic dipoles in order to obtain gauge invariant observables. We have provided an extensive analysis of the gauge problem of VCD in the disordered condensed phase. For the ordered condensed phase, an adaptation of the modern theory of magnetization has been devised, as presented in section 3.3. This derivation suggests that, in the liquid phase, the additional contributions due to itinerant currents should be negligible. For calculations of VCD spectra in the liquid phase, we have adopted an isotropic spatial decomposition scheme for analysis purpose. The results indicate that the TCF VCD spectra of chiral molecules in a polar solvent, in our case water, are very sensitive to insufficient sampling. The chirality fluctuations of the water, which only on average is achiral, introduce a noisy background of the actual VCD signal. This background originates from long-range inter-molecular correlations and is amplified by an additional scaling with the distance due to the gauge-transport. The rigorous solution of this problem is simply more sampling, which motivates further developments in this direction to decrease the computational costs, enabling longer simulation times. At present, we adopt the concept of scaled molecular moments and assume that the correlation functions of distant molecules decays sufficiently fast. Using this methodology, we have been able to calculate the first rigorously ab-initio VCD spectra in the condensed phase, including spectral features originating from chirality transfer.

The theory of VCD developed in this work is very general in the sense that the established approaches to VCD calculations can be obtained as the corresponding limits of this theory. It therefore provides enough methodological flexibility to adapt the level of theory to the corresponding system of interest, be it the use of classical molecular dynamics, the parametrization of molecular property surfaces or the effective normal mode analysis. Moreover, it establishes a natural starting point for further lines of research. These perspectives benefit from the favorable scaling of the implementation that allows for efficient probability current calculations along molecular dynamics of condensed phase systems at unprecedented time- and length scales.

One direction is the dynamical aspect of the theory of VCD. In analogy to the development of theoretical IRA spectroscopy,⁴⁸ one interesting question could be the study of nuclear quantum effects on the VCD spectrum. In the opposite direction, a coarser description of the environment in a hybrid QM/MM approach could give access to dynamical effects on the VCD spectra of larger molecular assemblies like e.g. biomolecules in solution. We have already taken first steps to explore the application of our methodology to dynamical VCD spectra of flexible molecules in solution. Further work in this direction will have to prove the reliability and robustness of the approach.

A second perspective for further developments is the possibility to access condensed phase VCD spectra of large scale systems. In this work, we have focused on isotropic systems in the disordered condensed phase, where the gauge problem could be addressed by making use of the disorder of the system. However, the

application of the theory and implementation to molecules in the ordered condensed phase requires further reasoning. In ordered systems with extended molecules, the long range correlations and possible itinerant currents have to be taken into account. Our proposed adaptation of the modern theory of magnetization for the framework of the NVPT provides the necessary starting point for this undertaking. Potential applications are e.g. parts of crystal structures of proteins or a strand of deoxyribonucleic acid (DNA).

In view of the linear response aspect of the developed theory, a further development could be the already mentioned analysis of the enhanced or amplified VCD of metal complexes. In these systems, the small energy gap between occupied and unoccupied states gives rise to enhanced responses. The discovered kinetic contribution to the NVPT VCD intensities might be important here. Moreover, the developed theory and implementation of NVPT VCD could be extended to vibrational Raman optical activity.¹⁷ The required additional quantity is the cross-polarizability, which can be obtained via the Sternheimer formalism in a similar manner to the NVPT theory. Also here, the implementational framework should give access to length- and time scales sufficient for AIMD-based dynamical spectra.

The interpretation of the vector potential matrix as a position dependent mass renormalization provides the basis for further applications of this theory. Since the vector potential matrix can be also obtained from non-adiabatic coupling vectors, this application is not limited to the Sternheimer formalism implementation. Beyond the first applications to non-adiabatic effects in hydrogen bonding and vibrational spectra of poly-atomic molecules, this theory could e.g. be used in explicit nuclear wave-packet dynamics.

Finally, the NVPT in principle gives access to the electronic probability current density. Despite the mentioned technical obstacles still to overcome, the NVPT provides a very efficient way for its calculation. Contrary to explicit electron dynamics, the NVPT can be used at isolated single points in time and nevertheless takes into account the dynamics of the electrons in a self-consistent manner. After a benchmark and comparison of the electronic probability current density from the NVPT and various other levels of theories, applications could be the visualization of electronic currents during chemical reactions or the determination of electronic reordering processes. Furthermore, the NVPT current density could be analyzed for its eddy-current contribution and compared with density derived currents.

THE ELECTRONIC SUSCEPTIBILITY FOR INTER-MOLECULAR INTERACTIONS

A different application of the linear response methodology has been the focus of the second line of research of this work. We have aimed for an efficient, density-based modeling scheme for inter-molecular interactions, employing response densities via an explicit representation of the electronic susceptibility response function.

The underlying conceptual idea is based on the observation that the electronic susceptibility yields the interacting electronic density response for perturbing potentials *independent* of the perturbation. This has to be compared to orbital-based response calculations, which require self-consistent solutions of the response equations for each novel perturbation potential. Since the perturbation Hamiltonian depends itself on the response of the electronic density, this self-consistent solution is comparatively much more costly. Once determined, the electronic susceptibility can instead be applied straightforwardly to changing perturbation potentials.

Our intended application of this method is the density-based modeling of inter-molecular interactions in a fragmentation approach. The overall system is fragmented into its molecular constituents and their in-

teractions are treated perturbatively. This methodology is known to yield reasonable interaction potentials in the linear response regime¹⁰ if orbital-based perturbation theory is employed. For a purely density-based evaluation, the expected accuracy is lower, however, a rigorous treatment of polarization effects might contribute to the development of transferable polarizable models with accuracies similar to polarizable force-fields. Instead of being parameterized for a particular application, the response density-based models should show a more robust transferability.

At the beginning of this research stood the idea to use the explicit spatial dependence of the electronic susceptibility in order to model short range inter-molecular interactions. This explicit spatial dependence has been obtained by means of an iterative spectral decomposition of the interacting static electronic susceptibility via a Lanczos diagonalization. In the spectral decomposition, the response function is represented as an outer product of the eigenfunctions, weighted with the eigenvalues. The application of the response function amounts to taking the inner products of the eigenfunctions with the perturbing potential, which has a much lower computational complexity compared with the original response calculation itself. First benchmarks of this spectral decomposition suggested that the electronic response density of small molecules can be accurately obtained employing a basis of few thousand eigenfunctions.

A few thousand eigenfunctions still pose considerable requirements for storage, computation and representation of their further properties. The Lanczos diagonalization yields the eigenfunctions in the plane wave representation, i.e. on a grid in real space. Since the molecular geometry changes during a molecular dynamics, also the eigenfunctions change. Therefore, for practical applications, the eigenfunction should be parameterized in terms of the nuclear positions, e.g. via an expansion in an atom centered basis set. This change of representation for several thousand eigenfunctions turned out to be a very demanding and inefficient task. This observation suggested further reasoning for an efficient representation and storage. In view of these considerations, we had to improve on the spectral decomposition representation to come up with a more practicable scheme.

The full spectral decomposition representation of the spatial dependence of the full response function has the advantage that both, inter- as well as intra-molecular perturbation potentials can be treated on the same footing. However, for the purpose of a fragmentation-based molecular dynamics simulations, we are mainly interested in the responses to inter-molecular perturbation potentials. Therefore, it is desirable to be able to partition the response function into a small part that describes inter-molecular interactions accurately and a large remainder, which accounts for the response to more complicated perturbation potentials. A priori, it is not clear whether such a partition exists at all, whether it is well-defined and what properties it has.

One central result of this work is the derivation of such a partition of the response function, termed “moment expansion” by us. As presented in section 2.4, it allows a very condensed representation of the relevant part of the response function for inter-molecular interactions. Starting from the observation that the relevance of a particular eigenfunction is not only determined by its eigenvalue but also by its overlap with the perturbation potential, the moment expansion yields transformed functions, the moment expanded states, which couple to the lowest orders of the series expansion of the perturbing potential. The resulting moment expanded states are well defined by their symmetry properties and can be labeled according to the symmetry of their multipole moments, which motivated the name. In terms of efficiency, the moment ex-

pansion reduces the number of required functions by about two to three orders of magnitude as compared to the spectral decomposition representation. This explicit representation greatly simplifies the calculation and improves the efficiency of the methodology.

After having devised the algorithm for the transformation, we analyzed and benchmarked its analytical and numerical properties. Important observations are the well-definition of transformation and representation, which is a priori non-trivial due to the origin dependence of the multipole moments and the truncation of the in principle infinite dimensional spectral decomposition representation. Furthermore, it is worthwhile to emphasize that the moment expanded representation yields an exact partition of the full response function, i.e. the coupling to the external potentials is partitioned exactly and the low dimensional part for inter-molecular interactions yields exact results.

This exact partition allowed a further step in the calculation of the moment expanded representation. As discussed in section 3.6, the expensive iterative diagonalization can be bypassed by making use of this exact partitioning. We have devised a simple iterative way of a direct calculation of the moment expanded representation with increasing orders of multipole symmetries. This direct moment expansion has been implemented in CPMD program package and greatly simplified the subsequent developments.

A particular appealing property of the moment expanded states are their symmetry properties, which directly connect their shape to well-defined physical observables. This connection provides elegant analytical rotation properties and, as important, assures that the moment expanded states are continuous functions of their parametric dependences as the molecular geometry or external electrostatic potentials.

This last observation motivates the use of a Taylor expansion of the response function in terms of the desired parametric dependences. For molecular dynamics, we are interested in the explicit molecular geometry dependence, which has been expressed in terms of Taylor expansions as presented in section 2.5. Corrections of the response function due to external field and external field gradients, as encountered in the near-field regime of inter-molecular interactions, are currently being examined.

In a next step, the moment expanded states had to be represented in an atom centered basis. For this change of representation, we had to solve a coupled non-linear optimization problem of the basis set exponents and basis set function prefactors. This change of representation is currently still ongoing and has not been included in this thesis.

The presented developments in this project have provided two important steps towards the use of the electronic susceptibility for inter-molecular interactions. Further work will have to integrate the response density calculations in a fragmented, density-based molecular dynamics framework. At this stage it is difficult to predict the accuracy of the resulting methodology. As already pointed out, it is clear that density-based methods cannot compete with orbital-based schemes. However, due to its first-principles character, the devised methodology might yield a transferable treatment of polarization effects. Moreover, it might provide a transferable post-processing scheme for classical molecular dynamics that allows to determine the molecular multipole moments on a polarizable force-field level of theory. Finally, the devised results might find use in different applications of the electronic susceptibility. One possible application is the use of the moment expanded states as a basis set for molecular random phase approximation or van der Waals calculations.

BIBLIOGRAPHY

- [1] R. Car and M. Parrinello. Unified approach for molecular dynamics and density-functional theory. *Phys. Rev. Lett.*, 55:2471–2474, Nov 1985.
- [2] D. Marx and J. Hutter. *Ab Initio Molecular Dynamics: Basic Theory and Advanced Methods*. Cambridge University Press, 1 edition, 5 2009.
- [3] P. Hohenberg and W. Kohn. Inhomogeneous electron gas. *Phys. Rev.*, 136:B864–B871, Nov 1964.
- [4] W. Kohn and L. J. Sham. Self-consistent equations including exchange and correlation effects. *Phys. Rev.*, 140:A1133–A1138, 1965.
- [5] S. Baroni, P. Giannozzi, and A. Testa. Green’s-function approach to linear response in solids. *Phys. Rev. Lett.*, 58:1861–1864, May 1987.
- [6] X. Gonze. Perturbation expansion of variational principles at arbitrary order. *Phys. Rev. A*, 52:1086–1095, Aug 1995.
- [7] X. Gonze. Adiabatic density-functional perturbation theory. *Phys. Rev. A*, 52:1096–1114, Aug 1995.
- [8] S. Baroni, S. de Gironcoli, A. Dal Corso, and P. Giannozzi. Phonons and related crystal properties from density-functional perturbation theory. *Rev. Mod. Phys.*, 73:515–562, Jul 2001.
- [9] A. Putrino, D. Sebastiani, and M. Parrinello. Generalized variational density functional perturbation theory. *J. Chem. Phys.*, 113(17), 2000.
- [10] D. M. Benoit, D. Sebastiani, and M. Parrinello. Accurate total energies without self-consistency. *Phys. Rev. Lett.*, 87:226401, Nov 2001.
- [11] G. Tabacchi, C. J. Mundy, J. Hutter, and M. Parrinello. Classical polarizable force fields parametrized from ab initio calculations. *J. Chem. Phys.*, 117(4), 2002.
- [12] G. Tabacchi, J. Hutter, and C. J. Mundy. A density-functional approach to polarizable models: A Kim-Gordon response density interaction potential for molecular simulations. *J. Chem. Phys.*, 123(7), 2005.
- [13] A. Putrino and M. Parrinello. Anharmonic Raman spectra in high-pressure ice from *Ab Initio* simulations. *Phys. Rev. Lett.*, 88:176401, Apr 2002.
- [14] D. Sebastiani and M. Parrinello. A new ab-initio approach for NMR chemical shifts in periodic systems. *J. Phys. Chem. A*, 105(10):1951–1958, 2001.
- [15] L. A. Nafie. Infrared and Raman vibrational optical activity: Theoretical and experimental aspects. *Annu. Rev. Phys. Chem.*, 48(1):357–386, 1997.
- [16] G. Magyarfalvi, G. Tarczay, and E. Vass. Vibrational circular dichroism. *WIREs Comput. Mol. Sci.*, 1(3):403–425, 2011.

- [17] L. A. Nafie. *Vibrational Optical Activity. Principles and Applications*. John Wiley & Sons Ltd., 1st edition, 2011.
- [18] T. Wu, X.-Z. You, and P. Bouř. Applications of chiroptical spectroscopy to coordination compounds. *Coord. Chem. Rev.*, 284:1 – 18, 2015.
- [19] L. G. Felipe, J. M. Batista Jr., D. C. Baldoqui, I. R. Nascimento, M. J. Kato, Y. He, L. A. Nafie, and M. Furlan. VCD to determine absolute configuration of natural product molecules: secolignans from *Peperomia blanda*. *Org. Biomol. Chem.*, 10:4208–4214, 2012.
- [20] E. De Gussem, P. Bultinck, M. Feledziak, J. Marchand-Brynaert, C. V. Stevens, and W. Herrebout. Vibrational circular dichroism versus optical rotation dispersion and electronic circular dichroism for diastereomers: the stereochemistry of 3-(1'-hydroxyethyl)-1-(3'-phenylpropanoyl)-azetidin-2-one. *Phys. Chem. Chem. Phys.*, 14:8562–8571, 2012.
- [21] S. Qiu, E. De Gussem, K. A. Tehrani, S. Sergeyev, P. Bultinck, and W. Herrebout. Stereochemistry of the tadalafil diastereoisomers: A critical assessment of vibrational circular dichroism, electronic circular dichroism, and optical rotatory dispersion. *J. Med. Chem.*, 56(21):8903–8914, 2013.
- [22] T. Burgi, A. Vargas, and A. Baiker. VCD spectroscopy of chiral cinchona modifiers used in heterogeneous enantioselective hydrogenation: conformation and binding of non-chiral acids. *J. Chem. Soc., Perkin Trans. 2*, pages 1596–1601, 2002.
- [23] M. Losada and Y. Xu. Chirality transfer through hydrogen-bonding: Experimental and ab initio analyses of vibrational circular dichroism spectra of methyl lactate in water. *Phys. Chem. Chem. Phys.*, 9:3127–3135, 2007.
- [24] M. Losada, P. Nguyen, and Y. Xu. Solvation of propylene oxide in water: Vibrational circular dichroism, optical rotation, and computer simulation studies. *J. Phys. Chem. A*, 112(25):5621–5627, 2008.
- [25] E. Debie, L. Jaspers, P. Bultinck, W. Herrebout, and B. Van Der Veken. Induced solvent chirality: A VCD study of camphor in CDCl₃. *Chem. Phys. Lett.*, 450(4–6):426 – 430, 2008.
- [26] V. P. Nicu, E. Debie, W. Herrebout, B. Van der Veken, P. Bultinck, and E. J. Baerends. A VCD robust mode analysis of induced chirality: The case of pulegone in chloroform. *Chirality*, 21(1E):E287–E297, 2009.
- [27] C. Merten and Y. Xu. Chirality transfer in a methyl lactate–ammonia complex observed by matrix-isolation vibrational circular dichroism spectroscopy. *Angew. Chem. Int. Ed.*, 52(7):2073–2076, 2013.
- [28] S. Murarka, Z.-J. Jia, C. Merten, C.-G. Daniliuc, A. P. Antonchick, and H. Waldmann. Rhodium(ii)-catalyzed enantioselective synthesis of troponoids. *Angew. Chem. Int. Ed.*, 54(26):7653–7656, 2015.
- [29] C. Merten, C. H. Pollok, S. Liao, and B. List. Stereochemical communication within a chiral ion pair catalyst. *Angew. Chem. Int. Ed.*, 54(30):8841–8845, 2015.

- [30] T. R. Faulkner, C. Marcott, A. Moscovitz, and J. Overend. Anharmonic effects in vibrational circular dichroism. *J. Am. Chem. Soc.*, 99(25):8160–8168, 1977.
- [31] T. A. Keiderling and P. J. Stephens. Vibrational circular dichroism of dimethyl tartrate. A coupled oscillator. *J. Am. Chem. Soc.*, 99(24):8061–8062, 1977.
- [32] L. A. Nafie and T. B. Freedman. Vibronic coupling theory of infrared vibrational transitions. *J. Chem. Phys.*, 78(12), 1983.
- [33] L. A. Nafie. Adiabatic molecular properties beyond the Born-Oppenheimer approximation. Complete adiabatic wave functions and vibrationally induced electronic current density. *J. Chem. Phys.*, 79(10):4950–4957, 1983.
- [34] P. J. Stephens. Theory of vibrational circular dichroism. *J. Phys. Chem.*, 89(5):748–752, 1985.
- [35] A. D. Buckingham, P. W. Fowler, and P. A. Galwas. Velocity-dependent property surfaces and the theory of vibrational circular dichroism. *Chem. Phys.*, 112(1):1–14, 1987.
- [36] P. J. Stephens, K. J. Jalkanen, R. D. Amos, P. Lazzeretti, and R. Zanasi. Ab initio calculations of atomic polar and axial tensors for hydrogen fluoride, water, ammonia, and methane. *J. Phys. Chem.*, 94(5):1811–1830, 1990.
- [37] L. A. Nafie. Electron transition current density in molecules. I. non-Born-Oppenheimer theory of vibronic and vibrational transitions. *J. Phys. Chem. A*, 101:7826, 1997.
- [38] T. B. Freedman, M.-L. Shih, E. Lee, and L. A. Nafie. Electron transition current density in molecules. 3. Ab initio calculations for vibrational transitions in Ethylene and Formaldehyde. *J. Am. Chem. Soc.*, 119:10620, 1997.
- [39] J. Bloino and V. Barone. A second-order perturbation theory route to vibrational averages and transition properties of molecules: General formulation and application to infrared and vibrational circular dichroism spectroscopies. *J. Chem. Phys.*, 136(12):124108, 2012.
- [40] C. Cappelli, J. Bloino, F. Lipparini, and V. Barone. Toward ab initio anharmonic vibrational circular dichroism spectra in the condensed phase. *J. Phys. Chem. Lett.*, 3(13):1766–1773, 2012.
- [41] R. G. Gordon. volume 3, chapter Correlation Functions for Molecular Motion. Elsevier, Jan 1968.
- [42] D. A. McQuarrie. *Statistical Mechanics*. University Science Books, 1976.
- [43] P. L. Silvestrelli, M. Bernasconi, and M. Parrinello. Ab initio infrared spectrum of liquid water. *Chem. Phys. Lett.*, 277(5–6):478 – 482, 1997.
- [44] M.-P. Gaigeot and M. Sprik. Ab initio molecular dynamics study of uracil in aqueous solution. *J. Phys. Chem. B*, 108(22):7458–7467, 2004.

- [45] M.-P. Gaigeot, R. Vuilleumier, M. Sprik, and D. Borgis. Infrared spectroscopy of n-methylacetamide revisited by ab initio molecular dynamics simulations. *J. Chem. Theory Comput.*, 1(5):772–789, 2005.
- [46] M.-P. Gaigeot, M. Martinez, and R. Vuilleumier. Infrared spectroscopy in the gas and liquid phase from first principle molecular dynamics simulations: application to small peptides. *Mol. Phys.*, 105:2857–2878, Oct 2007.
- [47] M. Heyden, J. Sun, S. Funkner, G. Mathias, H. Forbert, M. Havenith, and D. Marx. Dissecting the THz spectrum of liquid water from first principles via correlations in time and space. *Proc Natl Acad Sci USA*, 107(27):12068–12073, 2010.
- [48] R. Ramírez, T. López-Ciudad, P. Kumar P, and D. Marx. Quantum corrections to classical time-correlation functions: Hydrogen bonding and anharmonic floppy modes. *J. Chem. Phys.*, 121(9), 2004.
- [49] J. Horníček, P. Kaprálová, and P. Bouř. Simulations of vibrational spectra from classical trajectories: Calibration with ab initio force fields. *J. Chem. Phys.*, 127(8):084502, 2007.
- [50] H. Rhee, J.-H. Ha, S.-J. Jeon, and M. Cho. Femtosecond spectral interferometry of optical activity: Theory. *J. Chem. Phys.*, 129(9):094507, 2008.
- [51] H. Rhee, J.-H. Choi, and M. Cho. Infrared optical activity: Electric field approaches in time domain. *Acc. Chem. Res.*, 43(12):1527–1536, 2010.
- [52] M. Thomas and B. Kirchner. Classical magnetic dipole moments for the simulation of vibrational circular dichroism by ab initio molecular dynamics. *J. Phys. Chem. Lett.*, 7(3):509–513, 2016.
- [53] M. Born and R. Oppenheimer. Zur Quantentheorie der Molekeln. *Ann. Phys. (Berlin)*, 389(20):457–484, 1927.
- [54] A. Scherrer, F. Agostini, D. Sebastiani, E. K. U. Gross, and R. Vuilleumier. Nuclear velocity perturbation theory for vibrational circular dichroism: An approach based on the exact factorization of the electron-nuclear wave function. *J. Chem. Phys.*, 143(7):074106, 2015.
- [55] D. Cavagnat, L. Lespade, and T. Buffeteau. Vibrational absorption and circular dichroism studies of trans-(3S,4S)-d6-cyclopentene in the gas phase. *J. Phys. Chem. A*, 111(30):7014–7021, 2007.
- [56] H. Sato, Y. Mori, and A. Yamagishi. Conformational change of a chiral Schiff base Ni(ii) complex with a binaphthyl moiety: application of vibrational circular dichroism spectroscopy. *Dalton Trans.*, 42:6873–6878, 2013.
- [57] R. Resta. Quantum-mechanical position operator in extended systems. *Phys. Rev. Lett.*, 80:1800–1803, Mar 1998.
- [58] A. D. Buckingham. Permanent and induced molecular moments and long-range intermolecular forces. *Adv. Chem. Phys.*, 12:107–142, 1967.

- [59] A. J. Stone. Distributed multipole analysis, or how to describe a molecular charge distribution. *Chem. Phys. Lett.*, 83(2):233–239, 1981.
- [60] G. Náray-Szabó and G. G. Ferenczy. Molecular electrostatics. *Chem. Rev.*, 95(4):829–847, Jan 1995.
- [61] J. G. Angyán, C. Chipot, F. Dehez, C. Hättig, G. Jansen, and C. Millot. OPEP: a tool for the optimal partitioning of electric properties. *J. Comput. Chem.*, 24(8):997, Jun 2003.
- [62] T. Elking, D. Darden and R. J. Woods. Gaussian induced dipole polarization model. *J. Comput. Chem.*, 28(7):1261–1274, May 2007.
- [63] R. J. Wheatley. Gaussian multipole functions for describing molecular charge distributions. *Mol. Phys.*, 79(3):597–610, Jan 1993.
- [64] G. G. Hall and C. M. Smith. Fitting electron densities of molecules. *Int. J. Quant. Chem.*, 25(5):881–890, Jan 1984.
- [65] K. Eichkorn, O. Treutler, H. Öhm, M. Häser, and R. Ahlrichs. Auxiliary basis sets to approximate coulomb potentials. *Chem. Phys. Lett.*, 240:283–290, Jun 1995.
- [66] G. A. Cisneros, J.-P. Piquemal, and T. A. Darden. Intermolecular electrostatic energies using density fitting. *J. Chem. Phys.*, 123(4):044109, 2005.
- [67] B. Jeziorski, R. Moszynski, and K. Szalewicz. Perturbation theory approach to intermolecular potential energy surfaces of van der Waals complexes. *Chem. Rev.*, 94(7):1887–1930, 1994.
- [68] A. Heßelmann and G. Jansen. Intermolecular dispersion energies from time-dependent density functional theory. *Chem. Phys. Lett.*, 367(5–6):778–784, 2003.
- [69] A. J. Misquitta, B. Jeziorski, and K. Szalewicz. Dispersion energy from density-functional theory description of monomers. *Phys. Rev. Lett.*, 91:033201, Jul 2003.
- [70] R. G. Gordon and Y. S. Kim. Theory for the forces between closed-shell atoms and molecules. *J. Chem. Phys.*, 56(6), 1972.
- [71] Y. S. Kim and R. G. Gordon. Study of the electron gas approximation. *J. Chem. Phys.*, 60(5), 1974.
- [72] A. J. Stone and M. Alderton. Distributed multipole analysis. *Mol. Phys.*, 56(5):1047–1064, 1985.
- [73] J. D. Jackson. *Classical Electrodynamics*. Wiley, 3 edition, 8 1998.
- [74] A. J. Misquitta, A. J. Stone, and F. Fazeli. Distributed multipoles from a robust basis-space implementation of the iterated stockholder atoms procedure. *J. Chem. Theory Comput.*, 10(12):5405–5418, 2014.
- [75] A. J. Stone. Distributed polarizabilities. *Mol. Phys.*, 56(5):1065–1082, 1985.

- [76] C. R. Le Sueur and A. J. Stone. Practical schemes for distributed polarizabilities. *Mol. Phys.*, 78(5):1267–1291, 1993.
- [77] C. R. Le Sueur and A. J. Stone. Localization methods for distributed polarizabilities. *Mol. Phys.*, 83(2):293–307, 1994.
- [78] A. J. Misquitta and A. J. Stone. Distributed polarizabilities obtained using a constrained density-fitting algorithm. *J. Chem. Phys.*, 124(2):024111, 2006.
- [79] A. Stone. *The Theory of Intermolecular Forces*. Oxford University Press, 2nd edition, 4 2013.
- [80] R. Chelli, R. Righini, S. Califano, and P. Procacci. Towards a polarizable force field for molecular liquids. *J. Mol. Liq.*, 96-97:87, Jan 2002.
- [81] P. Paricaud, M. Predota, A. A. Chialvo, and P. T. Cummings. From dimer to condensed phases at extreme conditions: accurate predictions of the properties of water by a Gaussian charge polarizable model. *J. Chem. Phys.*, 122(24):244511, Jun 2005.
- [82] D. Martin and G. G. Hall. FSGO point charge models – their accuracy and extension to higher gaussians. *Theor. Chem. Acc.*, 59(3):281–290, Jan 1981.
- [83] R. J. Wheatley and J. B. O. Mitchell. Gaussian multipoles in practice: Electrostatic energies for intermolecular potentials. *J. Comput. Chem.*, 15(11):1187–1198, Jan 1994.
- [84] J.-P. Piquemal, N. Gresh, and C. Giessner-Prettre. Improved formulas for the calculation of the electrostatic contribution to the intermolecular interaction energy from multipolar expansion of the electronic distribution. *J. Phys. Chem. A*, 107(48):10353–10359, 2003.
- [85] J.-P. Piquemal, G. A. Cisneros, P. Reinhardt, N. Gresh, and T. A. Darden. Towards a force field based on density fitting. *J. Chem. Phys.*, 124(10):104101, 2006.
- [86] G. A. Cisneros, J.-P. Piquemal, and T. A. Darden. Generalization of the gaussian electrostatic model: Extension to arbitrary angular momentum, distributed multipoles, and speedup with reciprocal space methods. *J. Chem. Phys.*, 125(18):184101, 2006.
- [87] J.-P. Piquemal, R. Chelli, P. Procacci, and N. Gresh. Key role of the polarization anisotropy of water in modeling classical polarizable force fields. *J. Phys. Chem. A*, 111(33):8170–8176, 2007.
- [88] D. M. Elking, G. A. Cisneros, J.-P. Piquemal, T. A. Darden, and L. G. Pedersen. Gaussian multipole model (gmm). *J. Chem. Theory Comput.*, 6(1):190–202, 2010.
- [89] Q. Wang, J. A. Rackers, C. He, R. Qi, C. Narth, L. Lagardere, N. Gresh, J. W. Ponder, J.-P. Piquemal, and P. Ren. General model for treating short-range electrostatic penetration in a molecular mechanics force field. *J. Chem. Theory Comput.*, 11(6):2609–2618, 2015.

- [90] A. Scherrer, V. Vershinin, and D. Sebastiani. Eigensystem representation of the electronic susceptibility tensor for intermolecular interactions within density functional theory. *J. Chem. Theory Comput.*, 8(1):106–111, Jan 2012.
- [91] A. Scherrer and D. Sebastiani. Moment expansion of the linear density-density response function. *J. Comput. Chem.*, 37(7):665–674, 2016.
- [92] M. Born and K. Huang. *Dynamical Theory of Crystal Lattices*. Oxford at the Clarendon Press, 1st edition, 1954.
- [93] Ø. Burrau. Berechnung des Energiewertes des Wasserstoffmolekel-Ions (H_2^+) im Normalzustand. *Naturwissenschaften*, 15(1):16–17, 1927.
- [94] M. E. Tuckerman. *Statistical Mechanics: Theory and Molecular Simulation (Oxford Graduate Texts)*. Oxford University Press, 1 edition, 4 2010.
- [95] H. Hellmann. *Einführung in die Quantenchemie*. F. Deuticke (Leipzig), 1937.
- [96] R. P. Feynman. Forces in molecules. *Phys. Rev.*, 56:340–343, Aug 1939.
- [97] R. G. Parr and W. Yang. *Density-Functional Theory of Atoms and Molecules*. Oxford University Press, USA, 5 1994.
- [98] K. Burke. Perspective on density functional theory. *J. Chem. Phys.*, 136(15):150901, 2012.
- [99] A. D. Becke. Perspective: Fifty years of density-functional theory in chemical physics. *J. Chem. Phys.*, 140(18), 2014.
- [100] R. M. Martin. *Electronic Structure: Basic Theory and Practical Methods*. Cambridge University Press, 4 2004.
- [101] W. Ritz. Über eine neue Methode zur Lösung gewisser Variationsprobleme der mathematischen Physik. *J. Reine Angew. Math.*, 135:1–61, 1908.
- [102] A. D. Becke. Density-functional exchange-energy approximation with correct asymptotic behavior. *Phys. Rev. A*, 38:3098–3100, Sep 1988.
- [103] C. Lee, W. Yang, and R. G. Parr. Development of the Colle-Salvetti correlation-energy formula into a functional of the electron density. *Phys. Rev. B*, 37:785–789, Jan 1988.
- [104] J. P. Perdew, K. Burke, and M. Ernzerhof. Generalized gradient approximation made simple. *Phys. Rev. Lett.*, 77:3865–3868, Oct 1996.
- [105] J. P. Perdew and K. Schmidt. Jacob’s ladder of density functional approximations for the exchange-correlation energy. *AIP Conf. Proc.*, 577(1), 2001.
- [106] E. M. Lifshitz L. D. Landau. *Quantum Mechanics: Non-Relativistic Theory (Course of Theoretical Physics, Vol. 3)*. Butterworth-Heinemann, 3 edition, 1981.

- [107] T. Watermann, A. Scherrer, and D. Sebastiani. Linear response methods in quantum chemistry. In V. Bach and L. Delle Site, editors, *Many-Electron Approaches in Physics, Chemistry and Mathematics*, Mathematical Physics Studies, pages 97–110. Springer International Publishing, 2014.
- [108] R. M. Sternheimer. Electronic polarizabilities of ions from the Hartree-Fock wave functions. *Phys. Rev.*, 96:951–968, Nov 1954.
- [109] F. Mauri and S. G. Louie. Magnetic susceptibility of insulators from first principles. *Phys. Rev. Lett.*, 76:4246–4249, May 1996.
- [110] F. Mauri, B. G. Pfrommer, and S. G. Louie. *Ab Initio* theory of NMR chemical shifts in solids and liquids. *Phys. Rev. Lett.*, 77:5300–5303, Dec 1996.
- [111] G. H. Wannier. The structure of electronic excitation levels in insulating crystals. *Phys. Rev.*, 52:191–197, Aug 1937.
- [112] N. Marzari and D. Vanderbilt. Maximally localized generalized Wannier functions for composite energy bands. *Phys. Rev. B*, 56:12847–12865, Nov 1997.
- [113] T. A. Keith and R. F. W. Bader. Calculation of magnetic response properties using a continuous set of gauge transformations. *Chem. Phys. Lett.*, 210(1–3):223–231, 1993.
- [114] CPMD. Computer code, <http://www.cpmid.org/>.
- [115] D. R. Hamann, M. Schlüter, and C. Chiang. Norm-conserving pseudopotentials. *Phys. Rev. Lett.*, 43:1494–1497, Nov 1979.
- [116] L. Kleinman and D. M. Bylander. Efficacious form for model pseudopotentials. *Phys. Rev. Lett.*, 48:1425–1428, May 1982.
- [117] N. Troullier and J. L. Martins. Efficient pseudopotentials for plane-wave calculations. *Phys. Rev. B*, 43:1993–2006, Jan 1991.
- [118] P. Pulay. Ab initio calculation of force constants and equilibrium geometries in polyatomic molecules. *Mol. Phys.*, 17(2):197–204, 1969.
- [119] C. J. Pickard and F. Mauri. All-electron magnetic response with pseudopotentials: NMR chemical shifts. *Phys. Rev. B*, 63:245101, May 2001.
- [120] C. J. Pickard and F. Mauri. Nonlocal pseudopotentials and magnetic fields. *Phys. Rev. Lett.*, 91:196401, Nov 2003.
- [121] A. M. Kolorev. *Sov. J. Nucl. Phys.*, 6:256, 1968.
- [122] S. Ismail-Beigi, E. K. Chang, and S. G. Louie. Coupling of nonlocal potentials to electromagnetic fields. *Phys. Rev. Lett.*, 87:087402, Aug 2001.
- [123] P. E. Blöchl. Projector augmented-wave method. *Phys. Rev. B*, 50:17953–17979, Dec 1994.

- [124] S. Nosé. A unified formulation of the constant temperature molecular dynamics methods. *J. Chem. Phys.*, 81(1):511–519, 1984.
- [125] W. G. Hoover. Canonical dynamics: Equilibrium phase-space distributions. *Phys. Rev. A*, 31:1695–1697, Mar 1985.
- [126] J. W. Gibbs. *Elementary Principles in Statistical Mechanics*. New York: Charles Scribner’s Sons, 1902.
- [127] E. M. Lifshitz L. D. Landau. *Statistical Physics, Part 1 (Course of Theoretical Physics, Vol. 5)*. Pergamon Press, 3rd edition, 1969.
- [128] M. V. Berry. Quantal phase factors accompanying adiabatic changes. *Proc. R. Soc. A*, 392(1802):45–57, 1984.
- [129] R. D. King-Smith and D. Vanderbilt. Theory of polarization of crystalline solids. *Phys. Rev. B*, 47:1651–1654, Jan 1993.
- [130] R. Resta. Macroscopic electric polarization as a geometric quantum phase. *Eur. Phys. Lett.*, 22(2):133, 1993.
- [131] D. Vanderbilt and R. D. King-Smith. Electric polarization as a bulk quantity and its relation to surface charge. *Phys. Rev. B*, 48:4442–4455, Aug 1993.
- [132] R. Resta. Electrical polarization and orbital magnetization: the modern theories. *J. Phys.: Condens. Matter*, 22(12):123201, 2010.
- [133] N. A. Spaldin. A beginner’s guide to the modern theory of polarization. *J. Solid State Chem.*, 195:2–10, 2012.
- [134] S. F. Boys. Construction of some molecular orbitals to be approximately invariant for changes from one molecule to another. *Rev. Mod. Phys.*, 32:296–299, Apr 1960.
- [135] N. Marzari, A. A. Mostofi, J. R. Yates, I. Souza, and D. Vanderbilt. Maximally localized Wannier functions: Theory and applications. *Rev. Mod. Phys.*, 84:1419–1475, Oct 2012.
- [136] P. L. Silvestrelli, N. Marzari, D. Vanderbilt, and M. Parrinello. Maximally-localized Wannier functions for disordered systems: Application to amorphous silicon. *Solid State Commun.*, 107(1):7–11, 1998.
- [137] W. Kohn. Analytic properties of Bloch waves and Wannier functions. *Phys. Rev.*, 115:809–821, Aug 1959.
- [138] D. Sebastiani, G. Goward, I. Schnell, and M. Parrinello. NMR chemical shifts in periodic systems from first principles. *Comput. Phys. Commun.*, 147(1–2):707–710, 2002.
- [139] A. Scherrer, R. Vuilleumier, and D. Sebastiani. Nuclear velocity perturbation theory of vibrational circular dichroism. *J. Chem. Theory Comput.*, 9(12):5305–5312, 2013.

- [140] T. Thonhauser, D. Ceresoli, D. Vanderbilt, and R. Resta. Orbital magnetization in periodic insulators. *Phys. Rev. Lett.*, 95:137205, Sep 2005.
- [141] D. Ceresoli, T. Thonhauser, D. Vanderbilt, and R. Resta. Orbital magnetization in crystalline solids: Multi-band insulators, Chern insulators, and metals. *Phys. Rev. B*, 74:024408, Jul 2006.
- [142] A. D. McNaught and A. Wilkinson. *IUPAC. Compendium of Chemical Terminology, 2nd ed.* Blackwell Scientific Publications, Oxford, 1997.
- [143] W. S. Weiglhofer and A. Lakhtakia. *Introduction to Complex Mediums for Optics and Electromagnetics (SPIE Press Monograph Vol. PM123)*. SPIE Publications, 11 2003.
- [144] M. P. Silverman. Reflection and refraction at the surface of a chiral medium: comparison of gyrotropic constitutive relations invariant or noninvariant under a duality transformation. *J. Opt. Soc. Am. A*, 3(6):830–837, Jun 1986.
- [145] E. U. Condon. Theories of optical rotatory power. *Rev. Mod. Phys.*, 9:432–457, Oct 1937.
- [146] J. Lekner. Optical properties of isotropic chiral media. *Pure Appl. Opt.*, 5(4):417, 1996.
- [147] C. Altman and K. Suchy. *Reciprocity, Spatial Mapping and Time Reversal in Electromagnetics*. Springer, 2nd ed. 2011 edition, 7 2011.
- [148] L. D. Barron. *Molecular Light Scattering and Optical Activity*. Number 2. Cambridge University Press, Nov 2004.
- [149] D. J. Caldwell and H. J. Eyring. *Theory of Optical Activity (Monographs on Chemistry)*. Number 1. John Wiley & Sons Inc, Nov 1971.
- [150] A. E. Hansen and T. D. Bouman. Natural chiroptical spectroscopy: Theory and computations. *Adv. Chem. Phys.*, 44:454–644, 1980.
- [151] S. Abbate, G. Longhi, K. Kwon, and A. Moscowitz. The use of cross-correlation functions in the analysis of circular dichroism spectra. *J. Chem. Phys.*, 108(1):50–62, 1998.
- [152] L. Rosenfeld. Quantenmechanische Theorie der natürlichen optischen Aktivität von Flüssigkeiten und Gasen. *Z Physik*, 52(3-4):161–174, 1929.
- [153] R. Kubo. Statistical-mechanical theory of irreversible processes. I. General theory and simple applications to magnetic and conduction problems. *J. Phys. Soc. Jpn.*, 12(6):570–586, 1957.
- [154] G. Holzwarth, E. C. Hsu, H. S. Mosher, T. R. Faulkner, and A. Moscowitz. Infrared circular dichroism of carbon-hydrogen and carbon-deuterium stretching modes. Observations. *J. Am. Chem. Soc.*, 96(1):251–252, 1974.
- [155] L. A. Nafie, J. C. Cheng, and P. J. Stephens. Vibrational circular dichroism of 2,2,2-trifluoro-1-phenylethanol. *J. Am. Chem. Soc.*, 97(13):3842–3843, 1975.

- [156] L. A. Nafie, T. A. Keiderling, and P. J. Stephens. Vibrational circular dichroism. *J. Am. Chem. Soc.*, 98(10):2715–2723, 1976.
- [157] G. Holzwarth and I. Chabay. Optical activity of vibrational transitions: A coupled oscillator model. *J. Chem. Phys.*, 57(4), 1972.
- [158] J. A. Schellman. Vibrational optical activity. *J. Chem. Phys.*, 58(7), 1973.
- [159] L. A. Nafie and T. H. Walnut. Vibrational circular dichroism theory: a localized molecular orbital model. *Chem. Phys. Lett.*, 49(3):441–446, 1977.
- [160] C. J. Barnett, A. F. Drake, R. Kuroda, and S. F. Mason. A dynamic polarization model for vibrational optical activity and the infrared circular dichroism of a dihydro[5]helicene. *Mol. Phys.*, 41(2):455–468, 1980.
- [161] S. Abbate, L. Laux, J. Overend, and A. Moscovitz. A charge flow model for vibrational rotational strengths. *J. Chem. Phys.*, 75(7), 1981.
- [162] M. Moskovits and A. Gohin. Vibrational circular dichroism: effect of charge fluxes and bond currents. *J. Phys. Chem.*, 86(20):3947–3950, 1982.
- [163] T. B. Freedman and L. A. Nafie. Vibrational optical activity calculations using infrared and Raman atomic polar tensors. *J. Chem. Phys.*, 78(1), 1983.
- [164] P. L. Polavarapu. A comparison of bond moment and charge flow models for vibrational circular dichroism intensities. *Mol. Phys.*, 49(3):645–650, 1983.
- [165] R. Dutler and A. Rauk. Calculated infrared absorption and vibrational circular dichroism intensities of oxirane and its deuterated analogs. *J. Am. Chem. Soc.*, 111(18):6957–6966, 1989.
- [166] L. A. Nafie and T. B. Freedman. Vibrational circular dichroism theory: formulation defining magnetic dipole atomic polar tensors and vibrational nuclear magnetic shielding tensors. *Chem. Phys. Lett.*, 134(3):225–232, 1987.
- [167] L. A. Nafie. Velocity-gauge formalism in the theory of vibrational circular dichroism and infrared absorption. *J. Chem. Phys.*, 96:5687, 1992.
- [168] M. A. Lowe, G. A. Segal, and P. J. Stephens. The theory of vibrational circular dichroism: trans-1,2-dideuteriocyclopropane. *J. Am. Chem. Soc.*, 108(2):248–256, 1986.
- [169] N. Jiang, R. X. Tan, and J. Ma. Simulations of solid-state vibrational circular dichroism spectroscopy of (s)-alternarlactam by using fragmentation quantum chemical calculations. *J. Phys. Chem. B*, 115(12):2801–2813, Mar 2011.
- [170] K. L. Bak, P. Jørgensen, T. Helgaker, K. Ruud, and H. J. Aa. Jensen. Gauge-origin independent multiconfigurational self-consistent-field theory for vibrational circular dichroism. *J. Chem. Phys.*, 98(11), 1993.

- [171] K. L. Bak, P. Jørgensen, T. Helgaker, K. Ruud, and H. J. Aa. Jensen. Basis set convergence of atomic axial tensors obtained from self-consistent field calculations using London atomic orbitals. *J. Chem. Phys.*, 100(9), 1994.
- [172] V. P. Nicu, J. Neugebauer, S. K. Wolff, and E. J. Baerends. A vibrational circular dichroism implementation within a Slater-type-orbital based density functional framework and its application to hexa- and hepta-helicenes. *Theor. Chem. Acc.*, 119(1-3):245–263, 2008.
- [173] P. T. Panek and C. R. Jacob. Efficient calculation of anharmonic vibrational spectra of large molecules with localized modes. *ChemPhysChem*, 15(15):3365–3377, 2014.
- [174] S. Yang and M. Cho. Direct calculations of vibrational absorption and circular dichroism spectra of alanine dipeptide analog in water: Quantum mechanical/molecular mechanical molecular dynamics simulations. *J. Chem. Phys.*, 131(13), 2009.
- [175] J.-H. Choi and M. Cho. Direct calculations of mid- and near-IR absorption and circular dichroism spectra of chiral molecules using QM/MM molecular dynamics simulation method. *J. Chem. Theory Comput.*, 7(12):4097–4103, 2011.
- [176] K. L. C. Hunt and R. A. Harris. Vibrational circular dichroism and electric-field shielding tensors: A new physical interpretation based on nonlocal susceptibility densities. *J. Chem. Phys.*, 94(11), 1991.
- [177] G. Hunter. Conditional probability amplitudes in wave mechanics. *Int. J. Quantum Chem.*, 9(2):237–242, 1975.
- [178] A. Abedi, N. T. Maitra, and E. K. U. Gross. Exact factorization of the time-dependent electron-nuclear wave function. *Phys. Rev. Lett.*, 105:123002, Sep 2010.
- [179] A. Abedi, N. T. Maitra, and E. K. U. Gross. Correlated electron-nuclear dynamics: Exact factorization of the molecular wavefunction. *J. Chem. Phys.*, 137(22), 2012.
- [180] J. Frenkel. *Wave mechanics*. Clarendon, Oxford, 1934.
- [181] J. L. Alonso, J. Clemente-Gallardo, P. Echeniche-Robba, and J. A. Jover-Galtier. Comment on “Correlated electron-nuclear dynamics: Exact factorization of the molecular wave-function”. *J. Chem. Phys.*, 139(8):087101, 2013.
- [182] A. Abedi, N. T. Maitra, and E. K. U. Gross. Response to “Comment on ‘Correlated electron-nuclear dynamics: Exact factorization of the molecular wavefunction’”; [J. Chem. Phys. 139, 087101 (2013)]. *J. Chem. Phys.*, 139(8):087102, 2013.
- [183] F. Agostini, A. Abedi, Y. Suzuki, and E. K. U. Gross. Mixed quantum-classical dynamics on the exact time-dependent potential energy surface: a fresh look at non-adiabatic processes. *Mol. Phys.*, 111(22-23):3625–3640, 2013.
- [184] A. Abedi, F. Agostini, Y. Suzuki, and E. K. U. Gross. Dynamical steps that bridge piecewise adiabatic shapes in the exact time-dependent potential energy surface. *Phys. Rev. Lett.*, 110:263001, Jun 2013.

- [185] F. Agostini, A. Abedi, Y. Suzuki, S. K. Min, N. T. Maitra, and E. K. U. Gross. The exact forces on classical nuclei in non-adiabatic charge transfer. *J. Chem. Phys.*, 142(8):084303, 2015.
- [186] B. F. E. Curchod, F. Agostini, and E. K. U. Gross. An exact factorization perspective on quantum interferences in nonadiabatic dynamics. *ArXiv e-prints*, April 2016.
- [187] F. Agostini, S. K. Min, and E. K. U. Gross. Semiclassical analysis of the electron-nuclear coupling in electronic non-adiabatic processes. *Ann. Phys.*, 527(9-10):546–555, 2015.
- [188] F. G. Eich and F. Agostini. The adiabatic limit of the exact factorization of the electron-nuclear wave function. *ArXiv e-prints 1604.05098*, April 2016.
- [189] A. Abedi, F. Agostini, and E. K. U. Gross. Mixed quantum-classical dynamics from the exact decomposition of electron-nuclear motion. *Europhys. Lett.*, 106(3):33001, 2014.
- [190] F. Agostini, A. Abedi, and E. K. U. Gross. Classical nuclear motion coupled to electronic non-adiabatic transitions. *J. Chem. Phys.*, 141(21):214101, 2014.
- [191] S. K. Min, F. Agostini, and E. K. U. Gross. Coupled-trajectory quantum-classical approach to electronic decoherence in nonadiabatic processes. *Phys. Rev. Lett.*, 115:073001, Aug 2015.
- [192] F. Agostini, S. K. Min, A. Abedi, and E. K. U. Gross. Quantum-classical nonadiabatic dynamics: Coupled- vs independent-trajectory methods. *J. Chem. Theory Comput.*, 12(5):2127–2143, 2016.
- [193] A. Schild, F. Agostini, and E. K. U. Gross. Electronic flux density beyond the Born–Oppenheimer approximation. *J. Phys. Chem. A*, 120(19):3316–3325, 2016.
- [194] D. C. Langreth and J. P. Perdew. The exchange-correlation energy of a metal surface. *Solid State Commun.*, 17(11):1425–1429, Jul 1975.
- [195] D. C. Langreth and J. P. Perdew. Exchange-correlation energy of a metallic surface: Wave-vector analysis. *Phys. Rev. B*, 15:2884–2901, Mar 1977.
- [196] E. Runge and E. K. U. Gross. Density-functional theory for time-dependent systems. *Phys. Rev. Lett.*, 52:997, Mar 1984.
- [197] E. K. U. Gross and N. T. Maitra. Introduction to tddft. In M. A. L. Marques, N. T. Maitra, F. M.S. Nogueira, E. K. U. Gross, and A. Rubio, editors, *Fundamentals of Time-Dependent Density Functional Theory*, volume 837 of *Lecture Notes in Physics*, pages 53–99. Springer Berlin Heidelberg, 2012.
- [198] N. L. Doltsinis. Time-dependent density functional theory. In V. Bach and L. Delle Site, editors, *Many-Electron Approaches in Physics, Chemistry and Mathematics*, Mathematical Physics Studies, pages 135–151. Springer International Publishing, 2014.
- [199] T. Olsen and K. S. Thygesen. Accurate ground-state energies of solids and molecules from time-dependent density-functional theory. *Phys. Rev. Lett.*, 112:203001, May 2014.

- [200] A. Heßelmann, G. Jansen, and M. Schütz. Density-functional theory-symmetry-adapted intermolecular perturbation theory with density fitting: A new efficient method to study intermolecular interaction energies. *J. Chem. Phys.*, 122(1):014103, 2005.
- [201] R. Bukowski, R. Podestwa, and K. Szalewicz. Efficient calculation of coupled Kohn–Sham dynamic susceptibility functions and dispersion energies with density fitting. *Chem. Phys. Lett.*, 414(1–3):111 – 116, 2005.
- [202] H.-V. Nguyen, T. A. Pham, D. Rocca, and G. Galli. Improving accuracy and efficiency of calculations of photoemission spectra within the many-body perturbation theory. *Phys. Rev. B*, 85:81101, Feb 2012.
- [203] T. A. Pham, H.-V. Nguyen, D. Rocca, and G. Galli. GW calculations using the spectral decomposition of the dielectric matrix: Verification, validation, and comparison of methods. *Phys. Rev. B*, 87:155148, Apr 2013.
- [204] F. Caruso, P. Rinke, X. Ren, A. Rubio, and M. Scheffler. Self-consistent GW: All-electron implementation with localized basis functions. *Phys. Rev. B*, 88:075105, Aug 2013.
- [205] M. Fuchs and X. Gonze. Accurate density functionals: Approaches using the adiabatic-connection fluctuation-dissipation theorem. *Phys. Rev. B*, 65:235109, Jun 2002.
- [206] F. Furche and T. Van Voorhis. Fluctuation-dissipation theorem density-functional theory. *J. Chem. Phys.*, 122(16):164106, Apr 2005.
- [207] J. Toulouse, I. C. Gerber, G. Jansen, A. Savin, and J. G. Ángyán. Adiabatic-connection fluctuation-dissipation density-functional theory based on range separation. *Phys. Rev. Lett.*, 102:096404, Mar 2009.
- [208] J. F. Dobson and J. Wang. Successful test of a seamless van der Waals density functional. *Phys. Rev. Lett.*, 82:2123–2126, Mar 1999.
- [209] M. Dion, H. Rydberg, E. Schröder, D. C. Langreth, and B. I. Lundqvist. Van der Waals density functional for general geometries. *Phys. Rev. Lett.*, 92:246401, Jun 2004.
- [210] D. Lu, Y. Li, D. Rocca, and G. Galli. Abinitio calculation of van der Waals bonded molecular crystals. *Phys. Rev. Lett.*, 102:206411, May 2009.
- [211] J. F. Dobson and T. Gould. Calculation of dispersion energies. *J. Phys. Condens. Matter*, 24(7):073201, 2012.
- [212] A. Tkatchenko, A. Ambrosetti, and R. A. DiStasio. Interatomic methods for the dispersion energy derived from the adiabatic connection fluctuation-dissipation theorem. *J. Chem. Phys.*, 138(7):074106, Feb 2013.
- [213] A. Ambrosetti, A. M. Reilly, R. A. DiStasio, and A. Tkatchenko. Long-range correlation energy calculated from coupled atomic response functions. *J. Chem. Phys.*, 140(18):18A508, May 2014.

- [214] F. Furche. Molecular tests of the random phase approximation to the exchange-correlation energy functional. *Phys. Rev. B*, 64:195120, Nov 2001.
- [215] F. Furche. Developing the random phase approximation into a practical post-Kohn-Sham correlation model. *J. Chem. Phys.*, 129(11):114105, Sep 2008.
- [216] X. Ren, P. Rinke, C. Joas, and M. Scheffler. Random-phase approximation and its applications in computational chemistry and materials science. *J. Mater. Sci.*, 47(21):7447–7471, 2012.
- [217] D. Rocca. Random-phase approximation correlation energies from Lanczos chains and an optimal basis set: theory and applications to the benzene dimer. *J. Chem. Phys.*, 140(18):18A501, May 2014.
- [218] X. Ren, P. Rinke, G. E. Scuseria, and M. Scheffler. Renormalized second-order perturbation theory for the electron correlation energy: Concept, implementation, and benchmarks. *Phys. Rev. B*, 88:035120, Jul 2013.
- [219] J. E. Bates and F. Furche. Communication: Random phase approximation renormalized many-body perturbation theory. *J. Chem. Phys.*, 139(17):171103, Nov 2013.
- [220] N. Colonna, M. Hellgren, and S. de Gironcoli. Correlation energy within exact-exchange adiabatic connection fluctuation-dissipation theory: Systematic development and simple approximations. *Phys. Rev. B*, 90(12), Jan 2014.
- [221] B. Mussard, D. Rocca, G. Jansen, and J. G. Ángyán. Dielectric matrix formulation of correlation energies in the random phase approximation: Inclusion of exchange effects. *J. Chem. Theory Comput.*, 12(5):2191–2202, 2016.
- [222] P. Geerlings and F. De Proft. Conceptual DFT: the chemical relevance of higher response functions. *Phys. Chem. Chem. Phys.*, 10:3028–3042, 2008.
- [223] P. Geerlings, S. Fias, Z. Boisdenghien, and F. De Proft. Conceptual DFT: chemistry from the linear response function. *Chem. Soc. Rev.*, 43:4989–5008, 2014.
- [224] N. Sablon, F. De Proft, and P. Geerlings. The linear response kernel: Inductive and resonance effects quantified. *J. Phys. Chem. Lett.*, 1(8):1228–1234, 2010.
- [225] N. Sablon, F. De Proft, and P. Geerlings. The linear response kernel of conceptual DFT as a measure of electron delocalisation. *Chem. Phys. Lett.*, 498(1–3):192–197, 2010.
- [226] N. Sablon, F. De Proft, M. Sola, and P. Geerlings. The linear response kernel of conceptual DFT as a measure of aromaticity. *Phys. Chem. Chem. Phys.*, 14:3960–3967, 2012.
- [227] H. Hu and W. Yang. Free energies of chemical reactions in solution and in enzymes with ab initio quantum mechanics/molecular mechanics methods. *Ann. Rev. Phys. Chem.*, 59(1):573–601, 2008.
- [228] P. Pulay and T. Janowski. Efficient calculation of the energy of a molecule in an arbitrary electric field. *Int. J. Quant. Chem.*, 109(10):2113–2120, 2009.

- [229] T. Janowski, K. Wolinski, and P. Pulay. Ultrafast quantum mechanics/molecular mechanics Monte Carlo simulations using generalized multipole polarizabilities. *Chem. Phys. Lett.*, 530:1–9, 2012.
- [230] M. to Baben, J. O. Achenbach, and O. A. von Lilienfeld. Guiding ab initio calculations by alchemical derivatives. *J. Chem. Phys.*, 144(10):104103, 2016.
- [231] R. Balawender, M. A. Welearegay, M. Lesiuk, F. De Proft, and P. Geerlings. Exploring chemical space with the alchemical derivatives. *J. Chem. Theory Comput.*, 9(12):5327–5340, 2013.
- [232] K. Y. S. Chang, S. Fias, R. Ramakrishnan, and O. A. von Lilienfeld. Fast and accurate predictions of covalent bonds in chemical space. *J. Chem. Phys.*, 144(17):174110, 2016.
- [233] H. Lehmann. Über Eigenschaften von Ausbreitungsfunktionen und Renormierungskonstanten quantisierter Felder. *Il Nuovo Cimento (1943-1954)*, 11(4):342–357, 2008.
- [234] S. L. Adler. Quantum theory of the dielectric constant in real solids. *Phys. Rev.*, 126:413–420, Apr 1962.
- [235] N. Wiser. Dielectric constant with local field effects included. *Phys. Rev.*, 129:62–69, Jan 1963.
- [236] K. Yabana and G. F. Bertsch. Time-dependent local-density approximation in real time. *Phys. Rev. B*, 54:4484–4487, Aug 1996.
- [237] G. F. Bertsch, J.-I. Iwata, A. Rubio, and K. Yabana. Real-space, real-time method for the dielectric function. *Phys. Rev. B*, 62:7998–8002, Sep 2000.
- [238] I. Tavernelli. Electronic density response of liquid water using time-dependent density functional theory. *Phys. Rev. B*, 73:094204, Mar 2006.
- [239] Z. Boisdenghien, S. Fias, F. Da Pieve, F. De Proft, and P. Geerlings. The polarisability of atoms and molecules: a comparison between a conceptual density functional theory approach and time-dependent density functional theory. *Mol. Phys.*, 113(13-14):1890–1898, 2015.
- [240] S. Hamel, A. J. Williamson, H. F. Wilson, F. Gygi, G. Galli, E. Ratner, and D. Wack. First-principles calculations of the dielectric properties of silicon nanostructures. *Appl. Phys. Lett.*, 92:3115, Jan 2008.
- [241] D. Lu, F. Gygi, and G. Galli. Dielectric properties of ice and liquid water from first-principles calculations. *Phys. Rev. Lett.*, 100:147601, Apr 2008.
- [242] H. F. Wilson, D. Lu, F. Gygi, and G. Galli. Iterative calculations of dielectric eigenvalue spectra. *Phys. Rev. B*, 79:245106, Jun 2009.
- [243] A. Kaur, E. R. Ylvisaker, D. Lu, T. A. Pham, G. Galli, and W. E. Pickett. Spectral representation analysis of dielectric screening in solids and molecules. *Phys. Rev. B*, 87:155144, Apr 2013.
- [244] A. Savin, F. Colonna, and M. Allavena. Analysis of the linear response function along the adiabatic connection from the Kohn-Sham to the correlated system. *J. Chem. Phys.*, 115(15), 2001.

- [245] Z. Boisdenghien, C. Van Alsenoy, F. De Proft, and P. Geerlings. Evaluating and interpreting the chemical relevance of the linear response kernel for atoms. *J. Chem. Theory Comput.*, 9(2):1007–1015, 2013.
- [246] J. D. Walecka A. L. Fetter. *Quantum theory of many-particle systems*. Pure & Applied Physics. McGraw-Hill College, first edition edition, 1971.
- [247] R. P. Wehrum and H. Hermeking. On the response of arbitrary finite order and its relation to imaginary-time correlation functions. *J. Phys. C*, 7(6):L107, 1974.
- [248] E. K. U. Gross and W. Kohn. Local density-functional theory of frequency-dependent linear response. *Phys. Rev. Lett.*, 55:2850–2852, Dec 1985.
- [249] M. Petersilka, U. J. Gossmann, and E. K. U. Gross. Excitation energies from time-dependent density-functional theory. *Phys. Rev. Lett.*, 76:1212–1215, Feb 1996.
- [250] D. Bohm and D. Pines. A collective description of electron interactions. I. Magnetic interactions. *Phys. Rev.*, 82:625–634, Jun 1951.
- [251] J. Harris and R. O. Jones. The surface energy of a bounded electron gas. *J. Phys. F*, 4(8):1170, 1974.
- [252] O. Gunnarsson and B. I. Lundqvist. Exchange and correlation in atoms, molecules, and solids by the spin-density-functional formalism. *Phys. Rev. B*, 13:4274–4298, May 1976.
- [253] A. Görling and M. Levy. Correlation-energy functional and its high-density limit obtained from a coupling-constant perturbation expansion. *Phys. Rev. B*, 47:13105–13113, May 1993.
- [254] A. Savin, F. Colonna, and R. Pollet. Adiabatic connection approach to density functional theory of electronic systems. *Int. J. Quant. Chem.*, 93(3):166–190, 2003.
- [255] W. Yang, A. J. Cohen, F. De Proft, and P. Geerlings. Analytical evaluation of Fukui functions and real-space linear response function. *J. Chem. Phys.*, 136(14):144110, 2012.
- [256] C. Lanczos. An iteration method for the solution of the eigenvalue problem of linear differential and integral operators. *J. Res. Nat. Bur. Std.*, 45:225–282, 1950.
- [257] X. Ge and D. Lu. Local representation of the electronic dielectric response function. *Phys. Rev. B*, 92:241107, Dec 2015.
- [258] D. Rocca, R. Gebauer, Y. Saad, and S. Baroni. Turbo charging time-dependent density-functional theory with Lanczos chains. *J. Chem. Phys.*, 128(15):154105, 2008.
- [259] F. Kaoui and D. Rocca. Random phase approximation correlation energy using a compact representation for linear response functions: application to solids. *J. Phys. Condens. Matter*, 28(3):035201, 2016.

- [260] A. Scherrer, C. Dreßler, P. Ahlert, and D. Sebastiani. Generalization of the electronic susceptibility for arbitrary molecular geometries. *J. Chem. Phys.*, 144(14):144111, 2016.
- [261] A. C. Ihrig, A. Scherrer, and D. Sebastiani. Electronic density response to molecular geometric changes from explicit electronic susceptibility calculations. *J. Chem. Phys.*, 139(9):094102, Jan 2013.
- [262] C. J. Barnett, A. F. Drake, R. Kuroda, S. F. Mason, and S. Savage. Vibrational-electronic interaction in the infrared circular dichroism spectra of transition-metal complexes. *Chem. Phys. Lett.*, 70(1):8 – 10, 1980.
- [263] R. W. Bormett, S. A. Asher, P. J. Larkin, W. G. Gustafson, N. Ragunathan, T. B. Freedman, L. A. Nafie, S. Balasubramanian, and S. G. Boxer. Selective examination of heme protein azide ligand-distal globin interactions by vibrational circular dichroism. *J. Am. Chem. Soc.*, 114(17):6864–6867, 1992.
- [264] Y. He, X. Cao, L. A. Nafie, and T. B. Freedman. Ab initio VCD calculation of a transition-metal containing molecule and a new intensity enhancement mechanism for VCD. *J. Am. Chem. Soc.*, 123(45):11320–11321, 2001.
- [265] C. Merten, K. Hiller, and Y. Xu. Effects of electron configuration and coordination number on the vibrational circular dichroism spectra of metal complexes of trans-1,2-diaminocyclohexane. *Phys. Chem. Chem. Phys.*, 14:12884–12891, 2012.
- [266] S. R. Domingos, F. Hartl, W. J. Buma, and S. Woutersen. Elucidating the structure of chiral molecules by using amplified vibrational circular dichroism: From theory to experimental realization. *ChemPhysChem*, 16(16):3363–3373, 2015.
- [267] G. Lippert, J. Hutter, and M. Parrinello. A hybrid Gaussian and plane wave density functional scheme. *Mol. Phys.*, 92(3):477–488, 1997.
- [268] J. VandeVondele, M. Krack, F. Mohamed, M. Parrinello, T. Chassaing, and J. Hutter. Quickstep: Fast and accurate density functional calculations using a mixed gaussian and plane waves approach. *Comput. Phys. Commun.*, 167(2):103–128, 2005.
- [269] J. R. Cheeseman, M. J. Frisch, F. J. Devlin, and P. J. Stephens. Ab initio calculation of atomic axial tensors and vibrational rotational strengths using density functional theory. *Chem. Phys. Lett.*, 252(3–4):211 – 220, 1996.
- [270] G. Berghold, C. J. Mundy, A. H. Romero, J. Hutter, and M. Parrinello. General and efficient algorithms for obtaining maximally localized Wannier functions. *Phys. Rev. B*, 61:10040–10048, Apr 2000.
- [271] M. Heyden, J. Sun, H. Forbert, G. Mathias, M. Havenith, and D. Marx. Understanding the origins of dipolar couplings and correlated motion in the vibrational spectrum of water. *J. Phys. Chem. Lett.*, 3(16):2135–2140, 2012.

- [272] P. J. Stephens. Gauge dependence of vibrational magnetic dipole transition moments and rotational strengths. *J. Phys. Chem.*, 91(7):1712–1715, 1987.
- [273] K. J. Jalkanen, R. W. Kawiecki, P. J. Stephens, and R. D. Amos. Basis set and gauge dependence of ab initio calculations of vibrational rotational strengths. *J. Phys. Chem.*, 94(18):7040–7055, 1990.
- [274] M. Martinez, M.-P. Gaigeot, D. Borgis, and R. Vuilleumier. Extracting effective normal modes from equilibrium dynamics at finite temperature. *J. Chem. Phys.*, 125(14):144106, 2006.
- [275] D. C. Marinica, G. Grégoire, C. Desfrancois, J. P. Schermann, D. Borgis, and M. P. Gaigeot. Ab initio molecular dynamics of protonated dialanine and comparison to infrared multiphoton dissociation experiments. *J. Phys. Chem. A*, 110(28):8802–8810, 2006.
- [276] T. B. Freedman, K. M. Spencer, N. Ragunathan, L. A. Nafie, J. A. Moore, and J. M. Schwab. Vibrational circular dichroism of (s,s)-[2,3-2h₂]oxirane in the gas phase and in solution. *Can. J. Chem.*, 69(11):1619–1629, Jan 1991.
- [277] C. Merten, J. Bloino, V. Barone, and Y. Xu. Anharmonicity effects in the vibrational CD spectra of propylene oxide. *J. Phys. Chem. Lett.*, 4(20):3424–3428, 2013.
- [278] J. E. Bertie, S. L. Zhang, and C. D. Keefe. Infrared intensities of liquids XVI. Accurate determination of molecular band intensities from infrared refractive index and dielectric constant spectra. *J. Mol. Struct.*, 324(1):157–176, 1994.
- [279] A. D. Buckingham and M. B. Dunn. Optical activity of oriented molecules. *J. Chem. Soc. A*, pages 1988–1991, 1971.
- [280] J. Kubelka and T. A. Keiderling. The anomalous infrared amide I intensity distribution in ¹³C isotopically labeled peptide β -sheets comes from extended, multiple-stranded structures. An ab initio study. *J. Am. Chem. Soc.*, 123(25):6142–6150, 2001.
- [281] P. Bořr and T. A. Keiderling. Structure, spectra and the effects of twisting of β -sheet peptides. A density functional theory study. *J. Mol. Struct. THEOCHEM*, 675(1–3):95–105, 2004.
- [282] P. Bořr and T. A. Keiderling. Ab initio modeling of amide I coupling in antiparallel β -sheets and the effect of ¹³C isotopic labeling on infrared spectra. *J. Phys. Chem. B*, 109(11):5348–5357, 2005.
- [283] C. R. Jacob and M. Reiher. Localizing normal modes in large molecules. *J. Chem. Phys.*, 130(8):084106, 2009.
- [284] F. London. Théorie quantique des courants interatomiques dans les combinaisons aromatiques. *J. Phys. Radium*, 8(10):397–409, 1937.
- [285] K. Wolinski, J. F. Hinton, and P. Pulay. Efficient implementation of the gauge-independent atomic orbital method for NMR chemical shift calculations. *J. Am. Chem. Soc.*, 112(23):8251–8260, 1990.

- [286] J. R. Cheeseman, G. W. Trucks, T. A. Keith, and M. J. Frisch. A comparison of models for calculating nuclear magnetic resonance shielding tensors. *J. Chem. Physics*, 104(14), 1996.
- [287] M. Hamermesh. Galilean invariance and the Schrödinger equation. *Ann. Phys.*, 9(4):518 – 521, 1960.
- [288] B. I. Schneider and N. Nygaard. Orthogonal functions, discrete variable representation, and generalized Gauss quadratures. *J. Phys. Chem. A*, 106(45):10773–10776, 2002.
- [289] A. Scherrer, F. Agostini, D. Sebastiani, E. K. U. Gross, and R. Vuilleumier. On the mass of atoms in molecules: Beyond the Born-Oppenheimer approximation. *ArXiv e-prints 1605.04211*, May 2016.
- [290] H. Essén. The physics of the Born-Oppenheimer approximation. *Int. J. Quant. Chem.*, 12(4):721–735, 1977.
- [291] N. C. Handy and A. M. Lee. The adiabatic approximation. *Chem. Phys. Lett.*, 252(5–6):425–430, 1996.
- [292] W. Kutzelnigg. The adiabatic approximation I. the physical background of the Born-Handy ansatz. *Mol. Phys.*, 90(6):909–916, 1997.
- [293] A. S. Goldhaber. Newtonian adiabatics unified. *Phys. Rev. A*, 71:062102, Jun 2005.
- [294] W. Kutzelnigg. Which masses are vibrating or rotating in a molecule? *Mol. Phys.*, 105(19–22):2627–2647, 2007.
- [295] H. Kjaer and S. P. A. Sauer. On the relation between the non-adiabatic vibrational reduced mass and the electric dipole moment gradient of a diatomic molecule. *Theor. Chem. Account*, 122(3–4):137–143, 2009.
- [296] P. R. Bunker and R. E. Moss. The breakdown of the Born-Oppenheimer approximation: the effective vibration-rotation hamiltonian for a diatomic molecule. *Mol. Phys.*, 33(2):417–424, 1977.
- [297] D. W. Schwenke. Beyond the potential energy surface: Ab initio corrections to the Born-Oppenheimer approximation for H₂O. *J. Phys. Chem. A*, 105(11):2352–2360, 2001.
- [298] A. Owens, S. N. Yurchenko, A. Yachmenev, J. Tennyson, and W. Thiel. Accurate ab initio vibrational energies of methyl chloride. *J. Chem. Phys.*, 142(24):244306, 2015.
- [299] P. R. Bunker and R. E. Moss. The effect of the breakdown of the Born-Oppenheimer approximation on the rotation-vibration hamiltonian of a triatomic molecule. *J. Mol. Spect.*, 80(1):217–228, 1980.
- [300] John C. Tully. Perspective on “Zur Quantentheorie der Molekeln”. *Theor. Chem. Acc.*, 103(3–4):173–176, 2001.
- [301] G. A. Hagedorn. High order corrections to the time-dependent Born-Oppenheimer approximation I: Smooth potentials. *Ann. of Math.*, 124(3):571–590, 1986.

- [302] G. A. Hagedorn and A. Joye. Mathematical analysis of Born-Oppenheimer approximations. In *Spectral Theory and Mathematical Physics: A Festschrift in Honor of Barry Simon's 60th Birthday, Part 1: Quantum Field Theory, Statistical Mechanics, and Nonrelativistic Quantum Systems*, volume 76.1, pages 203–226. Amer. Math. Soc., Providence, RI, 2007.
- [303] G. Rigolin, G. Ortiz, and V. H. Ponce. Beyond the quantum adiabatic approximation: Adiabatic perturbation theory. *Phys. Rev. A*, 78:052508, Nov 2008.
- [304] R. Requist and O. Pankratov. Adiabatic approximation in time-dependent reduced-density-matrix functional theory. *Phys. Rev. A*, 71(4):062102–1–6, 2010.
- [305] D. Yang and A. Rauk. Sum rules for atomic polar and axial tensors from vibronic coupling theory. *Chem. Phys.*, 178(1–3):147 – 154, 1993.
- [306] W. B. Person and J. H. Newton. Dipole moment derivatives and infrared intensities. I. Polar tensors. *J. Chem. Phys.*, 61(3), 1974.
- [307] G. Hanna and R. Kapral. Quantum-classical Liouville dynamics of nonadiabatic proton transfer. *J. Chem. Phys.*, 122(24):244505, 2005.
- [308] K. Aidas, C. Angeli, K. L. Bak, V. Bakken, R. Bast, L. Boman, O. Christiansen, R. Cimiraglia, S. Coriani, P. Dahle, E. K. Dalskov, U. Ekström, T. Enevoldsen, J. J. Eriksen, P. Ettenhuber, B. Fernández, L. Ferrighi, H. Fliegl, L. Frediani, K. Hald, A. Halkier, C. Hättig, H. Heiberg, T. Helgaker, A. C. Hennum, H. Hettema, E. Hjertenæs, S. Høst, I.-M. Høyvik, M. F. Iozzi, B. Jansík, H. J. Aa. Jensen, D. Jonsson, P. Jørgensen, J. Kauczor, S. Kirpekar, T. Kjærgaard, W. Klopper, S. Knecht, R. Kobayashi, H. Koch, J. Kongsted, A. Krapp, K. Kristensen, A. Ligabue, O. B. Lutnæs, J. I. Melo, K. V. Mikkelsen, R. H. Myhre, C. Neiss, C. B. Nielsen, P. Norman, J. Olsen, J. M. H. Olsen, A. Osted, M. J. Packer, F. Pawłowski, T. B. Pedersen, P. F. Provasi, S. Reine, Z. Rinkevicius, T. A. Ruden, K. Ruud, V. V. Rybkin, P. Salek, C. C. M. Samson, A. S. de Merás, T. Saue, S. P. A. Sauer, B. Schimmelpfennig, K. Sneskov, A. H. Steindal, K. O. Sylvester-Hvid, P. R. Taylor, A. M. Teale, E. I. Tellgren, D. P. Tew, A. J. Thorvaldsen, L. Thøgersen, O. Vahtras, M. A. Watson, D. J. D. Wilson, M. Ziolkowski, and H. Ågren. The Dalton quantum chemistry program system. *WIREs Comput Mol Sci*, 4(3):269–284, 2014.
- [309] S. Fatehi and J. E. Subotnik. Derivative couplings with built-in electron-translation factors: Application to benzene. *J. Phys. Chem. Lett.*, 3(15):2039–2043, 2012.
- [310] M. J. Frisch, G. W. Trucks, H. B. Schlegel, G. E. Scuseria, M. A. Robb, J. R. Cheeseman, G. Scalmani, V. Barone, B. Mennucci, G. A. Petersson, H. Nakatsuji, M. Caricato, X. Li, H. P. Hratchian, A. F. Izmaylov, J. Bloino, G. Zheng, J. L. Sonnenberg, M. Hada, M. Ehara, K. Toyota, R. Fukuda, J. Hasegawa, M. Ishida, T. Nakajima, Y. Honda, O. Kitao, H. Nakai, T. Vreven, J. A. Montgomery, Jr., J. E. Peralta, F. Ogliaro, M. Bearpark, J. J. Heyd, E. Brothers, K. N. Kudin, V. N. Staroverov, R. Kobayashi, J. Normand, K. Raghavachari, A. Rendell, J. C. Burant, S. S. Iyengar, J. Tomasi, M. Cossi, N. Rega, J. M. Millam, M. Klene, J. E. Knox, J. B. Cross, V. Bakken, C. Adamo, J. Jaramillo,

- R. Gomperts, R. E. Stratmann, O. Yazyev, A. J. Austin, R. Cammi, C. Pomelli, J. W. Ochterski, R. L. Martin, K. Morokuma, V. G. Zakrzewski, G. A. Voth, P. Salvador, J. J. Dannenberg, S. Dapprich, A. D. Daniels, Ö. Farkas, J. B. Foresman, J. V. Ortiz, J. Cioslowski, and D. J. Fox. Gaussian 09 Revision D.01, 2009. Gaussian Inc. Wallingford CT.
- [311] H.-J. Werner, P. J. Knowles, G. Knizia, F. R. Manby, M. Schütz, et al. MOLPRO, version 2015.1, a package of ab initio programs, 2015.
- [312] E. M. Lifshitz L. D. Landau. *Electrodynamics of Continuous Media (Course of Theoretical Physics, Vol. 8)*. Pergamon Press, 2 edition, 1984.
- [313] R. Kubo, M. Toda, and N. Hashitsume. *Statistical Physics II: Nonequilibrium Statistical Mechanics*, volume 1 of (*Springer Series in Solid-State Sciences*). Springer, Jul 1985.
- [314] L. L. Hirst. The microscopic magnetization: concept and application. *Rev. Mod. Phys.*, 69:607–628, Apr 1997.
- [315] D. W. Noid, M. L. Koszykowski, and R. A. Marcus. A spectral analysis method of obtaining molecular spectra from classical trajectories. *J. Chem. Phys.*, 67(2), 1977.
- [316] A. Papoulis and S. U. Pillai. *Probability, Random Variables, and Stochastic Processes*. McGraw-Hill series in electrical and computer engineering. McGraw-Hill, 2002.
- [317] F. J. Zerilli. Tensor harmonics in canonical form for gravitational radiation and other applications. *J. Math. Phys.*, 11(7), 1970.
- [318] L. Blum and A. J. Torruella. Invariant expansion for two-body correlations: Thermodynamic functions, scattering, and the Ornstein–Zernike equation. *J. Chem. Phys.*, 56(1), 1972.
- [319] C. G. Gray and K. E. Gubbins. *Theory of Molecular Fluids: Fundamentals*. Oxford University Press, 1984.
- [320] A. R. Edmonds. *Angular Momentum in Quantum Mechanics (Investigations in Physics)*. Princeton University Press, reissue edition, 1 1996.
- [321] J. VandeVondele and J. Hutter. Gaussian basis sets for accurate calculations on molecular systems in gas and condensed phases. *J. Chem. Phys.*, 127(11):114105, 2007.
- [322] S. Goedecker, M. Teter, and J. Hutter. Separable dual-space Gaussian pseudopotentials. *Phys. Rev. B*, 54:1703–1710, Jul 1996.
- [323] C. Hartwigsen, S. Goedecker, and J. Hutter. Relativistic separable dual-space Gaussian pseudopotentials from H to Rn. *Phys. Rev. B*, 58:3641–3662, Aug 1998.
- [324] M. Krack. Pseudopotentials for H to Kr optimized for gradient-corrected exchange-correlation functionals. *Theor. Chem. Acc.*, 114(1-3):145–152, 2005.

- [325] S. Grimme. Semiempirical GGA-type density functional constructed with a long-range dispersion correction. *J. Comp. Chem.*, 27(15):1787–1799, 2006.
- [326] G. J. Martyna and M. E. Tuckerman. A reciprocal space based method for treating long range interactions in ab initio and force-field-based calculations in clusters. *J. Chem. Phys.*, 110(6), 1999.
- [327] G. Bussi, D. Donadio, and M. Parrinello. Canonical sampling through velocity rescaling. *J. Chem. Phys.*, 126(1):014101, 2007.
- [328] J. A. Schellman. Circular dichroism and optical rotation. *Chem. Rev.*, 75(3):323–331, 1975.
- [329] D. Bovi, A. Mezzetti, R. Vuilleumier, M.-P. Gageot, B. Chazallon, R. Spezia, and L. Guidoni. Environmental effects on vibrational properties of carotenoids: experiments and calculations on peridinin. *Phys. Chem. Chem. Phys.*, 13:20954–20964, 2011.
- [330] J. Crank and P. Nicolson. A practical method for numerical evaluation of solutions of partial differential equations of the heat conduction type. *Proc. Camb. Phil. Soc.*, 43(1):50–67, 1947.
- [331] R. A. Kendall, T. H. Dunning, and R. J. Harrison. Electron affinities of the first row atoms revisited. Systematic basis sets and wave functions. *J. Chem. Phys.*, 96(9):6796–6806, 1992.

LIST OF FIGURES

1.1	Schematic illustration of the first Hohenberg-Kohn theorem	8
1.2	Polarization of a one dimensional chain	16
1.3	Illustration of Wannier orbitals and the orbital-dependent position operator	17
1.4	Illustrations of circular birefringence, circular dichroism and elliptical polarization	22
2.1	Molecular structure of the (S)- d_2 -oxirane molecule	45
2.2	Vector potential of vibrational modes of oxirane	46
2.3	Vector potential of vibrational modes of (S)- d_2 -oxirane	46
2.4	Molecular structure of the (R)-propylene-oxide molecule	47
2.5	Molecular structure of the (R)-fluoro-oxirane molecule	47
2.6	Visualization of electronic currents	53
2.7	Molecular structure of the (R)- d_2 -oxirane molecule	56
2.8	Relative errors of sum rules in the common and distributed origin gauge	57
2.9	Dependence of sum rules on the distance between the mirror images	58
2.10	Molecular structure of the (R)-propylene-oxide molecule	58
2.11	Molecular structure of the (S)-norcamphor molecule	58
2.12	Molecular structure of the (R)- α -pinene molecule	58
2.13	Experimental and theoretical rotational strengths of (R)- d_2 -oxirane	58
2.14	Experimental and theoretical dipole strengths of (R)- d_2 -oxirane	58
2.15	Experimental and theoretical rotational strengths of (S)-norcamphor	58
2.16	Experimental and theoretical dipole strengths of (S)-norcamphor	59
2.17	Moduli of eigenvalues and weighted first order moments of H_2O	63
2.18	Convergence of the polarizability in the spectral decomposition	67
2.19	First order moment expanded states of H_2O	68
2.20	Hydrogen bonded water dimer with density response	68
2.21	Response density profile of the water dimer	68
2.22	Cumulative response projections	69
2.23	Hydrogen bonded water dimer with density response	73
2.24	Eigenstates in different geometries	74
2.25	First moment-expanded states in different geometries	75
2.26	Overlap between the explicitly calculated and the extrapolated states	76
2.27	Correlation of the vibrationally induced variations of the moment matrix	76
2.28	Correlation of the geometry dependence of the polarizability	76
2.29	Raman scattering intensities from vibrationally induced polarizability changes	77
3.1	Radially decomposed spectra of bulk (R)-propylene-oxide	88
3.2	Radially decomposed spectra of 7M (R)-propylene-oxide in water	88
3.3	Dynamical VCD spectrum of (S)- d_2 -oxirane in the gas phase	90
3.4	Dynamical VCD spectrum of (R)-propylene-oxide in the gas phase	91

3.5	Dynamical IRA and VCD spectra of bulk (R)-propylene-oxide	93
3.6	Dynamical IRA and VCD spectra of (R)-propylene-oxide in water (7M)	94
3.7	Dynamical IRA and VCD spectra of (R)-propylene-oxide in water (inf. diluted)	95
3.8	Cutoff dependence of the mean standard deviation of the VCD spectra	96
3.9	Stationary states with non-local potential	101
3.10	Boosted non-corrected stationary states	102
3.11	Currents and center of mass oscillations due to non-local potentials	102
3.12	Proton transfer potential energy surface and ground state density	116
3.13	Position dependent mass renormalization of the proton model	116
3.14	Molecular dynamics for O-H-O at different levels of theory	117
3.15	RMSD for BO and Ehrenfest dynamics and errors of excitation energies	118
B.1	Radially decomposed spectrum of bulk water	166
B.2	Radially decomposed spectra of diluted (R)-propylene-oxide in water	167

LIST OF TABLES

2.1	Rotational strengths (with corrections) of (S)-d ₂ -oxirane	46
2.2	Dipole and rotational strengths of (S)-d ₂ -oxirane	47
2.3	Dipole and rotational strengths (with corrections) of (R)-propylene-oxide	47
2.4	Dipole and rotational strengths (with corrections) of (R)-fluoro-oxirane	47
2.5	Basis set convergence of the sum rules	57
3.1	Normal and effective mode VCD spectra of (S)-d ₂ -oxirane	92
3.2	Harmonic frequencies and their non-adiabatic corrections	118
B.1	Computational details of the computational setups	168
C.1	A-matrix of the H ₂ molecule	174
C.2	A-matrix of the H ₂ O molecule	175

APPENDIX A

ELECTRONIC STRUCTURE METHODS

A.1 DERIVATION OF THE EXACT FACTORIZATION

We want to minimize the action functional

$$\mathcal{A}[\chi, \Phi_{\mathbf{R}}] = \int_{t_i}^{t_f} \langle \Psi | \hat{\mathcal{H}} - i\hbar \partial_t | \Psi \rangle dt \quad (\text{A.I.1})$$

until the variation with respect to $\chi^*(\mathbf{R}, t)$ is stationary

$$\delta_{\chi^*(\mathbf{R}, t)} \mathcal{A}[\chi, \Phi_{\mathbf{R}}] \stackrel{!}{=} 0 \quad (\text{A.I.2})$$

Explicitly written out, this reads

$$\langle \Phi_{\mathbf{R}}(t) | \hat{T}_n + \hat{\mathcal{H}}_{BO} + V_{n,ext}(\mathbf{R}, t) + V_{e,ext}(\mathbf{r}, t) - i\hbar \partial_t | \Phi_{\mathbf{R}}(t) \rangle \chi(\mathbf{R}, t) = 0. \quad (\text{A.I.3})$$

We note $\langle \Phi | \Phi \rangle = 1$, define $\mathbf{X} \equiv \langle \Phi | \nabla | \Phi \rangle$ and use the following identities

$$\langle \Phi | \nabla^2 \Phi \rangle = \nabla \cdot \langle \Phi | \nabla \Phi \rangle - \langle \nabla \Phi | \cdot | \nabla \Phi \rangle = \nabla \cdot \mathbf{X} - \langle \nabla \Phi | \cdot | \nabla \Phi \rangle \quad (\text{A.I.4})$$

$$(\nabla + \mathbf{X})^2 \chi = \nabla^2 \chi + 2\mathbf{X} \cdot \nabla \chi + \chi \nabla \cdot \mathbf{X} + \mathbf{X}^2 \chi \quad (\text{A.I.5})$$

to rewrite

$$\langle \Phi | \nabla^2 (\chi | \Phi) \rangle = (\nabla + \mathbf{X})^2 \chi - \mathbf{X}^2 \chi - \chi \langle \nabla \Phi | \cdot | \nabla \Phi \rangle. \quad (\text{A.I.6})$$

We use this for the action of the nuclear kinetic energy and introduce the vector potential $\mathbf{A}_\nu(\mathbf{R}, t) = \langle \Phi_{\mathbf{R}}(t) | -i\hbar \nabla_\nu | \Phi_{\mathbf{R}}(t) \rangle$

$$\begin{aligned} \langle \Phi_{\mathbf{R}}(t) | \hat{T}_n | \Phi_{\mathbf{R}}(t) \rangle \chi(\mathbf{R}, t) &= \sum_{\nu=1}^{N_n} \frac{1}{2M_\nu} \left[\left[-i\hbar \nabla_\nu + \mathbf{A}_\nu(\mathbf{R}, t) \right]^2 \chi(\mathbf{R}, t) \right. \\ &\quad \left. - \chi(\mathbf{R}, t) \left(\mathbf{A}_\nu(\mathbf{R}, t)^2 - \hbar^2 \langle \nabla_\nu \Phi_{\mathbf{R}}(t) | \cdot | \nabla_\nu \Phi_{\mathbf{R}}(t) \rangle \right) \right] \end{aligned} \quad (\text{A.I.7})$$

For the BO Hamiltonian and the time derivative, we obtain

$$\langle \Phi_{\mathbf{R}}(t) | \hat{\mathcal{H}}_{BO} | \Phi_{\mathbf{R}}(t) \rangle \chi(\mathbf{R}, t) = \epsilon_{BO}(\mathbf{R}, t) \chi(\mathbf{R}, t) \quad (\text{A.I.8})$$

$$\langle \Phi_{\mathbf{R}}(t) | -i\hbar \partial_t | \Phi_{\mathbf{R}}(t) \rangle \chi(\mathbf{R}, t) = \chi(\mathbf{R}, t) \langle \Phi(\mathbf{R}, t) | -i\hbar \partial_t | \Phi_{\mathbf{R}}(t) \rangle - i\hbar \partial_t \chi(\mathbf{R}, t) \quad (\text{A.I.9})$$

Finally we collect the terms in the nuclear Hamiltonian $\hat{\mathcal{H}}_n$ and the TDPES $\epsilon(\mathbf{R}, t)$

$$\hat{\mathcal{H}}_n = \sum_{\nu=1}^{N_n} \frac{\left[-i\hbar \nabla_\nu + \mathbf{A}_\nu(\mathbf{R}, t) \right]^2}{2M_\nu} + V_{n,ext}(\mathbf{R}, t) + \epsilon(\mathbf{R}, t) \quad (\text{A.I.10})$$

$$\begin{aligned} \epsilon(\mathbf{R}, t) &= \epsilon_{BO}(\mathbf{R}, t) - \sum_{\nu=1}^{N_n} \frac{1}{2M_\nu} \left(\mathbf{A}_\nu(\mathbf{R}, t)^2 + \hbar^2 \langle \nabla_\nu \Phi_{\mathbf{R}}(t) | \cdot | \nabla_\nu \Phi_{\mathbf{R}}(t) \rangle \right) \\ &\quad + \langle \Phi_{\mathbf{R}}(t) | V_{e,ext}(\mathbf{r}, t) - i\hbar \partial_t | \Phi_{\mathbf{R}}(t) \rangle \end{aligned} \quad (\text{A.I.11})$$

so that eq. (A.I.3) can be rewritten in the desired form as

$$i\hbar\partial_t\chi(\mathbf{R}, t) = \hat{\mathcal{H}}_n\chi(\mathbf{R}, t). \quad (\text{A.I.I2})$$

The variation with respect to $\Phi_{\mathbf{R}}^*(\mathbf{r}, t)$

$$\delta_{\Phi_{\mathbf{R}}^*(\mathbf{r}, t)}\mathcal{A}[\chi, \Phi_{\mathbf{R}}] \stackrel{!}{=} 0 \quad (\text{A.I.I3})$$

reads explicitly

$$\delta_{\Phi_{\mathbf{R}}^*(\mathbf{r}, t)}\mathcal{A}[\chi, \Phi_{\mathbf{R}}] = \chi^*(\mathbf{R}, t) \left(\hat{\mathcal{H}} - i\hbar\partial_t \right) \Phi_{\mathbf{R}}(\mathbf{r}, t) \chi(\mathbf{R}, t) = 0. \quad (\text{A.I.I4})$$

The time derivative yields

$$\begin{aligned} \chi^*(\mathbf{R}, t)(-i\hbar\partial_t)\Phi_{\mathbf{R}}(\mathbf{r}, t)\chi(\mathbf{R}, t) &= |\chi(\mathbf{R}, t)|^2(-i\hbar\partial_t)\Phi_{\mathbf{R}}(\mathbf{r}, t) \\ &\quad - \Phi_{\mathbf{R}}(\mathbf{r}, t)\chi^*(\mathbf{R}, t)\hat{\mathcal{H}}_n\chi(\mathbf{R}, t), \end{aligned} \quad (\text{A.I.I5})$$

which gives

$$i\hbar\partial_t\Phi_{\mathbf{R}}(\mathbf{r}, t) = \frac{1}{\chi(\mathbf{R}, t)} \left[\hat{\mathcal{H}}\Phi_{\mathbf{R}}(\mathbf{r}, t) - \Phi_{\mathbf{R}}(\mathbf{r}, t)\hat{\mathcal{H}}_n \right] \chi(\mathbf{R}, t). \quad (\text{A.I.I6})$$

In detail we use

$$\frac{1}{\chi}\nabla^2\Phi\chi = \nabla^2\Phi + 2\frac{(\nabla\chi)}{\chi}(\nabla\Phi) + \frac{\Phi}{\chi}\nabla^2\chi \quad (\text{A.I.I7})$$

$$\frac{\Phi}{\chi}(\nabla + \mathbf{X})^2\chi = \frac{\Phi}{\chi}\nabla^2\chi + \Phi\nabla \cdot \mathbf{X} + \frac{\Phi}{\chi}2\mathbf{X} \cdot \nabla\chi + \Phi\mathbf{X}^2 \quad (\text{A.I.I8})$$

to write

$$\frac{1}{\chi} \left[\nabla^2\Phi - \Phi(\nabla + \mathbf{X})^2 \right] \chi = (\nabla - \mathbf{X})^2\Phi + 2 \left(\frac{(\nabla\chi)}{\chi} + \mathbf{X} \right) \cdot (\nabla - \mathbf{X}). \quad (\text{A.I.I9})$$

This gives rise to the electron-nuclear coupling operator

$$\begin{aligned} \hat{U}_{en}^{coup}[\Phi_{\mathbf{R}}, \chi] &= \sum_{\nu=1}^{N_n} \frac{\left[-i\hbar\nabla_{\nu} - \mathbf{A}_{\nu}(\mathbf{R}, t) \right]^2}{2M_{\nu}} \\ &\quad + \frac{1}{M_{\nu}} \left(\frac{-i\hbar\nabla_{\nu}\chi(\mathbf{R}, t)}{\chi(\mathbf{R}, t)} + \mathbf{A}_{\nu}(\mathbf{R}, t) \right) \cdot (-i\hbar\nabla_{\nu} - \mathbf{A}_{\nu}(\mathbf{R}, t)). \end{aligned} \quad (\text{A.I.20})$$

Finally the electronic equation is obtained as

$$i\hbar\partial_t\Phi_{\mathbf{R}}(\mathbf{r}, t) = \left[\hat{\mathcal{H}}_e - \epsilon(\mathbf{R}, t) \right] \Phi_{\mathbf{R}}(\mathbf{r}, t) \quad (\text{A.I.21})$$

with the electronic Hamiltonian

$$\hat{\mathcal{H}}_e = \hat{\mathcal{H}}_{BO} + V_{e,ext}(\mathbf{r}, t) + \hat{U}_{en}^{coup}[\Phi_{\mathbf{R}}, \chi]. \quad (\text{A.I.22})$$

A.2 RELATING MICROSCOPIC AND MACROSCOPIC PERSPECTIVES

We relate the microscopic and macroscopic perspectives on VCD via energy dissipation. The complex admittances involved then are expressed in terms of classical TCFs.

A.2.1 ENERGY DISSIPATION

Macroscopically, Poynting's theorem relates the average energy dissipation per unit volume (loss L_{\pm}) to the negative divergence of the time averaged Poynting vector³¹²

$$L_{\pm}(\omega) = -\nabla \cdot \bar{\mathbf{S}}_{\pm}(\omega) = -\frac{c}{8\pi} \nabla \cdot \text{Re} [\tilde{\mathbf{E}}_{\pm} \times \tilde{\mathbf{H}}_{\pm}^*]. \quad (\text{A.2.1})$$

Using $\tilde{n}^2 = \tilde{\epsilon}\tilde{\mu}$, the result of §80 in ref.³¹² can be generalized to optically active media

$$L_{\pm}(\omega) = \frac{\omega}{8\pi} \left[\epsilon''(\omega) |\tilde{\mathbf{E}}_{\pm}|^2 + \mu''(\omega) |\tilde{\mathbf{H}}_{\pm}|^2 \right] \left[1 \pm \frac{1}{2} \frac{\Delta n''(\omega)}{n''(\omega)} \right]. \quad (\text{A.2.2})$$

In the microscopic perspective we use linear response theory,^{127,313} which provides an elegant connection of the macroscopic dissipation in terms of microscopic TCFs.^{41,42} The energy dissipation of linear irreversible processes is expressed in terms of complex admittances $\tilde{\chi}_{ij}$. In the following we assume time stationarity and vanishing equilibrium dipole moments. For a set of generalized displacements A_j coupling to a generalized periodic force $X_j = x_j \cos(\omega t + \delta_j)$, the system's response to a displacement B_i is given by the linear relation

$$B_i(t) = \sum_j \left[\chi'_{ij}(\omega) x_j \cos(\omega t + \delta_j) + \chi''_{ij}(\omega) x_j \sin(\omega t + \delta_j) \right]. \quad (\text{A.2.3})$$

The power loss is determined by the complex admittances $\tilde{\chi}_{ij}(\omega) = \chi'_{ij}(\omega) + i\chi''_{ij}(\omega)$ of the involved displacements via³¹³

$$L(\omega) = \frac{\omega}{2} \sum_{ij} \left[\chi'_{ij}(\omega) \sin(\delta_i - \delta_j) + \chi''_{ij}(\omega) \cos(\delta_i - \delta_j) \right] x_i x_j \quad (\text{A.2.4})$$

In our case, we use the interaction Hamiltonian in eq. (1.4.13). We directly omit the electric quadrupole term since it does not contribute in the isotropic average.¹⁴⁹ A further question arises, as to which fields to use as the generalized periodic forces. Following references,^{312,314} we use the experimentally controlled external fields that would also be present in absence of the medium. These are denoted as $\tilde{\mathbf{E}}_{\pm}$ and $\tilde{\mathbf{H}}_{\pm} = \tilde{\mathbf{B}}_{\pm}$, where we have $\tilde{\mathbf{E}}_{\pm} = \pm i\tilde{\mathbf{H}}_{\pm}$. Assuming total transmission at the interface of the medium, e.g. at the Brewster angle, we obtain the internal fields as $\mathbf{E}_{\pm} = \tilde{\mathbf{E}}_{\pm}$ and $\tilde{\mathbf{H}}_{\pm} = \frac{\tilde{n}}{\mu} \tilde{\mathbf{H}}_{\pm}$.⁷³ The relevant terms of the coupling Hamiltonian hence are given as

$$\hat{\mathcal{H}}_{\pm}^{(1)}(t) = -\hat{\boldsymbol{\mu}} \cdot \mathbf{E}_{\pm}(t) - \hat{\mathbf{m}} \cdot \tilde{\mathbf{H}}_{\pm}(t). \quad (\text{A.2.5})$$

Explicitly we have

$$\mathbf{E}_{\pm}(t) = \frac{|\tilde{\mathbf{E}}_{\pm}|}{\sqrt{2}} \left[\epsilon_1 \cos(\omega t) \pm \epsilon_2 \cos(\omega t - \frac{\pi}{2}) \right] \quad (\text{A.2.6})$$

$$\tilde{\mathbf{H}}_{\pm}(t) = \frac{|\tilde{\mathbf{H}}_{\pm}|}{\sqrt{2}} \left[\mp \epsilon_1 \cos(\omega t - \frac{\pi}{2}) + \epsilon_2 \cos(\omega t) \right] \quad (\text{A.2.7})$$

where we note $|\tilde{\mathbf{e}}_{\pm}| = |\tilde{\mathbf{h}}_{\pm}|$. The Hamiltonian in eq. (A.2.5) is

$$\hat{\mathcal{H}}_{\pm}^{(1)}(t) = -\frac{|\tilde{\mathbf{e}}_{\pm}|}{\sqrt{2}} \left[(\hat{\mu}_1 + \hat{m}_2) \cos(\omega t) \pm (\hat{\mu}_2 - \hat{m}_1) \cos(\omega t - \frac{\pi}{2}) \right]. \quad (\text{A.2.8})$$

Using eq. (A.2.4) We obtain the power losses due to the first component

$$L_{\mu_1, \mu_1}(\omega) = \frac{\omega}{4} |\tilde{\mathbf{e}}_{\pm}|^2 \chi''_{\mu_1 \mu_1}(\omega) \quad \text{and} \quad L_{m_1, m_1}(\omega) = \frac{\omega}{4} |\tilde{\mathbf{e}}_{\pm}|^2 \chi''_{m_1 m_1}(\omega) \quad (\text{A.2.9})$$

and the second component is analogue. The terms L_{μ_1, μ_2} and L_{m_1, m_2} vanish in the isotropic average. We define the isotropically averaged

$$L_{\overline{\mu} \cdot \overline{\mu}}(\omega) = \frac{1}{3} L_{\mu \cdot \mu}(\omega) \quad \text{and} \quad L_{\overline{\mathbf{m}} \cdot \overline{\mathbf{m}}}(\omega) = \frac{1}{3} L_{\mathbf{m} \cdot \mathbf{m}}(\omega) \quad (\text{A.2.10})$$

to obtain the final expressions of the isotropic losses

$$L_{\overline{\mu} \cdot \overline{\mu}}(\omega) = \frac{\omega}{6} |\tilde{\mathbf{e}}_{\pm}|^2 \chi''_{\mu \cdot \mu}^{ss}(\omega) \quad \text{and} \quad L_{\overline{\mathbf{m}} \cdot \overline{\mathbf{m}}}(\omega) = \frac{\omega}{6} |\tilde{\mathbf{e}}_{\pm}|^2 \chi''_{\mathbf{m} \cdot \mathbf{m}}^{ss}(\omega), \quad (\text{A.2.11})$$

where we have decomposed the susceptibility into its symmetric and anti-symmetric part

$$\tilde{\chi}(\omega) = \tilde{\chi}^s(\omega) + \tilde{\chi}^a(\omega). \quad (\text{A.2.12})$$

For the cross-terms we get

$$L_{m_1, \mu_1}(\omega) = \pm \frac{\omega}{4} |\tilde{\mathbf{e}}_{\pm}|^2 \chi'_{m_1 \mu_1}(\omega) \quad \text{and} \quad L_{m_2, \mu_2}(\omega) = \pm \frac{\omega}{4} |\tilde{\mathbf{e}}_{\pm}|^2 \chi'_{m_2 \mu_2}(\omega), \quad (\text{A.2.13})$$

which yields in the isotropic average

$$L_{\overline{\mathbf{m}} \cdot \overline{\mu}}(\omega) = \pm \frac{\omega}{3} |\tilde{\mathbf{e}}_{\pm}|^2 \chi'_{\mathbf{m} \cdot \mu}^a(\omega). \quad (\text{A.2.14})$$

Again, the cross-terms L_{μ_1, m_2} and L_{μ_2, m_1} vanish in the isotropic average. The resulting power loss depends via the cross-terms on the handedness of the radiation

$$L_{\pm}(\omega) = \frac{\omega}{6} |\tilde{\mathbf{e}}_{\pm}|^2 \left[\chi''_{\mu \cdot \mu}^{ss}(\omega) + \chi''_{\mathbf{m} \cdot \mathbf{m}}^{ss}(\omega) \pm 2 \chi'_{\mathbf{m} \cdot \mu}^a(\omega) \right]. \quad (\text{A.2.15})$$

Equating eqs. (A.2.2) and (A.2.15) and expressing the internal fields in terms of the external fields ($\tilde{\mathbf{H}}_{\pm} = \frac{\tilde{n}}{\tilde{\mu}} \tilde{\mathbf{h}}_{\pm}$) yields

$$\left[\epsilon''(\omega) + \mu''(\omega) \frac{|\tilde{\epsilon}(\omega)|}{|\tilde{\mu}(\omega)|} \right] \left[1 \pm \frac{1}{2} \frac{\Delta n''(\omega)}{n''(\omega)} \right] = \frac{4\pi}{3} \left[\chi''_{\mu \cdot \mu}^{ss}(\omega) + \chi''_{\mathbf{m} \cdot \mathbf{m}}^{ss}(\omega) \pm 2 \chi'_{\mathbf{m} \cdot \mu}^a(\omega) \right], \quad (\text{A.2.16})$$

where we identify the terms responsible for the mean absorbance

$$\epsilon''(\omega) = \frac{4\pi}{3} \chi''_{\mu \cdot \mu}^{ss}(\omega) \quad \text{and} \quad \mu''(\omega) = \frac{4\pi}{3} \frac{|\tilde{\mu}(\omega)|}{|\tilde{\epsilon}(\omega)|} \chi''_{\mathbf{m} \cdot \mathbf{m}}^{ss}(\omega) \quad (\text{A.2.17})$$

and the difference absorbance

$$\left[\epsilon''(\omega) + \mu''(\omega) \frac{|\tilde{\epsilon}(\omega)|}{|\tilde{\mu}(\omega)|} \right] \frac{\Delta n''}{n''} = \frac{16\pi}{3} \chi'_{\mathbf{m} \cdot \mu}^a(\omega) \quad (\text{A.2.18})$$

We are interested in the limit $\tilde{\mu} = 1$ and obtain

$$n''(\omega) = \frac{2\pi}{3n'(\omega)} \chi''_{\mu \cdot \mu}^{ss}(\omega) \quad \text{and} \quad \Delta n''(\omega) = \frac{8\pi}{3n'(\omega)} \chi'_{\mathbf{m} \cdot \mu}^a(\omega). \quad (\text{A.2.19})$$

A.2.2 CLASSICAL TIME CORRELATION FUNCTIONS

The complex admittances are related to the quantum response function³³ $\Phi_{\hat{B}\hat{A}}(t)$

$$\chi_{\hat{B}\hat{A}}(\omega) = \frac{1}{V} \int_0^\infty dt \Phi_{\hat{B}\hat{A}}(t) e^{i\omega t} \quad (\text{A.2.20})$$

where the volume V enters since the response function connects an extensive and an intensive quantity (e.g. the total dipole moment with the polarization). We approximate the quantum by the classical version of the Kubo transformed response function

$$\Phi_{\hat{B}\hat{A}}(\omega) \approx \Phi_{BA}(\omega) = \beta \langle \dot{A}(0) B(t) \rangle \stackrel{\text{stat.}}{=} -\beta \langle A(0) \dot{B}(t) \rangle. \quad (\text{A.2.21})$$

If the response function is even or odd under TR, we find

$$\chi'_{BA}(\omega) = \frac{1}{2V} \int_{-\infty}^\infty dt \Phi_{BA}^{\text{even}}(t) e^{i\omega t} \quad \text{and} \quad \chi''_{BA}(\omega) = \frac{1}{2Vi} \int_{-\infty}^\infty dt \Phi_{BA}^{\text{odd}}(t) e^{i\omega t}. \quad (\text{A.2.22})$$

Since $\langle \dot{\boldsymbol{\mu}} \cdot \boldsymbol{\mu}(t) \rangle$ is odd under TR, we obtain

$$\chi''_{\boldsymbol{\mu}\cdot\boldsymbol{\mu}}(\omega) = \frac{1}{2Vi} \int_{-\infty}^\infty dt \Phi_{\boldsymbol{\mu}\cdot\boldsymbol{\mu}}(t) e^{i\omega t} = \frac{\beta}{2V\omega} \int_{-\infty}^\infty dt \langle \dot{\boldsymbol{\mu}} \cdot \dot{\boldsymbol{\mu}}(t) \rangle e^{-i\omega t} \quad (\text{A.2.23})$$

where we have used stationarity and TR symmetry of the TCF in the last step. In turn, since $\langle \dot{\boldsymbol{\mu}} \cdot \mathbf{m}(t) \rangle$ is even under TR, we get

$$\chi'_{\mathbf{m}\cdot\boldsymbol{\mu}}(\omega) = \frac{1}{2V} \int_{-\infty}^\infty dt \Phi_{\mathbf{m}\cdot\boldsymbol{\mu}}(t) e^{i\omega t} = \frac{\beta}{2V} \int_{-\infty}^\infty dt \langle \dot{\boldsymbol{\mu}} \cdot \mathbf{m}(t) \rangle e^{-i\omega t}. \quad (\text{A.2.24})$$

Combining eqs. (A.2.23) and (A.2.24) with (A.2.19) yields the desired expression of eqs. (I.4.28) and (I.4.29) for the TCF IRA and VCD spectra.

In an ergodic regime the correlation functions can be evaluated using the Wiener-Khinchin theorem.^{151, 313, 315}

$$\int_{-\infty}^\infty dt \langle \dot{\boldsymbol{\mu}} \cdot \dot{\boldsymbol{\mu}}(t) \rangle e^{-i\omega t} = \lim_{T \rightarrow \infty} \frac{1}{2T} \left\langle \int_{-T}^T dt e^{i\omega t} \dot{\boldsymbol{\mu}}^*(t) \cdot \int_{-T}^T dt' e^{-i\omega t'} \dot{\boldsymbol{\mu}}(t') \right\rangle \quad (\text{A.2.25})$$

$$\int_{-\infty}^\infty dt \langle \dot{\boldsymbol{\mu}} \cdot \mathbf{m}(t) \rangle e^{-i\omega t} = \lim_{T \rightarrow \infty} \frac{1}{2T} \left\langle \int_{-T}^T dt e^{i\omega t} \dot{\boldsymbol{\mu}}^*(t) \cdot \int_{-T}^T dt' e^{-i\omega t'} \mathbf{m}(t') \right\rangle \quad (\text{A.2.26})$$

Since in practice we only have access to a finite simulation time T , we have to include a low-pass filter.³¹⁶ The available period is represented by the rectangle function \square via

$$A_T(t) = \square(t/T) A(t). \quad (\text{A.2.27})$$

This yields for the TCF on the interval $]-T, T[$

$$\langle AB(t) \rangle = \frac{1}{T \wedge (t/T)} \langle A_T B_T(t) \rangle = \frac{1}{T - |t|} \langle A_T B_T(t) \rangle. \quad (\text{A.2.28})$$

A.3 HARMONIC APPROXIMATIONS

The standard procedure to calculate VCD spectra is to invoke the double harmonic approximation of nuclear vibrations in terms of normal modes (NM) and the electronic contributions to the electric and magnetic dipole moments in terms of the atomic polar (APT) and atomic axial (AAT) tensors.¹⁷ We recover the same result in a stepwise approximation procedure.

A.3.1 HARMONIC MOTION: EFFECTIVE AND NORMAL MODES

For the interpretation of TCF spectra it is instructive to successively approximate the full spectrum via harmonic approximations. We employ the concept of effective modes (EM), which was originally developed for the IRA case.^{46,274} The EM analysis allows an attribution of TCF band intensities to their underlying molecular motion and hence provides a useful tool for the analysis and interpretation of theoretical spectra. Since only the nuclear velocities are required for their determination, no additional computational effort is required. The mathematical procedure to extract EMs from a molecular dynamics simulation is sketched in the following.

The EMs are defined from the Fourier transform velocity TCF, which is extracted directly from the AIMD trajectory. They are linear combinations of atomic displacements

$$\dot{q}_k(t) = \sum_i Z_{ki}^{-1} \dot{\zeta}_i(t) \quad (\text{A.3.1})$$

with internal coordinates $\zeta_i(t)$ constructed such that the corresponding power spectra

$$P_{kl}^{\dot{q}}(\omega) = \int_{-\infty}^{+\infty} \langle \dot{q}_k(0) \dot{q}_l(t) \rangle e^{i\omega t} dt \quad (\text{A.3.2})$$

are as localized as possible in frequency. The corresponding functional to be minimized is

$$\Omega^{(2)} = \sum_{k=1}^{3N-6} \left[\frac{\beta}{2\pi} \int_{-\infty}^{+\infty} |\omega|^4 P_{kk}^{\dot{q}}(\omega) d\omega - \left(\frac{\beta}{2\pi} \int_{-\infty}^{+\infty} |\omega|^2 P_{kk}^{\dot{q}}(\omega) d\omega \right)^2 \right].$$

By construction, EMs are orthonormal and equipartitioned

$$\langle \dot{q}_k \dot{q}_l \rangle = \frac{1}{2\pi} \int_{-\infty}^{+\infty} P_{kl}^{\dot{q}}(\omega) d\omega = k_B T \delta_{kl}. \quad (\text{A.3.3})$$

In the limit of low temperatures, the EMs correspond to the NMs when using the Cartesian coordinates as the $\zeta_i(t)$. They can be seen as the NMs obtained from a thermally averaged Hessian

$$\left\langle \frac{\partial^2 V}{\partial R_i \partial R_j} \right\rangle Z_{jk} = \langle \omega^2 \rangle m_i Z_{ik} \quad \text{s.t.} \quad Z_{ik} m_i Z_{il} = \delta_{kl}. \quad (\text{A.3.4})$$

with Cartesian nuclear coordinate components R_i and R_j . The calculation of NMs is usually done via diagonalization of the dynamical matrix after projection of translational and rotational degrees of freedom. The Hessian can be calculated via finite difference derivations or perturbatively^{2,9} employing the nuclear displacement perturbation described in section I.I.4.

Once the EMs or NMs $q_k(t)$ are determined, we can express their contribution to the fluctuation of the dipole moments

$$\dot{\mu}_\beta(t) \approx \sum_k \left\langle \frac{\delta \dot{\mu}_\beta}{\delta \dot{q}_k} \right\rangle \dot{q}_k(t) \quad \text{and} \quad m_\beta(t) \approx \sum_k \left\langle \frac{\delta m_\beta}{\delta \dot{q}_k} \right\rangle \dot{q}_k(t) \quad (\text{A.3.5})$$

with the moment-mode correlations

$$\left\langle \frac{\delta \dot{\mu}_\beta}{\delta \dot{q}_k} \right\rangle = \frac{\langle \dot{\mu}_\beta \dot{q}_k \rangle}{\langle \dot{q}_k \dot{q}_k \rangle} \quad \text{and} \quad \left\langle \frac{\delta m_\beta}{\delta \dot{q}_k} \right\rangle = \frac{\langle m_\beta \dot{q}_k \rangle}{\langle \dot{q}_k \dot{q}_k \rangle} \quad (\text{A.3.6})$$

The mode contributions to the total intensity are then simply

$$\langle D_k \rangle = \sum_{\beta=1}^3 \left\langle \frac{\delta \dot{\mu}_\beta}{\delta \dot{q}_k} \right\rangle \cdot \left\langle \frac{\delta \dot{\mu}_\beta}{\delta \dot{q}_k} \right\rangle \quad \text{and} \quad \langle R_k \rangle = \sum_{\beta=1}^3 \left\langle \frac{\delta m_\beta}{\delta \dot{q}_k} \right\rangle \cdot \left\langle \frac{\delta \dot{\mu}_\beta}{\delta \dot{q}_k} \right\rangle \quad (\text{A.3.7})$$

and the spectrum is given by

$$\alpha(\omega) = F(\omega) \sum_k \langle D_k \rangle P_{kk}^{\dot{q}}(\omega) \quad \text{and} \quad \Delta\alpha(\omega) = 4F(\omega) \sum_k \langle R_k \rangle P_{kk}^{\dot{q}}(\omega) \quad (\text{A.3.8})$$

with the prefactor $F(\omega) = \frac{4\pi^2\omega}{3V\hbar c n'(\omega)}$ and line shapes from the spectral density $P_{kk}^{\dot{q}}(\omega)$.

A.3.2 DOUBLE HARMONIC APPROXIMATION

In the double harmonic approximation, also the dipole moments are expanded to first order around their equilibrium values, introducing as expansion coefficients the APT \mathcal{P} in its position (r) and velocity (v) form and the AAT \mathcal{M}

$$\mu_\beta(t) \approx \sum_k \sum_{\nu=1}^{N_n} \sum_{\alpha=1}^3 \mathcal{P}_{\alpha\beta}^{\nu,r} S_{\alpha k}^\nu q_k(t) \quad (\text{A.3.9})$$

$$\dot{\mu}_\beta(t) \approx \sum_k \sum_{\nu=1}^{N_n} \sum_{\alpha=1}^3 \mathcal{P}_{\alpha\beta}^{\nu,v} S_{\alpha k}^\nu \dot{q}_k(t) \quad (\text{A.3.10})$$

$$m_\beta(t) \approx \sum_k \sum_{\nu=1}^{N_n} \sum_{\alpha=1}^3 \mathcal{M}_{\alpha\beta}^\nu S_{\alpha k}^\nu \dot{q}_k(t) \quad (\text{A.3.11})$$

The displacement vectors of the EMs or NMs $S_{\alpha k}^\nu = \frac{\partial \hat{R}_{\alpha}^\nu}{\partial q_k}$ describe the nuclear displacements in Cartesian coordinates. This yields the established expressions of the intensities in the double harmonic approximation¹⁷

$$\alpha(\omega) = F(\omega) \sum_k D_k \delta(\omega - \omega_k) \quad \text{and} \quad \Delta\alpha(\omega) = 4F(\omega) \sum_k R_k \delta(\omega - \omega_k) \quad (\text{A.3.12})$$

with dipole and rotational strengths as employed in section 1.4.2

$$D_k = \sum_{\nu,\nu'=1}^{N_n} \sum_{\alpha,\alpha',\beta=1}^3 \mathcal{P}_{\alpha\beta}^\nu S_{\alpha k}^\nu \mathcal{P}_{\alpha'\beta}^{\nu'} S_{\alpha' k}^{\nu'} \quad \text{and} \quad R_k = \sum_{\nu,\nu'=1}^{N_n} \sum_{\alpha,\alpha',\beta=1}^3 \mathcal{M}_{\alpha\beta}^\nu S_{\alpha k}^\nu \mathcal{P}_{\alpha'\beta}^{\nu'} S_{\alpha' k}^{\nu'}. \quad (\text{A.3.13})$$

APPENDIX B

GAUGE IN THE LIQUID PHASE AND FIRST APPLICATIONS

B.1 PROJECTED NUCLEAR VELOCITY PERTURBATION THEORY WITH DENSITY FUNCTIONAL PERTURBATION THEORY

We have already discussed the implementation of the NVPT in the plane wave electronic structure code CPMD^{54,139} and focus here on the projection aspect. The projected nuclear displacement Hamiltonian in eq. (3.2.3) is evaluated as

$$\hat{\mathcal{H}}_{KS}^{PNDP}(t) = \sum_{\nu=1}^{N_n} \sum_{\alpha=1}^3 \lambda_{\alpha}^{\nu}(t) \frac{\partial \hat{\mathcal{H}}_{KS}}{\partial R_{\alpha}^{\nu}}, \quad (\text{B.I.1})$$

yielding the first projected Sternheimer equation eq. (3.2.4), which has to be solved self-consistently due to the dependence of the perturbation Hamiltonian on the density response

$$-\hat{P}_e \left[\hat{\mathcal{H}}_{KS}^{(0)} - \epsilon_o^{(0)} \right] \hat{P}_e |\phi_o^{PNDP}(t)\rangle = \hat{P}_e \hat{\mathcal{H}}_{KS}^{PNDP}(t) |\phi_o^{(0)}\rangle. \quad (\text{B.I.2})$$

Here, $\hat{P}_e = 1 - \sum_{o=1}^{N_e} |\phi_o\rangle \langle \phi_o|$ is a projector on the unoccupied states. Correspondingly, we obtain the second Sternheimer equation eq. (3.2.6) as

$$\hat{P}_e \left[\hat{\mathcal{H}}_{KS}^{(0)} - \epsilon_o^{(0)} \right] \hat{P}_e |\phi_o^{(1)}(t)\rangle = \hat{P}_e |\phi_o^{PNDP}(t)\rangle,$$

which requires no self-consistency in the solution.

The evaluation of the current and magnetic dipole moments in eqs. (3.2.9) and (3.2.10) is done with respect to maximally localized Wannier orbitals φ_o

$$\dot{\mathbf{m}}^e(t) = \sum_{o=1}^{N_e} \langle \varphi_o^{(0)} | \hat{\mathbf{m}}^e | \varphi_o^{(1)}(t) \rangle_{\mathbf{r}} + \text{c.c.} \quad (\text{B.I.3})$$

$$\mathbf{m}^e(t) = \sum_{o=1}^{N_e} \langle \varphi_o^{(0)} | \hat{\mathbf{m}}^e | \varphi_o^{(1)}(t) \rangle_{\mathbf{r}} + \text{c.c.} \quad (\text{B.I.4})$$

This a priori projection yields numerically identical results to an a posteriori projection employing the electronic atomic polar tensor \mathcal{E} and the electronic atomic axial tensor \mathcal{I} .

$$\dot{m}_{\beta}^e(t) = \sum_{\nu=1}^{N_n} \sum_{\alpha=1}^3 \mathcal{E}_{\alpha\beta}^{\nu} \dot{R}_{\alpha}^{\nu}(t) \quad \text{with} \quad \mathcal{E}_{\alpha\beta}^{\nu} = \frac{\partial \langle \hat{m}_{\beta}^e \rangle}{\partial \dot{R}_{\alpha}^{\nu}} \quad (\text{B.I.5})$$

$$m_{\beta}^e(t) = \sum_{\nu=1}^{N_n} \sum_{\alpha=1}^3 \mathcal{I}_{\alpha\beta}^{\nu} \dot{R}_{\alpha}^{\nu}(t) \quad \text{with} \quad \mathcal{I}_{\alpha\beta}^{\nu} = \frac{\partial \langle \hat{m}_{\beta}^e \rangle}{\partial \dot{R}_{\alpha}^{\nu}}. \quad (\text{B.I.6})$$

B.2 RADially RESOLVED VIBRATIONAL SPECTRA

We wish to spatially decompose the total vibrational spectra in order to analyze their radial distribution and the dependence of the total spectra on the chosen gauge. To do so, we first show in which way the gauge transport term manifests itself in the decomposition. In a second step, we generalize the regularized decomposition procedure by Heyden et. al.^{47,271} for our purpose and finally discuss numerical results.

B.2.1 SYMMETRY DECOMPOSITION

The cross-correlation of a state variable $\mathbf{a} = \mathbf{a}(0)$ at time 0 with a second state variable $\mathbf{b}(t)$ at time t and distance $\mathbf{r}_{12}(t)$ is a rank two tensor field $\mathbf{T}(\mathbf{r}, t)$

$$\mathbf{T}(\mathbf{r}, t) = \left\langle (\mathbf{a} \otimes \mathbf{b}(t)) \delta(\mathbf{r} - \mathbf{r}_{12}(t)) \right\rangle, \quad (\text{B.2.1})$$

where both, \mathbf{a} and $\mathbf{b}(t)$, are vectors and functions of the system state in phase space. In our case, these could be the molecular electric, current or magnetic dipole moments at distance $\mathbf{r}_{12}(t)$ (in the molecular gauge). In a homogeneous isotropic fluid, the tensor can be expressed in terms of three radial functions

$$\begin{aligned} \mathbf{T}(\mathbf{r}, t) = & \Theta_0(r, t) \text{Id}_3 + \Theta_1(r, t) \sum_{ijk} \epsilon_{ijk} \hat{e}_i \otimes \hat{e}_j \hat{r}_k \\ & + \Theta_2(r, t) (3\hat{r}\hat{r} - \text{Id}_3), \end{aligned} \quad (\text{B.2.2})$$

which are symmetric (Θ_0, Θ_2) and anti-symmetric (Θ_1) under spatial inversion $\mathbf{r} \rightarrow -\mathbf{r}$.^{317–320} Here, we have denoted the unit vectors with a hat. Experimentally, we only observe the trace of the tensor and obtain all three symmetry contributions with the help of the auxiliary longitudinal function Θ_L^{ab} as

$$\Theta_0^{ab}(r, t) = \frac{1}{3} \text{Tr} \left[\frac{1}{4\pi} \int d\Omega \left\langle \mathbf{a} \mathbf{b}(t) \delta(\mathbf{r} - \mathbf{r}_{12}(t)) \right\rangle \right] \quad (\text{B.2.3})$$

$$\Theta_L^{ab}(r, t) = \frac{1}{4\pi} \int d\Omega \left\langle \mathbf{a} \hat{r} : \hat{r} \mathbf{b}(t) \delta(\mathbf{r} - \mathbf{r}_{12}(t)) \right\rangle \quad (\text{B.2.4})$$

$$\Theta_1^{ab}(r, t) = \frac{1}{8\pi} \int d\Omega \left\langle (\mathbf{a} \times \mathbf{b}(t) \cdot \hat{r}) \delta(\mathbf{r} - \mathbf{r}_{12}(t)) \right\rangle \quad (\text{B.2.5})$$

$$\Theta_2^{ab}(r, t) = \frac{1}{2} \left[\Theta_L^{ab}(r, t) - \Theta_0^{ab}(r, t) \right]. \quad (\text{B.2.6})$$

If we assume the particular form $\mathbf{b}(t) = \mathbf{r}_{12}(t) \times \mathbf{c}(t)$, as used in the gauge transport term, we obtain

$$\Theta_0^{ab}(r, t) = \frac{1}{3} r \Theta_1^{ca}(r, t), \quad (\text{B.2.7})$$

i.e. in chiral systems the anti-symmetric Θ_1^{ca} contributes to the spectrum.

B.2.2 REGULARIZATION PROCEDURE

Computationally, the evaluation of eqs. (B.2.4-B.2.5) via binning of molecular properties along a molecular dynamics is a formidable task. We therefore resort to the regularization technique employed by Heyden et al.,^{47,271} which we briefly review here. The starting point is a function of the form

$$f(\omega) = \int_{-\infty}^{\infty} dt e^{-i\omega t} \langle \mathbf{a}(0) \cdot \mathbf{b}(t) \rangle \quad (\text{B.2.8})$$

Instead of the bare molecular dipole moments, we introduce smooth local densities ρ^a , ρ^b , with regularization parameter σ as

$$\rho^a(\mathbf{r}, t) = \sum_{I=1}^{N_{mol}} \mathbf{a}_I(t) \frac{1}{(2\pi\sigma^2)^{\frac{3}{2}}} e^{-\frac{(\mathbf{r}-\mathbf{R}_I)^2}{2\sigma^2}}, \quad (\text{B.2.9})$$

such that

$$C_{ab}(t) = \langle \mathbf{a}(0) \cdot \mathbf{b}(t) \rangle = \lim_{\sigma \rightarrow 0} C_{ab}^\sigma(t) \quad (\text{B.2.10})$$

$$C_{ab}^\sigma(t) = \int d^3r \rho^a(\mathbf{r}, 0) \int d^3r' \rho^b(\mathbf{r}', t). \quad (\text{B.2.11})$$

Convolution and radial averaging yields

$$C_{ab}^\sigma(t) = \sum_{\alpha=1}^3 \int d^3r \int d^3\Delta r \rho_\alpha^a(\mathbf{r}, 0) \rho_\alpha^b(\mathbf{r} + \Delta\mathbf{r}, t) \quad (\text{B.2.12})$$

$$= \sum_{\alpha=1}^3 \int d^3\Delta r C_{\rho_\alpha^a \rho_\alpha^b}(\Delta\mathbf{r}, t). \quad (\text{B.2.13})$$

Using this approach, we define the spatially resolved component wise regularized correlation function

$$C_{\rho_\alpha^a \rho_\beta^b}(\Delta\mathbf{r}, t) = \int d^3r \rho_\alpha^a(\mathbf{r}, 0) \rho_\beta^b(\mathbf{r} + \Delta\mathbf{r}, t). \quad (\text{B.2.14})$$

The different symmetry contributions are then obtained as follows

$$\Theta_0^{ab}(r, t) = \lim_{\sigma \rightarrow 0} \frac{1}{12\pi} \int d\Omega \sum_{\alpha=1}^3 C_{\rho_\alpha^a \rho_\alpha^b}(\Delta\mathbf{r}, t) \quad (\text{B.2.15})$$

$$\Theta_L^{ab}(r, t) = \lim_{\sigma \rightarrow 0} \frac{1}{4\pi} \int d\Omega \sum_{\alpha, \beta=1}^3 C_{\rho_\alpha^a \rho_\beta^b}(\Delta\mathbf{r}, t) \Delta\hat{r}_\alpha \Delta\hat{r}_\beta \quad (\text{B.2.16})$$

$$\Theta_1^{ab}(r, t) = \lim_{\sigma \rightarrow 0} \frac{1}{8\pi} \int d\Omega \sum_{\alpha, \beta=1}^3 C_{\rho_\alpha^a \rho_\beta^b}(\Delta\mathbf{r}, t) \Delta\hat{r}_\gamma \epsilon_{\alpha\beta\gamma} \quad (\text{B.2.17})$$

and the total IRA spectrum is recovered via

$$C_{ab}(t) = \int dr 4\pi r^2 3\Theta_0^{ab}(r, t). \quad (\text{B.2.18})$$

B.2.3 CONVERGENCE OF TIME-CORRELATION FUNCTION VCD SPECTRA

Applied to IRA and VCD spectra, we obtain the final decompositions of IRA

$$\frac{1}{3} \text{Tr} \left[\int \frac{d\Omega}{4\pi} \left\langle \dot{\boldsymbol{\mu}} \dot{\boldsymbol{\mu}}(t) \delta(\mathbf{r} - \mathbf{r}_{12}(t)) \right\rangle \right] = \Theta_0^{\dot{\boldsymbol{\mu}} \dot{\boldsymbol{\mu}}}(r, t) \quad (\text{B.2.19})$$

and of VCD

$$\frac{1}{3} \text{Tr} \left[\int \frac{d\Omega}{4\pi} \left\langle \left(\dot{\boldsymbol{\mu}} \mathbf{m}(t) + \frac{1}{2c} \dot{\boldsymbol{\mu}}(\mathbf{r}_{12}(t) \times \dot{\boldsymbol{\mu}}(t)) \right) \delta(\mathbf{r} - \mathbf{r}_{12}(t)) \right\rangle \right] = \Theta_0^{\dot{\boldsymbol{\mu}} \mathbf{m}}(r, t) + \frac{1}{3c} r \Theta_1^{\dot{\boldsymbol{\mu}} \dot{\boldsymbol{\mu}}}(r, t). \quad (\text{B.2.20})$$

In systems with inversion symmetry $\mathbf{r} \rightarrow -\mathbf{r}$, the contributions $\Theta_0^{\mu\mu}(r, t)$ and $\Theta_1^{\mu\mu}(r, t)$ are, on average, zero.

In comparison to IRA spectra, the VCD contains the additional gauge transport term proportional to $r\Theta_1^{\mu\mu}(r, t)$. We have repeated the analysis of ref.⁴⁷ on the same dataset and computed the relevant anti-symmetric term in bulk water. The results are shown in fig. B.1 and reproduce the results of the original work. Even though there is no numerical equivalence between the use of the electric dipole and the current dipole moments, the interpretation of the result for our purpose is justified. We observe that the anti-symmetric contribution $\Theta_1^{\mu\mu}$ is much smaller than the observable $\Theta_0^{\mu\mu}$. The remaining high frequency oscillations are due to the fluctuations of the instantaneous chirality of water and would decrease with further sampling. This noise in the anti-symmetric contribution is instructive to distinguish between the desired signal and numerical artifacts in the other components. In the region of interest for our purpose, i.e. between 500 and 1700 cm^{-1} , the significant correlation only extends to the first solvation shell.

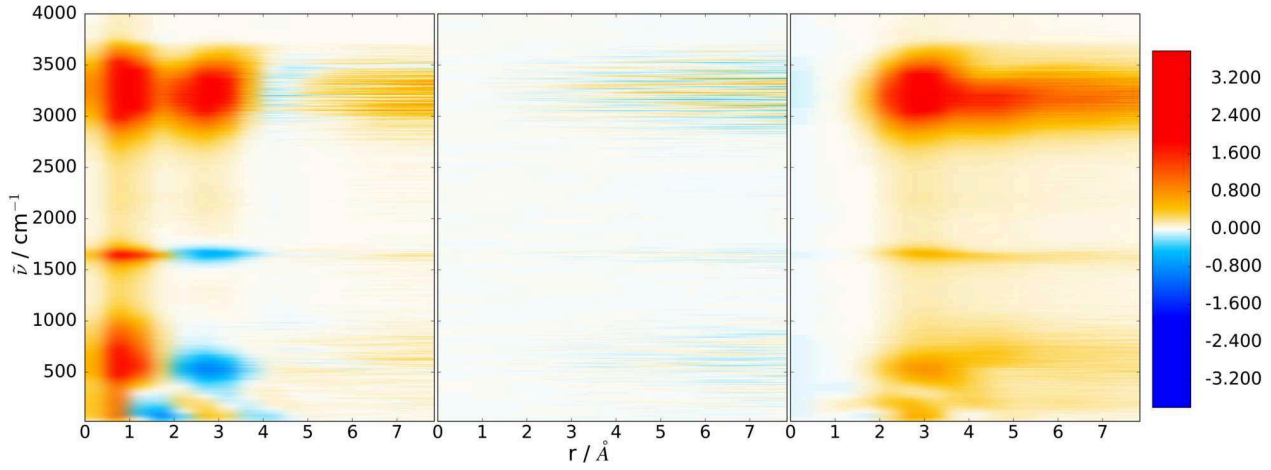


Figure B.1: Isotropic radial decompositions of the vibrational IRA spectrum of bulk water: 1. $\Theta_0^{\mu\mu}(r, \tilde{\nu})$. 2. $\Theta_1^{\mu\mu}(r, \tilde{\nu})$. 3. $\Theta_2^{\mu\mu}(r, \tilde{\nu})$. Intensity in $10^3 \text{Å}^{-1} \text{cm}^{-1}$. Trajectories provided by Heyden et al. from ref.⁴⁷

We have repeated the analysis for the case of a single (R)-propylene-oxide molecule solvated in water and the results of the IRA are in line with the bulk water (fig. B.2). Also here, we observe high frequency oscillations at large distances. Due to the smaller amount of sampling and the smaller simulation cell they start already earlier in this case. The solvent signal completely covers the molecular VCD spectrum, as opposed to the case of a higher concentration in fig. 3.2. The additional scaling of the anti-symmetric contribution $\Theta_1^{\mu\mu}$ with the radius r further blows up the noisy contribution to the total spectrum. This increases the amount of sampling necessary for a converged dynamical VCD spectrum as compared to the conventional dynamical IRA case. However, we can attribute the dominant contribution to the dynamical VCD spectrum to originate within the first solvation shell. Given the finite amount of sampling available, this analysis suggests to separate the significant part of the spectrum from the noisy background at long distances and justifies the localized correlation technique presented in section 3.2.3.

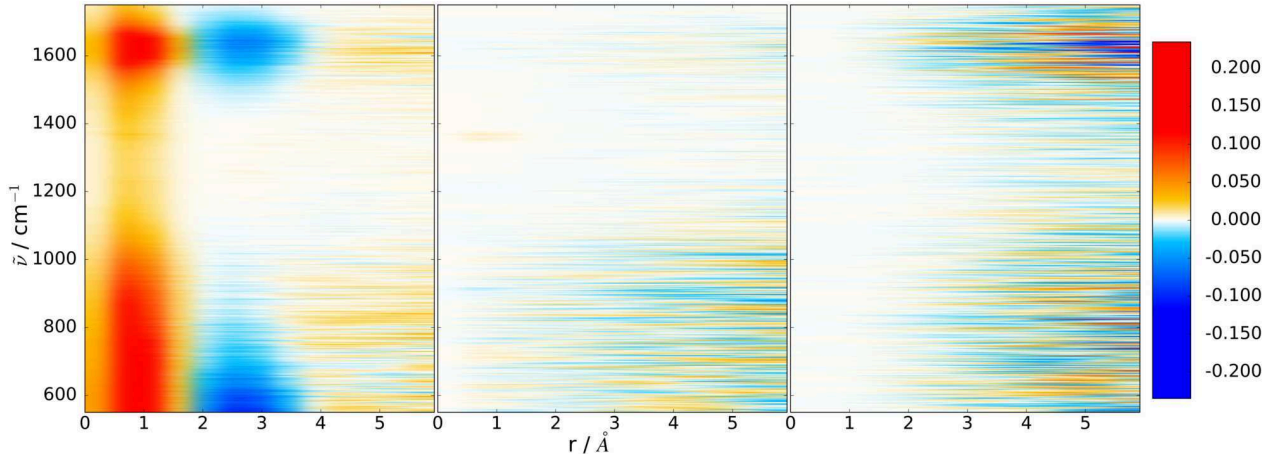


Figure B.2: Isotropic radial decompositions of the vibrational IRA and VCD spectra of a single (R)-propylene-oxide solvated in water: 1. $\Theta_0^{\mu\mu}(r, \tilde{\nu}) \cdot 10^{-4}$. 2. $\Theta_0^{\mu m}(r, \tilde{\nu})$. 3. $\frac{1}{3c} r \Theta_1^{\mu\mu}(r, \tilde{\nu})$. Intensities in $\text{\AA}^{-1} \text{cm}^{-1}$.

B.3 COMPUTATIONAL DETAILS

The presented projected NVPT has been implemented in our development version of the CPMD^{54,114,139} electronic structure package and will be part of future releases of the official code. The calculations have been performed using density functional perturbation theory^{8,9,107} with Troullier-Martins¹¹⁷ pseudopotentials and the BLYP^{102,103} functional. We have employed a plane wave cutoff of 70 Ry.

The BO AIMD have been generated with the CP2K^{267,268} program package using the TZV2P-MOLOPT-GTH basis³²¹ and GTH pseudo potentials^{322–324} with a 0.5 fs time step, a cutoff of 400 Ry and dispersion correction.³²⁵

The computational details of the six computational setups of (R)-propylene-oxide (RPO) and (S)-d₂-oxirane (SDO) are summarized in table B.1. The RPO bulk setup consists of 13 RPO and 1 propanal molecules, the solvated RPO setups of 7 RPO molecules in 34 H₂O molecules and 1 RPO molecule in 52 H₂O molecules. The propanal in the RPO bulk system has the same molecular formula as RPO but is not chiral. In the analysis of IRA and VCD spectra, its molecular dipole moments have been ignored. We have chosen simple cubic simulation cells, employing periodic boundary conditions in the bulk systems and a Poisson-solver³²⁶ in the isolated molecules. To obtain statistically independent initial conditions we have sampled microcanonical trajectories from thermostated molecular dynamics trajectories. Every 4 fs, the projected NVPT calculation of the electronic response properties has been carried out. All spectra shown have been smoothened in the frequency domain via convolution with a Gaussian filter with $\sigma = 2 \text{cm}^{-1}$.

We have followed ref.⁴⁷ in the choice of the sharpness parameter ($D = 0.25 \text{\AA}$) in eq. (3.2.25) and the regularization parameter ($\sigma = 0.4 \text{\AA}$) in eq. (B.2.9). For the representation of the normal and effective mode intensities, we use a Lorentzian line shape function^{17,328} with width $\gamma = 4 \text{cm}^{-1}$. The effective mode analysis has been performed with the MOLSIM package.^{46,329} As internal coordinates of SDO, we have chosen 6 distances, 5 bending and 4 torsion angles.

Table B.1: Computational details of the computational setups. The systems have been equilibrated (NVT) using the CSV_R³²⁷ and massive Nosé-Hoover^{124, 125} (mNH) thermostats with a time constant of 1 ps. All data shown are canonical averages over all microcanonical (NVE) trajectories.

System	(R)-propylene-oxide				(S)-d ₂ -oxirane
	bulk	7M	∞ diluted	isolated	isolated
Temp. (K)	340	340	340	340	10 / 300
Thermostat	CSV _R	CSV _R	CSV _R	mNH	mNH
Cell (Å)	11.8	11.92	11.85	14	12
ρ (g/cm ³)	0.82	1.00	1.00	-	-
# NVEs	3	2	8	40	40
t _{NVE} (ps)	20	20	20	20	10
t _{NVT} (ps)	2	2	2	1	1

APPENDIX C

ON THE MASS OF ATOMS IN MOLECULES

C.1 THE ADIABATIC LIMIT OF THE EXACT FACTORIZATION

We will argue in this section that (i) the correct scaling of the time variable is μ^2 , when the parameter μ^4 is used to scale the nuclear mass M_ν , and (ii) the term in the electron-nuclear coupling operator (ENCO) of Eq. (1.5.10) containing the nuclear wave function scales as well with μ^2 .

Statement (i) is obtained by taking the large mass limit, or small μ^4 limit, as in.³⁰¹ In this situation, the dynamics of the heavy nuclei becomes semi-classical and our scaling argument will make the nuclear kinetic energy tend towards a constant. In the classical limit, it is easy to see that at different values of μ^4 the trajectories of the nuclei can be superimposed if the physical time s is rescaled to a common time $t = \mu^2 s$. At each configuration $\underline{R}(s)$ along the dynamics, the scaling of the time variable has the effect of yielding a kinetic energy that is a constant of μ^4 . In other words, the velocities $\underline{V}(s)$ scale as μ^{-2} . Notice that this is possible as we do not scale the positions with μ^4 , and therefore the potential energy is not affected by the scaling. Using the common rescaled time t to describe the nuclear trajectory, it then becomes possible to make a convergence statement about the nuclear dynamics.

Following Ref.,³⁰¹ the nuclear wave packet can be considered to be a Gaussian wave packet localized at the position $\underline{R}(t)$, with momentum $\underline{P}(t)$:

$$\chi(\underline{R}, t) = \pi^{-3N_n/4} \mu^{-3N_n/2} (\det \underline{\sigma}(t))^{1/4} \times \exp \left[-\frac{(\underline{R} - \underline{R}(t))^T \underline{\sigma}(t) (\underline{R} - \underline{R}(t))}{2\mu^2} + \frac{i}{\hbar} \left(\frac{\underline{P}(t)}{\mu^2} \right) \cdot (\underline{R} - \underline{R}(t)) \right], \quad (\text{C.1.1})$$

with $\underline{\sigma}(t)$ a $(3N_n \times 3N_n)$ symmetric matrix yielding the spatial extension of the wave packet. From this expression, we prove statement (ii): $-i\hbar \nabla_\nu \chi / \chi$ scales as μ^{-2} thus

$$\lambda_\nu(\mathbf{R}, t) = \mu^2 \frac{-i\hbar \nabla_\nu \chi(\mathbf{R}, t)}{\chi(\mathbf{R}, t)} \quad (\text{C.1.2})$$

tends towards a quantity independent of μ .

C.2 SEPARATION OF THE CENTER OF MASS

We introduce the coordinate transformation according to eq. (3.5.55)

$$\mathbf{R}'_1 = \mathcal{R}_{\text{CoM}} = \frac{1}{M_{\text{tot}}} \left[\sum_{\nu=1}^{N_n} M_\nu \mathbf{R}_\nu + m \sum_{k=1}^{N_{el}} \langle \hat{\mathbf{r}}_k \rangle_{BO} \right] \quad (\text{C.2.1})$$

$$\mathbf{R}'_\nu = \mathbf{R}_\nu - \mathbf{R}_1 \quad \text{with } \nu \geq 2, \quad (\text{C.2.2})$$

with the position of the center of mass (CoM) defined in eq. (C.2.1) and $M_{\text{tot}} = \sum_\nu M_\nu + mN_{el}$ the total mass of the system. Such coordinate transformation is applied to the kinetic and potential energy terms in the

nuclear Hamiltonian (3.5.42). Since we have to evaluate the gradient of χ , we have to compute the Jacobian matrix of the transformation from Cartesian to internal coordinates. The Jacobian is a $(3N_n \times 3N_n)$ matrix, whose elements are

$$J_{\nu\nu'}^{ij} = \frac{\partial R_{\nu i}}{\partial R_{\nu' j}} = \begin{cases} \frac{1}{M_{tot}} \left(M_{\nu'} \delta_{ij} + \frac{m}{e} \mathcal{P}_{ji}^{\nu'} \right) & \text{if } \nu = 1 \\ -\delta_{1\nu'} \delta_{ij} + \delta_{\nu\nu'} \delta_{ij} & \text{if } \nu \geq 2 \end{cases} \quad (\text{C.2.3})$$

with $\mathcal{P}_{ji}^{\nu'}$ the electronic APT of eq. (3.5.52). It can be proved with some simple, but tedious, algebra that the determinant of the Jacobian is unity. In eq. (3.5.42) we replace $\underline{\nabla}$ with $\underline{\nabla}'$ according to

$$\begin{aligned} (-i\hbar\underline{\nabla})^T \underline{\mathcal{M}}^{-1} (-i\hbar\underline{\nabla}) &= \left[\underline{J}^T (-i\hbar\underline{\nabla}') \right]^T \underline{\mathcal{M}}^{-1} \left[\underline{J}^T (-i\hbar\underline{\nabla}') \right] \\ &= (-i\hbar\underline{\nabla}')^T \left(\underline{J} \underline{\mathcal{M}}^{-1} \underline{J}^T \right) (-i\hbar\underline{\nabla}') \end{aligned} \quad (\text{C.2.4})$$

where the position-dependent mass in the last term on the right-hand-side depends on \mathbf{R}' , namely

$$\underline{\mathcal{M}}^{-1}(\mathbf{R}') = \underline{J} \underline{\mathcal{M}}^{-1}(\mathbf{R}) \underline{J}^T. \quad (\text{C.2.5})$$

We rewrite the Jacobian matrix as the sum of two terms, \underline{J}^{CoM} and $\underline{J}^{int.}$: the first three rows of \underline{J}^{CoM} are the same as \underline{J} , thus given by eq. (C.2.3) for $\nu = 1$, i.e. $\left(J^{CoM} \right)_{\nu\nu'}^{ij} = \delta_{\nu 1} J_{\nu\nu'}^{ij}$, with each row composed by $3N_n$ entries, all other elements of \underline{J}^{CoM} are zeros; the first three rows of $\underline{J}^{int.}$ are zero and the remaining $3(N_n - 1)$ rows are the same as \underline{J} , thus given by the second expression in eq. (C.2.3). We now introduce the operator $\underline{\mathcal{T}}$, defined as $\mathcal{T}_{\nu\nu'}^{ij} = \delta_{ij} \delta_{\nu' 1}$, and we notice that the product of the position-dependent mass matrix and $\underline{\mathcal{T}}$ yields

$$\underline{\mathcal{M}}(\mathbf{R}) \underline{\mathcal{T}} = M_{tot} \left[\underline{J}^{CoM} \right]^T, \quad (\text{C.2.6})$$

as we now prove. First of all, we recall the expression of the position-dependent mass matrix,

$$\mathcal{M}_{\nu\nu'}^{ij}(\mathbf{R}) = M_{\nu} \delta_{\nu\nu'} \delta_{ij} + \mathcal{A}_{\nu\nu'}^{ij}(\mathbf{R}), \quad (\text{C.2.7})$$

then we write the matrix product with $\underline{\mathcal{T}}$ as the sum of their components, namely

$$\sum_{j=x,y,z} \sum_{\nu'=1}^{N_n} \mathcal{M}_{\nu\nu'}^{ij}(\mathbf{R}) \mathcal{T}_{\nu'\nu''}^{jk} = \left(M_{\nu} \delta_{ik} + \frac{m}{e} \mathcal{P}_{ik}^{\nu}(\mathbf{R}) \right) \delta_{\nu'' 1} = M_{tot} \left[\delta_{\nu'' 1} J_{\nu\nu''}^{ik} \right]^T \quad (\text{C.2.8})$$

where we used the sum rule of eq. (3.5.53) in the first equality and eq. (C.2.3) in the second. We identify the term in square brackets in the last equality as \underline{J}^{CoM} . Further relations that are used below are the following,

$$\underline{J}^{CoM} \underline{\mathcal{T}} = \begin{pmatrix} \underline{I}^{(3)} & \underline{0} \\ \underline{0} & \underline{0} \end{pmatrix} \quad (\text{C.2.9})$$

$$\underline{J}^{int.} \underline{\mathcal{T}} = \underline{0}. \quad (\text{C.2.10})$$

Eq. (C.2.5) is written by introducing the two components, CoM and *int.*, of the Jacobian as

$$\underline{\mathcal{M}}^{-1}(\mathbf{R}') = \underline{J}^{CoM} \underline{\mathcal{M}}^{-1}(\mathbf{R}) \left[\underline{J}^{CoM} \right]^T \quad (\text{C.2.11})$$

$$+ \underline{J}^{int.} \underline{\mathcal{M}}^{-1}(\mathbf{R}) \left[\underline{J}^{int.} \right]^T \quad (\text{C.2.12})$$

$$+ \underline{J}^{int.} \underline{\mathcal{M}}^{-1}(\mathbf{R}) \left[\underline{J}^{CoM} \right]^T \quad (\text{C.2.13})$$

$$+ \underline{J}^{CoM} \underline{\mathcal{M}}^{-1}(\mathbf{R}) \left[\underline{J}^{int.} \right]^T. \quad (\text{C.2.14})$$

Using eq. (C.2.6), the first term on the right-hand-side can be rewritten as

$$\begin{aligned} & \underline{\underline{J}}^{CoM} \underline{\underline{M}}^{-1}(\mathbf{R}) \left[\underline{\underline{J}}^{CoM} \right]^T \\ &= \frac{1}{M_{tot}} \underline{\underline{J}}^{CoM} \underline{\underline{M}}^{-1}(\mathbf{R}) \underline{\underline{M}}(\mathbf{R}) \underline{\underline{T}} \end{aligned} \quad (\text{C.2.15})$$

$$= \frac{1}{M_{tot}} \underline{\underline{J}}^{CoM} \underline{\underline{T}}, \quad (\text{C.2.16})$$

and from eq. (C.2.9) we obtain

$$\frac{1}{2} (-i\hbar \nabla')^T \left[\underline{\underline{J}}^{CoM} \underline{\underline{M}}^{-1}(\mathbf{R}) \left[\underline{\underline{J}}^{CoM} \right]^T \right] (-i\hbar \nabla') = \frac{\hat{P}_{CoM}^2}{2M_{tot}}. \quad (\text{C.2.17})$$

A similar procedure, which uses eq. (C.2.10), is employed to show that the cross-terms in eq. (C.2.14) do not contribute to the kinetic energy. Therefore, the final result reads

$$\hat{\mathcal{H}}_n = \frac{\hat{P}_{CoM}^2}{2M_{tot}} + \frac{1}{2} (-i\hbar \nabla')^T \underline{\underline{M}}(\mathbf{R}') (-i\hbar \nabla') + E(\mathbf{R}'). \quad (\text{C.2.18})$$

C.3 NUMERICAL DETAILS OF THE POSITION DEPENDENT MASS

C.3.1 NUMERICAL DETAILS OF THE O-H-O MODEL

A model system of a proton involved in a one-dimensional hydrogen bond like O – H – O is considered,²⁷⁵ with potential

$$\begin{aligned} V(r, R) = & D \left[e^{-2a(\frac{R}{2}+r-d)} - 2e^{-a(\frac{R}{2}+r-d)} + 1 \right] \\ & + Dc^2 \left[e^{-\frac{2a}{c}(\frac{R}{2}-r-d)} - 2e^{-\frac{a}{c}(\frac{R}{2}-r-d)} \right] + Ae^{-BR} - \frac{C}{R^6}. \end{aligned} \quad (\text{C.3.1})$$

Here r indicates the position of the proton measured from the center of the O – O bond and R stands for the O – O distance. The chosen parameters of the Morse potential are $D = 60$ kcal/mol, $d = 0.95$ Å, $a = 2.52$ Å⁻¹; $c = 0.707$ makes the potential for the proton asymmetric, mimicking a weak O – H – O bond. The other parameters are $A = 2.32 \times 10^5$ kcal/mol, $B = 3.15$ Å⁻¹ and $C = 2.31 \times 10^4$ kcal/mol/Å⁶. The full Hamiltonian of the system involves the $V(r, R)$ and the kinetic energies of the oxygen atoms and of the proton, namely

$$\hat{\mathcal{H}}(r, R_{O-}, R_{O+}) = \sum_{\nu=+,-} \frac{-\hbar^2 \nabla_{O\nu}^2}{2M_{O\nu}} + \frac{-\hbar^2 \nabla_r^2}{2M_H} + \hat{V}(r, R_{O-}, R_{O+}) \quad (\text{C.3.2})$$

$$= \sum_{\nu=+,-} \frac{-\hbar^2 \nabla_{O\nu}^2}{2M_O} + \hat{\mathcal{H}}_{BO}(r, R_{O-}, R_{O+}), \quad (\text{C.3.3})$$

where \hat{V} , according to eq. (C.3.1), depends only on the distance between the oxygen atoms, $R = |R_{O-} - R_{O+}|$.

In the static calculations, the adiabatic states have been computed by diagonalizing the BO Hamiltonian in Eq. (C.3.3) on a spatial grid 400×400 . The eigenvalues of the full Hamiltonian in Eq. (C.3.2) are determined using a Gaussian quadrature method with 20 points for R , the distance between the two heavy atoms,

and 34 for r , the displacement of the proton from the CoM of the heavy atoms. When the Hamiltonian with position-dependent dressed masses is used for computing the eigenvalues, R is again the distance between the two heavy atoms. In this case, as described in the text, the BO approximation has been introduced before separating the CoM motion and the eigenvalues of the Hamiltonian in internal coordinates (indicated by the prime symbols in Eq. (3.5.56)) have been computed.

In the dynamics we use the three coordinates, i.e. R_{O+} , R_{O-} and $r = r_H$, in order to test the conservation of the position of the CoM. The results in the paper are shown for the same number of periods in all cases, using: the velocity-Verlet algorithm to integrate the classical equations, with a time-step 1 fs; the Crank-Nicolson³³⁰ algorithm for the proton (quantum) equation in Ehrenfest, with a time-step 10^{-4} fs; the Euler algorithm if the force depends on the velocity (see Eq. (C.3.5)) with time-step 0.0625 fs, where the stability of the integration has been tested based on the energy conservation. The position of the proton is estimated as the expectation value of the position operator on the proton wave function at the instantaneous O – O geometry.

C.3.2 NORMAL MODE ANALYSIS

It is easy to prove that given a Lagrangian of the form

$$\mathcal{L}(\dot{\mathbf{R}}, \mathbf{R}) = \frac{1}{2} \dot{\mathbf{R}}^T \underline{\underline{\mathcal{M}}}(\mathbf{R}) \dot{\mathbf{R}} - E(\mathbf{R}), \quad (\text{C.3.4})$$

the classical Hamiltonian of eq. (3.5.44) can be derived as its Legendre-transform. Therefore, nuclear motion is classically governed by the Euler-Lagrange equation

$$\underline{\underline{\mathcal{M}}}(\mathbf{R}) \ddot{\mathbf{R}} = -\nabla E(\mathbf{R}) - \frac{1}{2} \dot{\mathbf{R}}^T [\nabla \underline{\underline{\mathcal{M}}}(\mathbf{R})] \dot{\mathbf{R}}. \quad (\text{C.3.5})$$

This classical equation of motion is integrated using the Euler algorithm as described in section C.3.1. If (i) we use internal coordinates, since the free motion of the CoM can be separated as in eq. (C.2.18), (ii) we introduce the harmonic approximation of $E(\mathbf{R})$ and (iii) we neglect the velocity-dependent term^{*}, we obtain

$$\ddot{\mathbf{R}} = -[\underline{\underline{\mathcal{M}}}^{-1}(\mathbf{R}_0) \underline{\underline{K}}(\mathbf{R}_0)] \mathbf{R}, \quad (\text{C.3.6})$$

with $\underline{\underline{K}}$ the Hessian matrix computed from the ground state electronic potential. The term in square brackets is evaluated at the equilibrium geometry \mathbf{R}_0 . The diagonalization of the matrix in square brackets yields corrected $\nu + \Delta\nu$ frequencies, as $\Delta\nu$ includes the effect of electrons that follow the motion of the nuclei non-adiabatically, namely not instantaneously.

C.3.3 CALCULATION OF THE \mathcal{A} -MATRIX

We have computed the \mathcal{A} -matrix using density functional perturbation theory^{7-9,107,139} as described in Ref.⁵⁴ and checked that the sum rule of Eq. (3.5.54) is satisfied. The numerical scheme has been implemented in the

^{*}In order to keep the procedure as simple as possible, we neglect the term in the equation of motion that explicitly depends on the velocity. Such term is quadratic in the *small* nuclear velocity. On the other hand, it contains spatial derivatives of the position-dependent mass, thus of the \mathcal{A} -matrix: the \mathcal{A} -matrix, in turn, depends on the non-adiabatic coupling vectors and on the BO energies, that we can correctly consider slowly varying in space, as we restricted ourselves to weakly non-adiabatic situations.

electronic structure package CPMD.¹¹⁴ Calculations have been performed using Troullier-Martins¹¹⁷ pseudopotentials in the Becke-Lee-Yang-Parr^{102,103} (BLYP) approximation of the exchange-correlation kernel. The molecular geometry is the equilibrium geometry at the BLYP level, employing the aug-cc-pVTZ basis set³³¹ in the Gaussian electronic structure program.³¹⁰

Table C.1 shows the results for the H₂ molecule. Remember that the \mathcal{A} -matrix is a $(3N_n \times 3N_n)$ matrix, with blocks

$$\left(\begin{array}{c|c} (\underline{\mathcal{A}}_{\text{H}_1\text{H}_1})^{ij} & (\underline{\mathcal{A}}_{\text{H}_1\text{H}_2})^{ij} \\ \hline (\underline{\mathcal{A}}_{\text{H}_2\text{H}_1})^{ij} & (\underline{\mathcal{A}}_{\text{H}_2\text{H}_2})^{ij} \end{array} \right) \quad (\text{C.3.7})$$

and indices i, j running over the Cartesian components x, y, z , so each block is a (3×3) matrix. The sum rule in eq. (3.5.53) reads, in this case,

$$\sum_{\nu, \nu'=1}^{N_n} \mathcal{A}_{\nu'\nu}^{xx}(\mathbf{R}) = \left[(\mathcal{A}_{\text{H}_1\text{H}_1})^{xx} + (\mathcal{A}_{\text{H}_1\text{H}_2})^{xx} + (\mathcal{A}_{\text{H}_2\text{H}_1})^{xx} + (\mathcal{A}_{\text{H}_2\text{H}_2})^{xx} \right] = 1.998 \simeq 2 \quad (\text{C.3.8})$$

and similarly for the other Cartesian components. This result is obtained by summing the entries of the matrix in table C.1, and we find indeed the total electronic mass ($m = 1, N_{el} = 2$) of the system as expected from eq. (3.5.53).

In the case of the H₂O molecules the use of non-local pseudopotentials poses additional technical complications that we discuss here. The BO Hamiltonian in eq. (3.5.47) contains a potential energy term corresponding to the pseudopotential, namely

$$\hat{H}_{BO} = \hat{T}_e + \hat{V}_{\text{loc}} + \hat{V}_{\text{nl}}. \quad (\text{C.3.9})$$

\hat{V}_{nl} , the non-local part of the pseudopotential, does not commute with the position operator¹²⁰ thus we have to take into account such correction when deriving the sum rules of eq. (3.5.53).

The evaluation of eq. (3.5.49) using only local pseudo potentials in the commutator in eq. (3.5.47) gives rise to the \mathcal{A} -matrix contribution due to the *local* pseudopotentials, in the following termed *local part* of the \mathcal{A} -matrix. The local part of the \mathcal{A} -matrix is indeed symmetric and has positive diagonal elements. However, it does not satisfy the sum rule of eq. (3.5.53). In order to correct for this error, we can calculate the correction due to the full commutator where also the effect of the non-local pseudopotential is included. For all $3N_n$ nuclear coordinates, labeled by the indices i, ν , we obtain a commutator for each Cartesian component j . The correction hence gives rise to a $(3N_n \times 3)$ -dimensional matrix Δ_{ν}^{ij} , i.e. the non-local contribution to the electronic APT. However, the appropriate dimension of the matrix to be used to correct the \mathcal{A} -matrix should be $(3N_n \times 3N_n)$, as the \mathcal{A} -matrix itself. Unfortunately, there is no protocol that allows us to match the dimensions of the two matrices, i.e. the \mathcal{A} -matrix and the correction matrix, based on some physical properties. Therefore, we develop such protocol according to the following prescription. The correction matrix is denoted $\Delta\mathcal{A}_{\nu\nu}^{ij}$. We add the symmetric part of the correction Δ_{ν}^{ij} corresponding to each nucleus to the diagonal parts of the blocks of the \mathcal{A} -matrix, i.e. for each nucleus ν :

$$\Delta\mathcal{A}_{\nu\nu}^{ij} = \frac{1}{2}(\Delta_{\nu}^{ij} + \Delta_{\nu}^{ji}) \quad \forall \nu, i, j. \quad (\text{C.3.10})$$

This correction leads to a correct sum rule for the \mathcal{A} -matrix whereas preserving all the known symmetry properties. We show the result of this operation in table C.2. In the case of the water molecule, we compute

$$\sum_{\nu, \nu'=1}^{N_n} \mathcal{A}_{\nu' \nu}^{xx}(\mathbf{R}) = 7.997 \simeq 8. \quad (\text{C.3.II})$$

The sum rule (3.5.53) yields a total mass of 8 ($m = 1, N_{el} = 8$), which is the number of electrons that are considered explicitly. The two $1s$ electrons of the oxygen atom are treated in the frozen core approximation.

Table C.1: Diagonal elements of the \mathcal{A} -matrix of the H_2 molecule (oriented along z-axis).

	Hydrogen 1	Hydrogen 2
Hydrogen 1	0.553 0.553 0.868	0.446 0.446 0.131
Hydrogen 2		0.553 0.553 0.868

Table C.2: Local part of the \mathcal{A} -matrix, i.e. $\tilde{\mathcal{A}}$, non-local pseudopotential correction Δ , symmetrized correction $\Delta\mathcal{A}$ and corrected \mathcal{A} -matrix of an isolated H_2O molecule (in xz-plane oriented along z-axis). The sum rule in eq. (3.5.53) yields, for the three Cartesian components xx , yy and zz , $mN_{el} = 7.998, 8.006, 7.993$, respectively.

$\tilde{\mathcal{A}}$	Oxygen		Hydrogen 1		Hydrogen 2	
Oxygen	6.500	6.323 5.989	0.190 -0.172 0.658	-0.091 0.415 0.287 0.314 0.527	0.190 0.172 0.020 -0.082 0.658	0.091 0.382 0.082 0.037 -0.287 0.314 0.527
Δ	Oxygen		Hydrogen 1		Hydrogen 2	
Correction	-0.395	-0.493 -0.415	-0.112 -0.093 -0.081	-0.081 -0.093 -0.133	-0.112 -0.093 0.081	0.081 -0.133
$\Delta\mathcal{A}$	Oxygen		Hydrogen 1		Hydrogen 2	
Oxygen	-0.395	-0.493 -0.415				
Hydrogen 1			-0.112 -0.093 -0.133	-0.081		
Hydrogen 2					-0.112 -0.093 -0.133	0.081
\mathcal{A}	Oxygen		Hydrogen 1		Hydrogen 2	
Oxygen	6.105	5.830 5.574	0.190 -0.172 0.546	-0.091 0.415 0.206 0.222 0.394	0.190 0.172 0.020 -0.082 0.546	0.091 0.382 0.082 0.037 -0.206 0.222 0.394

STATEMENT OF AUTHENTICITY

I hereby declare that I have written the present thesis independently, without assistance from external parties and without use of other sources than those indicated. The ideas taken directly or indirectly from external sources (including electronic sources) are duly acknowledged in the text. The material, either in full or in part, has not been previously submitted for grading at this or any other academic institution.

Place, Date

Signature

Arne Scherrer

Curriculum Vitae

Personal Information

First name / Surname **Arne Scherrer.**
Nationality **German.**
E-mail **arne.scherrer@chemie.uni-halle.de.**
Date of birth **15.07.1987.**

Education

2013–2016 **PhD student & research assistant**, *Martin-Luther-Universität Halle-Wittenberg & École Normale Supérieure Paris.*
2013 **Distinction (Studienpreis)**, *Physikalische Gesellschaft zu Berlin.*
2011–2013 **Master of Science in Physics**, *Freie Universität Berlin.*
2008–2012 **Bachelor of Science in Economics**, *FernUniversität Hagen.*
2007–2011 **Bachelor of Science in Physics**, *Freie Universität Berlin.*
2007 **Abitur**, *Werner-von-Siemens Gymnasium Berlin.*

Publications

- [1] A. Scherrer, F. Agostini, D. Sebastiani, E. K. U. Gross, and R. Vuilleumier. On the mass of atoms in molecules: Beyond the Born-Oppenheimer approximation. *ArXiv e-prints 1605.04211*, 2016.
- [2] A. Scherrer, C. Dreßler, P. Ahlert, and D. Sebastiani. Generalization of the electronic susceptibility for arbitrary molecular geometries. *J. Chem. Phys.*, 144(14):144111, 2016.
- [3] A. Scherrer and D. Sebastiani. Moment expansion of the linear density-density response function. *J. Comput. Chem.*, 37(7):665–674, 2016.
- [4] A. Scherrer, F. Agostini, D. Sebastiani, E. K. U. Gross, and R. Vuilleumier. Nuclear velocity perturbation theory for vibrational circular dichroism: An approach based on the exact factorization of the electron-nuclear wave function. *J. Chem. Phys.*, 143(7):074106, 2015.
- [5] T. Watermann, A. Scherrer, and D. Sebastiani. Linear response methods in quantum chemistry. In Volker Bach and Luigi Delle Site, editors, *Many-Electron Approaches in Physics, Chemistry and Mathematics*, Mathematical Physics Studies, pages 97–110. Springer International Publishing, 2014.
- [6] A. C. Ihrig, A. Scherrer, and D. Sebastiani. Electronic density response to molecular geometric changes from explicit electronic susceptibility calculations. *J. Chem. Phys.*, 139(9):094102, 2013.
- [7] A. Scherrer, R. Vuilleumier, and D. Sebastiani. Nuclear velocity perturbation theory of vibrational circular dichroism. *J. Chem. Theory Comput.*, 9(12):5305–5312, 2013.
- [8] A. Scherrer, V. Verschinin, and D. Sebastiani. Eigensystem representation of the electronic susceptibility tensor for intermolecular interactions within density functional theory. *J. Chem. Theory Comput.*, 8(1):106–111, 2012.